Technical Report Documentation Page

1. Report No.	2. Government Accession No.	3. Recipient's Catalog No.
FHWA/TX-09/0-4588-1 Vol. 2		

4. Title and Subtitle	5. Report Date
EFFECT OF VOIDS IN GROUTED, POST-TENSIONED CONCRETE BRIDGE CONSTRUCTION: VOLUME 2 – INSPECTION, REPAIR, MATERIALS, AND RISKS	February 2009 Published: September 2009
	6. Performing Organization Code

7. Author(s)	8. Performing Organization Report No.
David Trejo, Mary Beth D. Hueste, Paolo Gardoni, Radhakrishna G. Pillai, Kenneth Reinschmidt, Seok Been Im, Suresh Kataria, Stefan Hurlebaus, Michael Gamble, and Thanh Tat Ngo	0-4588-1 Vol. 2

9. Performing Organization Name and Address	10. Work Unit No. (TRAIS)
Texas Transportation Institute The Texas A&M University System College Station, Texas 77843-3135	11. Contract or Grant No. Project 0-4588

12. Sponsoring Agency Name and Address	13. Type of Report and Period Covered
Texas Department of Transportation Research and Technology Implementation Office P. O. Box 5080 Austin, Texas 78763-5080	Technical Report: September 2003-August 2008
	14. Sponsoring Agency Code

15. Supplementary Notes

Research performed in cooperation with the Texas Department of Transportation and the Federal Highway Administration.

Project Title: Effect of Voids In Grouted, Post-Tensioned Concrete Bridge Construction

URL: http://tti.tamu.edu/documents/0-4588-1-Vol2.pdf

16. Abstract

Post-tensioned (PT) bridges are major structures that carry significant traffic. These bridges are designed and constructed because they are economical for spanning long distances. In Texas, there are several signature PT bridges. In the late 1990s and early 2000s, several state highway agencies identified challenges with the PT structures: mainly corrosion of the PT strands. The Texas Department of Transportation (TxDOT) performed some comprehensive inspections of their PT bridges. A consultant's report recommended that all ducts be re-grouted. However, the environment in Texas is very different than the environments in which the corrosion of the PT strands were observed. The objective of this research was to evaluate the corrosion activity of strands for PT structures and to correlate this corrosion activity with general environmental and void conditions. To achieve this objective, time-variant probabilistic models were developed to predict the tension capacity of PT strands subjected to different environmental and void conditions. Using these probabilistic models, time-variant structural reliability models were developed. The probability of failure of a simplified PT structure subjected to HS20 and HL93 loading conditions was assessed. Both flexural failure and serviceability were assessed. Results indicate that the presence of water and chlorides can lead to significant corrosion rates and failure is dependent on this corrosion activity and the number of strands exposed to these conditions. These results are presented in Volume 1 of this report. To assist TxDOT with developing a plan to mitigate this corrosion, studies were performed to assess repair grout materials, inspection methods, and repair methods. In addition, a general methodology is presented on optimizing repairs. These topics are presented in Volume 2 of this report. An Inspection and Repair Manual was also developed from this research and is presented in a separate report. Results indicate that TxDOT should prevent water and chlorides from infiltrating the tendons — this can be achieved in part by repairing drain lines, ducts, and protecting anchor heads as these conditions can lead to early failure of PT bridges. Recommendations on inspections, repairs, and materials are provided, however, further research on the potential formation of galvanic coupling of strands embedded in both existing and new repair grouts need to be assessed.

17. Key Words	18. Distribution Statement
Post-tensioned Bridge; Corrosion; Electrochemistry, Strand, Reliability; Voids; Grout; Durability; Strength Reliability; Service Reliability; Deterioration	No restrictions. This document is available to the public through NTIS: National Technical Information Service Springfield, Virginia 22161 http://www.ntis.gov

19. Security Classif.(of this report)	20. Security Classif.(of this page)	21. No. of Pages	22. Price
Unclassified	Unclassified	342	

EFFECT OF VOIDS IN GROUTED, POST-TENSIONED CONCRETE BRIDGE CONSTRUCTION: VOLUME 2 – INSPECTION, REPAIR, MATERIALS, AND RISKS

by

David Trejo, Ph.D., P.E., Associate Research Engineer
Mary Beth D. Hueste, Ph.D., P.E., Associate Research Engineer
Paolo Gardoni, Ph.D., Assistant Research Engineer
Radhakrishna G. Pillai, Graduate Student Researcher
Kenneth Reinschmidt, Ph.D., P.E., Research Engineer
Seok Been Im, Graduate Student Researcher
Suresh Kataria, Graduate Student Researcher
Stefan Hurlebaus, Dr. Ing., Assistant Research Engineer
Michael Gamble, Graduate Student Researcher
Thanh Tat Ngo, Graduate Student Researcher

Zachry Department of Civil Engineering and
Texas Transportation Institute

Product 0-4588-1: Volume 2
Project 0-4588
Project Title: Effect of Voids in Grouted, Post-Tensioned Concrete Bridge Construction

Performed in cooperation with the
Texas Department of Transportation
and the
Federal Highway Administration

February 2009
Published: September 2009

TEXAS TRANSPORTATION INSTITUTE
The Texas A&M University System
College Station, Texas 77843-3135

DISCLAIMER

The contents of this report reflect the views of the authors, who are responsible for the facts and the accuracy of the data presented herein. The contents do not necessarily reflect the official view or policies of the Federal Highway Administration (FHWA) or the Texas Department of Transportation (TxDOT). References to specific products are for information only and do not imply any claim of performance for that particular product. This report does not constitute a standard, specification, or regulation. The researcher in charge was David Trejo, P.E. #93490.

ACKNOWLEDGMENTS

This project was conducted at Texas A&M University and was supported by the Texas Department of Transportation (TxDOT) and the Federal Highway Administration (FHWA) through the Texas Transportation Institute (TTI). This project had several advisors from TxDOT: their assistance and valuable input were very much appreciated. These engineers included Randy Cox (Program Coordinator), Jaime Sanchez (first Project Director), Maxine Jacoby (second Project Director), Dr. German Claros (third Project Director), and the following project advisors from TxDOT Bridge Division: Brian Merrill, Kenny Ozuna, Tom Rummel, Dean Van Landuyt, Keith Ramsey, Gilbert Silva, and Steve Strmiska. The authors would also wish to thank Matt Potter of the High Bay Structural Materials Laboratory, Duane Wagner, Cheryl Burt, Scott Dobrovolny, Robert Kocman, and Gary Gerke of TTI, Dr. Daren Cline of the Department of Statistics at TAMU, Dr. Ceki Halmen, Ramesh Kumar, Rhett Dotson, and Laura Bolduc (former and current graduate students at TAMU), and the many people at TxDOT who assisted with the bridge inspections.

EXECUTIVE SUMMARY

Post-tensioned (PT) bridges are effective structures from both engineering and economical perspectives. These bridge types have the ability to span long lengths and are often unique, graceful, and the most economical alternative. During construction, PT tendons are used to hold the precast girders together, resulting in a composite structure. The serviceability and performance of PT bridges are very much dependent on the tendons – without the tendons PT bridges would collapse. In the late 1990s and early 2000s state highway agencies (SHAs) identified voids in the grouted tendons. At some of these void locations the strands in the tendons were exhibiting corrosion deterioration, some significant. The Texas Department of Transportation (TxDOT) inspected several of their PT bridges and also found voids in the tendons. A consultant's report recommended that these voids be filled. However, these bridges are exposed to very different environmental conditions than the bridges that exhibited severe corrosion of the strands and the question was raised regarding the necessity to repair the voids, and thus proposed this research project: TxDOT 0-4588, *Effect of Voids in Grouted Post-Tensioned Concrete Bridge Construction*.

The objectives of TxDOT 0-4588 were to provide guidance on the corrosivity of PT strands under different environmental conditions, generate a general model to assess the reliability of PT bridges exhibiting corrosion of the strands, to provide recommendations for repair grout materials, and to provide recommendations for the inspection and repair of PT systems.

In late 2007 a PT bridge in Virginia experienced failure of a tendon. The tendon had been recently repaired (i.e., grouted), and it was believed that the failure could have been a result of galvanic cells formed by the different grout environments. The State of Virginia placed a

moratorium on repairing PT bridges. TxDOT also prevented repairs from being performed on their PT bridges. Unfortunately, the potential corrosion of strands resulting from a galvanic couple caused by embedment in different grout materials was not investigated as part of this research program, and no recommendations can be made on this mechanism of deterioration.

The research did perform extensive studies on the corrosion of strands in various environments. Results indicate that significant decreases in strand capacity occur when the stands are exposed directly to moisture and moisture containing chlorides. The research indicated that high humidity levels do not result in the same deterioration as the water and chloride exposure conditions, however, condensation can lead to higher corrosion rates. The results also indicated that oxygen and carbon dioxide levels have limited influence on the reduction of strand capacities. Using this information, the researchers developed a strand capacity model for the different environmental exposure conditions. Using a general cross section of a PT bridge, the researchers performed reliability analyses. These analyses indicated that PT bridges could fail soon after construction if the strands are subjected to high chloride-containing solutions. If the tendons are protected from these aggressive environments, the service life of these structures, based on corrosion of the strands, could exceed a hundred years. The research findings show the importance of protecting the strands from water and chlorides.

To this end, the researchers evaluated different inspection and repair techniques for tendons on PT bridges. The researchers also assessed the applicability of the current TxDOT specification for repair grouts. The research found that the pressure-vacuum repair procedure results in the best fillibality of the voids. This method was also identified as being the fastest and most economical. The research also proposed a new method for assessing repair grouts. These

repair methods and materials can be used if it is determined that galvanic cells do not form between the existing and repair grouts.

The researchers recommend that every effort be made to keep water and chlorides from the inside of tendons and PT girders. This should include the repair of drainage pipes, damaged ducts or leaking anchorage plates, or correcting any other issues that result in water penetrating the tendon and girder. Preventing the infiltration of water and chlorides into the tendons by performing these relatively simple tasks will likely extend the service life of PT bridges in Texas. The researchers also recommend that a study be performed on the influence of different grout types on corrosion of strands.

Table of Contents

Page

LIST OF FIGURES

LIST OF TABLES

1. INTRODUCTION

Volume-1 of this research report presented characteristics of post-tensioned bridges and described the environmental conditions of Texas. It also presented electrochemical and tension capacity (C_T) behavior of PT systems and the time-variant structural reliability of a typical PT bridge. Volume-2 presents the recommended procedures to inspect PT tendons for voids, to characterize PT grouts, and to repair voids in PT tendons. It should be noted that during the final year of this research project, a repaired tendon in a PT bridge in Virginia failed due to corrosion. This failure occurred approximately three years after being repaired. It is believed that this failure may have been caused by the galvanic cells that developed at the interface between existing and repair grouts. This corrosion mechanism was not investigated in this research. Repairs on PT bridges were not performed as a result of this concern. Research is needed to evaluate the potential impact of repair grouts on corrosion of PT strands. This volume also presents analytical models to assess economic risk associated with the mitigation strategies of PT bridges.

1.1. BRIDGE INSPECTION PROCEDURES

Recent bridge inspections conducted by various federal and state transportation agencies reported the presence of voids in grouted tendons (ASBI 2000a; FDOT 1999; FDOT 2001a; FDOT 2001b; Hansen 2007; NCHRP 1998a). Poor quality grout materials and poor grouting procedures have been cited as one of the causes for void formation in PT bridges (FDOT 2001a). In Volume-1 it was reported that voids can lead to significant amounts of strand corrosion, which in turn can lead to a reduction in both strand capacity and structural reliability. These findings indicate that water should be kept from infiltrating tendons and that voids may have to be filled or repaired to ensure good long-term performance of PT bridges. The first step to achieving more durable structures is to identify the voids and their locations. It is also necessary to obtain general geometrical characteristics of these voids such that the amount of grout materials required can be estimated and the grouting procedures can be selected. Hence, an inspection procedure is needed to identify voids, their locations, and to quantify the geometrical characteristics of voids.

The inspection of tendons in PT bridges can be expensive and cumbersome. This is because of the large mumber of tendons, insufficient and confined work space inside the PT girders, insufficient lighting inside the PT girders, and other constraints in the field. Inspection procedures that are easy to implement and less expensive and time consuming are needed to efficiently identify and quantify voids in PT tendons. Once voids are identified they may need to be filled with grout materials.

1.2. GROUT MATERIALS

In PT bridges, cementitious grout mixtures have been used to fill the PT ducts to protect the strands from the environment to prevent corrosion. Material characteristics of these grouts can have significant impacts on the long-term durability of PT bridges. The Post-Tensioning Institute (PTI) classifies grout materials into four classes based on material specifications and field requirements (PTI 2003a). Class A grout consists of cement and water only. Class B grout consists of portland cement, water, and mineral/chemical admixtures. Class C grout consists of pre-packaged, engineered grout material and water only. Class D grout is defined as any *special* grout designed by the engineer.

Class A and Class C grouts have been used in most PT bridges in Texas. Many Class C grouts with good flow characteristics are commercially available and being used in PT bridges. Three commercially available Class C grouts are Sikagrout 300PT®, Masterflow 816®, and Euco Cable grout PTX®. Information on the material characteristics and performance of these grouts are not available in the literature. Also, test procedures are not available to determine the capability of the grout materials to fill the voids (defined as fillability), especially small voids, in PT systems. A grout with good flow characteristics can have poor fillability. Current PT grout specifications typically have limited requirements for evaluating the fillability, which is a significant parameter for evaluating repair grouts. As such, these specifications may require modifications for grout materials in PT systems. In addition to good grout materials, it is necessary to have effective repair-grouting procedures to ensure proper filling of voids.

1.3. GROUTING PROCEDURES

There are two general grouting procedures used by the PT bridge industry. These are:

- pressure grouting (PG) and
- vacuum grouting (VG) procedures.

The PG procedure was initially developed for grouting of new PT systems. However, this procedure was found to be ineffective in filling the voids in an existing PT system. Therefore, the PT bridge industry developed the VG method. The VG method was found to be highly effective in filling voids in PT systems. However, the VG method was found to be very expensive and time consuming. This is because the VG method requires an air-tight PT system to effectively fill voids. The performance characteristics and personnel, time, and economic requirements, of these two procedures need to be quantified. In addition, a new grouting procedure with optimum performance characteristics and resource requirements needs to be developed.

The inspection, maintenance, and repair programs for PT bridges can be very expensive. Optimizing the inspection and repair while maximizing the effectiveness of the repair will make these procedures more economical.

1.4. ECONOMIC RISK

It is important to maintain the structural reliability and safety levels of PT bridges at higher than minimum required levels (say, threshold values). However, if these levels drop below a threshold value or have a probability to drop below the threshold values, appropriate maintenance and repair actions need to be performed. The objective is to not let the reliability or safety of a PT bridge drop below some critical threshold level as this would be unsafe to the traveling public. If identified early enough, corrosion may be slowed, thereby extending the life of the structure. However, it may be impractical to repair all the voids in PT bridges over a short period and such a decision could have significant economic risks. Moreover, no repair is needed if the existing conditions will not lead to a drop in the reliability and a safety levels. This

economic risk can be minimized by adopting a long-term strategy for bridge maintenance and repair.

All the bridges in a transportation network need to be maintained such that they are safe. Reliability degradation is considerably different for various PT bridges depending on many factors including the environmental conditions, the age of bridge, and the structural properties and characteristics of each bridge system. Management of a system of bridges becomes more challenging when constrained by limited annual maintenance budgets.

Considerable research has been done to develop optimization models to solve bridge management problems. Active research in the development of models for optimum bridge management include Mori and Ellingwood (1994a, 1994b); Estes and Frangopol (2003); and Kong and Frangopol (2003). Numerous optimization methodologies have been developed. Review of the literature shows that an improved optimization model is still, however, needed for the maintenance of PT bridges, in particular because the general models that have been developed have some limitations. These models may be quite difficult to use by decision-makers, to tell when and how a maintenance action should be taken for a specific bridge of the entire bridge system in a particular year during a time horizon. As the deterioration characteristics of PT bridges are quite different from other types of bridges, previous optimization models are not applicable to PT bridges.

1.5. RESEARCH MOTIVATION

Voids in existing PT ducts may have to be filled with grout (or repaired) to maintain some level at safety. To achieve this safety goal, voids and their locations have to first be identified. Once the voids are identified, the volume of voids needs to be determined such that the required amount of grout materials can be determined and a grouting procedure can be selected. The grout materials should have good fillability and other material characteristics to effectively fill these voids. Current grout specifications may also need to be modified to ensure good fillability. In addition, a grouting procedure needs to be developed to effectively fill the voids (if galvanic coupling is determined not to be a problem). This grouting procedure should be less expensive and time consuming than existing methods. Inspection, maintenance, and

repair programs need to be strategically scheduled such that the economic risk is minimized while ensuring safe PT bridges.

1.6. RESEARCH OBJECTIVES

The objectives of the research presented in this volume are:

- to develop feasible and approrpiate inspection procedures for PT systems;
- to identify critical material parameters affecting the performance of grouts (excluding galvanic coupling);
- to make recommendation for new specifications or modify existing specifications to improve the durability of PT systems;
- to develop and propose economically feasible repair-grouting procedures that result in good performance characteristics (this assumes that galvanic coupling does not occure at the existing–repair grout interface), and;
- to develop a repair schedule/strategy with optimum economic risk.

1.7. ORGANIZATION OF VOLUME-2

This document is organized using a section-subsection format as follows.

- Section 1 (the current section) started with a brief discussions on inspection, grout materials, grouting procedures, and economic risks of PT bridges. The research motivation and objectives were then presented.
- Section 2 provides a literature review of inspection strategies, grout material characteristics, repair procedures and economic risks of PT bridges.
- Section 3 presents the experimental program and results for void detection and damage assessment strategies
- Section 4 presents the experimental program and results from grout material characterization tests. Also, provided is the proposed modifications for the current PT grout specifications.
- Section 5 presents the experimental program and results on mitigation or repair strategies. The development of repair-grouting procedures is provided in this section.
- Section 6 presents the modeling of economic risk for PT bridges.
- Section 7 contains the conclusion from this research and recommendations for future research in this area.

2. LITERATURE REVIEW

2.1. INTRODUCTION

The corrosion of tendons has been a long-standing issue in PT structures because tendon corrosion can lead to the collapse of these bridges. In 1967, the sudden collapse of the Bickton Meadows Footbridge in the United Kingdom (UK) raised concerns about the durability of PT bridges, while the failure of Yns-y-Gwas Bridge in Wales, UK, further emphasized the severity of corrosion in PT systems (Pearson-Kirk 2003; Raiss 1995; Schokker et al. 2001a). Recently, the investigated failures of an external tendon in the Mid-Bay Bridge and a vertical loop tendon in the Sunshine Skyway Bridge called attention to the deficiencies in the inspection and maintenance methods of grouted ducts in PT structures (FDOT 2001a; Pielstick 2002). The Virginia Department of Transportation (VDOT) reported failures in external PT tendons in the Varina-Enon Bridge in 2007. As a result, they emphasized the need for an appropriate health monitoring system based on a failure analysis (Sprinkel and Napier 2008). Therefore, research in effective mitigation as well as feasible inspection of grouted ducts is required to better ensure the bridge integrity and safety.

The following sub-sections summarize previous research conducted in the area of grouting in PT systems, grout materials, inspection methods in PT structures, repair-grouting techniques in external PT systems, and economic risk assessment for PT systems.

2.2. MAJOR COMPONENTS OF PT SYSTEMS

The external PT bridge system consists of four main components, namely grout, strands, ducts, and anchorages. The following sub-sections present a review of these bridge components.

2.2.1. Grout materials

Most cementitious grouts are mixtures of cement with water (Warner 2004a). Because grouts have good flow and corrosion protection characteristics, they were used to cover strands in PT systems, fill cracks and other defects in structural concrete members, to stabilize rock and earth

masses, and other civil engineering applications. In grouted PT systems, the interstitial spaces between the ducts and the encased strands are supposed to be filled with cementitious grout. The main purpose of using cementitious grout is to protect the steel strands from external environment and potential corrosion.

Portland cement grout (a mixture of ASTM Type I cement and water) was commonly used to fill the void spaces of PT ducts. Good fluidity and economy were the main factors for using the portland cement grout. However, the use of this grout resulted in the formation of voids in PT systems. These voids were formed due to highly congested strands inside the ducts, formation of bleedwater that left voids upon evaporation, and improper grouting practices (PCI 1997; Woodward and Miller 1990).

Researchers investigated the use of mineral and chemical admixtures in developing high-performance grouts (Chaqui 2006; Hakansson et al. 1992; Hemmings and Cornelius 1991; Schokker et al. 2001b). At the same time, grout manufacturers developed various prepackaged cementitious grouts (e.g., Sikagrout 300PT®, Masterflow 816®, and Euco Cable grout PTX®). These prepackaged grouts claim to have improved volume stability, strength, and fluidity.

2.2.2. Post-tensioning strands

Post-tensioning strands that are generally used in most PT bridges are made of seven helically coiled wires (six outer wires helically coiled around one center wire) with a nominal diameter of 0.6 inches (15.24 mm). These strands meet the ASTM A416 specifications. According to PTI (1998), the minimum ultimate tensile strength (*MUTS*) of a strand is defined as the force equal to the nominal cross-sectional area of strand, or bar, times their nominal ultimate tensile stress. The *MUTS* of a 270 ksi (1860 MPa) grade, 0.6 inch (15.2 mm) diameter, seven-wire "as-received" strand meeting the ASTM A416 specifications is 58.6 kips (261 kN).

2.2.3. Post-tensioning ducts

As discussed in Volume-1 of this report, tendons are classified as internal and external systems. The duct systems for internal and external systems are different.

2.2.3.1. Ducts for internal tendons

For internal tendons, galvanized steel or high density polyethylene (HDPE) ducts are used. To ensure proper bonding with the adjacent concrete and to avoid slippage, the surfaces of these ducts are corrugated. Because galvanizing is supposed to reduce corrosion and friction losses in tendons, galvanized metal ducts were initially used in PT bridges (FHWA 2004; Ganz 2001). However, concerns about hydrogen embrittlement in PT strands were raised while using galvanized ducts; thus, corrugated, thick-walled plastic ducts were introduced in the internal PT system (FHWA 2004; Ganz 2001). Before the thick-walled plastic ducts were introduced, thin-walled corrugated polyethylene ducts were utilized between 1968 and 1974 (Della Vedova and Elsener 2006; Elsener 2004). However, the thin-walled plastic ducts were phased out due to excessive duct profile wobbling which can cause excessive friction losses while stressing. Also, the thin-walled ducts are easily damaged during stressing; grout leakage occurred frequently during grout injection (Ganz 2001). These issues led to the use of corrugated, thick-walled HDPE ducts by the early 1990s. Since then corrugated, thick-walled HDPE ducts have been used on PT bridges.

2.2.3.2. Ducts for external tendons

For external tendons, HDPE ducts with smooth surfaces are used. This is because the ducts are in contact with the box girder only at the deviator blocks and anchorages and therefore corrugated surfaces are not needed. Thick-walled HDPE pipe has been commonly used in external tendon systems. However, since HDPE ducts are not embedded in concrete they have to resist a significant pressure from the grout during injection without support from the external concrete. Thus, the European code specifies that external HDPE ducts have to be designed to resist an internal pressure of 145 psi (1 MPa) (Ganz 2001). The HDPE ducts used in the US are black in color and are opaque. This leads to difficulties in visually inspecting the quality of grouting and the presence of voids, if any, in the external tendons. Recently, transparent ducts have been used in a PT bridge in Japan to inspect grouting quality, the presence of potential voids, and corrosion (Ganz 2001).

2.2.3.3. Cross-sectional area of ducts

The total cross-sectional area of the strands in a duct should not exceed 40 to 45 percent of the inside cross-sectional area of ducts (VSL 2002). Circular ducts with smaller cross-sectional area could lead to difficulties associated with placing the strands inside the ducts (i.e., congestion) and then filling the congested areas inside the ducts with grout (Ganz 2001).

2.2.4. Anchorage blocks and diaphrams

Anchorage systems commonly consist of a concrete diaphragm, bearing plate, anchor head, and anchor wedges. Bearing plates, anchor heads, and anchor wedges are commercially available for different numbers of strands and strand diameters. These systems are suitable for 7, 12, and 19 strands. These systems are also available for strands with a nominal diameter of 0.5 and 0.6 inches (13 and 15 mm). To ensure the quality of the anchorage system, it must pass three basic tests: the static tensile test for verifying the durability of an anchorage system by post-tensioning, the load transfer test for confirming the effectiveness of a transferred load by post-tensioning, and the fatigue test for assessing the performance of an anchorage system (Ganz 2001).

2.3. INSPECTION OF PT SYSTEMS

The presence of voids in the grouted tendons in PT bridges have been identified on several bridges (ASBI 2000a; FDOT 1999; FDOT 2001a; FDOT 2001b; Hansen 2007; NCHRP 1998b). A study conducted on PT systems in Japan found that about 35 percent of PT systems contained voids (Woodward and Miller 1990). In another study, 30 percent of ducts in 1000 PT bridges in the UK contained voids while 19 percent of inspected PT bridges in the United States were found to have voids (Pearson-Kirk 2003). The inspection and detection of structural defects at an early stage could assist engineers in ensuring public safety, taking necessary actions to prevent further damage, and optimizing future inspection, maintenance, and repair costs.

In recent years, a considerable amount of research has been conducted in utilizing nondestructive testing and evaluation (NDT&E) methods to detect and locate damage and its severety in concrete structures. However, the implementation of NDT&E methods has

limitations, especially because of the noise generated during the field measurements, multiple interfaces between various elements of a structural system, and other reasons. To develop an effective NDT&E method, the following criteria should be satisfied: 1) high speed measurement, 2) ease of application, and 3) low cost. Following is a review of various NDT&E methods used in civil engineering applications.

2.3.1. Computerized tomography technique

The computerized tomography (CT) is a technique used to reconstruct images of an object projected by X-ray or Gamma (γ)-ray. This technology is used to determine several cross-sectional images of an object under projection where the intensity of the transmitting rays vary with the object's density. It has revolutionized the medical diagnostic field and is expanding fast in industrial fields (Herman 1980). The application of CT in concrete samples was performed by Martz et al. (1991). They applied the X-ray CT system to inspect voids and reinforcement bars in small concrete samples. In 1993, the authors studied the use of the γ-ray CT to perform more accurate inspections for voids and reinforcement bars in concrete specimens (Martz et al. 1993). Although CT is capable of producing detailed images of the structure, the device is expensive and requires accessibility to the concrete specimen from both sides which limits its application in the field.

2.3.2. Impact-echo technique

The impact-echo (IE) method uses mechanical impacts to generate a stress pulses in concrete. This method has been studied by several researchers (Carino and Sansalone 1990; Carino and Sansalone 1992; Pessiki and Carino 1988; Sansalone and Carino 1989) and yielded successful measurements for flaw detection. Because the impact generates a high energy pulse and can penetrate deep into the concrete, the IE method is particularly promising. Moreover, it produces a better signal-to-noise ratio than other ultrasonic techniques because of its low attenuation in composite materials such as concrete (Karaoğuz et al. 1998). Carino and Sansalone (1992) applied the IE method to detect simulated voids in grouted post-tensioning ducts which were located in a 3.3-ft (1-m) thick concrete wall specimen. Although the IE method can detect small voids, it is difficult to produce an image of the structure as well as it is difficult

to apply directly in small grouted ducts such as external tendons. Moreover, the IE method is rather time intensive for inspection of large specimens. To resolve this limitation a movable IE scanner system was developed by Tinkey et al. (2005). The scanning system was applied to internal ducts. However, it was difficult to detect voids when the concrete cover was thicker than the diameter of the embedded ducts. Also, the IE scanner system is incapable of identifying voids when the ducts are partially filled with water (Tinkey et al. 2005). The authors concluded that a scanning system could not detect voids well when the diameter of the ducts was small and the concrete covers were large.

2.3.3. Magnetic flux leakage technique

The magnetic flux leakage (MFL) technique is a promising technique in the NDT&E field because it is capable of detecting corrosion in embedded steels or metallic materials. This technique employs the use of magnetic field sensors called superconducting quantum interference devices (SQUIDs). These sensors are relatively sensitive and have a large dynamic range for inspection. Krause et al. (2001) studied the inspection of ruptured tendons in pre-stressed concrete structures using a SQUID system. It was reported that the MFL method was applied successfully to the detection of corrosion in external polymer ducts (Tilly 2002). Although the MFL technique is effective in detecting corrosion in metallic materials, it cannot evaluate other discontinuities such as voids and cracks. To prevent tendons from corroding, it is necessary to identify the existence of voids before severe corrosion in tendons occurs.

2.3.4. Ultrasonic technique

Ultrasonics is defined as the study dealing with sound, having a frequency of 18 kHz and higher (Blitz and Simpson 1996). The ultrasonic technique can be used in concrete structures to identify concrete thickness (Krause et al. 1995), elastic modulus, and detecting flaws such as cracks, voids, etc. (Schickert 1995). Martin et al. (2001) performed tests on 1.6-inch (40-mm) grouted duct specimens with simulated voids by measuring the time-of-flight of transmitted pulses. These tests required the use of several receivers in a grid pattern on the surface of specimens. Although this technique depicted successful results for detecting voids in PT concrete beams, it is relatively time-consuming and costly because of the large number of transducers

required. Iyer et al. (2003; 2005) evaluated the ultrasonic C-scan imaging system to verify the detection of corrosion and voids in specimens. The specimens were grouted in square PVC ducts with one strand in the center. They identified two different levels of corrosion and voids in specimens using the C-scan.

In general, ultrasonic testing systems can be classified into three types: ultrasonic pulse echo (UPE) method, ultrasonic pulse velocity (UPV) method, and pitch catch method (Kundu 2000). The UPE method employs a single transducer that generates pulses and measures reflected pulses. This method consists of having a transducer on the surface of a specimen that transmits ultrasonic pulses. The emitted pulses are then reflected from layers or discontinuities in the concrete such as cracks and voids. The reflected pulse waves are then recorded at the transducer on the surface for further processing. The UPE transducer is moved over the entire surface of the specimen in small increments to monitor the inside condition continuously. In the UPV method, two transducers are utilized: one for excitation and the other for detection. Usually, these transducers are located on opposite sides of a specimen to measure signals directly. Alternatively, for the pitch catch method, the transducers are on the same side of the specimen. In these three methods, contact transducers are normally used, so a couplant, such as water, is needed between the transducers and the surface of the specimen.

Although the application of ultrasonic techniques is limited in real structures, they can be promising if limitations can be resolved. Alternatives have been studied that involve non-contact ultrasonic systems such as air-coupled ultrasound (Martínez et al. 2003; Mendelsohn and Wiener-Avnear 2002), or laser ultrasound (Kil et al. 1998; Scruby and Drain 1990). Air-coupled ultrasound works typically in the frequency range of 50 to 100 kHz for application in concrete structures; however, it has the disadvantage of low signal amplitudes due to the impedance mismatch between the interfaces (transducer-air-specimen). However, Blum (2003) studied the increased signal amplitude using several combined air-coupled ultrasonic transducers into an array for generation of ultrasound. Laser ultrasonics may be used for the generation and detection of elastic waves. These laser techniques provide numerous benefits over conventional piezoelectric techniques (Hurlebaus et al. 1998). Since optical techniques are non-contact techniques, they do not cause any errors associated with couplant thickness and/or applied pressure, which are present when contact piezoelectric transducers are used. Couplant on the

specimen surface can cause small changes in observed arrival times of surface acoustic waves. These small errors can become critical when the measured velocities are used for the calculation for the localization of discontinuities. Another benefit of optical methods is that they are point techniques, which may be used on any specimen regardless of size or geometry. A laser source provides the benefit of being broadband, that is, the resulting signal has components over a wide frequency bandwidth. Finally, using laser detection has the benefit of making absolute measurements with high fidelity (resonance free). However, laser ultrasonics are expensive and application in the field is difficult due to laser safety requirements.

2.3.5. Sounding technique

For the inspection of external PT ducts, the sounding inspection is generally performed to identify the existence of voids in ducts (FDOT 2001a). Although the sounding inspection might contain errors, it is easy to execute in the field and is a very rapid method for detecting voids in ducts. In addition, an inspection using a borescope can be utilized near the location having an "irregular sounding" in order to inspect voids and corrosion directly (FDOT 2001a). A borescope consists of flexible optic fibers with a small eyepiece (the diameter is less than 0.16 inches (4 mm)) at one end. This equipment has been used mainly in the field of medicine and inspection for small equipment. Although void inspections using a borescope requires access holes, it can give a clear and concise image of hidden areas within ducts.

2.3.6. Summary

Most non-destructive inspection techniques detect structural defects using the propagation of elastic waves. However, the shrinkage of Class A grout causes problems for typical damage detection. The shrinkage of cement material creates a gap between the interface of the grout and the duct, and as a consequence does not transmit elastic waves. This shrinkage separation does not increase the risk of corrosion, as does a grout void; however, it does increase the errors associated with void detection. Therefore, further research is required to reduce the negative effects of the shrinkage gap in ducts.

2.4. GROUT MATERIAL CHARACTERISTICS

2.4.1. Grout fresh characteristics

This section includes a discussion on the fresh characteristics of grout that can impact the durability of PT structures. The fresh grout characteristics that were considered in this research are presented in the following sections.

2.4.1.1. Bleed

Powers (1939) defined bleeding of a cement paste or mortar as the sedimentation of the suspended cement or sand particles. In other words, the individual cement or sand particles settle in the solution under the influence of gravity leaving the excess water on the top when the cement paste or mortar is at rest. Grout bleeding occurs in layers in which the upper layer of cement paste or mortar has higher water-cement ratio (w/c) as compared to the lower layers. This results in weak, porous, and less durable paste at the upper surfaces. ASTM C940, Standard Test Method for Expansion and Bleeding of Freshly Mixed Grouts for Preplaced-Aggregate Concrete in the Laboratory, is the standard specification to evaluate the bleed of cement grouts.

A typical bleed test in a vertical channel is shown in Figure 2-1. The cylinder at the left contains freshly mixed grout. With time, settlement of cement particles takes place leaving excess water on the top. This is shown in the cylinder on the right. The grout level decreases with time in actual structures in a manner somewhat similar to the one shown in Figure 2-1.

Research conducted to study the effect of strands on grout bleed indicates that bleeding of grout in ducts for post-tensioning is largely influenced by the interstices between the king wire and the perimeter wires that act as capillary tubes (PTI 2003b; Schupack 2004). This bleed water results in the formation of air voids in the PT ducts after the water evaporates or is reabsorbed into the grout (Earley 2004). A wick-induced bleed test (Modified ASTM C940) is used to measure the bleeding in grouts when PT strands are present. The bleed water can be greatly reduced through good dispersion of the solids with high shear mixing. Non-bleeding properties

of grouts can also be achieved by the addition of anti-bleeding admixtures to the cement grout (Schokker et al. 2001b).

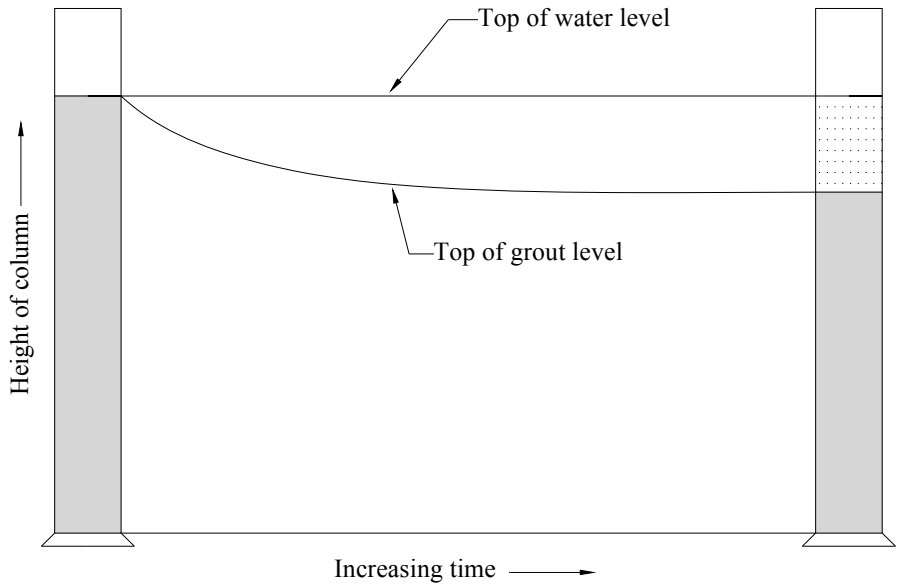

Figure 2-1. Illustration of a typical bleed process in graduated cylinder (ASTM C940).

An investigation of the corrosion of in-place tendons on demolished bridges in California concluded that corrosion of strands was significant at major void locations (Schupack 2004). Schupack (2004) noticed that the void formation was mainly due to the bleeding of grout. He designed the "Schupack pressure bleed test" which was included in the PTI Guide Specification for Grouting of Post-Tensioned Structures (PTI 2001) as a grouting standard in 2001. This test is very useful in predicting the bleed resistance of a particular grout mixture. The recommended maximum allowable bleed for pre-packaged Class C grouts as given by Schokker et al. (2002) for a maximum tendon elevation change between 6 ft (1.8 m) and 100 ft (30.5 m) is zero percent bleed at air pressure of 50 psi (0.34 MPa).

Grout bleeding is an important parameter and needs to be measured for each grout mixture. Grout bleeding results in formation of voids in the PT ducts. Strands can be exposed to aggressive external environments due to formation of the voids and corrosion of these strands

can occur. This void formation may, sometimes, reduce the effective grout cover on the strands which in turn reduces the time to initiation of corrosion of strands. The Schupack pressure bleed test should be performed if the maximum difference in elevation of longitudinal tendons is 6 ft (1.8 m) or for vertical tendons with heights of 20 ft (6.1 m) and more (PTI 2003).

2.4.1.2. Viscosity

Viscosity of a fluid is defined as a measure of the fluid's resistance to flow. A fluid can be "thick" or "thin" based on its ability to flow under a constant applied stress. Water and alcohols are some examples of thin fluids whereas oil and gels are thick fluids. Viscosity is defined by considering laminar shear of fluid between two parallel plates (Figure 2-2). It is postulated that for uniform flow of fluids between parallel plates the shear stress between the layers is proportional to the velocity gradient (Ritchie 1965). To express this, the following equation is used:

$$\tau = \eta\left(\frac{dv}{dx}\right) \tag{2.1}$$

where τ is the shear stress, η is coefficient of viscosity, and $\frac{dv}{dx}$ is velocity gradient.

Fluids are categorized into two types based on their flow behavior. These are Newtonian and Non-Newtonian fluids. Water is a Newtonian fluid in which the stress is directly proportional to the rate of strain. Figure 2-3 shows the shear stress behavior of Newtonian fluids. The slope of the shear stress-shear rate curve in Figure 2-3 represents the viscosity (η) of fluids. A typical relationship between the shear stress (τ), and shear rate (γ) is shown by Equation 2.2:

$$\tau = \eta\,\gamma \tag{2.2}$$

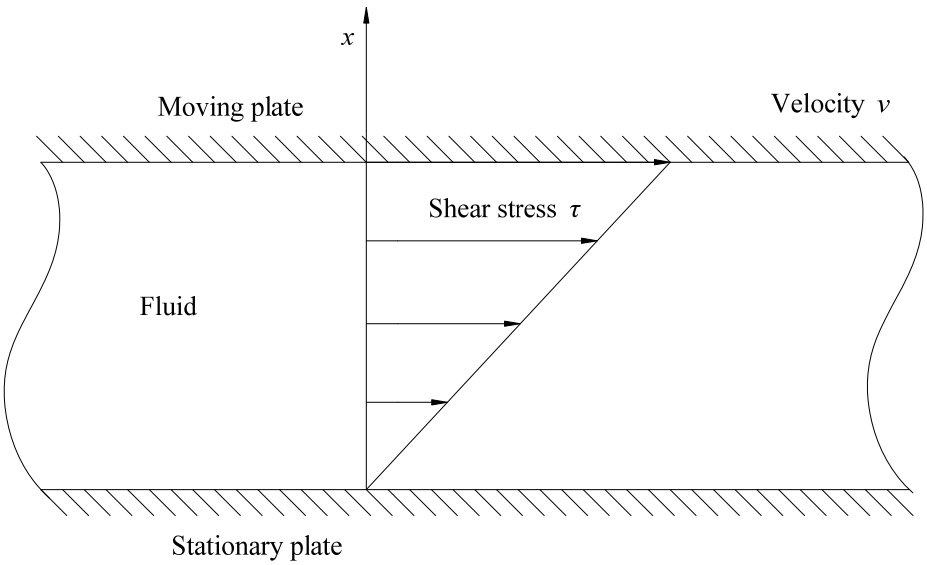

Figure 2-2. Laminar shear of fluid between two plates.

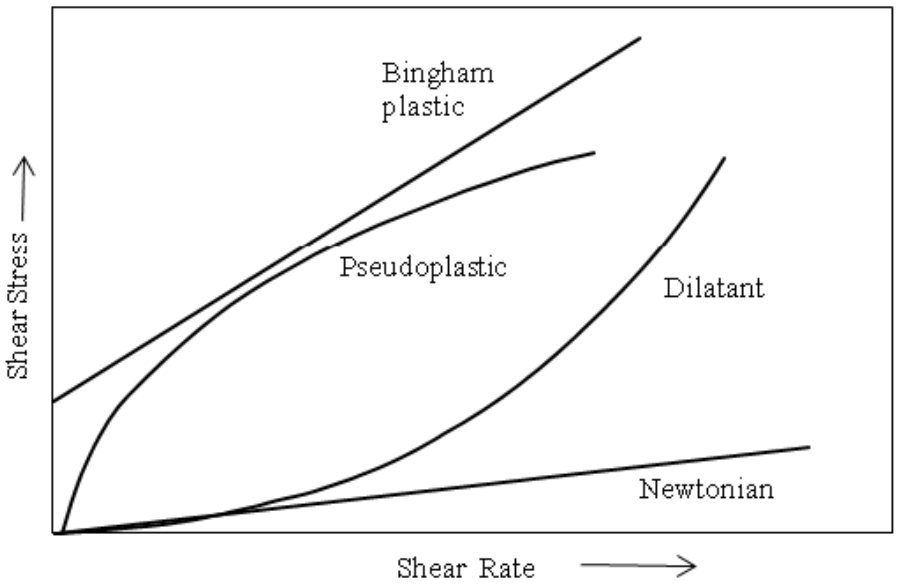

Figure 2-3. Newtonian and non-newtonian flow behavior.

A non-Newtonian fluid, on the other hand, exhibits a non-linear behavior. Non-Newtonian fluids are categorized by behavior type which is based on the fluid's change in

viscosity in response to variations in shear rate. The three main types of flow behavior are: Bingham plastic, dilatant, and pseudoplastic (Ferraris 1999). Bingham fluids behave as a solid under static conditions and need a certain amount of stress, also known as "yield stress," to induce the flow. This type of behavior is shown in Equation (2.3) represents the Bingham model:

$$\tau = \tau_0 + \eta\gamma \tag{2.3}$$

where τ is shear stress, τ_0 is the yield stress, η is the viscosity and γ is the shear rate (Ferraris 1999). Dilatant fluids, as shown in Figure 2-3, are those in which the viscosity increases as the shear rate increases. Pseudoplastic fluids, on the other hand, exhibit a decrease in viscosity with the increase in shear rate.

Some fluids also exhibit change in viscosity with time under the influence of constant shear rate. Viscosity of Newtonian fluids does not change with time. Non-Newtonian fluids, on the other hand, exhibit a change in viscosity with time. Hence viscosity of these fluids is referred to as dynamic viscosity. Based on the nature of the change in viscosity, fluids are sub-divided into two categories: thixotropic and rheopectic (Ritchie 1965). Viscosity of the thixotropic fluids decreases with time when stress is applied. A rheopectic fluid's viscosity increases with time as the stress is applied (Ferraris 1999).

Most cement grouts exhibit a non-Newtonian flow behavior as they require a certain magnitude of yield stress or cohesion to make them flowable. These cementitious grouts can be categorized into pseudoplastic fluids as their viscosity reduces as the shear stress is increased. Because they require a positive stress of some magnitude to initiate movement they are also considered as thixotropic pseudoplastic fluids.

Hakansson et al. (1992) studied the rheology of cementitious grouts. The authors suggested that an increase in fineness increases the yield stress and the viscosity. The authors also noted that the rheological properties of a grout are affected by the paste water to

cementitious materials ratio[1] (w/cm), fineness of the cement particles, the type of cement, mixing time, and cement hydration. Mixing time also plays a major role. Temperature and pressure also have an effect on viscosity. When temperature and pressure increases, viscosity decreases (Warner 2004). Hence, the mixing should be consistent in order to obtain reproducible properties.

Because the rheological properties of a grout are influenced by various factors it is important to measure viscosity characteristics of grouts in order to evaluate their flow properties. Because this test requires a comprehensive test procedure and an expensive setup, it is not advisable to perform this test in the field. Rather, a relationship between the viscosity and fluidity characteristics of grout can be determined by testing agencies or manufacturers as needed. Tests have been performed in this study to evaluate both the viscosity and fluidity characteristics and to study whether a correlation exists between the two.

2.4.1.3. Fluidity

A fluid is a substance that continually changes its shape when stress is applied. Fluids are categorized into two types based on their flow properties as discussed in section 2.4.1.2. Newtonian fluids are the fluids in which the stress is directly proportional to the strain rate. Non-Newtonian fluids show non-linear behavior of shear stress to the strain rate and have higher viscosities due to which a positive pressure is required to pump such fluids through a duct (Warner 2004).

Grout fluidity is a measure of how fluid the grout mixture is and is a measure of the flowability of the grout. It is inversely proportional to the viscosity of a grout. This grout property is considered important as compared to other characteristics because it affects the fillability of the tendon (VSL 2002). The rheological behavior of all cementitious grouts is dominated by several physical and chemical factors such as w/cm, particle size distribution, fineness, addition and type of supplementary cementitious materials, and chemical admixtures.

[1] w/cm is the ratio of the weight of water to the weight of cement and other supplementary cementitious materials.

Portland cement grout was extensively used in the construction of PT structures with the main objective of filling the voids. Pore spaces in PT ducts are typically small due to the presence of strands and low viscosity grouts are necessary. To achieve the desired flow that could fill void spaces in the PT ducts, the w/c was often adjusted to meet fluidity requirements. However, other characteristics are affected, mainly volume stability.

Challenges with grouting PT ducts due to the volume stability of grouts led researchers to develop grouts with better dimensional stability without the loss of fluidity. Various high-performance grouts were developed using ASTM Type I and III cements along with supplementary cementitious materials (SCM), water reducing admixtures, superplasticizers, and aluminum powders (Chaqui 2006; Hope and Ip 1988; Schokker et al. 2001b). These grouts have been reported to perform better in terms of their fluidity and dimensional stability when compared with traditional portland cement grouts.

Increasing demand of high-performance grouts in PT applications led various organizations to develop pre-packaged PT grouts. These pre-packaged PT grouts eased the on-site grout mixing requirements and are believed to contain one or more chemical and mineral admixtures. These grouts typically exhibit thixotropic, pseudoplastic flow behavior (Yahia and Khayat 2003), and the conventional method of evaluating their flow properties (ASTM C939: Standard Test Method for Flow of Grout for Preplaced-Aggregate Concrete (Flow Cone Method)) does not address this true flow behavior.

TxDOT issued specifications for measuring efflux time of thixotropic grouts (Tex-437-A). This TxDOT standard is also known as the modified ASTM C939 test procedure to measure the efflux time of thixotropic grouts and is also contained in the PTI grout specification manual (2003b). According to the Method 2 of Tex-437-A standard specification, the flow cone is filled with freshly mixed grout up to the top and the time it takes to flow the initial 2.11 pints (1000 ml) grout from the ½-inch (12.7 mm) orifice is measured as the grout's efflux time.

Because most prepackaged grouts are thixotropic grouts, the Method 2 of Tex-437-A standard can evaluate the fluidity characteristic of the grout more accurately. Also, it is a simple test procedure and can be conducted in the field for each batch of mixture. Therefore, this standard may be applicable to evaluate the efflux time of grout mixtures in the field.

2.4.1.4. Wet density

Quality control of freshly prepared grouts is essential to ensure proper filling of PT ducts. An increase in the water content of the grout can initiate bleed, which can led to formation of voids in the PT ducts. The American Petroleum Institute (API) provides Specification RP 13B-1, Recommended Practice Standard Procedure for Field Testing Water-Based Drilling Fluids to measure specific gravity of grouts. Also referred to as the Baroid Mud Balance test, this test is used to measure the specific gravity of drilling fluids. Although this test procedure is used to measure the density of grouting fluids for drilling purposes, it can also be used as a good quality control device to provide information on the water-powder ratio[2] (w/p) of the mixture in the field prior to placement in the duct.

The Baroid Mud Balance provides a measure of the consistency of the grout produced in the field (Clark and Ganz 2002). A comparison of the wet density of the freshly mixed grouts at the inlet (mixer) and outlet (grout vent) of the grout pump is a means of verifying the quality of field produced grout. Ideally, the density of the grout at the outlet should never be less than the density at the inlet of grout pump. Similar densities ensure no sedimentation of the grout. According to the Federal Highway Administration's Post-Tensioning Tendon Installation and Grouting Manual, the consistency and density of field produced, pre-packaged, thixotropic grouts can be checked by measuring the grout density at both the mixer and grout vent (FHWA 2004).

2.4.1.5. Fillability

Many tests are available to evaluate the fresh characteristics of PT grouts. These tests include efflux time, bleed, viscosity, and wet density. However, there are no established standard specifications that can estimate to what extent a freshly prepared PT grout can fill voids in PT ducts. Tests such as the bleed test (or wick-induced bleed test) only attempt to explain whether the grout to be used in PT applications will result in void formation. The flow cone test provides

[2] w/p is the ratio of weight of water to the weight of all cementing materials including non-cementing powders. It is different from w/cm as other than the cementitious materials, this powder may contain fine aggregates which are unknown as the PT grout materials are proprietary.

a measure of the fluidity, not fillability. Note that a concrete mixture with a ½-inch (12.7 mm) maximum size aggregate can exhibit high fluidity but would not fill the voids in a PT duct. No test method or standard is currently available to assess the fillability of grouts through small pore size openings such as that found in PT ducts.

Various studies have been conducted on grouts for purposes of injecting them in joints or cracks of rock strata for geotechnical purposes. Researchers have shown that these grouts cannot pass through a specific aperture and put limits on the minimum aperture through which the grout can be injected (Amadei 2000; Moon and Song 1997). Eriksson et al. (2000) have shown that this aperture size varies for various grouts and an evaluation of the minimum aperture of each grout is necessary to find out the penetrability of that particular grout.

Eriksson and Stille (2003) developed a test method to measure and evaluate the penetrability of cement based grouts. The test method includes a penetrability meter that gives parameters for making grouting penetration predictions. The parameters obtained from the penetrability meter test are the minimum and critical aperture of the grout. The authors defined the minimum aperture as the aperture through which no grout can pass and the critical aperture as the opening through which an infinite volume of grout can flow. Because the particle size and other characteristics of various grouts differ due to their different production methods, the minimum and critical aperture limits differ significantly with the type of grout.

In this study, a fillability test setup was developed. This setup is similar to the penetrability meter developed by Eriksson and Stille (2003). The objective behind using this fillability meter is to differentiate and/or assess various pre-packaged PT grouts in terms of their performance to fill small voids in PT systems. The fillability meter design and test procedure is discussed in the next section.

2.4.2. Grout hardened characteristics

This section includes a discussion on the hardened characteristics of grout that can impact the durability of PT structures. The hardened characteristics that were considered in this research are presented in the following subsections.

2.4.2.1. Compressive strength

A normal portland cement grout (ASTM Type I cement and water) was used in most PT bridges constructed in the Texas until approximately 2000. Grout bleeding and void formation was found to be the main cause of corrosion of PT strands in most of these PT bridges. A careful evaluation of the grouts' fresh properties (bleed and fluidity) would provide valuable information for determining proper grouting requirement and materials for successful future post-tensioning. Compressive strength, on the other hand, does not provide a direct measurement of a grout's ability to fill the voids in PT ducts. Instead, this property is considered to provide an indication of the grout quality with respect to its bond and shear strength, and possibly an indication of its durability.

2.4.2.2. Dimensional stability

Various physical factors such as surrounding temperature, humidity, and chemical factors such as carbonation shrinkage, sulfate attack, and alkali-aggregate reactions affect the dimensional stability of the hardened grout specimens (Kosmatka et al. 2002). Hence, it is important to measure the effect of these physical and chemical factors on the volume stability of the cementitious grouts.

Shrinkage of cement grouts in PT structures is an important durability issue. This volume change of the grout can result in formation of voids in PT ducts. Drying shrinkage in portland cement grout is affected by its water content. As the water content is lowered, drying shrinkage is reduced, but the flow properties are also affected (grout become less fluid as the water content is lowered). Studies have shown that the addition of SCMs such as fly ash also reduces the drying shrinkage and increases the flow. Chemical admixtures, on the other hand, have been reported to have little or no effect on the drying shrinkage of cement paste (Kosmatka et al. 2002).

Grout cracking in the PT ducts is another important parameter that needs to be assessed. If cracks develop in the hardened grout, the PT strands can be exposed to the external environment and corrosion can initiate. Cracking in the hardened grout can be either temperature cracking or drying shrinkage or due to external agents such as sulfate attack. Changes in the

relative humidity and temperature can cause grout cracking if the hardened grout is directly exposed to the environment which may be the case with cracked ducts. Cracking due to the drying shrinkage can be controlled by controlling the curing process after placement. Cracking due to sulfate attack can be controlled by selecting suitable cement and admixtures (Mindess et al. 2003).

Various pre-packaged, high-performance grouts that have been developed for post tensioning applications are believed to be non-shrinking grouts. A careful evaluation of the volume change of these grouts is required to improve the durability of PT structures.

2.4.3. Grout durability characteristics

This section includes a discussion on characteristics that can impact the durability of PT structures. The durability characteristics that were considered in this research are presented in the following sections.

2.4.3.1. Chloride diffusivity

In PT bridges, corrosion of strands can be a serious problem as corrosion can reduce a bridge's performance and safety. Strand corrosion in PT structures has been identified as being mainly due to the use of poor grouting practices and materials. Generally, the PT ducts are filled with cementitious grout to prevent the strands from being exposed to aggressive corrosive agents. But due to the use of dimensionally unstable grout and poor grouting practices, ducts may not be filled fully, resulting in voids and exposure of strands to these aggressive environments. Moreover, the use of precast elements and inadequate detailing of joints and drainage in modern bridges can make them more susceptible to corrosion (Gallagher 1989; Goodwin 2002). Woodward (1980) investigated 12 bridges in the UK and found voids in the ducts of 10 bridges.

In many cases, strand corrosion is initiated by the presence of water and chlorides near the strands. Chlorides can penetrate through the grout. This ingress of chlorides through uncracked grout is diffusion controlled and depends on the apparent chloride diffusion coefficient, D_a. The chlorides diffuse from a place of higher concentration to a place of lower concentration. This is described by Fick's Second Law (Mindess et al. 2003):

$$\frac{\partial C}{\partial t} = D_a \frac{\partial^2 C}{\partial x^2} \tag{2.4}$$

where, C = chloride concentration [mass %], t = exposure time [seconds], D_a = diffusion coefficient [inch^2/seconds (m^2/seconds)], and x = depth below the exposed surface [inch (m)].

The chloride concentration at any depth and any time can be obtained by solving this differential equation. ASTM C1556-03, Standard Test Method for Determining the Apparent Chloride Diffusion Coefficient of Cementitious Mixtures by Bulk Diffusion, (ASTM C1556-03) provides a test procedure to determine the diffusion coefficient of a cementitious material. The chloride ion concentration at any depth x and time t, $C(x,t)$ as explained in ASTM C 1556-03 is given by the Equation (2.5):

$$C(x,t) = C_s - (C_s - C_i) \times erf\left(\frac{x}{\sqrt{4D_a t}}\right) \tag{2.5}$$

where, C_s = chloride ion concentration at the surface of a concrete specimen [mass %], C_i = initial chloride-ion concentration of the specimen [mass %], and erf = error function described in Equation (2.6):

$$erf(z) = \frac{2}{\sqrt{\pi}} \times \int_0^z \exp(-u^2)du \tag{2.6}$$

where z refers to the expression $\frac{x}{\sqrt{4D_a t}}$ and u is a regression variable. The value of this error function corresponding to the specific depth x and time t can be obtained from standard mathematical reference books (Beyer 1978).

It should be noted that the rate of transport of chlorides in a round duct will be different than that shown in Equation (2.5). Diffusion in a round duct is two-dimensional (Equation (2.5) is for one-dimensional flow) and is given by Equation (2.7) (Poulsen and Mejlbro 2006):

$$\frac{1}{D_a}\frac{\partial C}{\partial t} = \frac{\partial^2 C}{\partial x^2} + \frac{\partial^2 C}{\partial y^2} \tag{2.7}$$

Because the current ASTM standard (ASTM C 1556) to measure chloride diffusivity of concrete specimens assumes one-dimensional rate of transport of chlorides, the one-dimensional flow rate is assumed to evaluate diffusivity of PT grouts.

Because grouts provide a protective cover to the strands, the resistance of these grouts to the transport of chlorides is critical. Because of this, diffusion rates will be determined for grouts assessed in this study. It should be noted that diffusivity measurements are relatively time consuming and it is anticipated that this testing will not be required for all grout placements.

2.4.3.2. pH

In PT bridges, the strands are surrounded by grout, which is supposed to protect the strands from being exposed to aggressive agents. In a normal PT duct, the embedded strand is covered by the grout. The pore spaces in the paste contain a highly alkaline solution (with a pH higher than 12), which inhibits the corrosion of the strands by creating a passive environment for the strands (Locke 1986).

Hence, there is a need to determine the pH of the pore solution of grouts because lower pH values increase the chance of corrosion of PT strands. Because there are no ASTM standards available to test the pH of the pore solution it is difficult to measure. In this research, the pH of the pore solution was assessed using the method explained by Barneyback and Diamond (1981) and is discussed later.

2.5. REPAIR-GROUTING METHODS

2.5.1. General recommendations for grouting

Extensive research has been done in the area of improving grout materials, grouting procedures, grout protection, and grout placement training (ASBI 2000b; Hope and Ip 1988; Pearson-Kirk 2003; Pielstick 2002; Raiss 1995; Schokker et al. 2001b; Smith and Wood 2001; Woodward and Miller 1990). Woodward and Miller (1990) suggested the use of suitable admixtures for good grout properties. They also emphasized the use of high performance grout materials, grouting equipment, and appropriate locations for grout vents. The authors also mentioned the necessity of having trained experts for initial-grouting and repair-grouting in order to reduce the formation of large voids. Raiss (1995) summarized appropriate tests for each construction step for effective management of PT structures. The author explained the details of a grout protection system that prevents the ingress of detrimental materials inducing corrosion. He also mentioned the importance of developing high performance grouts and effective grout procedures. Smith and Wood (2001) stressed the necessity for trial-grouting and provided practical feedback for grouting operations to improve performance in the field. Pearson-Kirk (2003) studied the previous investigation of PT bridges and concluded that the local voids were not critical to strand corrosion. He noted that the main cause of strand corrosion was the ingress of water or deleterious chemical agents from damaged ducts. He focused on the improvement of grout materials, grouting procedures, and grout protections. The American Segmental Bridge Institute (ASBI 2000b) provided statements about proper grouting requirements, and they mentioned the need for a training program for practical grouting. In addition, a significant amount of research has been performed on improving grout materials. These studies were performed and tested to reduce grout bleeding using various admixtures (Hope and Ip 1988; Qian et al. 2004; Schokker et al. 2001b).

2.5.2. Pressure grouting method

The PG method was initially used to fill the grouts in PT systems, especially initial-grouting. In the PG method, the grout is injected into the tendon with the aid of external pressure, typically using a pressure pump. This method does not require the duct system to be air-tight. In fact,

relief valves or air outlets typically have to be installed to avoid bursting of ducts and to improve grouting. This method requires less preparation work and is cost-effective. However, further research is needed to evaluate (1) the effectiveness, (2) the performance, and (3) the economic feasibility of this method to fill the voids.

2.5.3. Vacuum grouting method

While a lot of research has been carried out on the initial-grouting of PT systems, significantly less research has been done on the repair-grouting (i.e., repair of voids). Raiss (1995) recommended the vacuum grouting (VG) method for repair. However, he mentioned that it could be ineffective when the ducts are not in an air-tight condition. Moreover, most studies recommend the VG method for filling large voids in ducts (FDOT 2001a; FHWA 2004; Pielstick 2002; Shoji et al. 2003; VSL 2002). Shoji et al. (2003) reported the use of the water-jet method for safe drilling and application of VG method. The Federal Highway Administration (FHWA) recommended the application of VG method (FHWA 2004). A report by VSL (2002) described the repair-grouting by using the VG method, where the vacuum pump can be used to reduce pressure in the duct by 80 percent. Figure 2-4 shows the vacuum control and grouting equipment developed by VSL International Ltd.

Figure 2-4. Vacuum Control and Grouting Equipment for Voided Tendons (VSL 2002).

If the duct system in not completely air-tight, the air from outside might leak into the duct system, and the remaining vacuum pressure might not be sufficient to aid the grouting process. The Constellation Group LLC developed an equipment to detect the drop in vacuum pressure and measure the void volume. This equipment can help the engineer in to verify if the vacuum pressure has been built and estimate the amount of grout needed, prior to grouting.

Table 2-1. Leak Detection and Void Measuring Equipment (CGLLC 2009).

2.5.4. Comparison of vacuum and pressure grouting procedures

FDOT studied the performance of the VG and PG methods. In this study (FDOT 2001a), prototype, horizontal tendon specimens (see Figure 2-5 and Figure 2-6) were grouted using VG and PG methods and the effectiveness in filling the voids were evaluated. Figure 2-7 shows the cross-section of tendons repaired using PG and VG methods. Figure 2-7(a) shows that the PG method did not completely fill the voids. Figure 2-7(b) shows that the VG method completely filled the voids in tendons. Based on this finding, FDOT recommended VG method over PG method to fill the voids in PT bridges in Florida.

However, it should be noted that the PG method could not fill the voids because of the potential back-pressure that could have developed and prevented the in-flow of grout. This back-pressure might have been developed because the single grout port in each specimen (indicated by the horizontal arrow in Figure 2-5) was located on the anchor plate and there were no grout outlets or vents (Figure 2-6) elsewhere on the test setup. These outlets or vents are necessary to completely fill the voids using PG method. Therefore, the PG method need to be re-evaluated by performing grouting tests on prototype tendon specimens with air outlets.

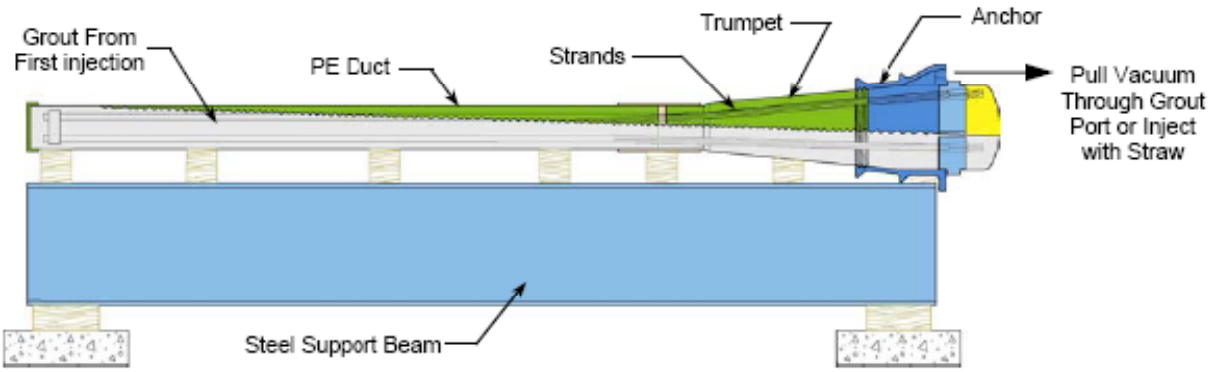

Figure 2-5. Schematic of the Prototype Tendon Specimen used in FDOT study to Compare the Performance of Vacuum and Pressure Grouting methods (FDOT 2001a).

(a) (b)

Figure 2-6. Grouting tests conducted by FDOT: (a) Pressure grouting and (b) Vacuum grouting methods (FDOT 2001).

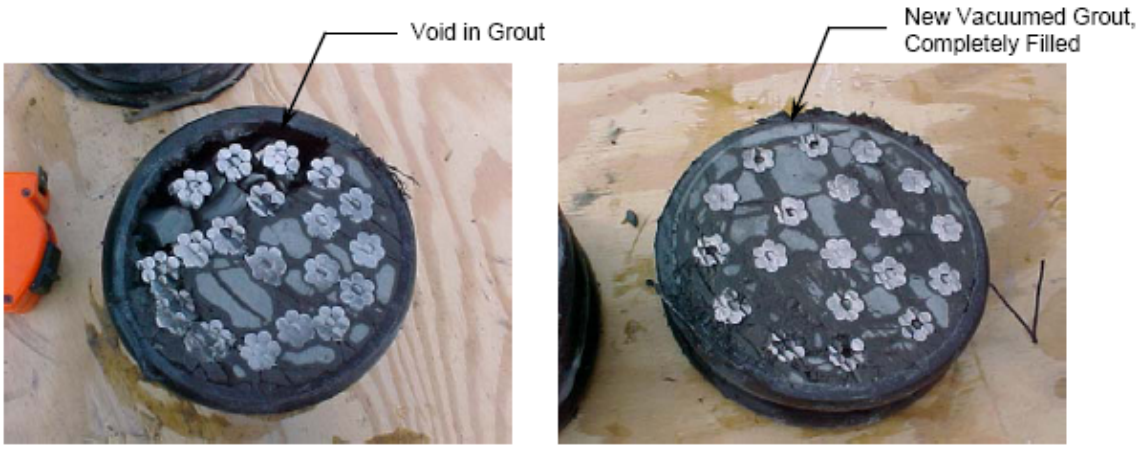

Figure 2-7. Mock-up Test Sections after Repair: Pressure Injection (a) and Vacuum Injection (b) (FDOT 2001).

Although the VG method is effective for filling voids, it is time-consuming and costly. To perform the VG method, a vacuum system is connected to the duct and the pressure in the ducts is reduced. Once the pressure stabilizes, the vacuum pump is closed off from the system and fresh grout is allowed to flow into the duct, filling the voids. This method is effective for filling voids; however it is difficult to form an air-tight tendon such that a constant vacuum pressure can be maintained inside the tendon. Significant preparation time is required to make the tendons air-tight. This process often takes weeks or even months making the VG method practically unfeasible and economically less viable.

A new repair-grouting method that utilizes the advantages of both VG and PG methods needs to be developed. Such a method is developed in Subsection 5.1.4.3.

2.6. ECONOMIC RISK MODELING

This section provides a review of literature on different bridge management approaches, popular software packages, and deterioration and reliability models of structural systems.

2.6.1. Bridge management approaches

Adey et al. (2003) compared a Supply and Demand System (SDS) approach proposed by Adey (2002) with two existing bridge management systems (BMSs), the Supply Bridge (SB) approach and the Supply and Demand Bridge (SDB) approach. In the SDS approach, an optimal management strategy is to maintain a system of bridges at an adequate level of service while minimizing the expected additional costs or penalties if the level of service is not adequate. The authors pointed out the inability of SB and SDB to find optimal management strategies when the performance of a system of multiple bridges is simultaneously affected adversely by natural hazards such as hurricanes, floods, and earthquakes. The SB approach was supposed to be based only on the condition of a bridge without considering user demands, and it is currently used in BMSs, including the Pontis and BRIDGIT. Application of these two software packages is discussed in the next paragraph. The objective of using the SB approach was to minimize the total probability of inadequate performance of every bridge in a system. The objective of using the SDB approach was to minimize the total expected additional costs in case a system of bridges does not provide an adequate service level. In their study, assumptions about the probability of inadequate performance were made for comparison of the three approaches (SDS, SB, and SDB), and the deterioration model used is not stated. One of the important conclusions is that repair of a bridge with the highest probability of inadequate service in a bridge system does not necessarily produce the maximum benefits.

2.6.2. Software packages for bridge management

Pontis and BRIDGIT are software packages and have been widely used by transportation agencies for bridge management. Inspection and inventory data of bridges including condition of structural elements of a bridge can be updated and stored in Pontis based on the coding guidelines of the National Bridge Inventory System (Thompson et al. 2003). Using a Markovian Decision Process (Hu and Yue 2008), Pontis assists in the prediction of future condition of a bridge and suggests an optimal preservation of the bridge with maximum benefits given a specified or constrained budget. BRIDGIT aids decision-makers in the optimal allocation of constrained resources to a system or network of bridges in order to obtain the greatest benefits from preservation of the system (Hawk and Small 1998). Robert et al. (2003) presented how the

US transportation agencies make use of Pontis to produce an optimal preservation policy for their bridges. Pontis is used not only in the transportation departments of 39 states and territories of the nation, including the State of Texas, but also in other countries. Pontis can be customized so that stored inspection data and structural element models can be used to predict deterioration of bridges at both network and individual bridge levels. Robert et al. (2003) identified that transportation agencies could supplement or replace a set of commonly recognized (CoRe) elements in Pontis; however, this customization was unacceptable to Federal Highway Administration and was discouraged by the American Association of State Highway and Transportation Officials (AASHTO). It was concluded that it has been difficult to use Pontis effectively and to find information for supporting network-level decision-making (Thompson et al. 2003) despite the advantages of this software package.

2.6.3. Deterioration and reliability models for structural systems

It is important to analyze the entire structural system of a bridge as well as its structural components such as abutments, decks, and bents so that the performance or reliability level of each structural component of a bridge and the bridge itself in a network can be predicted. Structural performance effects of maintenance expenditures for individual bridges and can be evaluated correctly for cost-effectiveness assessment (Yanev et al. 2003). Accuracy of a mathematical model of a bridge structure must be confirmed before an optimal preservation policy for each bridge in a network of bridges can be developed effectively. As shown in Kuznetsov et al. (2003), the City of Moscow was successful in incorporating this module of structural analysis into their bridge management system. The authors pointed out that changes in the structural condition of various structures over time in the city had been objectively evaluated.

Uncertainties always exist in the bridge management process because of uncertainties in design, analysis, and construction of bridges, associated expenditures, variations in load history, and environmental conditions. Kong and Frangopol (2003) suggested that the reliability of a bridge or a network of bridges be modeled in probabilistic terms to account for these uncertainties. Reliability analysis is time varying, and it should be updated based on inspection data. Without maintenance intervention, reliability deteriorates with time often because of strength degradation of materials due to aging, loss of material due to corrosion, damages due to

natural hazards, and users' increasing demands. Effects of corrosion and seismic hazard on the life cycle cost (LCC) of reinforced concrete bridges were investigated by Kumar et al. (2008). The authors developed a probabilistic approach to compute LCC regarding two deterioration processes and found that the cumulative seismic damage has greater effects on the reliability of bridges in earthquake prone regions than corrosion. Choe et al. (2008a; 2008b) developed probabilistic capacity models and evaluated the seismic fragility of reinforced concrete bridges when these bridges are exposed to various corrosive environments. These studies account for different types of uncertainties related to the process of design and construction of these structures including in environmental conditions, material properties, structural geometry, water-to-cement ratios, and curing conditions. Pillai et al. (2009) presented a methodology to assess the flexural reliability of corroding segmental PT bridges. In their studies, a typical PT bridge was exposed to different corrosive environmental conditions, and the time-dependent reliability index was investigated with consideration of void existence in the tendons of prestressing strands.

It was pointed out in Huang et al. (2008) that nondestructive testing methods can provide valuable data for reducing uncertainties in the reliability assessment of a bridge and better evaluating its actual conditions. Updating reliability of highway bridges with inspection results from the Pontis bridge management system was investigated by Estes and Frangopol (2003). An assumption of linear deterioration of reliability over time was made for bridges although reliability deterioration depends on limit states of failure of structural components and can be nonlinear. The authors, however, emphasized the importance of evaluating three major components of a reliability model: load or demand model, resistance or capacity model, and material deterioration model. The authors provided a useful methodology for quantifying the reliability of bridges with reinforced concrete and steel structural components based on visual inspection, in which the experience of inspectors was taken into consideration. Because structural models can behave rather differently from real bridges due to structural analysis simplifications, the reliability model quantities should be updated from inspection data and become the base for optimum life-cycle inspection and repair planning. When bridge performance measures or indices are incorporated in accordance with the safety-based goals of the federal bridge program (Sivakumar et al. 2003), priorities can be taken into consideration in the optimum planning model.

Maintaining the performance of concrete structures was investigated by Mori and Ellingwood (1994a). They developed a conceptual methodology for determining inspection/repair strategies to keep the performance or reliability index of a structure above a specified limit. The evaluation of the reliability or failure probability of a structure or structural component was based on the probability density function of the damage intensity that was updated after an inspection or repair using a Bayesian approach. The expected amount of damage in a time interval was described as a Poisson process and was assumed to be dependent on the surface area or volume of a structural component. However, the amount of damage may not be appropriate for evaluating strength of a component because the location of damage in a component is more important. Effects of inspection/repair operations on reliability of structures were investigated by assuming all detected damages are repaired completely. This is not always feasible, especially in the case when only a limited budget for maintenance is provided for bridges in a transportation network.

In the second paper on maintaining the reliability of concrete structures, Mori and Ellingwood (1994b) developed a methodology to optimize maintenance strategies for structures so that the expected future cost of the structures (including cost of structural failure) can be minimized while their performance is still kept higher than a specified limit of safety during their life cycle. In their study, a constant cost of replacement was assumed for structural components with detected damages. However, it was suggested that this cost should be a function of damage intensities, which were determined based on their time-dependent growth model. The design load combination in ACI Standard 318 (1989) with factored loads of 1.4 for dead load and 1.7 for live load was used to determine the flexural demand on the structures studied but is too conservative and is not able to well represent the real demand; the probability of failure is, therefore, excessively high. The authors concluded that the solution of optimum inspection/repair strategies was sensitive to the relative costs of inspection, repair, and failure. Their studies also showed optimum solutions usually need extensive computational resources and require significant time for running computer programs even though their study examples focused on only reinforced concrete structures. For prestressed concrete structures, extensive computation is necessary to evaluate a deterioration model for optimization purposes, and advanced knowledge of this type of structure as well as programming skills are needed. Later, two methodologies to optimize the

maintenance/repair strategies of PT bridges will be introduced; this will be followed by numerical examples of applications.

3. DETECTION OF VOIDS IN POST-TENSIONED BRIDGES: EXPERIMENTAL PROGRAM AND RESULTS

3.1. INTRODUCTION AND OBJECTIVES

The literature review provided in Subsection 2.3 found that an effective inspection method is required to identify voids and their locations in post-tensioned systems. This section describes the experimental program and results on the research performed on void detection and measurement methods. At first, preliminary testing and results are discussed. Details of test specimens, test methodologies, and the analysis plan are then described. The results from this study are then presented.

The objectives of this section are:

- to develop an effective method for identifying voids in PT system.
- to develop a method to estimate the volume of voids in PT system.

3.2. PRELIMINARY TESTING AND RESULTS

In the preliminary testing, the Impact-Echo (IE) and Ultrasonic Pulse Velocity (UPV) techniques were found to be ineffective in detecting voids in PT systems. This is because the interface between the HDPE ducts and cementitious grout obstructed the elastic waves used in these techniques. As a result of this, these non-destructive techniques are not effective for field applications. The IE technique is sensitive to vibration. The IE technique is generally useful in detecting voids in the thick concrete webs of the box girders. However, they are not effective in detecting voids in the 4-inch (102 mm) diameter tendon specimens. The UPV method requires a couplant between the transducers and the surface of the specimens. This is a time-consuming process and probably inpractical to be used on long tendon systems in PT bridges.

3.3. VOID DETECTION AND ASSESSMENT: EXPERIMENTAL PROGRAM

The section first presents the details of prototype external tendon (PET) test specimens and explains how to fabricate the artificial voids in PET specimens. The visual and sounding

inspection methods are then presented. Finally, a procedure to estimate the effectiveness of sounding inspection method in estimating void volume is discussed.

3.3.1. Experimental setup

PET specimens were designed, fabricated, and used to evaluate the sounding inspection method. The schematic of a PET specimen is shown in Figure 3-1.

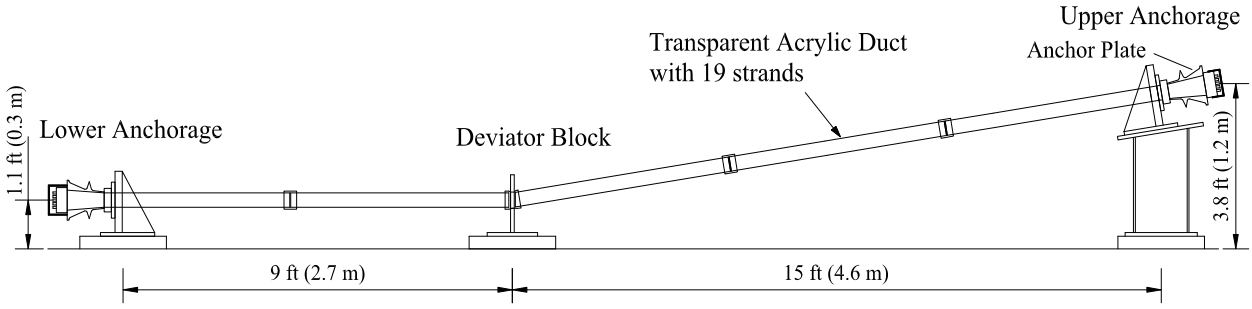

Note: For clarity the 19 strands inside the acrylic duct are not shown.

Figure 3-1. Prototype External Tendon Speicmen.

This PET specimen consists of a lower anchorage, a deviator block, an upper anchorage, and 19 strands inside a transparent acrylic duct. The inside diameter of the acylic duct is 4 inches (0.1 m). To straighten the strands and mimic field conditions, the 19 strands were tensioned to 0.8 ksi (5.52 MPa), which is equal to 0.3% of their ultimate strength. After stressing the strands, the interstitial spaces between the stands and duct were filled with Class A grout. Figure 3-2 (a) and (b) show hand grout pump and pressure grout pump, respectively. The grout was injected through the grout hole near the lower anchorage using a hand grout pump [Figure 3-2 (a)]. The hand grout pump was used (instead of pressure grout pump) to better control the grout level and void size in the PET specimens. Artificial voids were then formed in the top anchorage zone and at five locations along the duct to simulate improper grouting procedures. Schematic of these voids and their locations are shown in Figure 3-3.

The main void near the top anchorage zone is formed by filling the grout only upto the 'initial grout level' as indicated in Figure 3-4. The five void locations along the duct system were fabricated by extracting grout from these locations using a vacuum pump and flask. This vacuum pump and flask setup is shown in Figure 3-5. Through preliminary studies, an appropriate time for making the voids was determined to be 2 hours after the initial grouting. To insert the vacuum tube to extract the fresh grout at each void location, a 1-inch (0.025-m) diameter hole was drilled into the duct before initial grouting. After removing the grout, the duct was later sealed with a pipe saddle tap to prevent the leakage of repair grout (Figure 3-6).

Figure 3-2. (a) Hand Grout Pump and (b) Pressure Grout Pump (www.chemgrout.com).

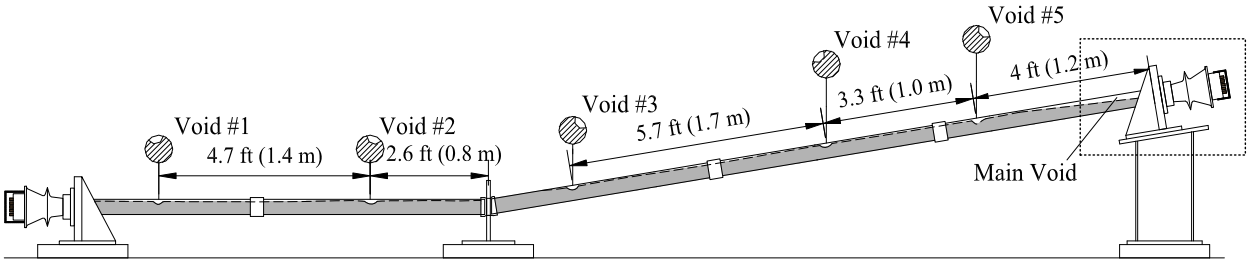

Figure 3-3. Void Locations on the PET Specimen.

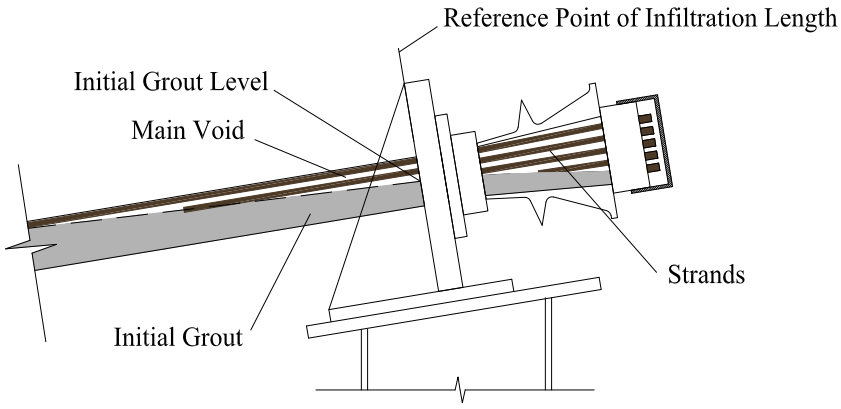

Figure 3-4. Close-up View of the Main Void Near the Top Anchorage of the PET Specimen.

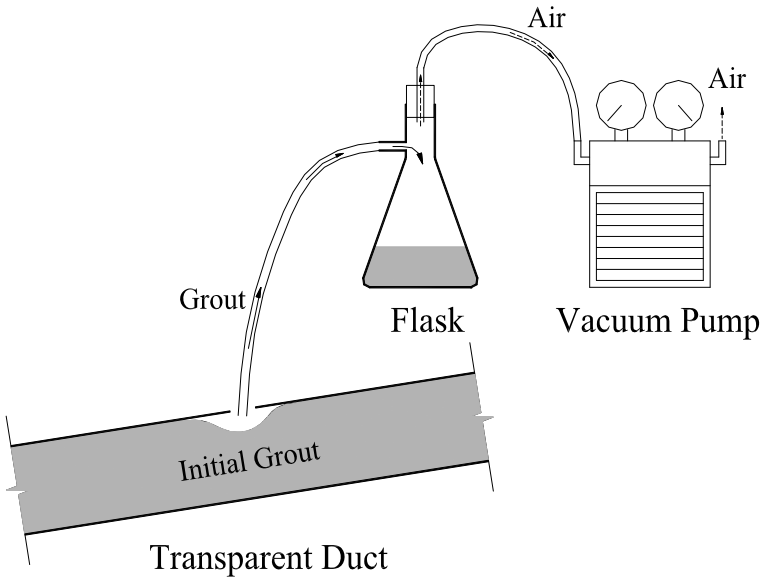

Figure 3-5. Schematic Showing the Setup Used for Making Making Artificial Voids in PET Specimen.

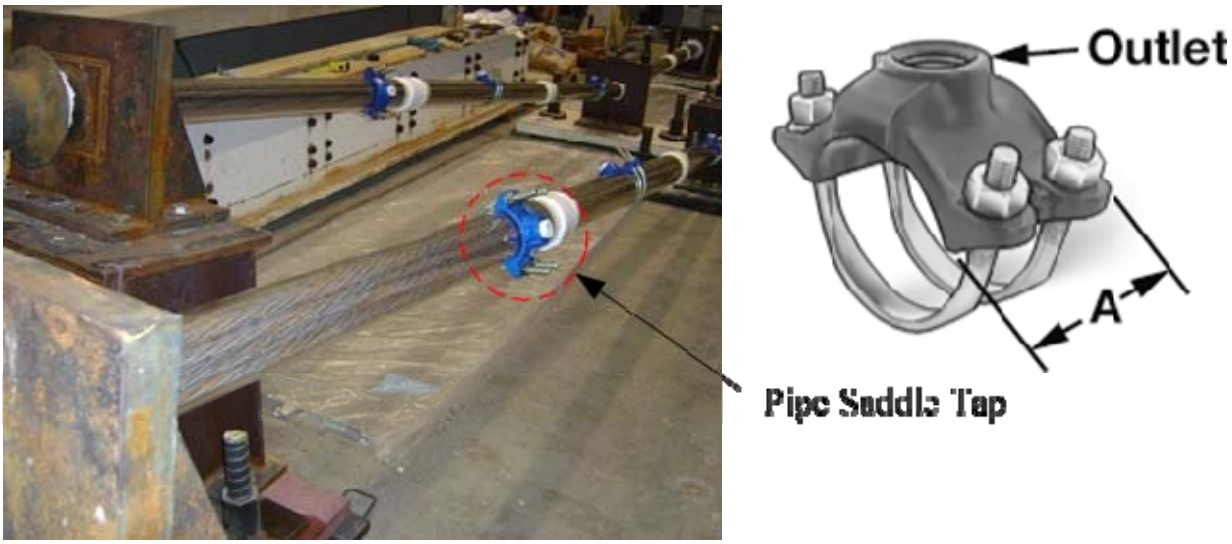

Figure 3-6. Transparent Acrylic Ducts and Pipe Saddle Tap Used on PET Specimens.

As shown in Figure 3-3, the main void at the top anchorage zone and the five other small voids along the duct are connected by a top surface void line along the duct. These void lines are called "bleed lines" (also known as "bug holes") and are formed by the evaporation of bleed water from the grout and entrapped air pockets (PCI 1997). A total of 16 PET specimens were fabricated and tested in this research.

3.3.2. Visual inspection

Transparent acrylic ducts were used to facilitate visibility during the initial and repair grouting procedures. The voids in the PET specimens were visually inspected and drawn on a "void mapping sheet." The "void mapping sheet" is discussed later.

3.3.3. Sounding inspection

Sounding inspection method used in this study used a steel tapping hammer to identify the existence of voids in ducts. Figure 3-7 shows these steel tapping hammers. The presence of voids was identified by detecting a high pitch and irregular sound, while tapping. In this

research, soundings were recorded at every inch in the surveyed intervals (1 ft, 0.305 m) of specimens. Although the assessment of sounding is subjective and depends on the inspector's judgement, it was classified as high and low pitch sounds. Following this method, void profiles of PET systems were drawn on "void mapping sheets."

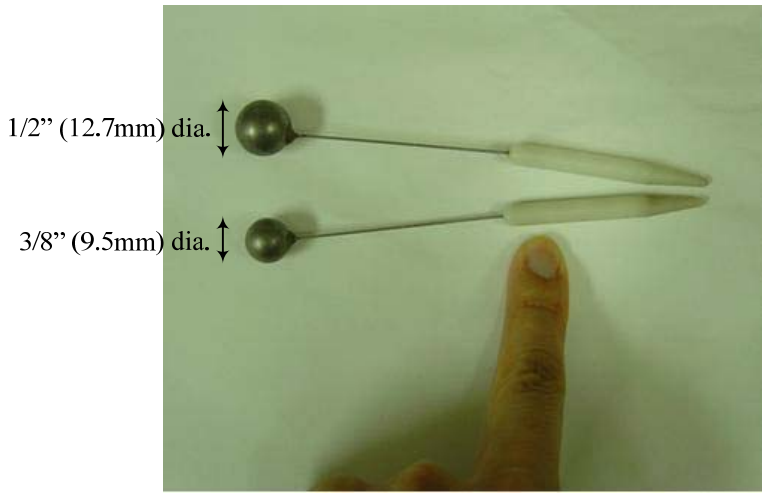

Figure 3-7. Steel Tapping Hammer for Sounding Inspection.

3.3.4. Void mapping sheet

Void profiles developed from the sounding and visual inspections were mapped on scaled sheets called "void mapping sheets." Irregular soundings are recorded on the "unrolled drawing" of PT ducts as shown in Figure 3-8 and Figure 3-9.

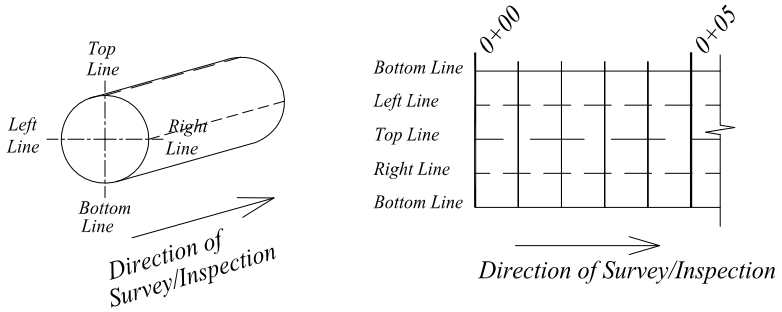

Figure 3-8. Unrolled Drawing of PT Ducts in the "Void Mapping."

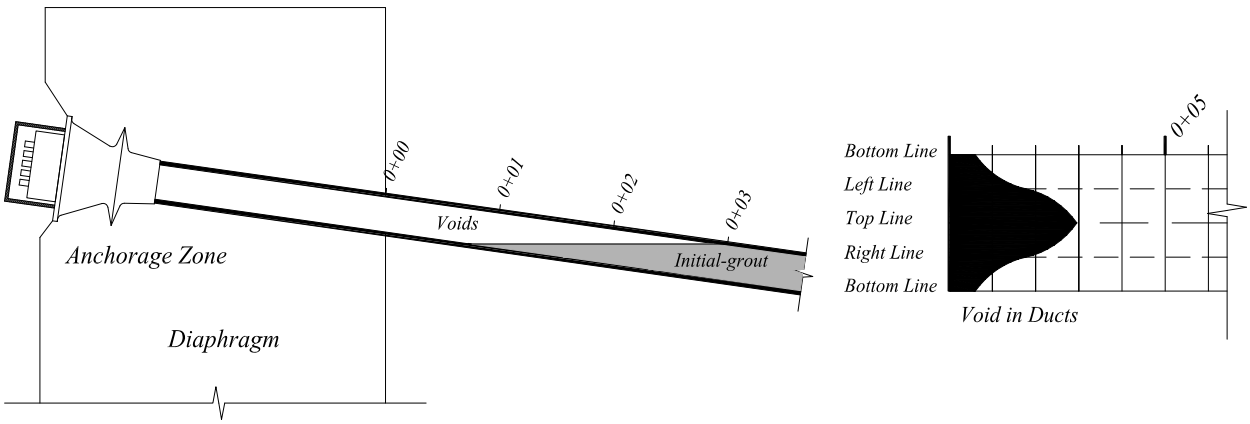

Figure 3-9. Marking Voids on the "Void Mapping Sheet."

3.3.5. Comparison of void profiles obtained using visual and sounding inspections

A comparison of void profiles obtained using the sounding and visual inspections was performed to assess the accuracy of the sounding inspections.

The void maps obtained from the visual nad sounding inspection were drawn in AutoCAD® and the area at every foot (0.305 m) interval was determined. The calculated areas were then used to compare the effectiveness of the sounding inspection method.

3.4. VOID DETECTION AND ASSESSMENT: RESULTS

This section provides the detailed results of sounding inspections of Specimen VG-C1-2, which was repaired by the VG method using Class C1 grout. Although some errors were identified with the sounding technique, this research shows that the sounding technique is relatively accurate and there exists a correlation between irregular soundings and the existence of voids. This section also provides a summary of a procedure on how to estimate repair grout volumes from sounding inspection data. The detailed results of all other specimens are shown in Appendix B.

3.4.1. Effectiveness of sounding inspection

A sounding inspection is generally performed to identify the existence of voids in ducts (FDOT 2001a). Because of the general uncertainty associated with sounding inspections, a detailed inspection using a borescope can be conducted to confirm the existence of a void. To evaluate the effectiveness of sounding inspections, a *t*-test is performed that compares the differences between sounding and visual inspections. Void profiles found by both sounding and visual inspection methods are provided in the form of void maps for every specimen. The difference between the sounding inspection and the void inspection was estimated at intervals of one per foot (0.305 m) for the entire specimen. Figure 3-10 shows the initial void profiles found by the sounding inspection and the visual inspection before repairing the specimen (VG-C1-2). The areas of both void profiles were estimated using AutoCAD® and are provided in Table 3-1.

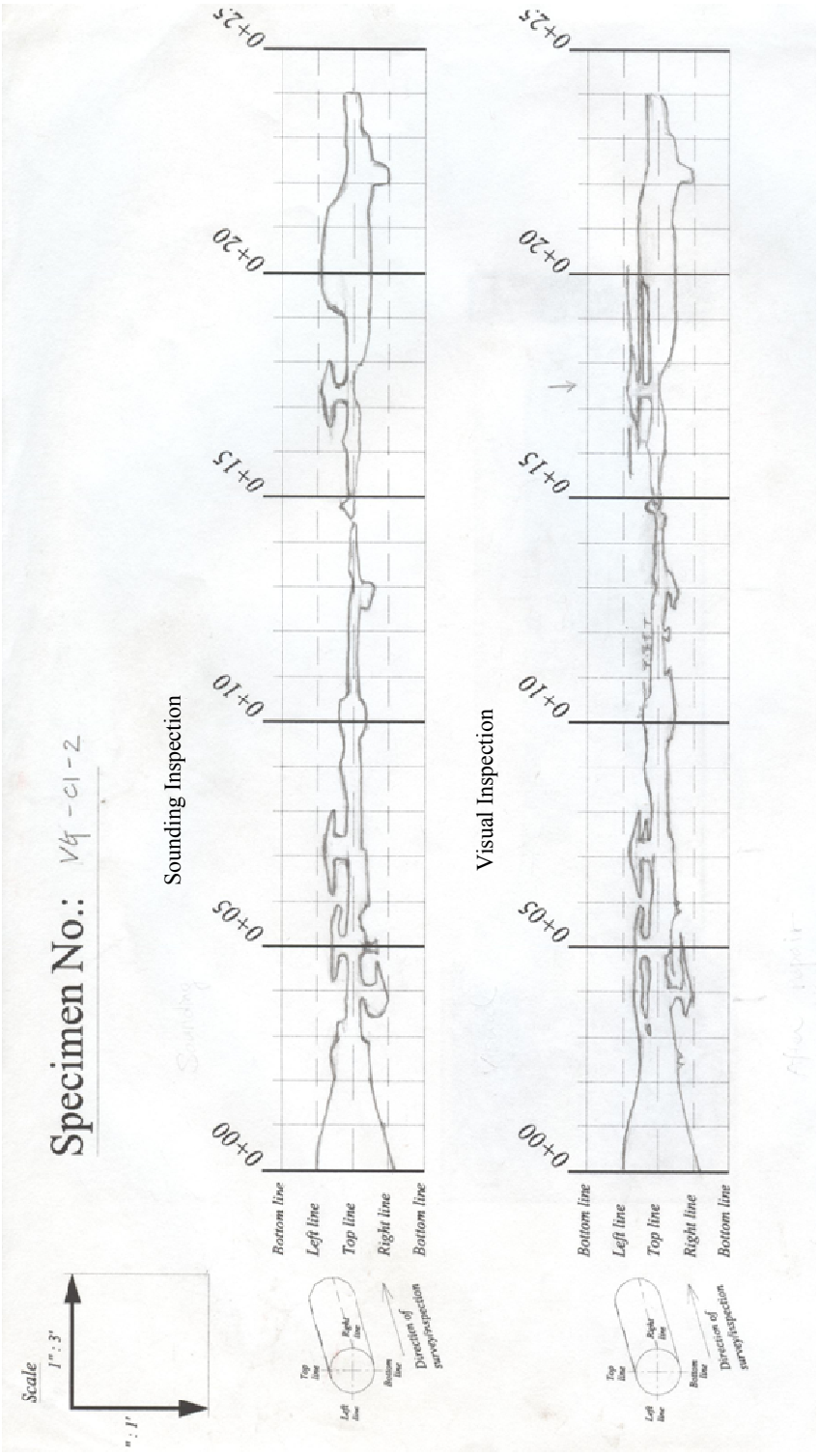

Figure 3-10. Void Map of Specimen VG-C1-2.

Table 3-1. Estimation of Void Profile in Specimen VG-C1-2.

Section, ft (m)	Sounding Inspection (SI), inch^2 (10^{-4} m^2)	Visual Inspection (VI), inch^2 (10^{-4} m^2)	SI - VI, inch^2 (10^{-4} m^2)
0~1 (0~0.3)	73.60 (474.9)	73.20 (472.2)	0.41 (2.6)
1~2 (0.3~0.6)	50.58 (326.3)	53.34 (344.2)	-2.76 (-17.8)
2~3 (0.6~0.9)	38.69 (249.6)	41.93 (270.5)	-3.25 (-20.9)
3~4 (0.9~1.2)	31.94 (206.1)	41.46 (267.5)	-9.52 (-61.4)
4~5 (1.2~1.5)	30.48 (196.7)	37.46 (241.7)	-6.98 (-45.0)
5~6 (1.5~1.8)	28.80 (185.8)	34.93 (225.3)	-6.13 (-39.6)
6~7 (1.8~2.1)	29.49 (190.2)	31.78 (205.0)	-2.29 (-14.8)
7~8 (2.1~2.4)	32.32 (208.5)	35.88 (231.5)	-3.55 (-22.9)
8~9 (2.4~2.7)	19.04 (122.8)	20.34 (131.2)	-1.30 (-8.4)
9~10 (2.7~3.0)	21.75 (140.3)	24.93 (160.8)	-3.18 (-20.5)
10~11 (3.0~3.4)	20.76 (133.9)	30.52 (196.9)	-9.77 (-63.0)
11~12 (3.4~3.7)	11.59 (74.7)	20.07 (129.5)	-8.49 (-54.7)
12~13 (3.7~4.0)	17.75 (114.5)	18.33 (118.3)	-0.58 (-3.7)
13~14 (4.0~4.3)	11.31 (73.0)	14.30 (92.3)	-2.99 (-19.3)
14~15 (4.3~4.6)	7.50 (48.4)	10.33 (66.6)	-2.83 (-18.3)
15~16 (4.6~4.9)	11.10 (71.6)	12.19 (78.7)	-1.09 (-7.0)
16~17 (4.9~5.2)	19.93 (128.6)	22.50 (145.2)	-2.57 (-16.6)
17~18 (5.2~5.5)	26.44 (170.6)	27.76 (179.1)	-1.32 (-8.5)
18~19 (5.5~5.8)	23.16 (149.4)	33.98 (219.3)	-10.83 (-69.9)
19~20 (5.8~6.1)	46.90 (302.6)	39.19 (252.8)	7.72 (49.8)
20~21 (6.1~6.4)	51.61 (333.0)	39.85 (257.1)	11.76 (75.9)
21~22 (6.4~6.7)	41.21 (265.9)	37.33 (240.8)	3.88 (25.0)
22~23 (6.7~7.0)	35.74 (230.6)	37.21 (240.0)	-1.47 (-9.5)
23~24 (7.0~7.3)	19.61 (126.5)	21.06 (135.9)	-1.45 (-9.4)

The void profiles and the area estimates for all other specimens are provided in Appendix B. In the analysis, void maps generated from visual inspections are considered to represent the actual existence of voids as it was possible to confirm their existence through the transparent acrylic ducts. The differences between the void quantities from the sounding inspections and the

visual inspections were compared using the null and alternate hypotheses (H_0 and H_1) as follows:

$$H_0 : \mu_{\text{Sounding Inspection - Visual Inspection}} = 0$$
$$H_1 : \mu_{\text{Sounding Inspection - Visual Inspection}} \neq 0 \quad (3.1)$$

where, $\mu_{\text{Sounding Inspection – Visual Inspection}}$ is the mean of the population for differences between void areas detected from the sounding inspections and visual inspections.

The results of the *t*-test are provided in Table 3-2. Figure 3-11 shows the data distributions. From the analysis, the null hypothesis is rejected at the 0.05 level of significance; therefore, the voids identified from the sounding inspection do not accurately represent the existence of voids in ducts.

Table 3-2. The *t*-test for Difference between Sounding and Visual Inspections.

Difference	Mean	Standard Deviation	Sample size	*t*-test	*p*-value
Sounding - Visual	-1.0743	7.7295	360	-2.637	0.002

However, a correlation analysis between sounding and visual inspections reveals a highly positive linear correlation (correlation coefficient is 0.906) between the actual voids in the test specimens and sounding inspections. Interpretation of this correlation reveals that the voids detected by sounding inspections are inaccurate when considering the magnitude of a void, but are relatively accurate at determining the location and existence of a void. This relationship will be shown in the next section. While the sounding inspection lacks the ability to detect extremely small voids and requires experienced personnel, it can be an effective tool for inspecting voids because of its ease of application and relative accuracy.

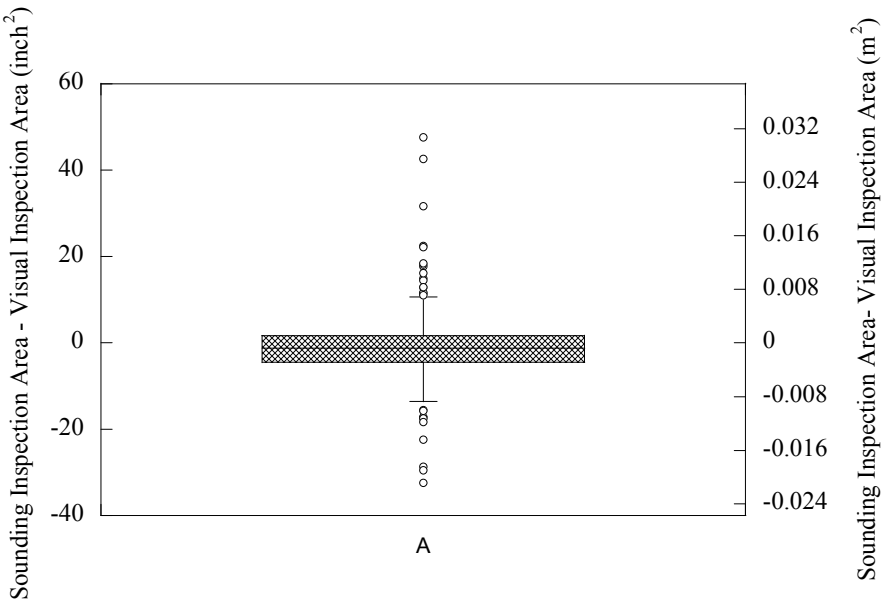

Figure 3-11. Box and Whisker Plot for the Difference between Sounding Inspection and Visual Inspection.

3.4.2. Volume estimation of voids in ducts by sounding inspection

The volume of repair grout can be estimated using a volumeter, which is an instrument that measures the volume of voids in ducts, using air pressure. However, using a volumeter requires that ducts are in sealed conditions to correctly estimate void volumes. While volumeters are equipped with some leak compensation abilities, significant errors can occur. A volumeter is capable of estimating the entire volume of an external tendon. However, for this to be accomplished in the field the repair grouting has to be performed twice from each end because test results indicate that repair grouts cannot fill all the voids in the entire tendon at one time. Therefore, alternative methods for measuring the volume of voids are required for repair methods in ducts.

In this research, estimates of the required volume for repair grout were made using the data obtained from sounding and visual inspections. The void areas obtained from visual and sounding inspection (A_{VI} and A_{SI}) were found to be linearly correlated (Figure 3-12). The corresponding equation is as follows:

$$A_{VI} = 0.844A_{SI} + 4.371$$
$$(A_{VI} = 0.844A_{SI} + 28.199 \text{ for SI unit}) \quad (3.2)$$

where, A_{VI} is the estimated area by visual inspection, which is assumed here to be the actual area of voids, in inch^2 (10^{-4} m^2 for SI unit), A_{SI} is the estimated area by the sounding inspection in inch^2 (10^{-4} m^2 for SI unit). To prevent the underestimation of voids, the upper limit (U.L.) equation for a 0.05 level of significance can be used as follows:

$$A_{VI} = 0.844A_{SI} + 18.522 \text{ (U.L.)}$$
$$(A_{VI} = 0.844A_{SI} + 119.499 \text{ (U.L.) for SI unit}) \quad (3.3)$$

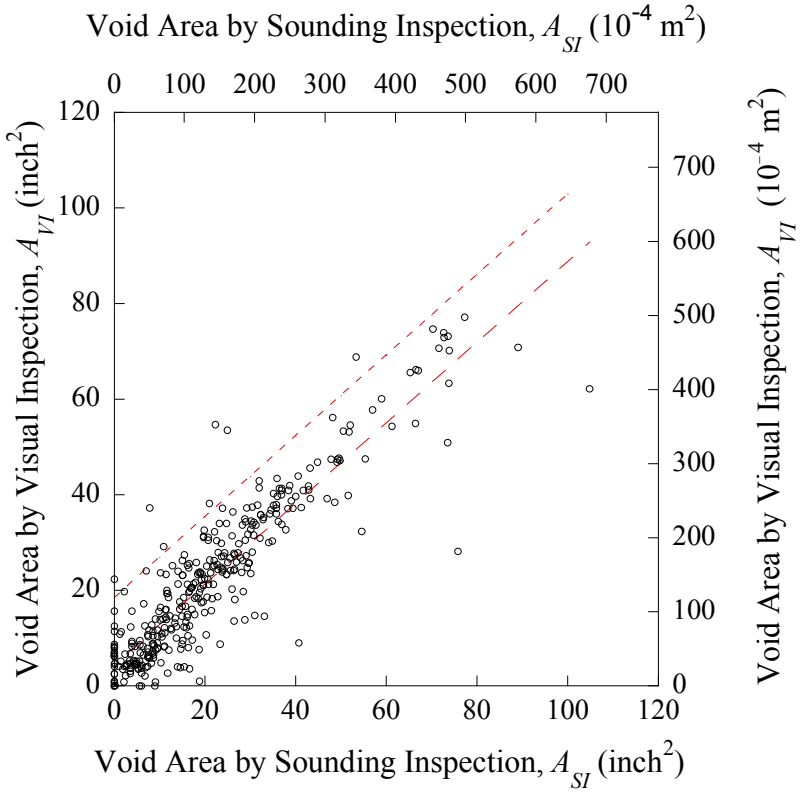

Figure 3-12. Scatter Plots between the Void Areas Obtained from Sounding and Visual Inspections.

From volumetric estimations of repaired grouts from the test specimens, the relationship between void areas by visual inspection and the volume of repair grouts used for the specimens are provided in Figure 3-13. The repaired volume of each specimen was obtained from the sections of the cut tendon. For cut sections, the approximate repaired volume was determined using the average void area at both ends multiplied by the cut length. The equation for the relation between void areas determined from the visual inspections and the grout volume is estimated as follows:

$$V_{req} = 0.165 A_{VI} + 25.150$$
$$(V_{req} = 0.420 A_{VI} + 412.138 \text{ for SI unit}) \quad (3.4)$$

where, A_{VI} is the estimated area by visual inspection in inch^2 (10^{-4} m^2 for SI unit) and V_{req} is the estimated repair volume of the specimen in inch^3 (10^{-6} m^3 for SI units). To ensure enough grout for repair, the upper limit equation (95% confidence limit) for this relationship is given by:

$$V_{req} = 0.165A_{VI} + 62.152 \quad \text{(U.L.)}$$
$$(V_{req} = 0.420A_{VI} + 1018.501 \quad \text{(U.L.)} \quad \text{for SI unit}) \tag{3.5}$$

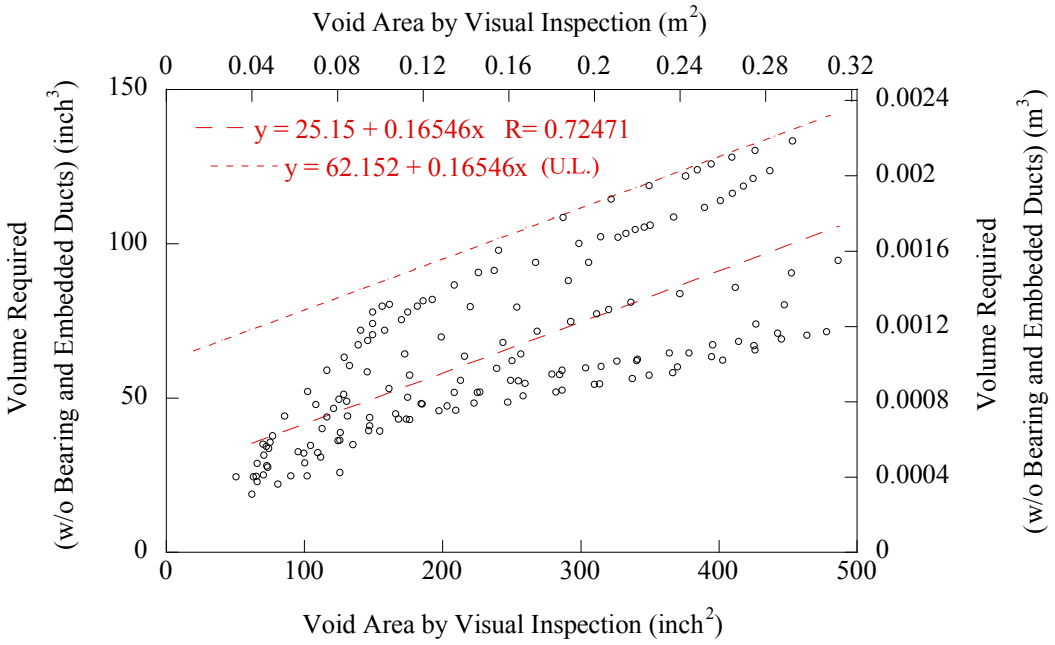

Figure 3-13. Scatter Plot between the Void Areas from Visual Inspection and the Void Volume Repaired.

The repair volume of each specimen was estimated based on the cross sections of each test specimen. However, this relationship does not include the void volume contained in embedded ducts and bearing plate in diaphragm; the embedded duct and bearing plate in the concrete diaphragm in the field cannot be examined by the sounding inspection. To ensure sufficient grout is prepared, the volume estimates of the repair grout should be performed assuming that the embedded ducts and bearing plate contain no grout.

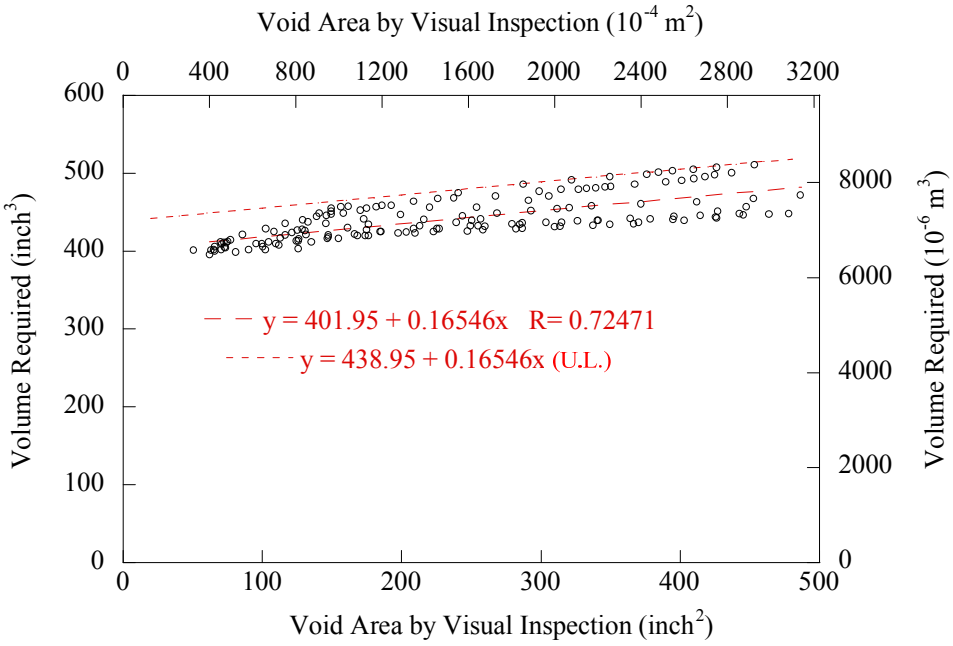

Figure 3-14. Scatter Plot between Void Area by Visual Inspection and Void Volume Repaired (Including the volume of the Voids in Bearing Plate and Ducts inside the Upper Anchorage).

Figure 3-14 shows the relationship between void area determined from visual inspections and the volume of repaired grouts in the test specimens (including the volume of voids in bearing plate and ducts inside the upper anchorage). Sounding inspections are applied to the test specimens that have only partially filled ducts to the reference point (Section 3.3.1). The volumetric effect of having an empty bearing plate and 5 inches (0.127 m) of empty ducts embedded at the anchorage are considered in Figure 3-14. The equations considering the volume of the embedded ducts and bearing plate are defined as:

$$V_{req,BP\&ED} = 0.165A_{VI} + 401.95$$
$$(V_{req,BP\&ED} = 0.420A_{VI} + 6586.79 \quad \text{for SI unit}) \tag{3.6}$$

where, A_{VI} is the estimated area by visual inspection in inch^2 (10^{-4} m^2 for SI unit) and $V_{req,BP\&ED}$ is the estimated repair volume of the specimen, which includes the void volume of the empty bearing plate and 5 inches (0.127m) embedded ducts, in inch^3 (10^{-6} m^3 for SI units). The upper limit equation (95% confidence limit) for this relationship is given by:

$$V_{req,BP\&ED} = 0.165A_{VI} + 438.95 \text{ (U.L.)}$$
$$(V_{req,BP\&ED} = 0.420A_{VI} + 7193.1 \text{ (U.L.)} \quad \text{for SI unit}) \tag{3.7}$$

This upper limit equation should be used to ensure that sufficient grout for repair grouting.

Simply, the equations indicate that one-quarter cubic foot (0.007 m^3) of grout would be needed to fill a typical void caused by using Class A grout. Additional grout will also be needed and this depends on the area identified as having voids using the sounding inspection method.

From Equations 3.3 and 3.5, the repair volume can be approximately estimated from the sounding inspection. The equation of the repair volume, which does not contain the volume of bearing plate and embedded ducts, is defined as follows:

$$V_{req} = 0.139A_{SI} + 65.208$$
$$(V_{req} = 0.354A_{SI} + 1068.691 \text{ for SI unit}) \tag{3.8}$$

From bearing plate designs and diaphragm thicknesses, bridges have different grout volume requirements for anchorage zones. Thus, the void volume in bearing plate and embedded ducts has to be added to Equation (3.8) to apply in the field.

Figure 3-15 provides examples of the void profiles obtained from sounding inspection While this inspection shows the existence of voids, it lacks the ability to show void size and the

condition of the strands inside. Hence, a detailed inspection using a borescope would be beneficial to assess voids and strand corrosion. From a detailed inspection using a borescope, it was determined if tendons needed repair work. In both examples in Figure 3-15, it was determined that repair grouting was needed. The required volume of the repair grout can be estimated as follows. Although this volume may be different in actual structures, the obtained volume can be simply determined from the sounding inspection and ensures sufficient volumes for repair.

In the case of example (a) in Figure 3-15, the value of A_{SI} can be estimated from 3 ft (0.91 m) to 10.2 ft (3.07 m). Note that the void profile between 0 ft (0 m) and 3 ft (0.91 m) represents a nearly empty duct. To ensure sufficient amounts of repair grout void areas that exceed the "Left Line" and "Right Line" [see Figure 3-15 (a)] are considered as empty. Thus, the bearing plate, the embedded ducts in the diaphragm, and an additional 3 ft (0.91 m) along the ducts are considered to be empty in this case (see Figure 3-15). A_{SI}, can be estimated from 3 ft (0.91 m) to 10.3 ft (3.14 m), and the repair grout volume, V_{req}, can be obtained from Equation (3.8). The volume of the empty bearing plate and ducts has to be estimated and added to V_{req} to provide the total required volume for repair grouting.

In the case of example (b), the value of A_{SI} can be estimated from 0 ft (0 m) to 9.7 ft (2.92 m) - the bearing plate and embedded ducts in the diaphragm are considered to be empty. The estimated A_{SI} can be used to determine V_{req} obtained from Equation (3.8). The volume of the bearing plate and duct embedded in the diaphragm is estimated assuming it is empty. The total volume required can again be obtained by adding these two volumes.

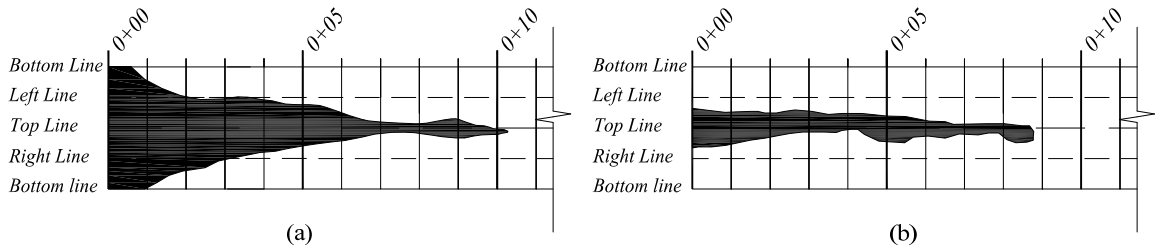

Figure 3-15. Examples of Void Profiles Obtained from Sounding Inspection Method.

The upper limit equations shown in Equations 3.3 and 3.5 can be applied in the field when external tendons are contained in 4-inch (0.1-m, inside diameter) ducts and void profiles are determined using sounding inspections. Therefore, a void profile developed using a sounding inspection method can be used to predict the grout volume required for repair as well as the appropriate locations for detailed inspections using a borescope.

3.5. INSPECTION OF PT BRIDGES

This research developed a separate manual for the inspection and repair of PT bridges. The reader is encouraged to review that document if procedures on inspecton or repair are needed. An overview of inspection is provided here.

The corrosion of tendons has been a long-standing issue in PT structures because the PT tendons perform a significant role in the structural integrity of the system. In addition, severe tendon corrosion can lead to the collapse of an entire bridge. Thus, it is critical to proactively protect tendons from corrosion. For PT tendons with severe corrosion, tendon replacement may be required; however, this can be expensive. Therefore, it would be advantageous to detect tendon corrosion in its early stages, not only to ensure public safety, but also to prevent severe damage and to reduce structural maintenance and repair costs.

Ideally, bridge inspection should be performed at regular intervals to ensure bridge performance. As with most bridges, PT bridges are inspected every two years. However, more detailed inspections may be needed – these can be expensive and time consuming and

monitoring all bridges in great detail may not be necessary. Detailed bridge inspections should be able to be performed in a timely manner and repairs should be dependent on damage levels. This research provides an inspection manual that provides strategies for inspection and analysis of external PT tendon system to maintain bridge performance when corrosion is present (0-4588-2). This inspection manual categorizes bridges and spans based on environmental conditions, factors inducing corrosion, and structural/non-structural damages caused by corrosion. This approach can reduce the time for bridge inspection significantly; thus enabling bridge management to be performed more effectively.

4. GROUT MATERIAL CHARACTERIZATION: EXPERIMENTAL PROGRAM AND RESULTS

4.1. INTRODUCTION

This chapter primarily deals with evaluating the fresh, hardened, and durability characteristics of pre-packaged grouts and developing standard specifications to select PT grout for grouting new and existing PT bridges. Various test variables were identified and evaluated to assess the fresh, hardened, and durability characteristics of the pre-packaged PT grouts.

This section comprises of descriptions of the various test variables used for the research, a brief discussion of the test matrix, details of the mixing procedures performed, and a discussion of the test procedures used in the research. This section also includes the design and proposed procedures for the fillability test setup developed as a part of this research to evaluate the grout's filling ability inside a PT duct.

4.2. TEST VARIABLES

Four variables were identified, and the experiments were performed to study the effects of each variable on the grout characteristics. A detailed description of the test variables is presented in the following sections.

4.2.1. Grout classes

The specification developed by PTI provides minimum performance requirements for a specific grout to be used in protecting and bonding tendons in PT applications (PTI 2003b). According to the PTI specifications (2003), grouts are divided in four classes based on the material specifications and field requirements. These classes are designated as classes A, B, C, or D. Class A is the normal portland cement grout with a maximum w/c of 0.45 and is intended to be used in non-aggressive exposure environments. Class B grouts contains SCMs and is for use in aggressive exposure environments. Class C grouts are pre-packaged PT grouts that can be used for both aggressive and non-aggressive exposure conditions (PTI 2003b). Class D grout is a

specially prepared PT grout to be used in specific conditions where the grout performance characteristics can be carefully controlled.

Class A grout has been used in the construction of most existing PT bridges constructed before the year 2000 and does not exhibit thixotropic properties. Class B, C, and D grouts contain admixtures and may be thixotropic (PTI 2003b). Commercially available prepackaged grouts are Class C grouts and are also referred to as high-performance grouts. Three commercially available high-performance grouts that are being tested for this research are identified as grouts Class C-1, C-2, and C-3. These three grouts and a Class A control grout are shown in Table 4-1 along with their respective identification. Because the contents of these pre-packaged PT grouts are unknown, the ratio of water to all pre-packaged grout ingredients will be referred to as the water-powder ratio (w/p). Table 4-1 also shows the manufacturer's recommended w/p for the grouts considered in this research.

Table 4-1. Pre-packaged Grouts along with their Identification Labels.

Grout	ID	Recommended w/p
ASTM Type I cement	Class A	0.44
Master flow 816 grout	Class C-1	0.30
Sika 300PT grout	Class C-2	0.26
Euco Cable grout PTX	Class C-3	0.27

4.2.2. Grout mixer types

The post-tensioning of new bridges requires a large volume of the grouts (approximately 8 ft^3 (0.23 m^3) of grout required for a standard 150 ft (45.7 m) long PT duct). Hence, a large field grout mixer with high shear action is desirable. A variety of high-shear mixers and colloidal mixers are available for this purpose. In repairing the voided ducts of existing PT bridges, a relatively small quantity of grout [less than 1 ft^3 (0.028 m^3)] is often required. In these cases the

larger field grout mixers may not be applicable for repairs and common practice is to prepare smaller quantities of grouts with hand drills. Two models of portable corded drill mixers were considered in this research. A need for a mixer that could impart high-shear action to achieve the best possible mixing in the shortest time was desirable. Two corded drill mixers with rotating speeds of 2500 and 4000 rpm (identified as M1 and M2 mixers respectively) were selected to evaluate the effect of mixer speed on the characteristics of grout. Figure 4-1 shows the mixing paddle used with M1 and M2 mixers.

Figure 4-1. Mixing Paddle used with M1 and M2 Mixers.

In addition to the standard drill mixers, two hand-held high shear mixers, manufactured by Desoi of Germany, were procured and used to produce grout mixtures. Figure 4-2 shows the high shear mixer by Desoi. These high shear mixers were used to mix various grouts but it was found that these mixers overheated when mixing relatively small volumes. Because of this, it was decided not to further evaluate grout characteristics mixtures with these high shear mixers.

Figure 4-2. High Shear Mixer from Desoi (showing the shear mixer).

4.2.3. Mixing volume

While performing experiments it was observed that mixing volume may have an effect on the efflux time of the grout. Therefore, the volume of the mixture was also considered as a potentially influencing variable. The mixture volume ranges used in this research were 0.25, 0.50, and 0.75 ft^3 (0.0071, 0.0142, and 0.0213 m^3), respectively.

4.2.4. Water-powder ratio

Maintaining exact w/p when large batches of grout are being mixed in the field is difficult. Because the fresh characteristics of many pre-package grouts are sensitive to changes in w/p, and the w/p can influence the hardened characteristics of the grout, the performance of grouts as a function of w/p was also investigated. All three grout manufacturers specify a recommended w/p for their product. These different w/p values and their influence on grout characteristics were also investigated.

To evaluate the sensitivity of w/p on grout characteristics, the w/p was varied from -5 % to +15 % of the recommended w/p. Table 4-2 shows the w/p values used in this research. The test matrix for this research is shown in Table 4-3. This table shows all test variables evaluated to study the grout characteristics.

Table 4-2. w/p for all Four Grouts used in Experiment.

Grout	5% lower w/p	Recommended w/p	15% higher w/p
Class A	0.41	0.44	0.51
Class C-1	0.27	0.30	0.35
Class C-2	0.25	0.26	0.30
Class C-3	0.26	0.27	0.31

Table 4-3. Test Matrix Based on Grout Type, w/p, and Mixture Volume.

Mixer Type	Grout Type	w/p	Mixture Volume ft^3 (m^3)		
			0.25 (0.007)	0.5 (0.014)	0.75 (0.021)
M1	Class A	0.42	√	√	√
		0.44a	√	√	√
		0.51	√	√	√
	Class C-1	0.29	√	√	√
		0.30b	√	√	√
		0.35	√	√	√
	Class C-2	0.25	√	√	√
		0.26c	√	√	√
		0.30	√	√	√
	Class C-3	0.26	√	√	√
		0.27d	√	√	√
		0.31	√	√	√
M2	Class A	0.42	√	√	√
		0.44a	√	√	√
		0.51	√	√	√
	Class C-1	0.29	√	√	√
		0.30b	√	√	√
		0.35	√	√	√
	Class C-2	0.25	√	√	√
		0.26c	√	√	√
		0.30	√	√	√
	Class C-3	0.26	√	√	√
		0.27d	√	√	√
		0.31	√	√	√

a = Recommended w/p for Class A
b = Recommended w/p for Class C-1
c = Recommended w/p for Class C-2
d = Recommended w/p for Class C-3
√ = Indicates grout was evaluated as part of this research

4.2.5. Mixing procedure

It is important to achieve a uniform mixing procedure and to prepare the grout in the same way to achieve repeatability of test results. The grouts were mixed using one of the mixers (M1 or M2) discussed in Section 4.2.2. The mixing was performed in 10-gallon (38.85 liter) cylindrical containers for mixture sizes greater than 0.50 ft^3 (0.0142 m^3) and in a 5-gallon (18.93 liter)

cylindrical container for mixture sizes of 0.25 ft^3 (0.0071 m^3). The following mixing procedure was used:

- The appropriate amount of water was measured and added to the container; the grout was then added slowly to the water within the first 30 seconds while the mixer was rotated at a slow rate.
- A stop watch was started when half of the grout was added to the water; the mixer was rotated at its maximum mixing speed after all grout was added to the water.
- The mixer was stopped after 1 minute and the dry grout was scraped from sides of the container. The mixer was not stopped for more than 30 seconds.
- The grout was then remixed for an additional 4 minutes.
- All mixes were prepared at a room temperature of 75±4 °F (23.8±2.3 °C). The mixing time for each grout was determined based on the efflux time values. Required mixing times for the grouts are shown in Table 4-4.

Table 4-4. Mixing Time.

Grout	Mixing time (minutes)
Class A	5
Class C-1	5
Class C-2	6
Class C-3	20

4.3. TESTS PERFORMED

Table 4-5 shows the tests that were conducted as part of this research. The test standards that were used for each test are also shown in the Table 4-5. Brief descriptions of each test procedure including the standard followed are presented next.

Table 4-5. Test Procedures and the Corresponding Standards Followed.

Tests	Standard followed	Description
Fluidity	Modified ASTM C939 (Tex-437-A)	Test of fresh grout characteristic
Wick-induced bleed	Tex-441-A	Test of fresh grout characteristic
Compressive strength	ASTM C942	1, 3, 7, 28, 56 day strength test
Volume Change	ASTM C1090	1, 3, 7, 14, 28 day test
Initial Set	ASTM C953	Test of fresh grout characteristic
Mixture density	Baroid Mud Balance	Test of fresh grout characteristic
Chloride diffusion	ASTM C1556	Hardened
Viscosity	Brookfield Rheometer	Test of fresh grout characteristic
pH	None	Hardened

4.3.1. Wick-induced bleed

The wick-induced bleed test was performed on all grout types following TxDOT standard, Tex-441-A: Wick Induced Bleed Test of Freshly Mixed Grouts. This method is similar to the PTI's wick induced bleed test (PTI 2003b). All grouts with three different w/p, three different mixture volumes, and two mixer types were tested to study the effect of w/p, mixture volume, and mixer type on the rate and amount of bleeding. Three samples per grout mixture were evaluated based on the TxDOT specifications (Tex-441-A). Figure 4-3 shows the wick-induced bleed test. The final bleeding was determined by evaluating the average of three bleed cylinders using the following equation:

$$\text{Final Bleeding}, \% = \frac{V_w \times 100}{V_s} \tag{4.1}$$

where V_w is the volume of bleed water in pints (ml) and V_s is the volume of the sample at the beginning of the test in pints (ml).

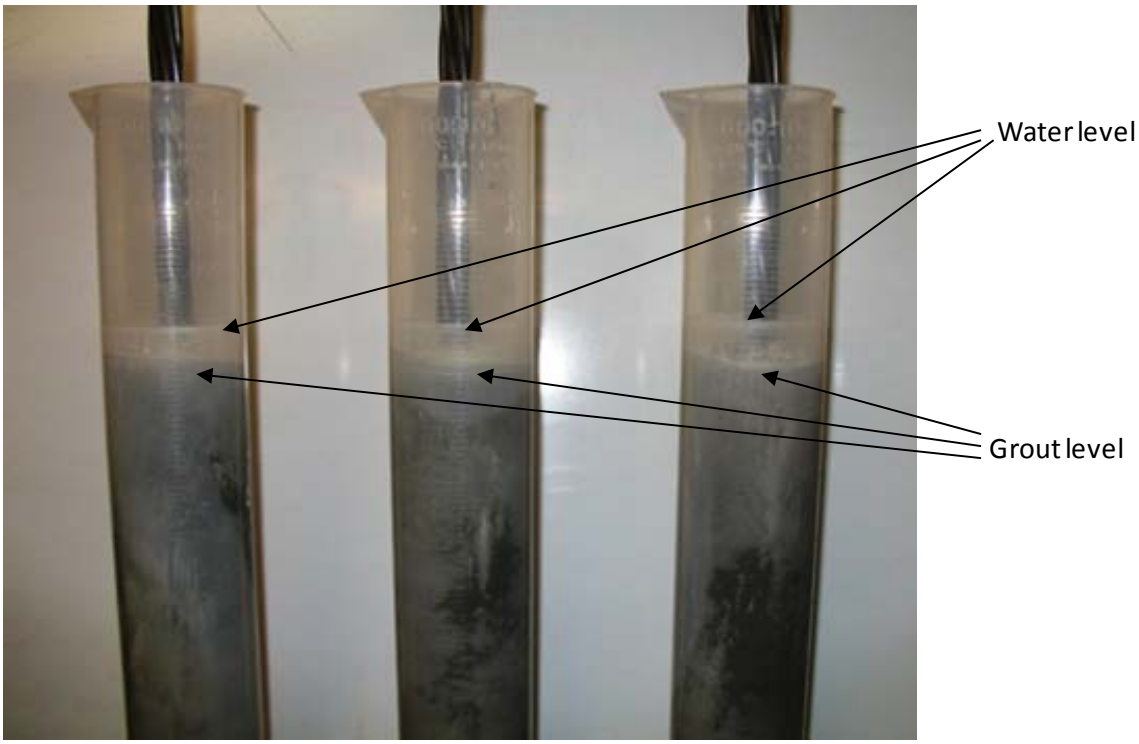

Figure 4-3. Wick-induced bleed test according to TxDOT standards (Tex-441-A).

4.3.2. Viscosity

Viscosity is an important flow characteristic that should be evaluated to assist in predicting the flow of grout inside a PT duct. There has always been the issue of whether a low or high

viscosity grout will perform better in filling voids inside PT ducts. Findings from Schupack (2004) determined that a more viscous, thixotropic grout will achieve better water retention capacity.

Viscosity tests were performed using a Digital Programmable Rheometer by Brookfield Engineering. This test used three pieces of equipment. A DV-III+ Digital Programmable Rheometer (Figure 4-4) was used to measure the viscosity of the grout with a spindle attached to the rheometer. A Model D Helipath™ Stand, also by Brookfield Engineering (Figure 4-4) was used to raise and lower the rheometer to obtain viscosity measurements at different depths and a temperature probe was used to measure the temperature in the grout during the test.

Figure 4-4. Brookfield Rheometer and HelipathTM Stand Used for the Viscosity Test.

The Helipath™ stand moves the rheometer at a constant velocity of 7/8 inch (22.22 mm) per minute. The adjustable stops were placed so that the rheometer is able to move 1.75 inches (44.45 mm) in two minutes. The top stop was also adjusted so that when the container is filled with grout, the spindle is immersed 0.5 inch (12.7 mm) into the grout. Special T-bar spindles (spindle A and B) were used for this test. The rheometer was used with the Rheocalc v2.4

software. The Rheometer was set to spin at 12 rpm, to take readings every 15 seconds, and to run for 30 minutes, so viscosity variation with respect to time could also be studied.

This test program had three objectives. The first was to determine the viscosity of the grouts using a Brookfield Rheometer. Second, the viscosity was evaluated and compared to the efflux time to determine if there is a correlation between the efflux time and the viscosity of a grout; a correleation could provide contractors with information on the fillability of these grouts. Third, viscosities at different depths were evaluated to assess the measurement of viscosity at different depths. This was important because the viscosity of the grout at the top of the duct may be different from the viscosity at the bottom of the duct due to settlement of grout particles. This will assist the researchers in determining whether void formations from viscosity changes are more likely at lower or higher locations at the duct.

The Helipath™ stand also allows the spindle to cut through fresh material, eliminating the channeling effect that is produced by conventional spindles. It is one of the goals of this test to use the viscosity variation with respect to depth to determine the homogeneity of the grout. It is expected that the more homogeneous a grout mixture is, the less the viscosity will vary with respect to depth. This information is important in PT applications as it provides information on the variation in flow in a duct. A detailed description of the procedures to perform this test is shown in Appendix A, Section A.1.

4.3.3. Fluidity

The flow cone test is a test that determines the efflux time of freshly prepared grouts. The flow cone test was performed in the laboratory following Tex-437-A: Test for Flow of Grout Mixtures (Flow Cone Method) (TxDOT 1999). This test can be performed both in the laboratory and in the field, and the efflux time is determined by measuring the time taken to flow a certain amount of grout through a discharge tube of the flow cone.

Because the grouts used (Class C-1, C-2, and C-3) were identified as being thixotropic grouts, Method 2 of the standard (Tex-437-A) was followed. Figure 4-5 shows the schematic diagram of the flow cone as specified in the Tex-437-A standard specifications. According to this method, the cone was filled to the top with freshly prepared grout and the time required for

2.11 pints (1000 ml) of grout to flow from the cone was reported as the efflux time. The required efflux time from the current TxDOT standard for thixotropic grouts to be used in PT ducts based on Method 2 of the standard is:

- 9 to 20 seconds immediately after mixing, and
- 30 seconds maximum with 30 minutes standing time after initial mixing and remixed for 30 seconds before testing.

The flow cone test was performed for all grouts with three different w/p levels, three different mixture volumes, and two different mixers.

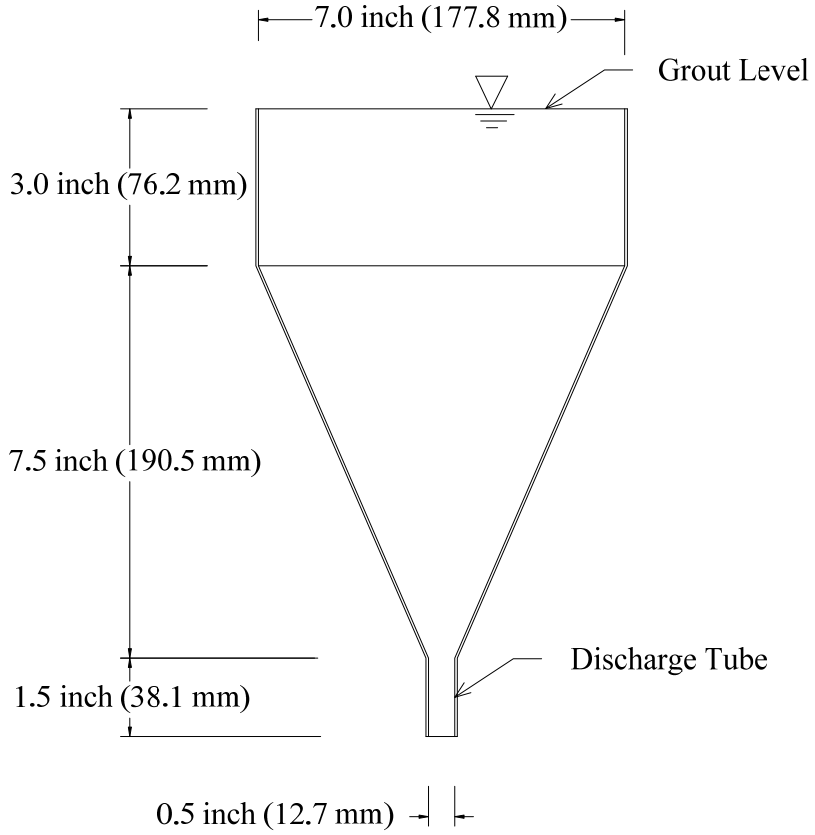

Figure 4-5. Schematic Diagram of Flow Cone as per Tex-437-A Specification.

4.3.4. Wet density

The grout's wet density was measured following the American Petroleum Institute's RP 13B-1 (Baroid mud balance), to ensure the quality of freshly mixed grouts. One test per grout mixture was performed for all grout mixtures with varying w/p, mixer type, and mixture volume. A discussion of the results of this test is presented later.

To use the Baroid mud balance test as a quality control device, tests have been performed to predict the grout's wet density using the mixture's w/p and powder's dry density. Since the grout's dry density varies from batch to batch it was decided to measure the powder's representative dry density in the field using the Baroid mud balance. This dry density is not a measure of the grout's specific gravity. Instead it is measured in the field to predict the grout's wet density after mixing. The procedure to measure dry density of grout is described in the Appendix A, Section A.2.

The dry density values along with the corresponding mixture's w/p and observed wet density have been used to predict the wet density of the resulting grout mixture. A relationship between the observed and predicted wet density of grout has been formulated. A discussion on the wet density model is present in Section 4.4.

4.3.5. Compressive strength

The compressive strength test was performed on all grouts following Tex-442-A: Determining Compressive Strength of Grouts (TxDOT 2006), which is identical to ASTM C942-99: Standard Test Method for Compressive Strength of Grouts for Preplaced-Aggregate Concrete in the Laboratory (ASTM Stantard C 942 1986). The compressive strength of three 2-inch (51-mm) grout cubes were determined using this test method at 1-, 3-, 7-, 28-, and 56-day test ages. Stainless steel and brass cube molds conforming to ASTM C109-05: Standard Test Method for Compressive Strength of Hydraulic Cement Mortars (Using 2-inch Cube Specimens), were used to cast the cubes. For each mixture, the compressive strength was expressed as the average of three cube compressive strengths at each of the selected test ages.

4.3.6. Volume change

ASTM C1090-01 (2005), Standard Test Method for Measuring Changes in Height of Cylindrical Specimens of Hydraulic-Cement Grout, was followed to evaluate the expansion/shrinkage of all grouts. One test per grout mixture was performed for all grouts with varying w/p, mixer type, and mixture volume. Expansion/shrinkage measurements were taken after 1, 3, 7, 14, and 28 days as specified in ASTM C1090. Figure 4-6 shows the micrometer bridge set used to measure the change in the height of the cylindrical specimen.

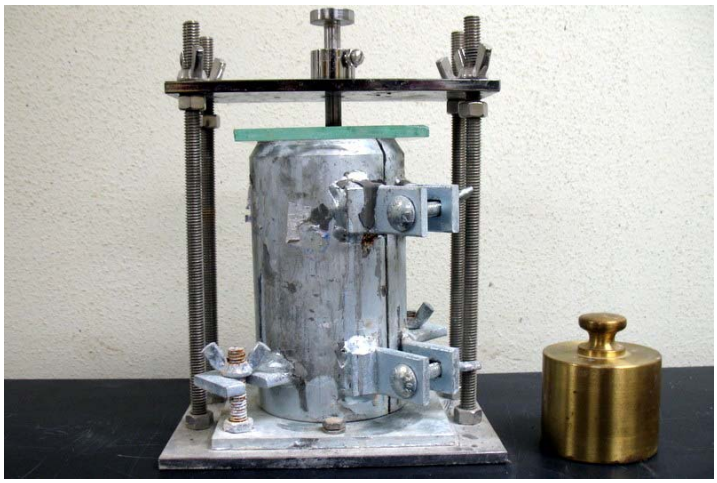

Figure 4-6. Volume Change Apparatus Conforming to ASTM C1090 Used to Measure Change in Height of Cylindrical Specimens.

4.3.7. Chloride diffusion

ASTM C1556-03 test standard was followed to determine the apparent chloride diffusion coefficient of the PT grouts corresponding to their manufacturers' recommended w/p. Mixture volumes of 0.50 ft^3 (0.0142 m^3) were produced using both the M1 and M2 mixers. Cylinders (3 inch × 6 inch [51 mm × 102 mm]) were cast for all combinations of mixtures and cured for 28 days in a 100 percent humidity environment.

Figure 4-7 provides a detailed description of the cylindrical sample and sections tested. The test specimens were prepared by cutting sections parallel to the ends. The top 2.95 inch (75

mm) of the cylinder sample was used as test specimen, the next 0.79 inch (20 mm) thick slice was used to determine the initial chloride content, and the remaining sample was discarded. The test specimens were then coated with epoxy on all sides except for the finished (or cut) surface and exposed to the exposure solution. After 35 days of ponding, powdered samples were collected following the profile grinding procedure in ASTM C1556 (2003).

For all samples a total of five depths were ground and tested. These depths were determined from the recommended depth interval table in ASTM C1556 (2003). The five chosen depth intervals were the top three depths and depth 6 and 8 respectively and are shown in Table 4-6. The chloride content was determined for each sample and then, using the initial chloride content, the apparent chloride diffusion coefficient D_a was determined using the equation in the standard (refer to Equation (2.5)). Note that this is one-dimensional flow and only provides a relative measure of chloride resistance for PT ducts.

Table 4-6. Chosen Depth Intervals in Inches (mm) based on ASTM C1556 Standard.

Grout type	Class A		Class C-1		Class C-2		Class C-3	
	inch	mm	inch	mm	inch	mm	inch	mm
Depth 1	0-0.04	0-1	0-0.04	0-1	0-0.04	0-1	0-0.04	0-1
Depth 2	0.04-0.12	1-3	0.04-0.08	1-2	0.04-0.08	1-2	0.04-0.08	1-2
Depth 3	0.12-0.20	3-5	0.08-0.12	2-3	0.08-0.12	2-3	0.08-0.12	2-3
Depth 6	0.43-0.55	11-14	0.24-0.31	6-8	0.20-0.24	5-6	0.20-0.24	5-6
Depth 8	0.71-0.87	18-22	0.39-0.47	10-12	0.31-0.39	8-10	0.31-0.39	8-10

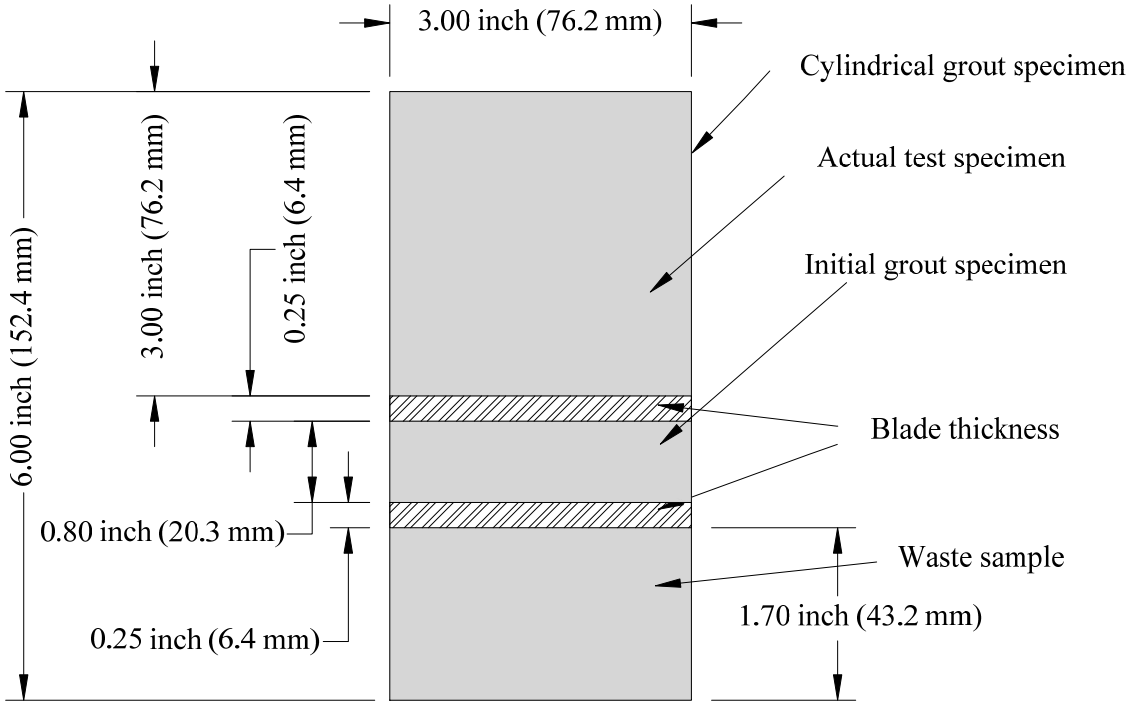

Figure 4-7. Cylindrical Specimen for Chloride Diffusion.

4.3.8. Alkalinity

The pH of the grout's pore solution was measured by extracting the pore solution of the grout cylinders after 28 days of curing. Three cylindrical samples, 2 inch by 4 inch (51 mm x 102 mm), were cast for each combination. Figure 4-8 shows the pore fluid expression device used to extract the pore solution. A detailed test procedure is shown in Appendix A, Section A.3.

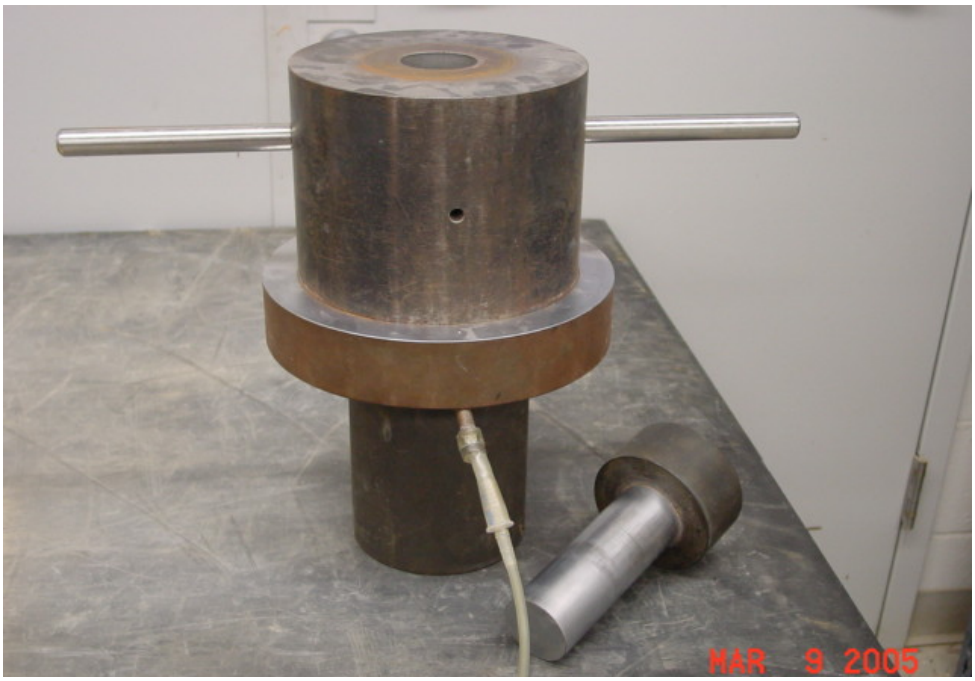

Figure 4-8. Pore Fluid Expression Device to Measure pH of Pore Solution.

4.3.9. Fillability meter

The fillability meter was designed with the aim of evaluating various grouts in terms of their ability to fill small voids in PT ducts. Freshly prepared grout was placed under pressure and the minimum and maximum filter sizes at which there is no flow and good flow was determined. The fillability meter vessel was fabricated using PVC Schedule 40 and Schedule 80 pressure fittings. The meter consists of a pressurized vessel with a capacity of 0.07 ft^3 (2000 ml), a pressure hose connection through which pressure can be applied, and a set of filters.

Figure 4-9 shows a cross-section of the fillability meter. After the fillability meter was fabricated, pilot tests were performed to test for leaks. The meter was tested at 60 psi (0.42 MPa) pressure. Fillability tests were then performed to study the fillability of various grouts. Ten different 2-inch (51-mm) diameter pore size filters were used and the sizes of the pore opening were as follows:

- 0.0055 inch (140 μm)
- 0.007 inch (178 μm)
- 0.009 inch (229 μm)
- 0.015 inch (381 μm)
- 0.021 inch (533 μm)
- 0.03 inch (762 μm)
- 0.034 inch (864 μm)
- 0.054 inch (1372 μm)
- 0.065 inch (1651 μm)
- 0.08 inch (2032 μm)

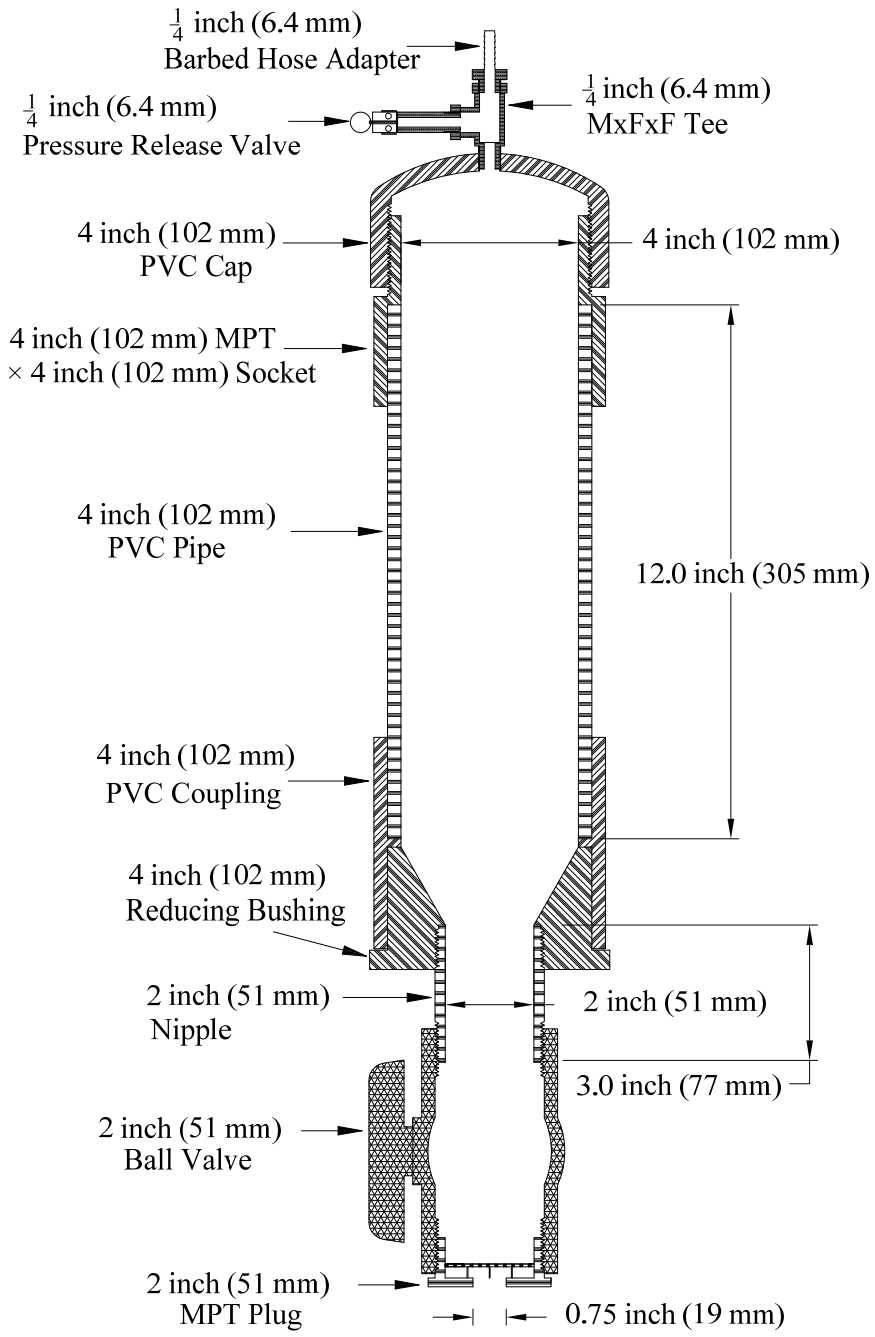

Figure 4-9. Detailed Sketch of Fillability Meter.

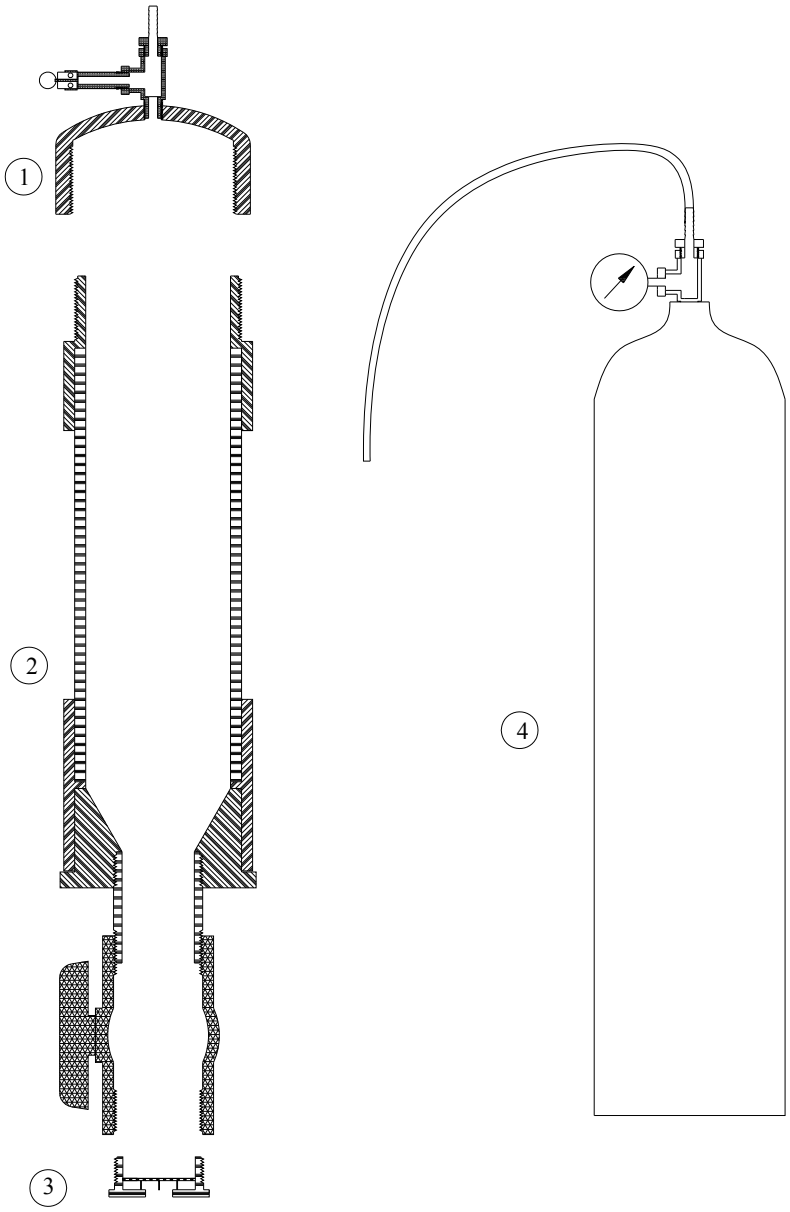

Fillability meter parts:
1. Top cap with attached barbed hose adapter for connecting with air supply
2. Grout vessel with 2 inch (51 mm) valve at hte bottom to control the flow of grout through filter.
3. Male pipe thread plug with filter.
4. Pressurized air supply cylinder.

Figure 4-10. Fillability Meter Parts for Use in Fillability Test.

The fillability test was performed on the Class C grouts. The steps to perform the test were:

- Mount the grout vessel (2) shown in Figure 4-10 to the table near the compressed air supply (4).

- Close the grout outlet valve at the bottom of grout vessel (2).
- Place a 2 inch (51 mm) diameter stainless steel wire cloth woven filter in the 2 inch (51 mm) Male Pipe Thread (MPT) Plug (3) and affix it to the ball valve of the grout vessel.
- Prepare a grout mixture following manufacturer's recommended w/p to produce at least 0.25 ft^3 (0.0071 m^3) of grout. Immediately after mixing, perform a flow cone test following Tex-437-A standard to measure the efflux time of the resulting grout mixture.
- Measure 4.23 pints (2000 ml) of freshly prepared grout in a scoop, pour it into the grout vessel (2) and close the top 4 inch (102 mm) cap with the threaded connection (1). Attach pressure hose to the ¼ inch (6.3 mm) barbed adapter and apply pressure equal to 20 psi (0.14 MPa).
- Maintain the pressure at 20 psi (0.14 MPa) and open the bottom 2 inch (51 mm) valve and collect the grout flowing through the filter in a 2.12 pints (1 l) graduated cylinder with a resolution of 0.02 pints (10 ml). Release the pressure if no grout or all grout flows through the filter. Measure the volume of grout collected in the graduated cylinder and document this volume.

After the fillability test is performed, a plot of volume passed versus the filter size can provide an indication of the filling ability of a particular grout. To express the fillability in terms of a number, the fillability index is defined as the average percent volume retained on the chosen filters. This can be defined in the same way as the fineness modulus of fine aggregates. The fillability index (FI) is expressed as:

$$FI = \frac{\sum_{i}^{n} \%VR_i}{100} \tag{4.2}$$

where n is the number of different sized filters, and $\%VR_i$ is the percentage of total volume retained on the ith filter.

Table 4-7 shows a typical observation table used to record the volume of grout passed through various filters. Columns 3 shows the filter sizes. Column 4 is used to record the volume of grout passed through the specific filter. Once the volume of grout passed through all filters has been recorded then the percent volume passed from the total volume of 4.23 pints (2000 ml) can

be calculated. The VR_i can be determined by subtracting the percent volume passed from 100. The fillability index can then be calculated using Equation (4.2). Higher values indicate coarser, less flowable grouts.

Table 4-7. Example Table Showing Observations for the Fillability Index.

Grout	Filter No.	Filter size, inch (μm)	Volume passed, pints (ml)	Percent volume passed	Percent volume retained (VRi)
(1)	(2)	(3)	(4)	(5)	(6)
Grout class	#10	0.08 (2032)	4.23 (2000)	100	0
	#12	0.065 (1651)	4.23 (2000)	100	0
	#16	0.054 (1372)	4.23 (2000)	100	0
	#20	0.034 (864)	4.23 (2000)	100	0
	#24	0.03 (762)	4.23 (2000)	100	0
	#30	0.021 (533)	2.94 (1390)	69.5	30.5
	#40	0.015 (381)	0.82 (390)	19.5	80.5
	#60	0.009 (229)	0.13 (60)	3	97
	#80	0.007 (178)	0.02 (10)	0.5	99.5
	#100	0.0055 (140)	0 (0)	0	100
			Fillability Index, FI =		4.1

4.4. RESULTS: GROUT MATERIAL CHARACTERISTICS

4.4.1. Fresh characteristics

The results on how mixer-type, mixture volume, and w/p influences the fresh characteristics of grout are presented in this section.

4.4.1.1. Wick-induced bleed

The wick-induced bleed test was performed for all grouts following Tex-441-A. Three tests for each grout mixture were performed and an average of three bleed cylinders was expressed as the overall percent bleed. Figure 4-11 and Figure 4-12 show the grout bleed results of the grouts for the three w/p values and both mixers. The research indicates that grouts C-1, C-2, and C-3 did not bleed. The Class A grout (w/p = 0.44) exhibited an average bleed of approximately 2 percent.

The Class C grouts (C-1, C-2, and C-3) meet the maximum permissible bleed recommended by the PTI 2003 and the current TxDOT specifications.

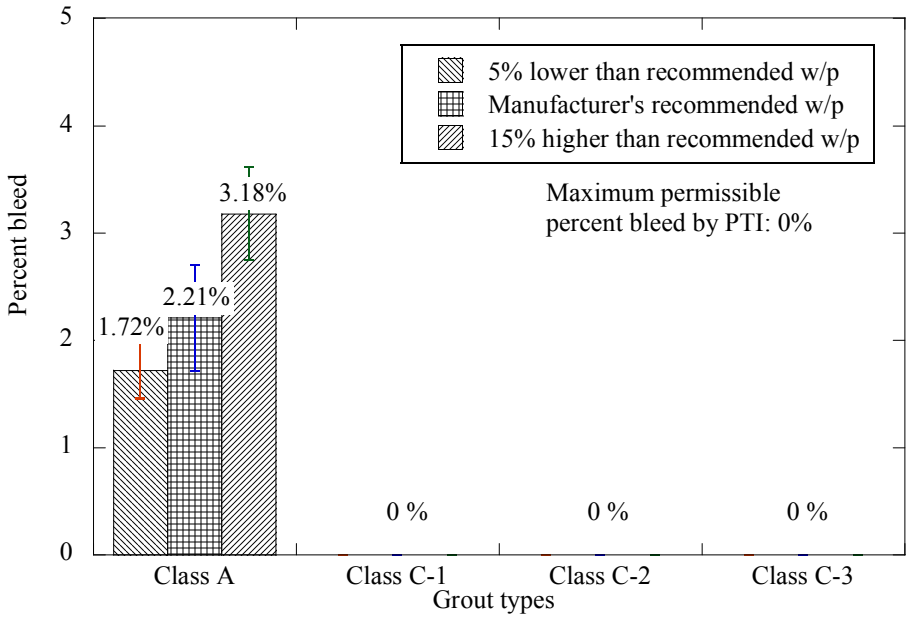

Figure 4-11. Wick-induced Bleed Results for Grouts Based on Different w/p Using M1 Mixer.

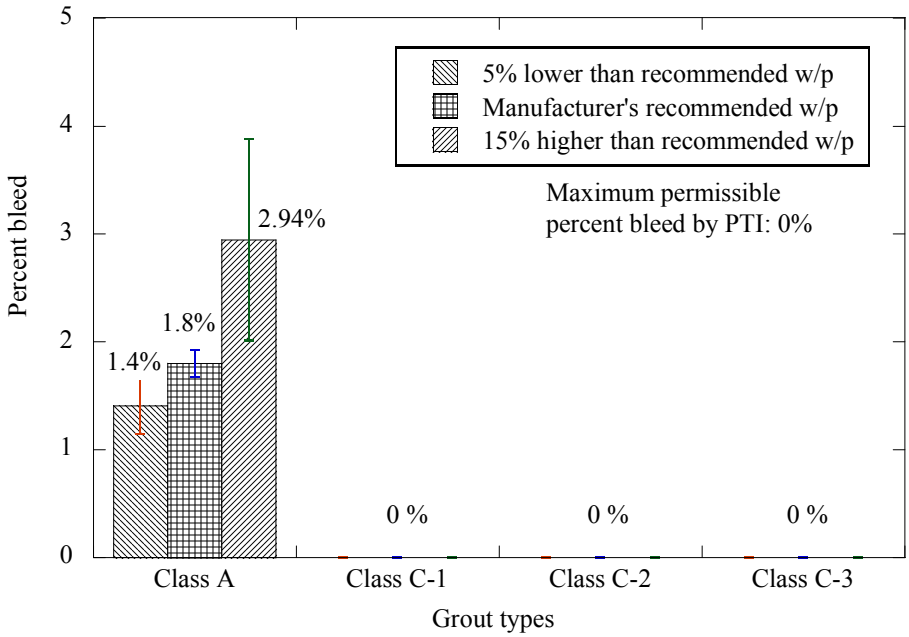

Figure 4-12. Wick-induced Bleed Results for Grouts Based on Different w/p Using M2 Mixer.

The variation of Class A grout bleed water with respect to the w/p, mixture volume, and mixer type is shown in Figure 4-13. Here, the L, R, and H represent the corresponding 5% lower (0.42), recommended (0.44), and 15% higher (0.51) w/p's, respectively. The values 0.25, 0.50, and 0.75 represent the size of the mixture volume as 0.25, 0.50, and 0.75ft^3 (0.0071, 0.0142, and 0.0213 m^3). Because a set of three bleed cylinders were tested for each mixture, the lines on the top of the bars represent the standard deviation in the bleed results obtained from three cylinders.

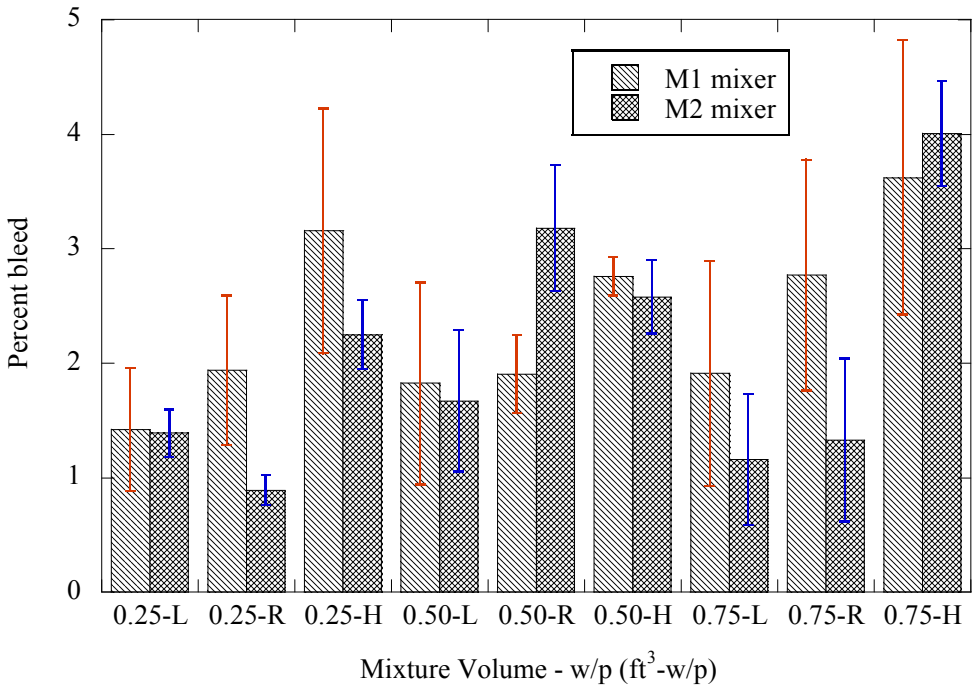

Figure 4-13. Wick-induced Bleed Results for Class A Grout.

A randomized single factor analysis of variance (ANOVA) test was performed to determine whether the change in mixture volume reduces the bleeding of grout. For the sake of simplicity, it was assumed that the percent bleed varies linearly with the mixture volume. By assuming a linear statistical model, the observations can be described as shown below:

$$Y_{ij} = \mu + \tau_i + \varepsilon_{ij} \begin{cases} i = 1, 2, ..., a \\ j = 1, 2, ..., n \end{cases} \tag{4.3}$$

where Y_{ij} is a random variable denoting the (*ij*)th observation, μ is a parameter common to all treatments referred to as the overall mean, τ_i is a parameter associated with the *i*th treatment called the *i*th treatment effect, and ε_{ij} is the random error component that is assumed to be normally distributed with a zero mean and σ^2 variance. The null hypothesis H_0 and alternate hypothesis H_1 formulated for this purpose are defined as shown below:

$$H_0 = \tau_1 = \tau_2 = \tau_3 = 0$$
$$H_1 = \tau_i \neq 0 \text{ for at least one } i \quad (4.4)$$

Assuming a 5% level of significance, the single factor ANOVA test results are presented in Table 4-8. From the analysis results, it can be concluded that sufficient evidence is not available to reject the null hypothesis H_0. Mixture volume does not significantly affect the percent bleed of the Class A grout.

Table 4-8. Single Factor ANOVA for Wick-induced Bleed Result of Class A Grout Assessing Effect of Mixture Volume on the Bleed.

Source of Variation	Sum of Squares	Degrees of freedom	Mean Sum of Squares	F statistic	F critical	*p*-value
Mixture volume	0.0017	2	0.0009	0.0017	5.14330	0.9983
Within (SSe)	3.1155	6	0.5193			
Total	3.1172	8				

Once it was identified that the mixture volume does not significantly affect the grout bleed, the effect of mixer type and w/p on the bleed rate were evaluated by assuming a two-factorial linear model as follows:

$$Y_{ijk} = \mu + \tau_i + \alpha_j + (\tau\alpha)_{ij} + \varepsilon_{ijk} \begin{cases} i = 1,2 \\ j = 1,2,3 \\ k = 1,...,9 \end{cases} \quad (4.5)$$

The hypotheses for both treatment variables (mixer type and w/p) and their interaction are shown as:

1. $H_0 = \tau_1 = \tau_2 = 0$
   $H_1 = \tau_i \neq 0$ for at least one i
2. $H_0 = \alpha_1 = \alpha_2 = \alpha_3 = 0$
   $H_1 = \alpha_j \neq 0$ for at least one j
3. $H_0 = (\tau\alpha)_1 = (\tau\alpha)_2 = ... = (\tau\alpha)_k = 0$
   $H_1 = (\tau\alpha)_k \neq 0$ for at least one k

(4.6)

Table 4-9 summarizes the results obtained from the two-factorial statistical analysis for the hypotheses discussed above. At a 5% level of significance it is concluded that the mixer type has no significant effect on the grout bleed whereas the w/p significantly affects the grout bleed. Because Class C grouts (C-1, C-2, and C-3) did not exhibit any bleed, no analysis is needed to evaluate the effect of either mixture volume, w/p, or the mixer type on the bleed.

Table 4-9. Two-factorial ANOVA for Wick-induced Bleed Result of Class A Grout Assessing Effect of Mixer Type and w/p on the Bleed.

Source of Variation	Sum of Squares	Degrees of freedom	Mean Sum of Squares	F statistic	F critical	*p*-value
Mixer Type	1	1	1	1.130	4.043	0.293
w/p	22	2	11	24.373	3.191	0.000
Interaction	0	2	0	0.261	3.191	0.772
Within (SSe)	22	48	0			
Total	44	53				

4.4.1.2. Viscosity

The time-dependent viscous behaviors of the grouts were studied. For each grout and mixture type viscosity measurements were taken for a minimum of 30 minutes. Figure 4-14 and Figure 4-15 show the viscosity as a function of time for the Class A, C-2, and C-3 grouts while mixing with their recommended w/p using the M1 and M2 mixers. The viscosity of the grouts increased with time as would be expected due to hydration.

The viscosity measurements show that grout C-2 exhibits a much lower viscosity when compared to grout C-3 at the corresponding manufacturer's recommended w/p. It was also observed that, for Class C grouts (C-2 and C-3) the mixture prepared with the M2 mixer resulted in relatively low viscous mixtures as compared to the mixture prepared with the M1 mixer. Class A grout showed a sharp increase in viscosity with time. This could be due to the initiation of hydration of the Class A grout. Based on the results obtained from the viscosity tests, it can be concluded that the Class C-2 grout exhibits lower viscosity values than the Class C-3 grout, making them more likely to fill voids.

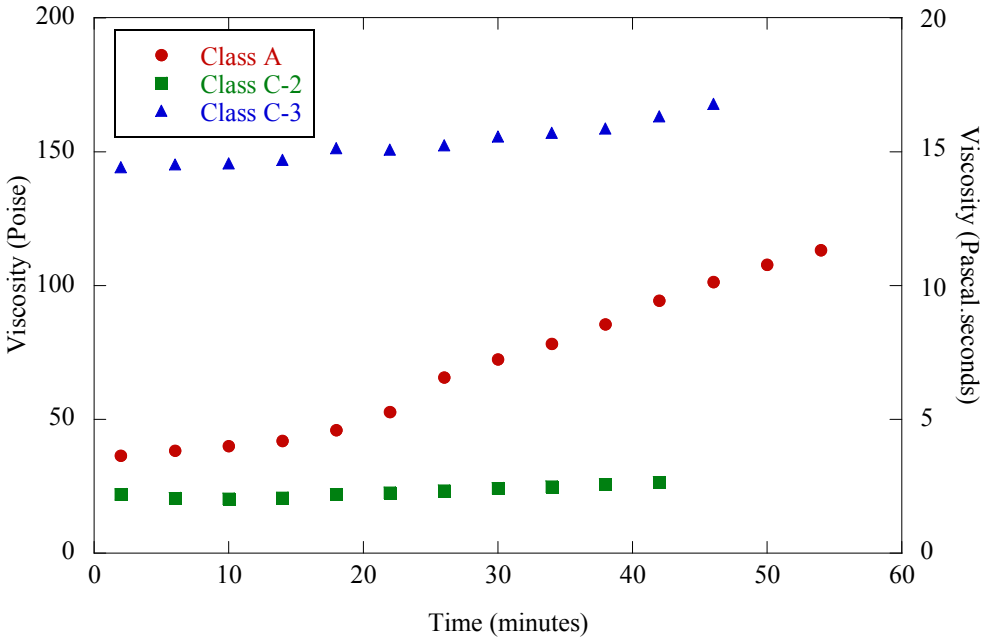

Figure 4-14. Time-dependent Viscosity of Class A, C-2, and C-3 Grouts Mixed with M1 mixer.

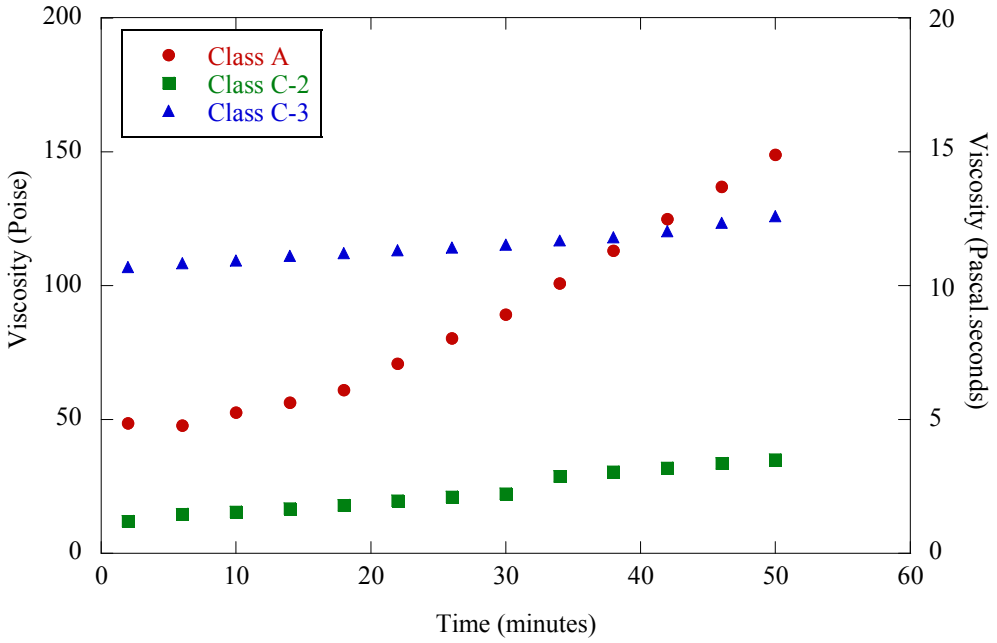

Figure 4-15. Time-dependent Viscosity of Class A, C-2, and C-3 Grouts Mixed with M2 Mixer.

To evaluate the effect of mixer type on the viscosity of grouts, a *t*-test was performed. In the null hypothesis, it is assumed that the mixer type does not produce any significant difference in viscosity. Hence, the null and alternate hypotheses are defined as follows:

$$H_0 : \mu_1 - \mu_2 = 0$$
$$H_1 : \mu_1 - \mu_2 \neq 0 \qquad (4.7)$$

where μ_1 and μ_2 are the average viscosities of grouts corresponding to M1 and M2 mixers, respectively. Table 4-10 shows the results of the *t*-test performed to compare the effect of mixer on the viscosity of grouts. Assuming a 0.05 level of significance, it is concluded that mixer type significantly affects viscosity of the Class C-3 grout. The M2 mixer results in lower viscosity values. It is also concluded that sufficient evidence is not available to reject the null hypotheses for Class A and C-2 grouts. Hence, mixer type does not significantly affect the viscosity of Class A and C-2 grouts. Although the viscosities of all grouts are not significantly affected by the mixer type, the M2 mixer could provide better mixing.

Table 4-10. Summary Statistics for the *t*-test to compare Effect of Mixer on the Viscosity of Grout.

Source of Variation	Grout	t_0	*t* critical	*p*-value
Mixer Type	A	1.802	2.379	0.087
	C2	0.003	2.379	0.998
	C3	12.499	2.379	0.000

4.4.1.3. Fluidity

The fluidity of the grouts can be assessed by evaluating the efflux time for each grout mixture. One test was performed for each mix as specified by the Tex-437-A specifications. The currently accepted values for efflux time according to the Tex-437-A standard are:

- Between 9 and 20 seconds for efflux time measured immediately after mixing,
- Less than 30 seconds for efflux time measured 30 minutes after the mixing.

The results obtained from the testing are shown in Figure 4-16, Figure 4-17, Figure 4-18, and Figure 4-19. These figures show the variation of the efflux time as the mixture volume changes. The efflux time measurements shown in these graphs are from mixes with w/p values equal to their manufacturers' recommended w/p and using M1 and M2 mixers for mixing.

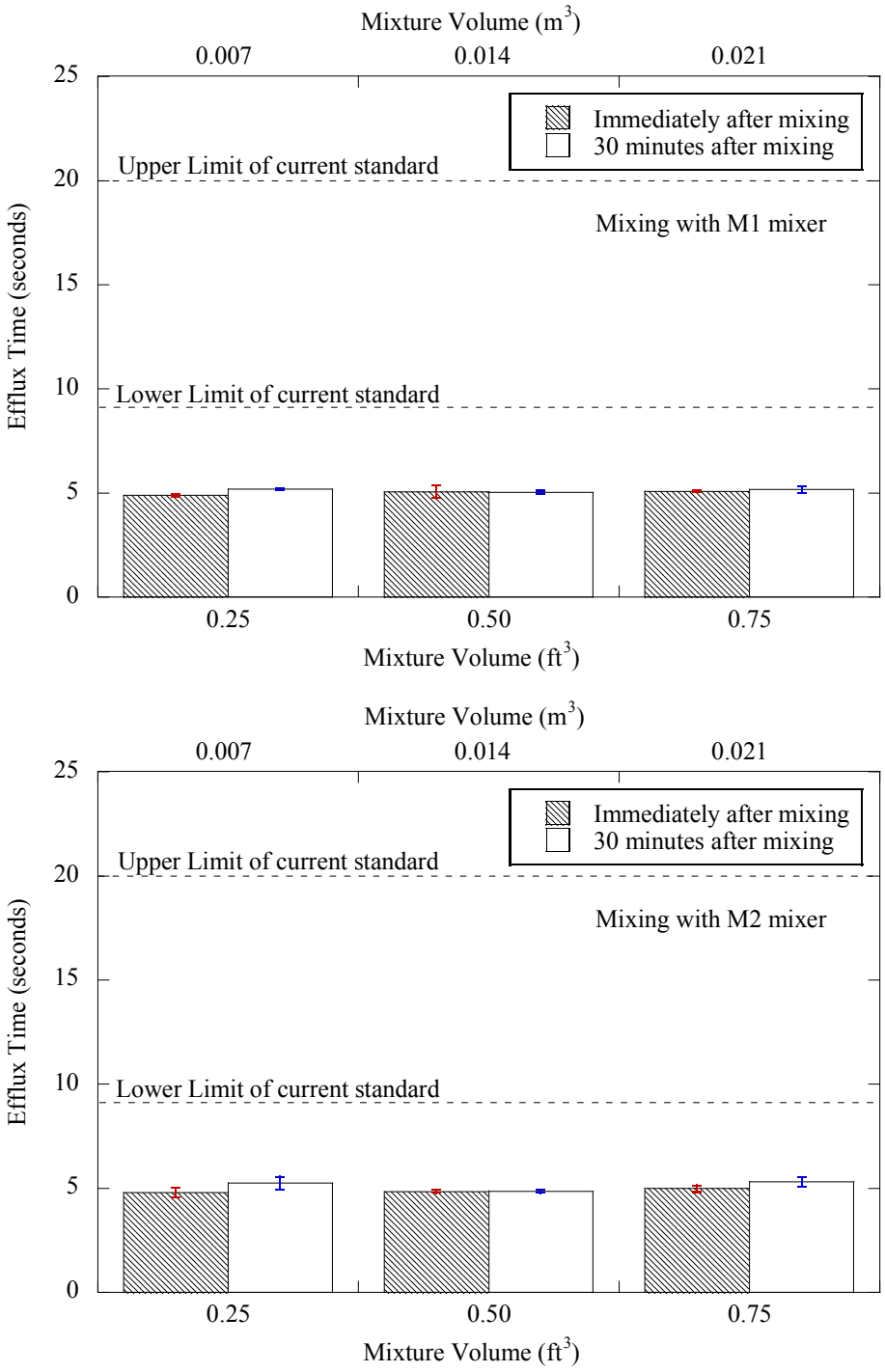

Figure 4-16. Efflux Time versus the Volume of Mixture for Class A Grout: (a) Using M1 Mixer and (b) Using M2 Mixer.

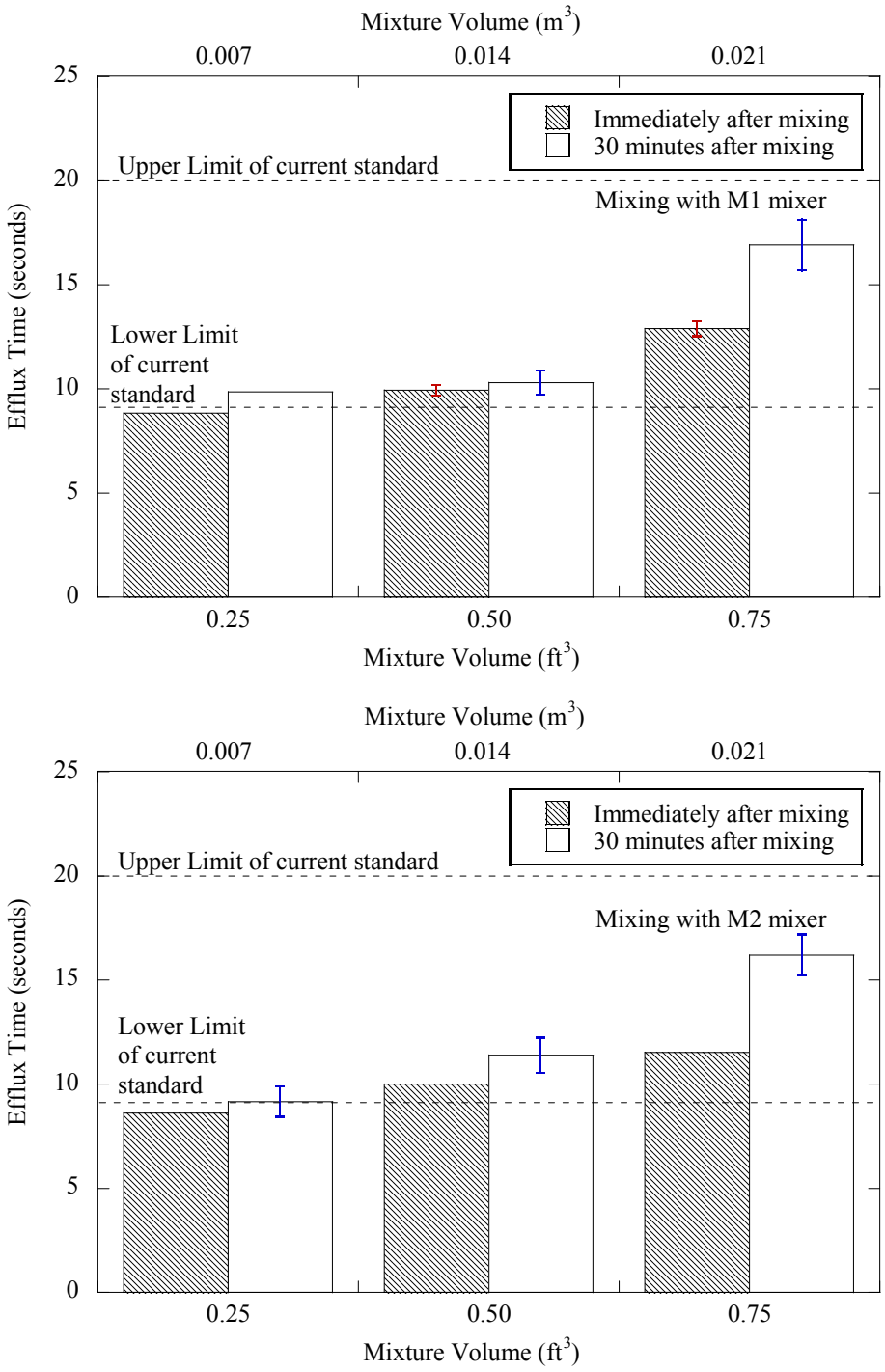

Figure 4-17. Efflux Time versus the Volume of Mixture for Class C-1 Grout: (a) Using M1 Mixer and (b) Using M2 Mixer.

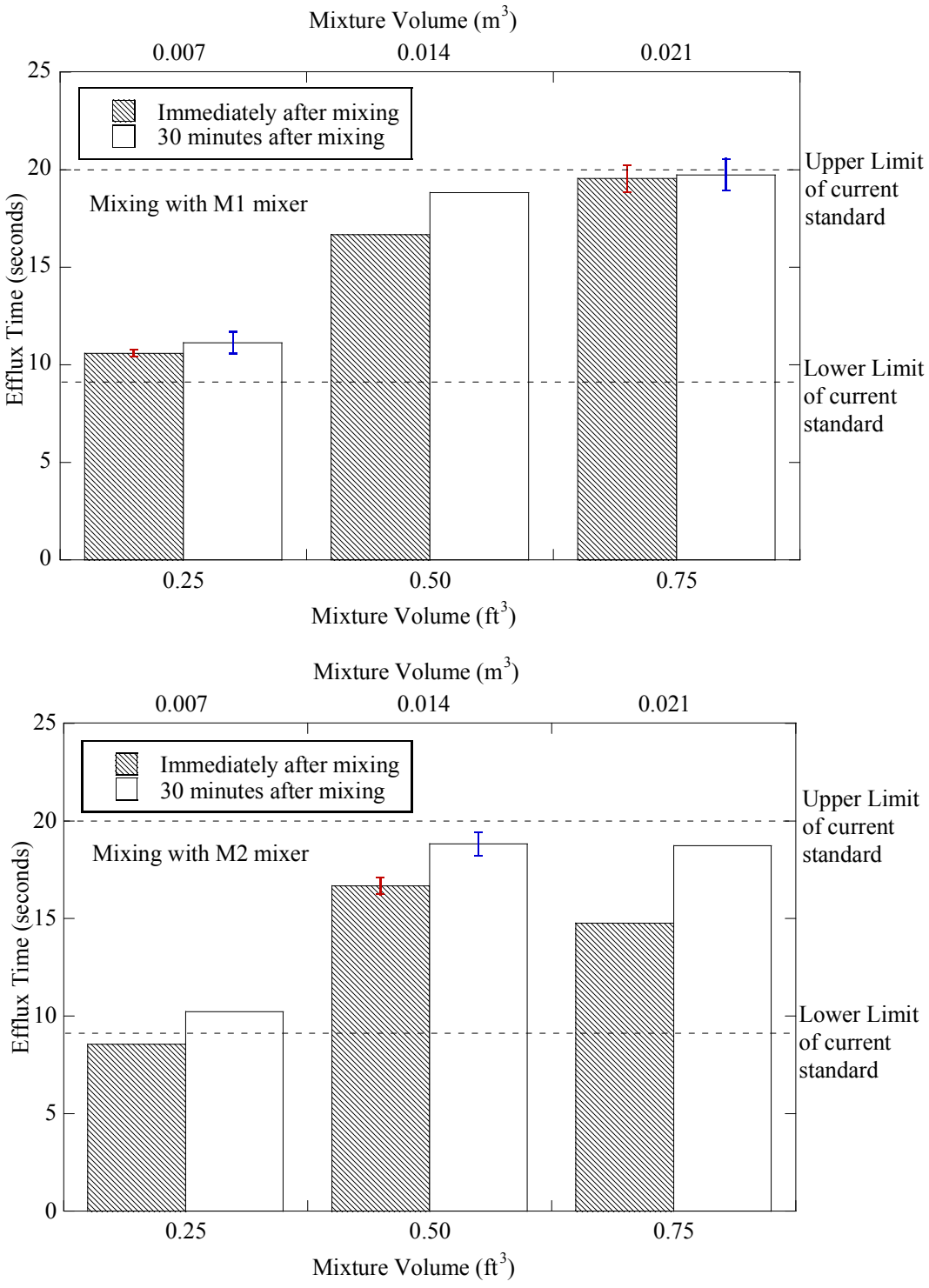

Figure 4-18. Efflux Time versus the Volume of Mixture for Class C-2 Grout, (a) Using M1 Mixer and (b) Using M2 Mixer.

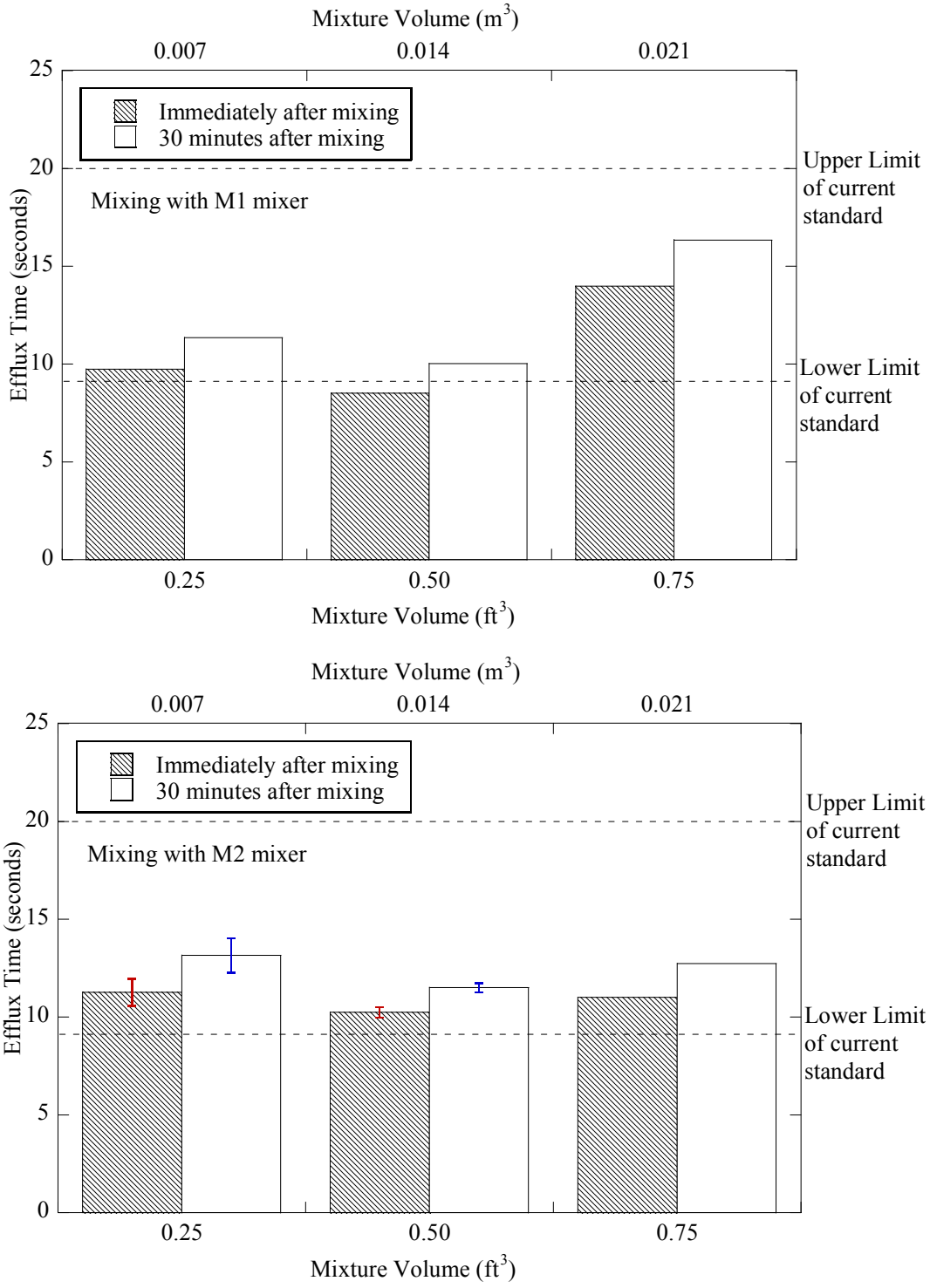

Figure 4-19. Efflux Time versus the Volume of Mixture for Class C-3 Grout, (a) Using M1 Mixer and (b) Using M2 Mixer.

A general observation can be made that as the mixture volume increases from 0.25 ft^3 (0.0071 m^3) to 0.75 ft^3 (0.0213 m^3), the efflux time increases. A comparison can be made between the efflux times of all grouts, which concludes that Class A has a lower efflux time as compared to other grouts, although Class A grout does not meet the current TxDOT minimum efflux time requirements (minimum 9 seconds).

Figure 4-20 (a) and (b) show the sensitivity of efflux time as a function of w/p for the grouts mixed with M1 and M2 mixers respectively. The base case for the w/p sensitivity analysis is the manufacturer's recommended w/p for all grouts. Experiments were performed for the recommended w/p, a w/p 5% lower than that recommended by the manufacturer, and a w/p 15% higher than that recommended by the manufacturer.

From Figure 4-20, it can be seen that as the w/p increases the efflux time decreases. The Class C-1 and C-3 grouts have nearly the same efflux time for the corresponding w/p. The C-2 grout has a lower efflux time when compared to the Class C-1 and C-3 grouts.

One reason for this could be that the Class C-2 grout has a manufacturer's recommended w/p of 0.26 which is lower than that for Class C-1 and C-3 grouts. It should also be pointed out that the efflux time of the grouts mixed with M2 mixer were lower than the corresponding efflux times using the M1 mixer.

The viscosity results for Class C-2 and C-3 grouts (Figure 4-14 and Figure 4-15) also indicate that the viscosity values of these grouts were higher while mixing with the M1 mixer when compared to the M2 mixer. A higher viscosity indicates higher efflux time. It can be concluded that mixing with a higher rpm mixer results in a more fluid grout mixture.

Grouts C-1, C-2, and C-3 do not meet the current TxDOT's requirements for minimum efflux time as the w/p is increased to 15% of the manufacturer's recommended w/p. It should be noted that the recommended w/p should be achieved in the field.

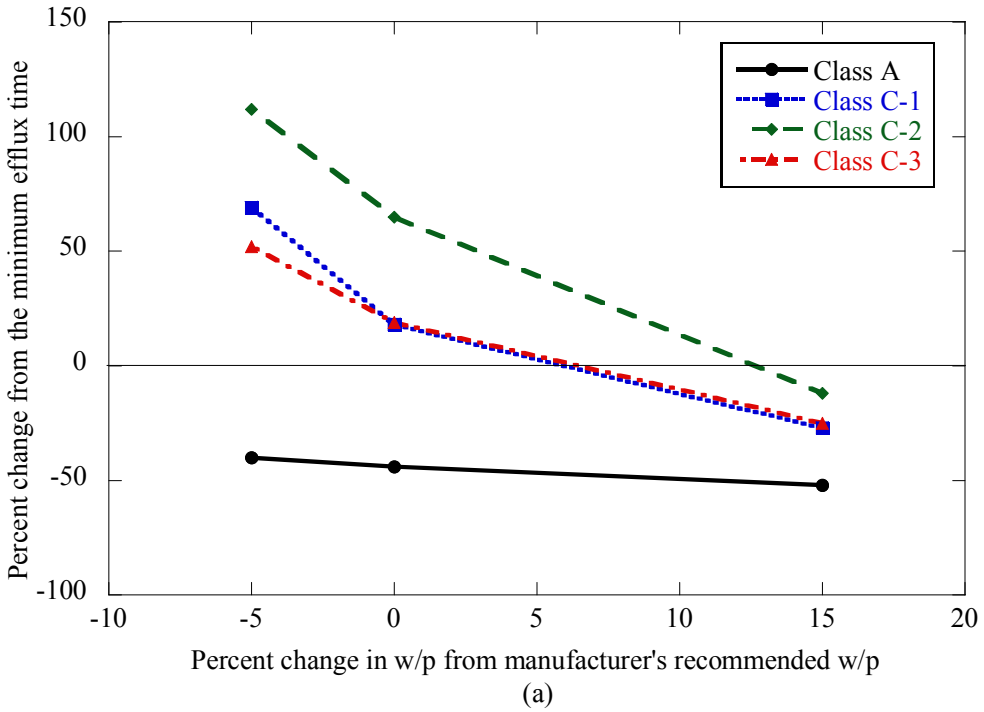

(a)

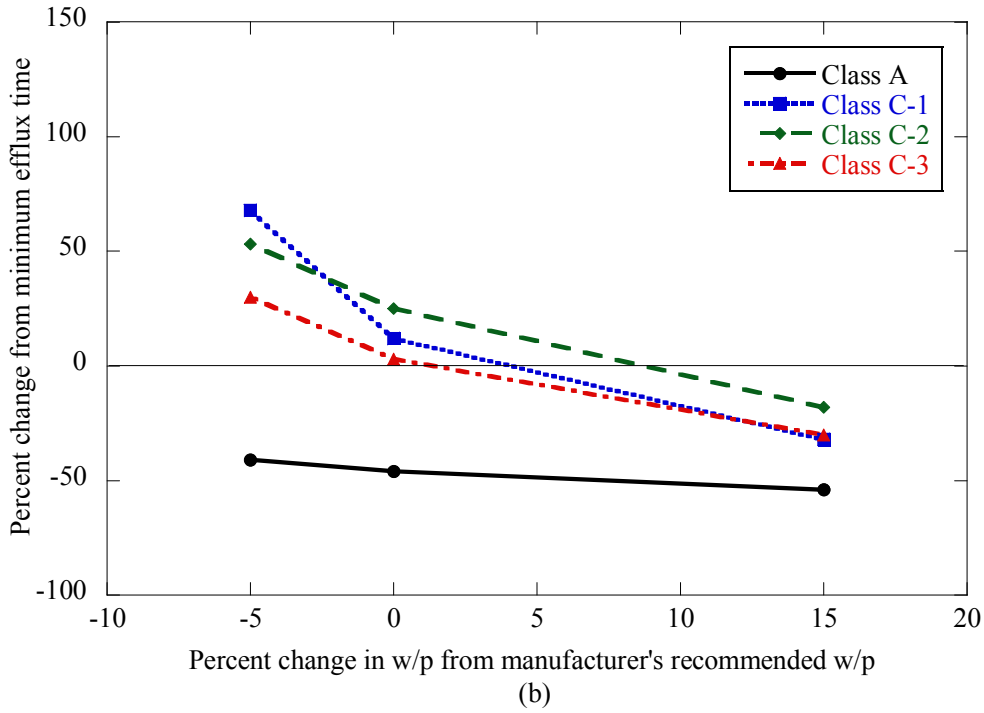

(b)

Figure 4-20. Efflux Time Sensitivity to the w/p for All Four Grout Types (a) Using M1 Mixer, and (b) Using M2 Mixer.

Three mixture volumes were used in the test matrix to study the effect of mixing volume on the efflux time of grouts. A randomized complete block design (RCBD) model was used to test the effect of mixture volume. The linear statistical model is represented by Equation (4.8) shown below:

$$Y_{ij} = \mu + \tau_i + \beta_j + \varepsilon_{ij} \begin{cases} i = 1,2,3 \\ j = 1,2,3 \end{cases} \tag{4.8}$$

where μ is the overall mean efflux time, τ_i is the effect of the *i*th treatment (mixture volume), β_j is the *j*th block (w/p), and ε_{ij} is the random error term, which is assumed to be independent and normally distributed with a mean of zero and variance σ^2. To test the equality of the treatments effects (mixture volume), the RCBD is used and it is assumed that the treatment and blocks (w/p) do not interact. The testing hypotheses are shown in Equation (4.9) below:

$$\begin{aligned} &H_0 = \tau_1 = \tau_2 = \tau_3 = 0 \\ &H_1 = \tau_i \neq 0 \text{ for at least one } i \end{aligned} \tag{4.9}$$

A summary of the RCBD ANOVA results is shown in the Table 4-11. The *p*-value for the analysis performed on Class A is close to 0.05, hence assuming the test statistic it can be conclude that the mixture volume has significant influence on the efflux time of Class A grout. However, at a 5% level of significance, the null hypothesis cannot be rejected for any of the

three Class C grouts under study. Hence, it can be concluded that the mixture volume does not significantly affect the efflux time at a 5% level of significance.

Table 4-11. Summary Statistics of RCBD ANOVA Test with Mixture Volume as Treatments.

Source of Variation	Grout	F-statistic	F critical	*p*-value
Mixture Volume	Class A	6.505	6.944	0.055
	Class C-1	3.372	6.944	0.139
	Class C-2	5.907	6.944	0.064
	Class C-3	1.719	6.944	0.289

The effect of mixer type was studied to evaluate whether mixer type influences grout characteristics and to determine whether one mixer type is more effective than another. Two small mixers M1 and M2 with helical paddles were used to study the effect of the mixer type on grout characteristics. Efflux time observations were averaged from the three mixture volume test results obtained and used in statistical analysis. To study the effect of mixer type on the efflux time, a RCBD analysis of variance was performed. Equation (4.10) represents the linear statistical model:

$$Y_{ij} = \mu + \tau_i + \beta_j + \varepsilon_{ij} \begin{cases} i = 1,2 \\ j = 1,2,3 \end{cases} \tag{4.10}$$

where μ is an overall mean, τ_i is the effect of the *i*th treatment, β_j is the *j*th block, and ε_{ij} is the random error term, which is assumed to be normally and independently distributed with mean zero and variance σ^2. The testing hypotheses are shown in Equation (4.11):

$$H_0 = \tau_1 = \tau_2 = 0$$
$$H_1 = \tau_i \neq 0 \text{ for at least one } i \tag{4.11}$$

A summary of the RCBD ANOVA results is shown in the Table 4-12. The test results indicate that, at a 5% level of significance, the null hypothesis cannot be rejected, for any of the Class C grouts under study. It can be concluded that the mixer types used in the study do not significantly affect the efflux time for Class C grouts. Efflux time of the Class A grout, on the other hand, is significantly affected by the mixer type at the 5% level of significance.

Table 4-12. Summary Statistics for RCBD ANOVA with Mixer Type as Treatments.

Source of Variation	Grout	F-statistic	F critical	*p*-value
Mixer Type	Class A	158.281	18.513	0.006
	Class C-1	6.675	18.513	0.123
	Class C-2	5.312	18.513	0.148
	Class C-3	1.791	18.513	0.313

It was determined from the analysis that the mixer type has no significant effect on the fluidity of Class C grouts, which means that the any of the two mixers (M1 and M2) can be used for mixing the grout. However, from a practical point of view, it is advisable to use the higher speed mixer (M2 mixer) to achieve a more homogenous and consistent grout mixture. There are some issues associated with the M2 mixer. The M2 mixer overheated when more than one bag of grout mixture was mixed. This problem was solved by using two similar mixers and using the second one when the first mixer started overheating. Hence, it is recommended that if the M2 mixer is used then:

- not more than one bag of grout should be mixed at once
- have two mixers and use one after the other in case of overheating of the mixer

Grout fluidity is an indirect measure of the viscosity of the grout and a correlation may exist between these characteristics. To carry out correlation analyses between the efflux time and viscosity, viscosity measurements immediately after mixture (time zero) and 30 minutes after the mixture were extracted from the collected data. A correlation analysis was then performed between the two corresponding measurements for each grout type.

The correlation coefficients between the efflux time and the grout viscosity for all grouts were evaluated. The correlation coefficient typically ranges from -1 to 1. A correlation coefficient of zero indicates no correlation between the efflux time and viscosity, a correlation coefficient close to 1 indicates a good positive correlation between the efflux time and viscosity, whereas a correlation coefficient close to negative one (-1) indicates a good negative correlation between the same.

Table 4-13 and Table 4-14 illustrate the correlation coefficients for the Class A, C-2, and C-3 grouts mixed with the different mixers. The Class C-1 grout is not included in the correlation analysis because the viscosity tests were not performed on the Class C-1 grout. The correlation coefficients between the efflux time and viscosity of the grouts came out to be greater than 0.7 which demonstrate that a higher efflux time implies higher viscosity. It can be concluded that a lower efflux time indicates in lower viscosity which corresponds to higher fluidity.

While preparing the grout mixtures, the actual rotation speeds of both mixers were measured using a tachometer. A correlation analysis was performed to study the correlation between the actual mixer rotation speed and efflux time of the resulting mixture. The correlation coefficients between the efflux time and the actual rpm for all grouts were evaluated and are shown in Table 4-15 and Table 4-16. Results show the correlation coefficient from the M1 and M2 mixers for the Class A, C-1, C-2 and C-3 grouts.

Table 4-13. Correlation Coefficients between Efflux Time and Viscosity for Class A, C-2, and C-3 Grouts Mixed with M1 Mixer.

Viscosity		Efflux Time					
		Class A		Class C-2		Class C-3	
		0 min	30 min	0 min	30 min	0 min	30 min
Class A	0 min	0.979	-	-	-	-	-
	30 min	-	0.904	-	-	-	-
Class C-2	0 min	-	-	0.981	-	-	-
	30 min	-	-	-	0.989	-	-
Class C-3	0 min	-	-	-	-	0.782	-
	30 min	-	-	-	-	-	0.764

Table 4-14. Correlation Coefficients between Efflux Time and Viscosity for Class A, C-2, and C-3 Grouts Mixed with M2 Mixer.

Viscosity		Efflux Time					
		Class A		Class C-2		Class C-3	
		0 min	30 min	0 min	30 min	0 min	30 min
Class A	0 min	0.774	-	-	-	-	-
	30 min	-	0.533	-	-	-	-
Class C-2	0 min	-	-	0.986	-	-	-
	30 min	-	-	-	0.919	-	-
Class C-3	0 min	-	-	-	-	0.850	-
	30 min	-	-	-	-	-	0.841

Table 4-15. Correlation Coefficients between Efflux Time and Mixer rpm for Class A, C-1, C-2, and C-3 Grouts Mixed with M1 Mixer.

Actual rpm	Efflux Time			
	Class A	Class C-1	Class C-2	Class C-3
Class A	-0.4735			
Class C-1		-0.4738		
Class C-2			-0.4172	
Class C-3				-0.2028

Table 4-16. Correlation Coefficients between Efflux Time and Mixer Speed for Class A, C-1, C-2, and C-3 Grouts Mixed with M2 Mixer.

Actual rpm	Efflux Time			
	Class A	Class C-1	Class C-2	Class C-3
Class A	-0.4332			
Class C-1		-0.1989		
Class C-2			-0.6853	
Class C-3				-0.4237

The correlation coefficients between the efflux time and mixer rpm for most grouts are between -0.5 and 0, which indicates a weak negative correlation between the efflux time and actual mixing speed. This negative correlation between the efflux time and mixer rpm is expected because as the mixer rpm increases the mixture becomes more fluid which in turn results in a mixture with a lower efflux time. Hence, the efflux time of the mixture decreases as the mixer rpm increases. The speed of the mixer depends on the w/p and the volume of the mixture. When the w/p increases, the mixer rotates at a faster speed. When the mixture volume increases, the mixer rotating speed decreases. Figure 4-21 shows the variation of mixer rpm with the change in w/p for the M1 and M2 mixers. It can be concluded from the results that as the w/p increases the mixer rpm increases. Similarly Figure 4-22 shows the variation of mixer rpm as the volume of mixture changes from 0.25 ft^3 (0.007 m^3) to 0.75 ft^3 (0.021 m^3) for M1 and M2 mixers.

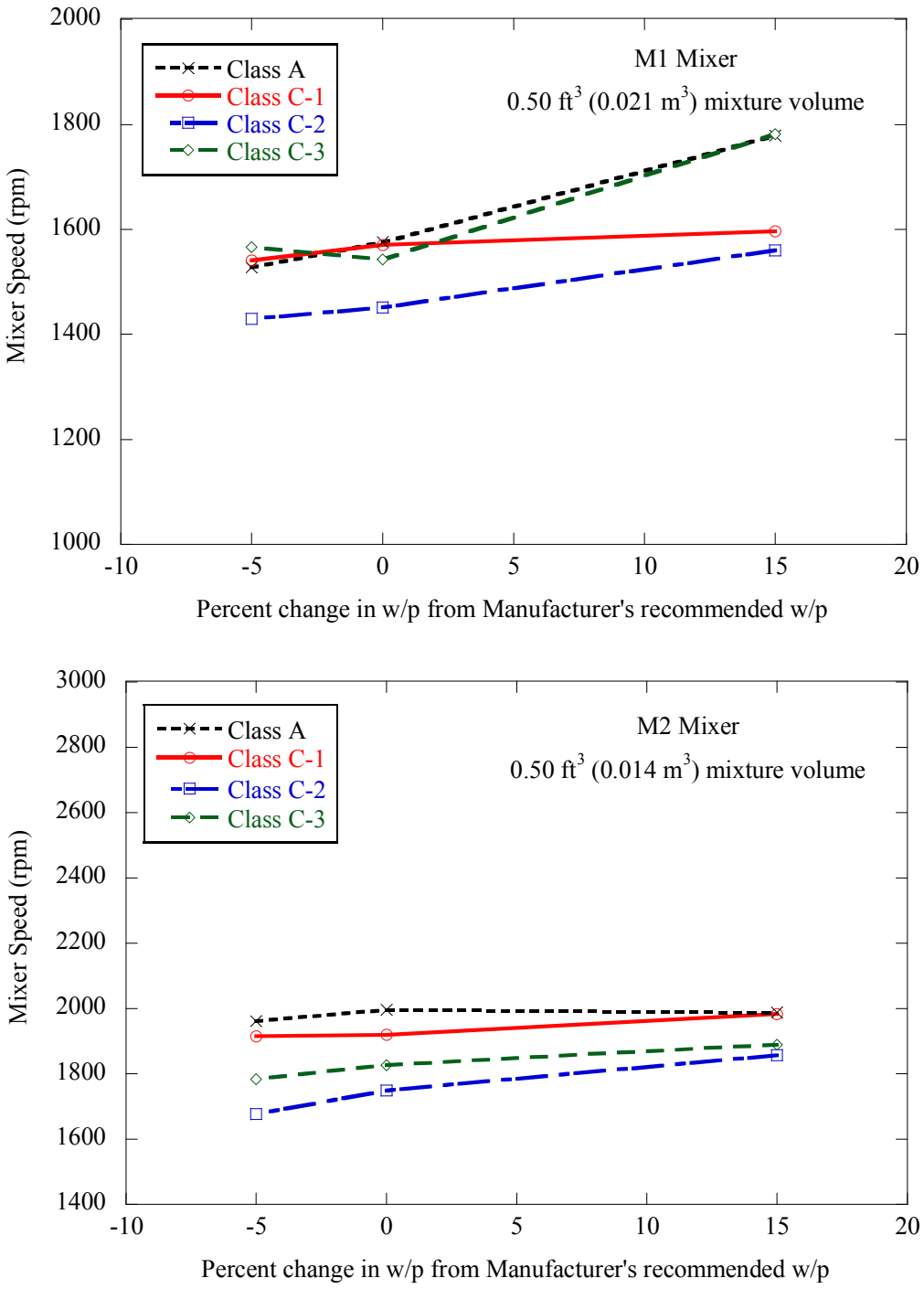

Figure 4-21. Change in Mixer Speed with the Grout's w/p for Both (a) M1 and (b) M2 Mixers.

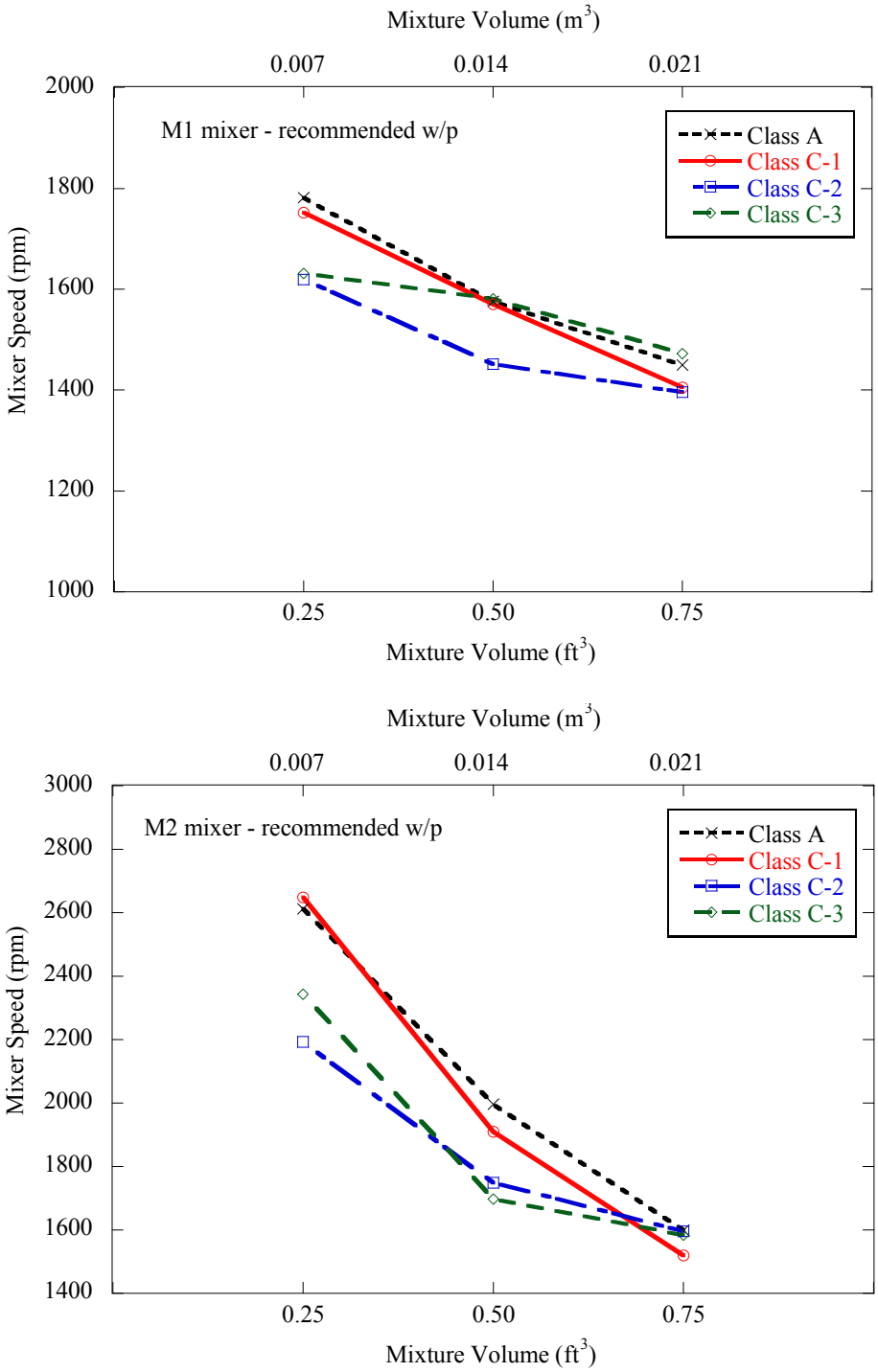

Figure 4-22. Change in Mixer Speed with Mixture Volume for Both (a) M1 and (b) M2 Mixers.

The M1 mixer shows more scatter when compared to the M2 mixer results for increasing w/p. However, the M2 mixer shows more scatter when compared to the M1 mixer as the mixture

volume changes. Because a higher speed mixer is desirable to achieve high shearing during mixing, the M2 mixer may provide a better shearing action with the higher average speed when compared to the M1 mixer.

4.4.1.4. Wet density

The Baroid mud balance was used to measure the wet density of freshly prepared grout mixtures. The average grout density and the range of grout density obtained from the tests for the recommended w/p mixtures are presented in the Table 4-17. The test results indicate that the range of Class C-1 and C-3 grouts is narrow and shows very little variation of grout density.

These grout ranges were calculated by performing repeat tests on all grouts to evaluate the variability of the mud balance test. These lower and upper grout ranges were approximately plus or minus one standard deviation ($\pm 1\sigma$), which is approximately equal to plus or minus 0.5 percent of the mean grout wet density.

Table 4-17. Average Grout Density Measured Using Baroid Mud Balance.

Grout type	Density		Density Range			
	lb/gal	g/cm^3	Minimum		Maximum	
			lb/gal	g/cm^3	lb/gal	g/cm^3
Class A	15.62	1.87	15.5	1.86	15.7	1.88
Class C-1	17.57	2.11	17.5	2.10	17.6	2.11
Class C-2	17.55	2.10	17.4	2.08	17.7	2.12
Class C-3	16.35	1.96	16.3	1.95	16.4	1.97

To determine the relationship between the w/p, dry density, and the wet density, tests were performed to evaluate the dry density as described in Section 4.3.4. Table 4-18 shows the dry density for Class C grouts along with their corresponding manufacturer's recommended w/p and wet densities.

Table 4-18. Dry and Wet Densities of Class C Grouts along with Corresponding Manufacturer's Recommended w/p.

Grout type	w/p	Dry Density		Wet Density	
		lb/gal	g/cm^3	lb/gal	g/cm^3
Class C-1	0.30	7.1	0.85	17.5	2.10
		7.0	0.84	17.5	2.10
		7.1	0.85	17.6	2.11
Class C-2	0.26	9.1	1.09	17.4	2.08
		9.1	1.09	17.6	2.11
		9.0	1.08	17.5	2.10
Class C-3	0.27	8.2	0.98	16.3	1.95
		7.9	0.95	16.4	1.97
		8.1	0.97	16.3	1.95

Using the observations shown in Table 4-18, the following model was developed to predict the theoretical wet density of the resultant grout mixture:

$$\rho_{\text{predicted}} = \theta_0 + \theta_1\left(\text{w/p}\right) + \theta_2\left(\rho_{\text{dry}}\right) + \sigma\varepsilon \tag{4.12}$$

where $\rho_{\text{predicted}}$ is the theoretical wet density predicted by the model, ρ_{dry} is the grout's dry density, θ_0, θ_1, and θ_2, are model parameters, σ is the model error and ε is the random error term and assumed to be normally distributed with a zero mean and unit standard deviation. The term $\sigma\varepsilon$ is collectively called as model error.

The posterior statistics of the wet density model are shown in Table 4-19. The regression coefficients for the linear regression model are shown in column 2. A *t*-test was also performed to determine whether the independent model variables (w/p and the ρ_{dry}) are significant. The *p*-values show that at 5% level of significance, the model variables are significant and the linear

regression model holds good. The R^2 value for the regression model was determined to be 0.87, which indicates that the model accounts for about 87% of the variability in the wet density.

Table 4-19. Posterior Statistics of the Wet Density Model.

Model Name	MAPE (%)	Parameters	Mean	Standard Deviation	CoV	Correlation Coefficients between θ_i	
						θ_0	θ_1
Wet Density	1.02	θ_0	-28.4	9.1	-0.32	1	
		θ_1	104.6	20.7	0.20	-0.99	1
		θ_2	2.1	0.4	0.21	-0.98	0.96

The mean absolute percent error (MAPE) of the wet density model is 1.02% which is a reasonable value. The model standard deviation, σ, is also reasonable (i.e., 0.31) considering the limited amount of data available and the inherent scatter observed among data points.

The wet density model developed to predict the grout's wet density is given by the Equation (4.13):

$$\rho_{\text{predicted}} = -28.4 + 104.6\left(\text{w/p}\right) + 2.1\left(\rho_{\text{dry}}\right) \tag{4.13}$$

Using this linear model shown in Equation (4.13), the grout's wet density can be predicted by using the w/p and dry density and can be compared with the observed grout's wet density (ρ_{observed}) measured in the field using the Baroid mud balance test. The validation plot for wet density model is shown in Figure 4-23. This plot indicates that the model provides a reasonably good prediction of the observed grout's wet density.

Based on the accuracy of the model, it can be concluded that if the ρ_{observed} falls within the one standard deviation region ($\sigma = \pm 0.31$) of $\rho_{\text{predicted}}$ then no serious alteration in the grout's w/p

is observed in the field. Equation (4.14) presents the criterion relating the $\rho_{observed}$ (measured using Baroid mud balance test in the field) with $\rho_{predicted}$ [calculated using the Equation (4.13)].

$$\rho_{observed} = \rho_{predicted} \pm 0.31 \tag{4.14}$$

The Baroid mud balance test can be used in the field as a quality control measure. Any significant change in grout wet density can be determined instantly and necessary actions should be taken to ensure proper grouting of PT ducts. Therefore, the Baroid mud balance test is recommended in the field. The observed wet density can be compared with the manufacturer's specified wet density corresponding to the w/p.

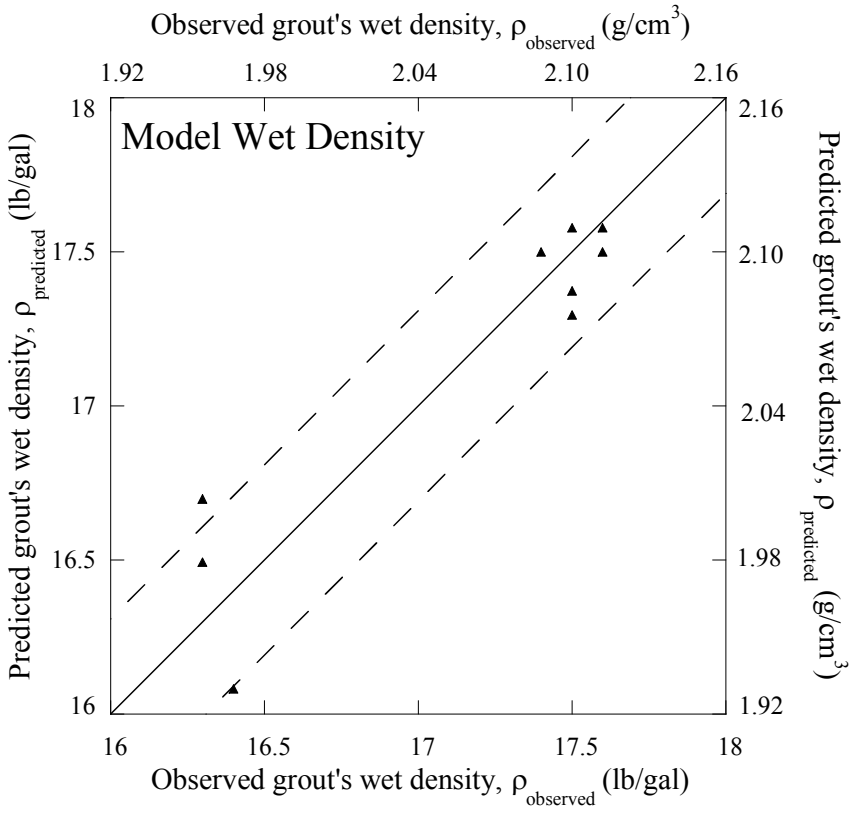

Figure 4-23. Validation Plot for the Wet Density Model.

4.4.1.5. Initial setting time

The initial setting time results for the grouts are shown in Figure 4-24 and Figure 4-25 when mixing with M1 and M2 mixers respectively. All grouts used in the research (Class A, C-1, C-2, and C-3 grouts) exhibit an initial setting time between 4 and 11 hours, which fulfills the current TxDOT requirements.

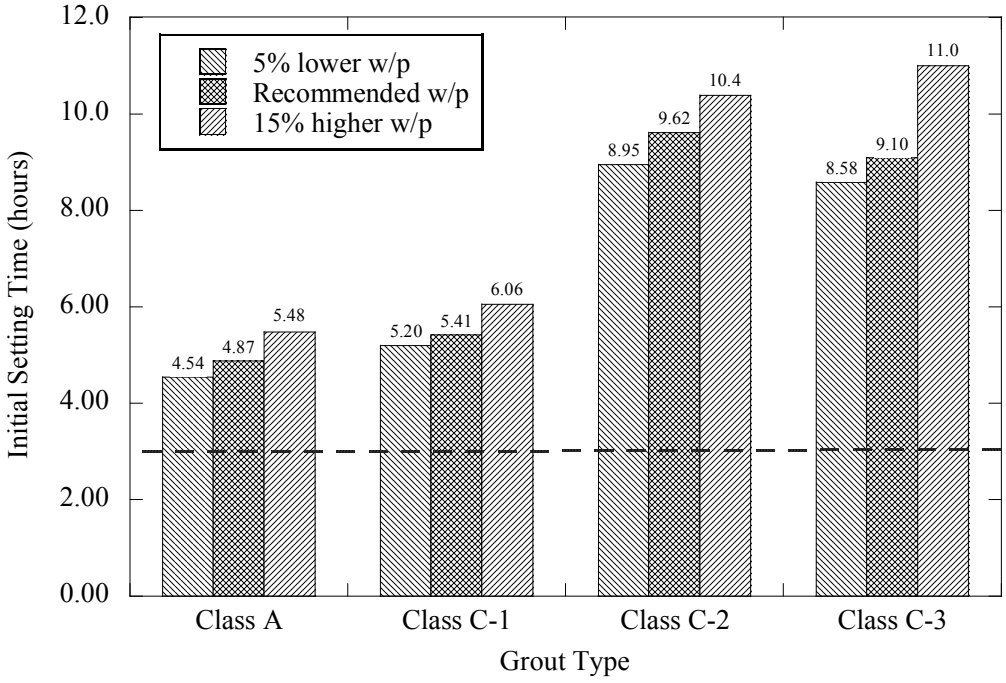

Figure 4-24. Initial Setting Time for Class A, C-1, C-2 and C-3 Grouts when Mixed with M1 Mixer.

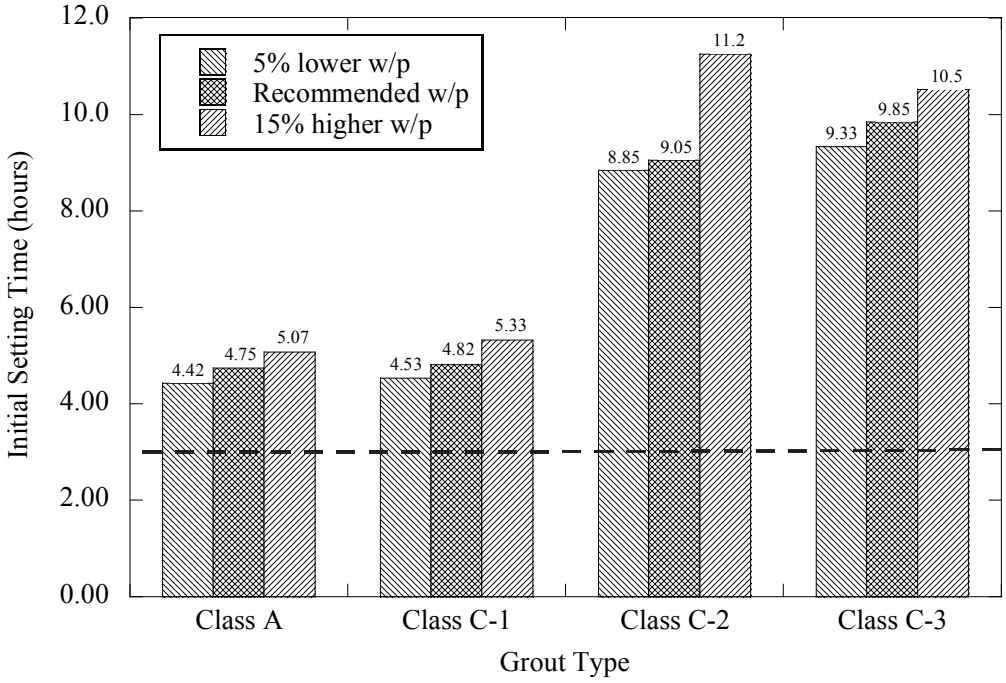

Figure 4-25. Initial Setting Time for Class A, C-1, C-2 and C-3 Grouts when Mixed with M2 Mixer.

Although initial setting time is not related to the workable time of the grout, it is assumed that grouts with a low initial setting time tends to stiffen early, thereby reducing the time available to successfully place the grout without significant loss in other grout characteristics. All initial setting tests were performed in the laboratory where the temperature and other climatic conditions were controlled, and it should be noted that the conditions are not controlled in the field while grouting the PT ducts. The temperature in the field may be higher than the laboratory temperature which can accelerate the initial setting of grouts. Hence, from a practical point of view, less time will be available to place the grout in the field in hot temperatures.

It is therefore recommended that the minimum required lower initial setting time is increased from three hours to four hours. It is assumed that there is a chance that an increase in the initial setting time can increase the time available to place the grout in the field.

4.4.2. Hardened characteristics

Compressive strength and dimensional stability results are presented in this section.

4.4.2.1. Compressive strength

The compressive strength test was performed on all four grouts for five different test ages following the Tex-442-A. At each test age, an average of 3 cube strengths was reported. Figure 4-26, Figure 4-27, and Figure 4-28 show the average compressive strength for all grouts at 1, 3, 7, 28, and 56 day test ages. Values are reported for the manufacturer's recommended w/p, and -5% and +15% of the manufacturer's recommended w/p. Values were averaged for the M1 and M2 mixers.

One-day strengths were higher in the Class C-1 grout while at 3, 7, 28, and 56 days, the average compressive strength for both Class C-1 and C-2 grouts are nearly the same. The Class C-3 grout results indicate low strengths when compared to the Class C-1 and C-2 grouts at all five sample ages. The Class A grout results in a much lower strength when compared to the Class C-1, C-2, and C-3 grouts. However, all strengths are sufficient for use in PT systems.

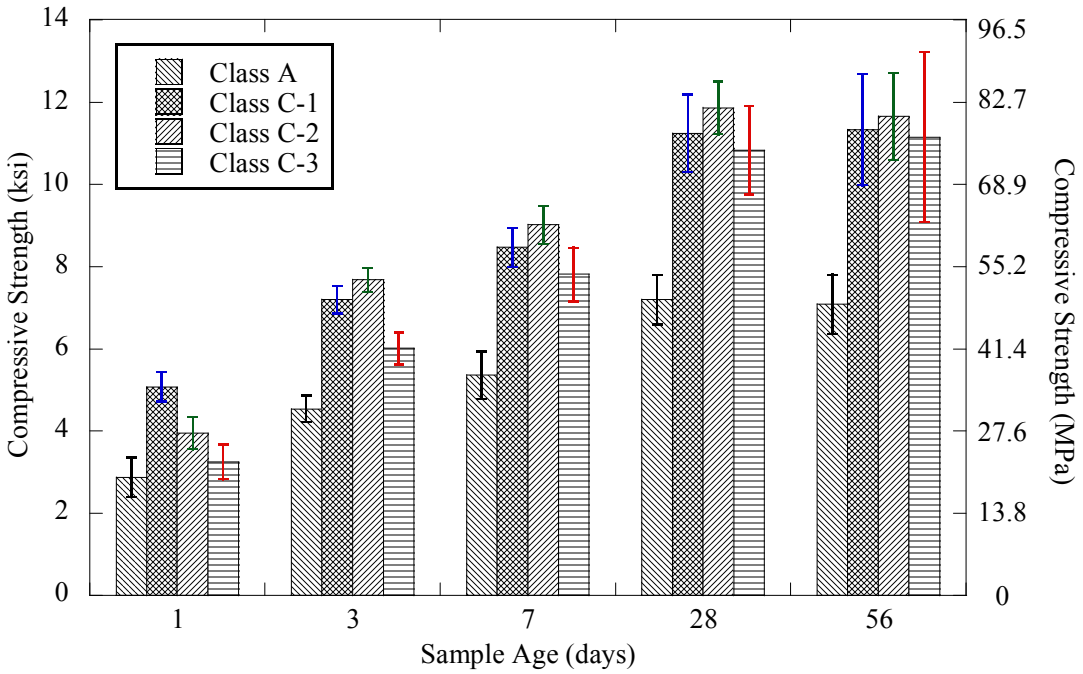

Figure 4-26. Compressive Strength Results at Various Sample Ages for Four Grout Types at Low w/p.

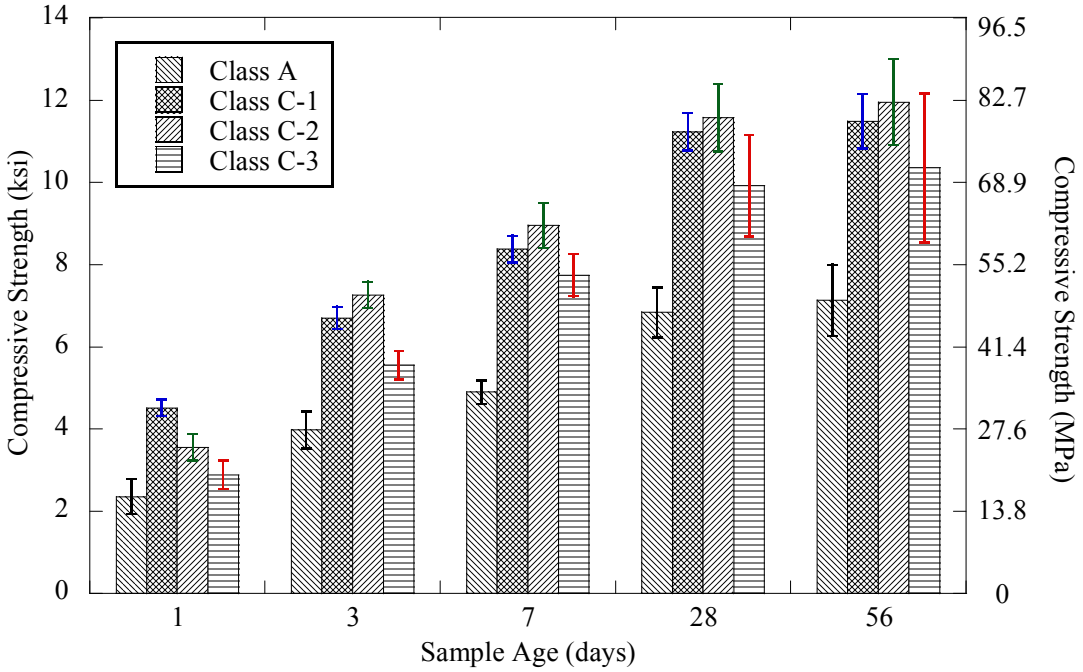

Figure 4-27. Compressive Strength Results at Various Sample Ages for the Grout Types at Recommended w/p.

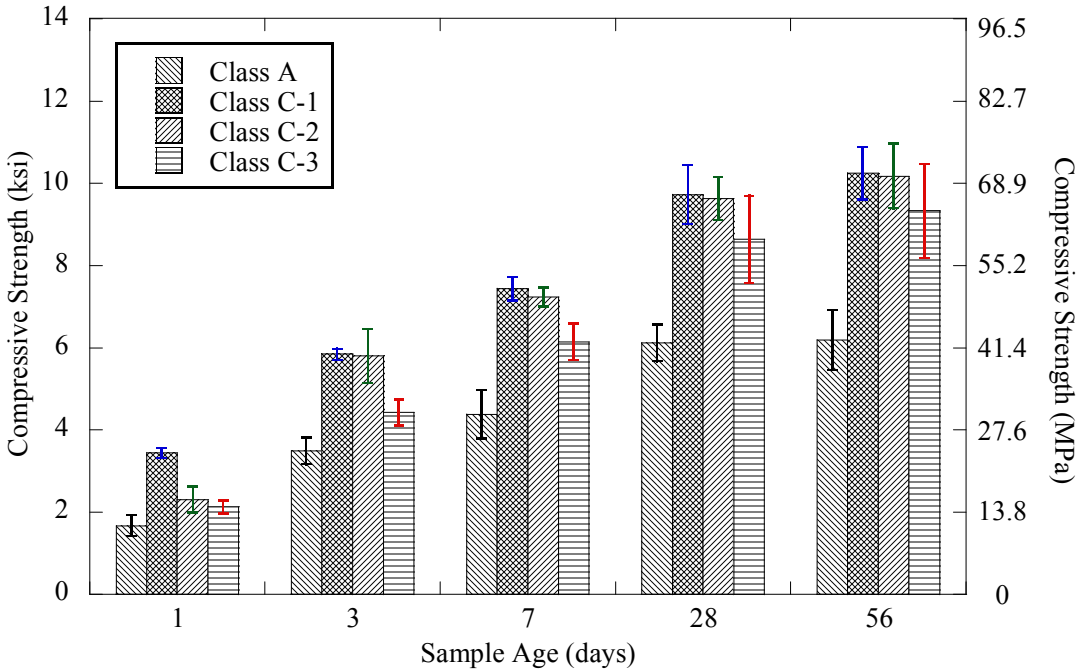

Figure 4-28. Compressive Strength Results at Various Sample Ages for the Grout Types at High w/p.

In some of the Class C grouts, SCMs may have been included to improve the grout's strength characteristics. A higher compressive strength, however, may not enhance the performance of the grout in PT applications. To evaluate the effect of mixer type, mixture volume, w/p, and sample age on the grout's compressive strength, a four-factor-factorial fixed-effects ANOVA was defined.

The four-factor-factorial experiment was considered to analyze the effect of all factors on the grout's compressive strength. The four factors are mixer type (MIXER), volume of mixture (VOL), w/p of the mixture (WP), and the age of the sample (AGE). The four-factor-factorial experiment also analyzes the interactions among the factors along with their individual effects. The aim of this analysis is to determine the effect of the four factors on the compressive strength of the grouts. Interactions such as the MIXER-VOL and MIXER-WP are important for the research as one mixer type may perform better than the other as the mixture volume changes. Similarly, the mixer's performance may also change as the grout's w/p is altered. Other two-way interactions such as MIXER-AGE, VOL-AGE, etc., and other higher order interactions are less significant in determining the suitable mixer type that can produce better grout mixture. For the sake of simplicity, all other two-way, three-way and four-way interactions were ignored. The four-factor-factorial model is defined as:

$$Y_{ijklm} = \mu + \tau_i + \alpha_j + \beta_k + \gamma_l + (\tau\alpha)_{ij} + (\tau\beta)_{ik} + \varepsilon_{ijklm} \begin{cases} i = 1,2 \\ j = 1,2,3 \\ k = 1,2,3 \\ l = 1,2,...,5 \\ m = 1,2,3 \end{cases} \tag{4.15}$$

where μ is the overall mean effect, τ_i is the effect of the ith level of mixer type, α_i is the effect of the jth level of mixture volume, β_j is the kth effect of w/p and γ_k is the l^{th} effect of sample age, $(\tau\alpha)_{ij}$ is the effect of the interaction between mixer type and mixture volume, $(\tau\beta)_{ik}$ is the effect of the interaction between mixer type and w/p, and ε_{ijklm} is a random error component having a normal distribution with mean zero and variance σ^2.

The null and alternate hypotheses for all factors are as follows:

$$
\begin{aligned}
&1.\ H_0 = \tau_1 = \tau_2 = 0 && \text{(no main effect of mixer type)}\\
&\quad H_1 = \tau_i \neq 0 \text{ at least one } i\\
&2.\ H_0 = \alpha_1 = \alpha_2 = \alpha_3 = 0 && \text{(no main effect of mixture volume)}\\
&\quad H_1 = \alpha_j \neq 0 \text{ at least one } j\\
&3.\ H_0 = \beta_1 = \beta_2 = \beta_3 = 0 && \text{(no main effect of w/p)}\\
&\quad H_1 = \beta_k \neq 0 \text{ at least one } k\\
&4.\ H_0 = \gamma_1 = \gamma_2 = \ldots = \gamma_5 = 0 && \text{(no main effect of sample age)}\\
&\quad H_1 = \gamma_l \neq 0 \text{ at least one } l\\
&5.\ H_0 = (\tau\alpha)_{11} = (\tau\alpha)_{12} = (\tau\alpha)_{23} = 0 && \text{(no interaction)}\\
&\quad H_1 = \text{at least one } (\tau\alpha)_{ij} \neq 0\\
&6.\ H_0 = (\tau\beta)_{11} = (\tau\beta)_{12} = (\tau\beta)_{23} = 0 && \text{(no interaction)}\\
&\quad H_1 = \text{at least one } (\tau\beta)_{ik} \neq 0
\end{aligned}
\qquad (4.16)
$$

Once the hypotheses were defined, fixed effects ANOVA was performed to test these hypotheses on the grouts. Table 4-20, Table 4-21, Table 4-22, and Table 4-23 summarize the ANOVA results obtained while studying the effect of various factors on the compressive strength of the grouts. The *p*-values for all the test statistics are shown in the last column of the table. The *p*-values reveal that at a 5% level of significance there is no main effect of mixer type or mixture volume (i.e., *p*-value > α). It also shows that the w/p and sample age have a significant effect on the grout's compressive strength, which was expected.

The two interactions, one between the mixer type and mixture volume and the other between the mixer type and the w/p were also evaluated to study the combined effect. The *p*-values shown in the table reveals that there is no significant interaction among these pairs.

Table 4-20. ANOVA Computations for the Hypotheses for Class C-1 Grout.

Source	Degrees of Freedom	Type III Sum of Squares	Mean Square	F statistic	*p*-value
MIXER	1	18,096	18,096	0.05	0.8205
VOL	2	541,745	270,873	0.77	0.4628
WP	2	91,477,275	45,738,637	130.47	<.0001
AGE	4	1,721,932,257	430,483,064	1,227.97	<.0001
MIXER*VOL	2	1,156,711	578,355	1.65	0.1941
MIXER*WP	2	130,394	65,197	0.19	0.8304

Table 4-21. ANOVA Computations for the Hypotheses for Class C-2 Grout.

Source	Degrees of Freedom	Type III Sum of Squares	Mean Square	F statistic	*p*-value
MIXER	1	6,444,098	6,444,098	18.02	<.0001
VOL	2	445,593	222,797	0.62	0.537
WP	2	178,057,154	89,028,577	248.91	<.0001
AGE	4	2.339E+09	584,853,109	1,635.2	<.0001
MIXER*VOL	2	4,275,840	2,137,920	5.98	0.003
MIXER*WP	2	741,983	370,992	1.04	0.356

Table 4-22. ANOVA Computations for the Hypotheses for Class C-3 Grout.

Source	Degrees of Freedom	Type III Sum of Squares	Mean Square	F statistic	*p*-value
MIXER	1	17,550,778	17,550,778	21.84	<.0001
VOL	2	1,440,247	720,123	0.9	0.4095
WP	2	132,518,900	66,259,450	82.44	<.0001
AGE	4	2,128,961,223	532,240,306	662.24	<.0001
MIXER*VOL	2	23,679,875	11,839,938	14.73	<.0001
MIXER*WP	2	1,799,269	899,635	1.12	0.3281

Table 4-23. ANOVA Computations for the Hypotheses for Class A Grout.

Source	Degrees of Freedom	Type III Sum of Squares	Mean Square	F statistic	*p*-value
MIXER	1	93,305.2	93,305.2	0.35	0.5546
VOL	2	1,449,147	724,573	2.72	0.0679
WP	2	50,499,058	25,249,529	94.71	<.0001
AGE	4	782,453,651	195,613,413	733.76	<.0001
MIXER*VOL	2	2,932,457	1,466,228	5.5	0.0046
MIXER*WP	2	3,765,538	1,882,769	7.06	0.001

To determine which treatment pairs are significantly different, *Fisher's least significant difference (LSD)* method is used. The null hypothesis for comparing all pairs of means (μ_i, μ_j) by the Fisher's LSD is:

$$H_0 : \mu_i = \mu_j \quad \text{for all} \, i \neq j \tag{4.17}$$

According to the Fisher's LSD, the pair of means μ_i, μ_j would be declared significantly different if

$$| \bar{y}_{i.} - \bar{y}_{j.} | > \text{LSD} \tag{4.18}$$

where the LSD, is defined as:

$$\text{LSD} = t_{\alpha/2, a(n-1)} \sqrt{\frac{2MS_E}{n}} \tag{4.19}$$

where $t_{\alpha/2,a(n-1)}$ is a two sided *t*-statistic with α level of significance, a is the number of levels in a particular treatment, n is the sample size, and MS_E is the mean square error (Montgomery and Runger 2007).

Table 4-24 summarizes the results obtained from Fisher's LSD test to identify which treatment level means are different for all grouts. Column 3 of the table lists the treatment levels for all treatment types and column 4 lists the Fisher's least LSD in compressive strength for each treatment evaluated using Equation (4.16) to determine whether the treatment levels are significantly different.

The last column of Table 4-24 reveals that for all grouts, the mixer type and mixture volume does not significantly affect the compressive strength, assuming a 0.05 level of significance. It is already well understood that the compressive strength increases as the w/p decreases. But in this experiment, the w/p values assessed are the recommended w/p, 5% lower than the recommended w/p, and 15% higher than the recommended w/p. So, the recommended w/p and 5% lower than the recommended w/p does not significantly affect the compressive strength at the 5% level of significance, although the compressive strength corresponding to the lower w/p is slightly higher than the recommended w/p. Fisher's LSD method also reveals that the 28-day and 56-day compressive strengths are not significantly different at the 5% level of significance, indicating only small quantities of SCMs are likely present.

Table 4-24. Summary of Multiple Comparisons Following the ANOVA Based on LSD.

Grout (1)	Treatment (2)	Treatment Levels (3)	Result (4)
Class A	Mixer type	M1, M2	No significant difference
	Mixture volume	0.25, 0.50, 0.75	No significant difference
	w/p	0.41, 0.44, 0.51	0.41 and 0.44 not significantly different
	Age	1, 3, 7, 28, 56	28 day and 56 day strength not significantly different
Class C-1	Mixer type	M1, M2	No significant difference
	Mixture volume	0.25, 0.50, 0.75	No significant difference
	w/p	0.27, 0.30, 0.35	0.27 and 0.30 not significantly different
	Age	1, 3, 7, 28, 56	28 day and 56 day strength not significantly different
Class C-2	Mixer type	M1, M2	No significant difference
	Mixture volume	0.25, 0.50, 0.75	No significant difference
	w/p	0.25, 0.26, 0.30	0.25 and 0.26 not significantly different
	Age	1, 3, 7, 28, 56	28 day and 56 day strength not significantly different
Class C-3	Mixer type	M1, M2	No significant difference
	Mixture volume	0.25, 0.50, 0.75	No significant difference
	w/p	0.26, 0.27, 0.31	0.41 and 0.44 not significantly different
	Age	1, 3, 7, 28, 56	28 day and 56 day strength not significantly different

4.4.2.2. Dimensional stability

The dimensional stability of cylindrical specimens was measured for all grouts following ASTM C1090. Various mixtures were prepared as noted in Table 4-3 and one specimen was cast for

each mixture as specified by the standard. The change in height at 3, 7, 14, and 28 days with respect to the height at one day was measured using a micrometer.

Table 4-25 shows the percent change in height after 28 days with respect to the height at one day for the different mixers for the Class C-1 grout. The measured percent change in height of the cylindrical specimens was less than 0.04% for all samples. This was close to the measuring limit of the micrometer. To determine whether the percent change in length is significantly different from zero a *t*-test was performed, and the proposed null and alternate hypotheses for mean percent change in height μ_i are as shown in Equation (4.20):

$$\begin{aligned} &H_0 : \mu_i = 0 \\ &H_1 : \mu_i \neq 0 \ \text{ for at least one } i \end{aligned} \tag{4.20}$$

The last column of Table 4-25 shows the *p*-values of the *t*-tests performed, and these *p*-values reveal that the null hypothesis at the 5% level of significance for both M1 and M2 mixer cannot be rejected. Therefore, the mean percent change in height of the cylindrical specimens is not significantly different from zero.

Table 4-25. Percent Change in Height and *t*-test for Class C-1 Grout.

Mixer type	Mixture volume, ft^3 (m^3)	Mixture w/p	Percent change in height	t_0	*p*-value
M1	0.25 (0.007)	0.27	0.008	2.049	0.096
	0.25 (0.007)	0.30	-0.004		
	0.25 (0.007)	0.35	0.021		
	0.50 (0.014)	0.27	-0.004		
	0.50 (0.014)	0.30	0.038		
	0.75 (0.021)	0.30	0.029		
M2	0.25 (0.007)	0.27	0.000	2.010	0.115
	0.50 (0.014)	0.27	-0.004		
	0.50 (0.014)	0.30	0.021		
	0.50 (0.014)	0.35	0.033		
	0.75 (0.021)	0.27	0.021		

Similar hypotheses were formed for the C-2, C-3, and A grouts and the percent change in height for each mixture along with the t-statistics are shown in Table 4-26, Table 4-27, and Table 4-28 for these grouts. The *p*-values for these grouts reveal that the mean percent changes in height of the cylindrical specimens are not significantly different from zero at the 5% level of significance.

Table 4-26. Percent Change in Height and *t*-test for Class C-2 Grout.

Mixer type	Mixture volume, ft^3 (m^3)	Mixture w/p	Percent change in height	t_0	*p*-value
M1	0.50 (0.014)	0.25	-0.008	0.988	0.379
	0.50 (0.014)	0.26	0.017		
	0.50 (0.014)	0.30	-0.013		
	0.75 (0.021)	0.25	0.033		
	0.75 (0.021)	0.26	0.013		
M2	0.25 (0.007)	0.26	0.004	0.542	0.607
	0.25 (0.007)	0.30	0.000		
	0.50 (0.014)	0.25	0.004		
	0.50 (0.014)	0.30	-0.013		
	0.75 (0.021)	0.25	-0.004		
	0.75 (0.021)	0.30	0.000		

Table 4-27. Percent Change in Height and *t*-test for Class C-3 Grout.

Mixer type	Mixture volume, ft^3 (m^3)	Mixture w/p	Percent change in height	t_0	*p*-value
M1	0.25 (0.007)	0.27	0.004	0.091	0.929
	0.50 (0.014)	0.27	-0.013		
	0.50 (0.014)	0.31	-0.004		
	0.75 (0.021)	0.26	0.003		
	0.75 (0.021)	0.27	0.011		
M2	0.25 (0.007)	0.26	-0.006	1.149	0.294
	0.25 (0.007)	0.31	0.000		
	0.50 (0.014)	0.26	0.004		
	0.50 (0.014)	0.27	-0.010		
	0.75 (0.021)	0.27	-0.002		

Table 4-28. Percent Change in Height and *t*-test for Class A Grout.

Mixer type	Mixture volume, ft^3 (m^3)	Mixture w/p	Percent change in height	t_0	*p*-value
M1	0.25 (0.007)	0.42	0.006	0.066	0.949
	0.25 (0.007)	0.44	0.000		
	0.25 (0.007)	0.51	-0.017		
	0.50 (0.014)	0.42	0.002		
	0.50 (0.014)	0.44	-0.006		
	0.50 (0.014)	0.51	-0.013		
	0.75 (0.021)	0.42	0.015		
	0.75 (0.021)	0.44	-0.002		
	0.75 (0.021)	0.51	0.013		
M2	0.25 (0.007)	0.42	0.000	0.664	0.525
	0.25 (0.007)	0.44	0.000		
	0.25 (0.007)	0.51	0.000		
	0.50 (0.014)	0.42	0.004		
	0.50 (0.014)	0.44	0.004		
	0.50 (0.014)	0.51	0.008		
	0.75 (0.021)	0.42	0.000		
	0.75 (0.021)	0.44	-0.002		
	0.75 (0.021)	0.51	-0.006		

Although, the *t*-statistic test results indicate that there is no significant shrinkage or expansion for any of the four grouts evaluated in this research, an interesting example shows that ignoring even a small shrinkage of 0.001 inch (25.4 μm) per 6-inch (153 mm) grout sample can lead to the substantial shrinkage in a PT duct. The resolution of the micrometer used to perform the volume change test (ASTM C1090) is 0.001 inch. This indicates that the consequences of using such equipment could result in significant voids in the field due to shrinkage. Now, consider a 150-ft (45.7 m) span PT duct. If the shrinkage of 0.001 inch is ignored then the actual shrinkage in the 150-ft (45.7 m) PT duct is 3.6 inch (91.44 mm). Shrinkage of less than 2 inches (51 mm) is large enough to cause corrosion of strands. Therefore, the resolution of the 0.001-inch (25.4 μm) equipment could result in a grout that is considered to be non-shrinkage, but voids could still form. It is therefore recommended that the resolution of Micrometer Bridge should be increased to measure the shrinkage smaller than 0.001 inch (25.4 μm).

4.4.3. Durability characteristics

The results obtained from the chloride diffusion and pH tests are presented in this section.

4.4.3.1. Chloride diffusion

The chloride diffusion tests were performed following ASTM C1556 test method as discussed in Section 4.3.7. Three samples for each grout were tested with the manufacturer's recommended w/p. The chloride diffusion coefficients obtained for the grouts mixed with the M1 and M2 mixers are shown in Table 4-29. The diffusion coefficient for the Class C-3 grout was the lowest followed by Class C-1 and C-2 grouts. The diffusion coefficient of Class A grout was found to be approximately six times higher than the Class C grouts.

Table 4-29. Chloride Diffusion Coefficient Results for All Grouts.

Mixer	Grout	Diffusion Coefficient, D	
		ft^2/s	m^2/s
M1	Class A	7.00×10^{-11}	6.50×10^{-12}
	Class C-1	1.25×10^{-11}	1.16×10^{-12}
	Class C-2	2.86×10^{-11}	2.66×10^{-12}
	Class C-3	1.21×10^{-11}	1.12×10^{-12}
M2	Class A	-	-
	Class C-1	1.58×10^{-11}	1.47×10^{-12}
	Class C-2	1.89×10^{-11}	1.76×10^{-12}
	Class C-3	1.14×10^{-11}	1.06×10^{-12}

The chloride diffusion coefficient for high performance grouts is higher than the control grout (Class A grout). Assuming a ¼-inch (6.3 mm) clear cover for PT strands, the critical chloride threshold of 0.1% by weight of cementitious materials and the surface chloride concentration of 0.289% by weight of cementitious materials (Alonso et al. 2008), the time to initiation of corrosion for Class A and Class C grouts can be calculated using Equation (2.5). Note that this is only a comparative assessment and these times to corrosion are not representative of strands in PT bridges. The time to initiation of corrosion for Class A grout is 40.4 days whereas it is 198.8, 118.7, and 240.7 days for the Class C-1, C-2, and C-3 grouts, respectively.

4.4.3.2. Alkalinity

The *pH* tests were performed following the test method described in Section 4.3.8. Three cylindrical specimens of 2 inches x 4 inches (51 mm x 102 mm) were initially cast to study the effect of mixer type on the *pH* of pore solution for all grouts. However, the pore solution extracted from one sample was not enough to measure the *pH* of the pure solution. Therefore, three samples were used and the combined pore solution extracted by the three specimens was used to measure the corresponding pH values. Table 4-30 summarizes the *pH* values of the grout mixtures. Figure 4-29 and Figure 4-30 show the *pH* values of the grout pore solutions when mixed with the M1 and M2 mixers.

Table 4-30. *pH* of Pore Solutions Extracted from Grout Samples.

Mixer type	w/p	Grout type			
		Class A	Class C-1	Class C-2	Class C-3
M1	-5%	13.09	12.78	12.81	12.93
	Recommended	12.92	12.91	12.87	12.95
	+15%	12.94	12.87	12.74	*
M2	-5%	13.15	12.91	12.84	12.73
	Recommended	13.16	12.91	12.75	13.06
	+15%	12.58	12.98	12.86	12.91

* indicates test not performed for the particular mixture

Various research indicates that the corrosion of steel starts if the *pH* drops below a certain value because the passive oxide layer is destroyed at lower *pH* values. Mindess et al. (2003) noted that this passive oxide layer is destroyed if the *pH* of the pore solution drops below 11.5, and Locke (1986) noted a pH value to be 12. Assuming a more conservative case, the *pH* of the grout pore solution should be more than 12 for protection of strands from corrosion. The *pH* values for all grouts while mixing with the M1 and M2 mixers are well above 12. Therefore, it is concluded that all Class C grouts are protective.

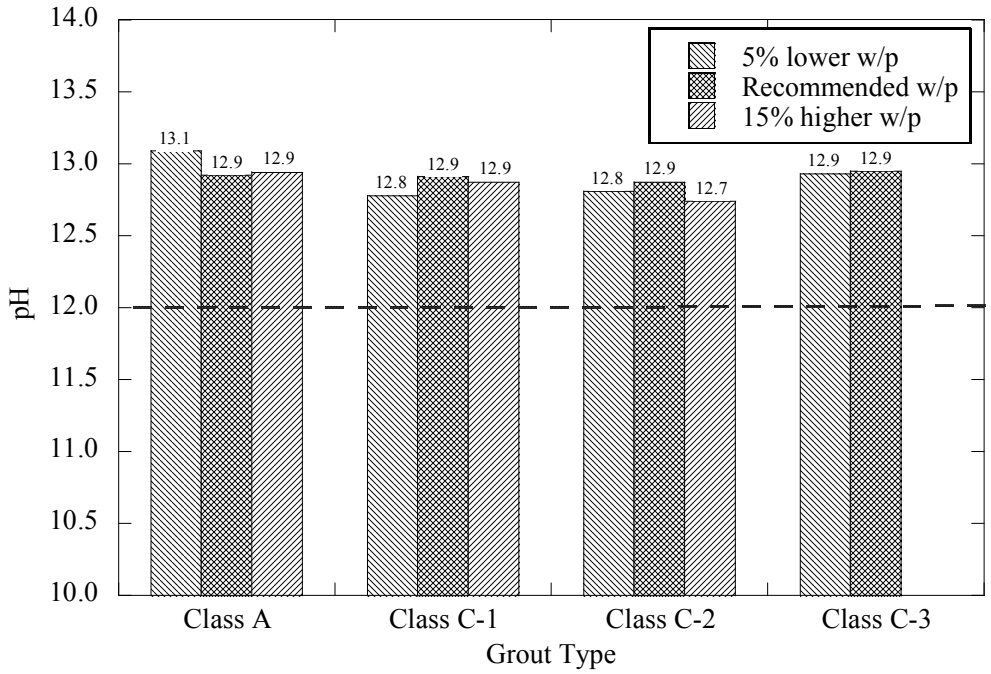

Figure 4-29. *pH* Values of the Pore Solution of Grouts Mixed with M1 Mixer.

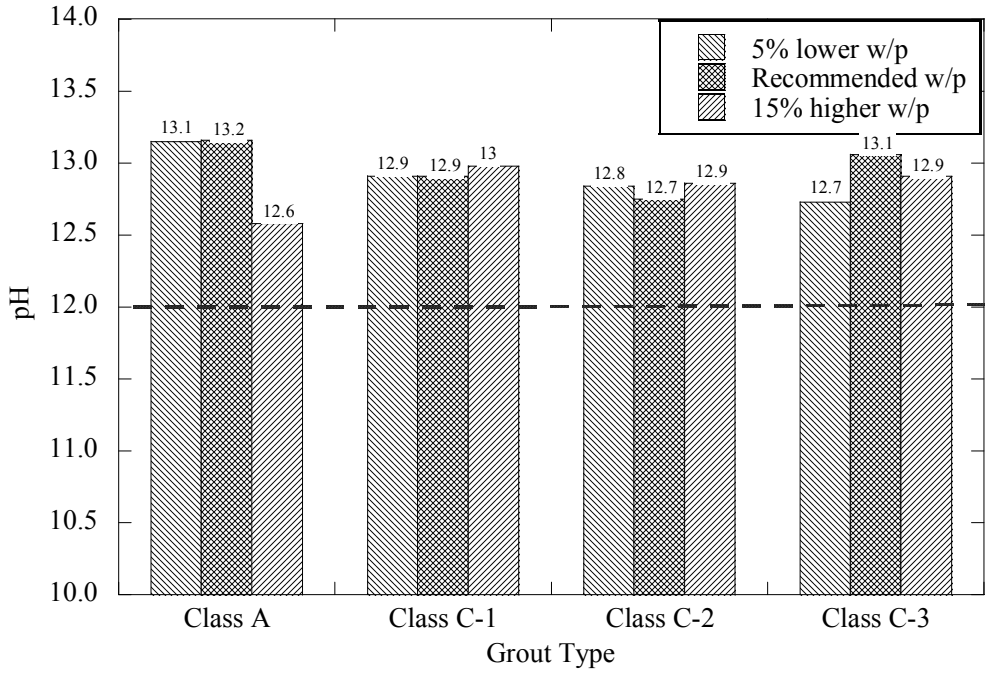

Figure 4-30. *pH* Values of the Pore Solution of Grouts Mixed with M2 Mixer.

4.4.4. Fillability

The fillability test was performed using a fillability meter. To study the repeatability of the test procedure, triplicate fillability tests were performed on four grouts in the study. The results obtained from the fillability meter are shown in the Figure 4-31 along with the standard deviation.

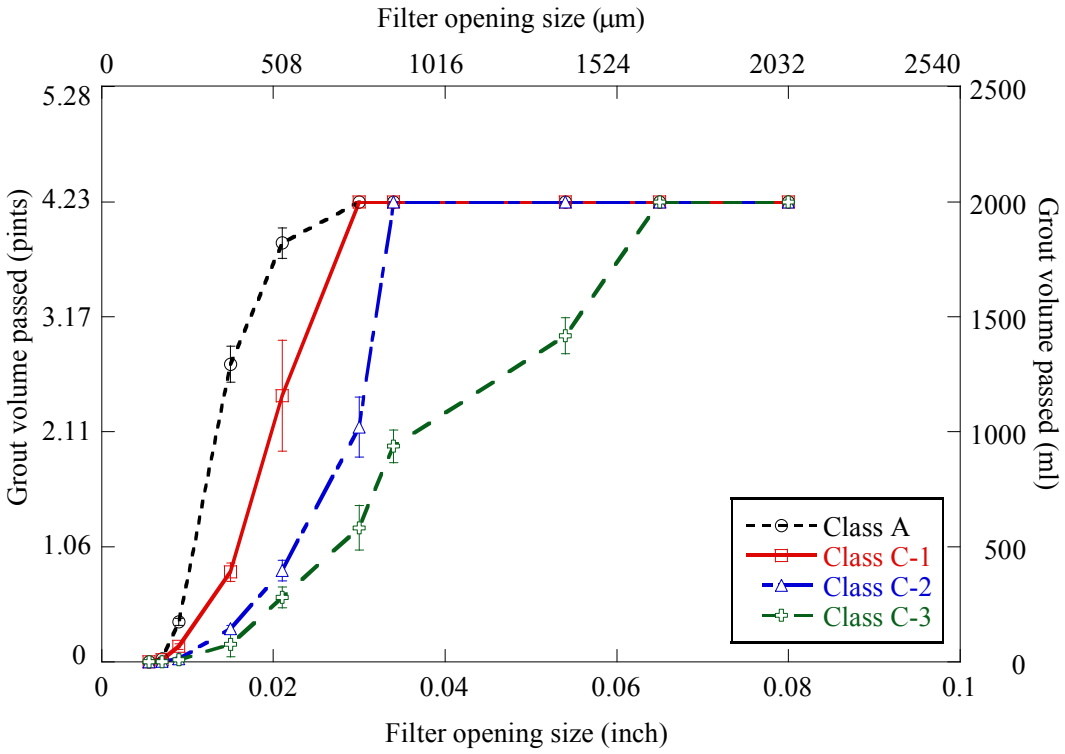

Figure 4-31. Fillability Test Results.

The results show that among the three Class C grouts, the Class C-1 grout is more fillable when compared to the C-2 and C-3 grouts. The Class C-2 grout also exhibits fillability slightly lower than the Class C-1 grout. The Class C-3 grout did not perform well in terms of the fillability. Results indicate that the Class C-1 grout can easily pass through a 0.034-inch (864

μm) sieve opening. Results also indicate that 19.5% of the Class C-1 grout can flow through a 0.015-inch (381-μm) sieve opening whereas only 6.5% and 0.5% of Class C-2 and C-3 grouts passed through the same sieve opening before being clogged by the grout.

The fillability test results categorize the grouts based on their ability to pass through small voids. The fillability index was calculated using Equation (4.2). The fillability index calculations for Class A, C-1, C-2 and C-3 grouts are shown in Table 4-31, Table 4-32, Table 4-33, and Table 4-34, respectively. The fillability index values from the test results are 3.3, 4.1, 5.3 and 7.5 respectively for Class A, C-1, C-2 and C-3 grouts. Lower values of the fillability indices indicate that the grout can "fill" smaller voids.

Table 4-31. Fillability Index Calculations for Class A Grout.

Grout	Filter No.	Filter Size, inch (μm)	Volume passed, pints (ml)	Percent volume passed	Percent volume retained (VRi)
Class A	#10	0.08 (2032)	4.227 (2000)	100	0
	#12	0.065 (1651)	4.227 (2000)	100	0
	#16	0.054 (1372)	4.227 (2000)	100	0
	#20	0.034 (864)	4.227 (2000)	100	0
	#24	0.03 (762)	4.227 (2000)	100	0
	#30	0.021 (533)	3.994 (1890)	94.5	5.5
	#40	0.015 (381)	2.916 (1380)	69	31
	#60	0.009 (229)	0.359 (170)	8.5	91.5
	#80	0.007 (178)	0.042 (20)	1	99
	#100	0.0055 (140)	0	0	100
				Fillability Index, FI =	3.3

Table 4-32. Fillability Index Calculations for Class C-1 Grout.

Grout	Filter No.	Filter Size, inch (μm)	Volume passed, pints (ml)	Percent volume passed	Percent volume retained (VRi)
Class A	#10	0.08 (2032)	4.227 (2000)	100	0
	#12	0.065 (1651)	4.227 (2000)	100	0
	#16	0.054 (1372)	4.227 (2000)	100	0
	#20	0.034 (864)	4.227 (2000)	100	0
	#24	0.03 (762)	4.227 (2000)	100	0
	#30	0.021 (533)	2.938 (1390)	69.5	30.5
	#40	0.015 (381)	0.824 (390)	19.5	80.5
	#60	0.009 (229)	0.127 (60)	3	97
	#80	0.007 (178)	0.021 (10)	0.5	99.5
	#100	0.0055 (140)	0 (0)	0	100
				Fillability Index, FI =	4.1

Table 4-33. Fillability Index Calculations for Class C-2 Grout.

Grout	Filter No.	Filter Size, inch (μm)	Volume passed, pints (ml)	Percent volume passed	Percent volume retained (VRi)
Class A	#10	0.08 (2032)	4.227 (2000)	100	0
	#12	0.065 (1651)	4.227 (2000)	100	0
	#16	0.054 (1372)	4.227 (2000)	100	0
	#20	0.034 (864)	4.227 (2000)	100	0
	#24	0.03 (762)	1.881 (890)	44.5	55.5
	#30	0.021 (533)	0.845 (400)	20	80
	#40	0.015 (381)	0.275 (130)	6.5	93.5
	#60	0.009 (229)	0.021 (10)	0.5	99.5
	#80	0.007 (178)	0 (0)	0	100
	#100	0.0055 (140)	0 (0)	0	100
				Fillability Index, FI =	5.3

Table 4-34. Fillability Index Calculations for Class C-3 Grout.

Grout	Filter No.	Filter Size, inch (μm)	Volume passed, pints (ml)	Percent volume passed	Percent volume retained (VRi)
Class A	#10	0.08 (2032)	4.142 (1960)	98	2
	#12	0.065 (1651)	2.409 (1140)	57	43
	#16	0.054 (1372)	1.987 (940)	47	53
	#20	0.034 (864)	1.014 (480)	24	76
	#24	0.03 (762)	0.697 (330)	16.5	83.5
	#30	0.021 (533)	0.296 (140)	7	93
	#40	0.015 (381)	0.021 (10)	0.5	99.5
	#60	0.009 (229)	0 (0)	0	100
	#80	0.007 (178)	0 (0)	0	100
	#100	0.0055 (140)	0 (0)	0	100
				Fillability Index, FI =	7.5

Because three fillability tests were performed on all grouts, the fillability indices for all grouts along with their standard deviation in fillability index are shown in Table 4-35. The average fillability indices for Class A, C-1, C-2, and C-3 grouts are 3.39, 4.19, 5.21, and 6.73 respectively. The low values of standard deviation in fillability indices values show the repeatability of the fillability test.

Table 4-35. Fillability Index Along with the Standard Deviations for All Grouts.

Grouts	Fillability Index				
	1	2	3	Average	Standard Deviation
Class A	3.3	3.4	3.4	3.35	0.08
Class C-1	4.1	4.3	4.2	4.19	0.13
Class C-2	5.3	5.2	5.2	5.21	0.06
Class C-3	7.5	6.4	6.3	6.73	0.67

Based on the tests performed on the three Class C grouts and the Class A grout, the Class A grout possesses higher fillability (indicated by a lower fillability index). However, Class A grout bleeds are not acceptable for filling post-tensioning ducts. Among the Class C grouts, Class C-1 grout was found to possess higher fillability when compared to the Class C-2 and C-3 grouts. Because all Class C grouts met to the TxDOT material specifications for grouts for

post-tensioning applications, any of the three grouts can be used for PT applications. However, Class C-1 grout was found to fill more voids when compared with Class C-2 and C-3 grouts. In general, a grout with a low fillability index should be preferred for PT applications.

4.4.5. Summary of results

A summary of various grout characteristics evaluated in this research for Class A, C-1, C-2, and C-3 grouts is presented in Table 4-36. The values shown in the Table 4-36 are overall mean values obtained in the test program. Based on the experimental results, grout characteristics that meet the current TxDOT specification DMS-4670: Grouts for post-tensioning were evaluated for each grout and the results are presented in Table 4-37. Table 4-37 indicates that the Class C grouts (C-1, C-2, and C-3) met the current TxDOT grouting specifications, whereas Class A grout did not meet the current specifications. It is also noted that the three Class C grouts are seemingly good for grouting PT ducts according to the current TxDOT specifications. However, the current specifications do not well characterize the Class C grouts. Therefore, it is difficult to determine which grouts can fill voids efficiently to prevent voids and corrosion of the strands. The requirements for grouts shown in Table 5-31 require modification and additional tests should be included to better characterize the grouts.

Table 4-36. Summary of the Test Results Obtained for Each Grout Characteristic.

Grout Characteristic	Class A	C-1	C-2	C-3
Wick-induced bleed, %	2.05	0	0	0
Fluidity (immediately after mixing), seconds	4.95	10.32	13.03	9.99
Viscosity (immediately after mixing), Poise (Pascal.seconds)	42.53 (4.25)	-	17.09 (1.71)	106.96 (10.70)
Wet density, lb/gal (g/cm^3)	15.62 (1.87)	17.57 (2.11)	17.55 (2.10)	16.35 (1.96)
Initial setting time, hours	4.81	5.12	9.34	9.47
Compressive strength, ksi (MPa)	6.84 (47.18)	11.24 (77.48)	11.57 (79.77)	9.17 (63.22)
Volume change, %	0	0	0	0
Chloride diffusivity (10^{-11}), ft^2/s (m^2/s)	7.00 (0.65)	1.42 (0.13)	2.38 (0.22)	1.18 (0.11)
pH	13.04	12.91	12.81	13.01
Fillability, FI	3.35	4.19	5.21	6.73

Table 4-37. Grout Characteristics that Met Current DMS-4670 Specification.

Grout Characteristic	Class A	C-1	C-2	C-3
Wick-induced bleed	×	√	√	√
Fluidity (immediately after mixing)	×	√	√	√
Viscosity (immediately after mixing)	NR	NR	NR	NR
Wet density	NR	NR	NR	NR
Initial setting time	√	√	√	√
Size gradation	√	√	√	√
Compressive strength	√	√	√	√
Volume change	√	√	√	√
Chloride diffusivity	NR	NR	NR	NR
pH	NR	NR	NR	NR
Fillability, FI	NR	NR	NR	NR

√ indicates grout meet current DMS-4670 specifications

× indicates grout did not meet current DMS-4670 specifications

NR indicates grout characteristic not required in current DMS-4670 specifications

4.4.6. Proposed changes to current TxDOT specification

The current TxDOT specifications for PT grouting applications are contained in DMS-4670, *Grouts for Post-Tensioning.* Research indicates that these specifications should be modified. The requirements for maximum particle size gradation should be modified. The requirements for two grout characteristics, fluidity and initial setting times, should also be modified. Also, two new test methods, the wet density and fillability test, should be added to the current specifications. The following pages show the newly proposed modified DMS-4670 specifications. The additions

to this specification are underlined, and all requirements that are proposed to be removed have been struck through.

TxDOT's modified material specification for selection of grouts for post-tensioning applications is shown on the following pages with suggested modifications based on findings from this research (TxDOT 2004).

4.4.6.1. Modified DMS-4670 specifications

Departmental Material Specifications - DMS-4670, Grouts for Post-Tensioning[1]

Overview

Effective Date: August 2004 (New Specification). This Specification governs for the prequalification procedure, packaging, and material properties of thixotropic grouts for post-tensioning.

Material Producer List

The Materials and Pavements Section of the Construction Division (CST/M&P) maintains the list of qualified manufacturers of thixotropic grouts for post-tensioning. Only manufacturers of thixotropic grouts for post-tensioning on the Material Producer List can be used on Department projects.

The Department reserves the right to conduct random sampling of materials from prequalified manufacturers for testing and to perform random audits of documentation. Department representatives may sample material from the manufacturing plant, the project site, and the warehouse. CST/M&P reserves the right to test samples to verify compliance with this Specification.

Prequalification Requests

To prequalify material, submit a letter to the Texas Department of Transportation, Construction Division, Director of the Materials & Pavements Section (CP51), 125 East 11th Street, Austin, Texas 78701-2483, and include the company name, physical and mailing address, and contact person and phone number.

Prequalification Requirements

Manufacturers requesting prequalification must meet the following requirements.

- Test all grouts with results meeting the minimum material requirements of this Specification.
- Provide an independent laboratory test report from a laboratory audited and inspected by the Cement Concrete Research Laboratory, certifying compliance of the material to this Specification.
- Submit a minimum of one bag of grout for testing to the Texas Department of Transportation, Construction Division, Materials and Pavements Section (CP51), 9500 Lake Creek Parkway, Austin, Texas 78717.

All materials submitted for prequalification tests are at no cost to the Department.

Packaging and Labeling

Prepackage grout in plastic lined or coated bags. Grout bags must indicate the brand name, date of manufacture, lot number, and mixing instructions. The grout supplier must provide the Contractor and Engineer with a copy of the quality control data sheet for each lot number and shipment sent to the jobsite.

[1] Source: TxDOT (2004)

Material Properties

No grout may contain aluminum powder, gas generating components that produce hydrogen gas, carbon dioxide, or oxygen, expansive admixtures or admixtures containing chlorides. The grout must meet the material requirements stated in the following table:

Material Requirements of Grout

Property	Requirement	Test Method
Total Chloride Ions	Maximum 0.08% by weight of cementitious material	ASTM C1152
Fine Aggregate (if used),	Gradation Maximum Size ≤ No. ~~50~~ 100 Sieve	Tex-401-A
Volume Change	0.0% to 0.1% expansion at 24 hr. and 0.0% to 0.2% at 28 days	ASTM C1090[1]
Bleeding	Maximum 0.0% at 3 hr.	Tex-441-A (see *Note*)
Compressive Strength (Average of 3 cubes)	> 3000 psi at 7 days and > 5000 psi at 28 days	Tex-442-A (see *Note*)
Initial Set of Grout	Minimum ~~3~~ 4 hr., Maximum 12 hr.	ASTM C953
Fluidity - Efflux Time from Flow Cone: (a) Immediately after mixing (b) 30 min. after mixing with remixing for 30 sec.	Minimum ~~9~~ 5 sec., Maximum 20 sec. Maximum 30 sec.	Tex-437-A Method 2
Permeability at 28 days	Maximum 2,500 Coulombs; At 30 V for 6 hr.	ASTM C1202[2]
Wet density	$\rho_{observed} = \rho_{predicted} \pm 0.31$ $\rho_{predicted} = -28.4 + 104.6\,(w/p) + 2.1\,(\rho_{dry})$	Baroid mud balance
Fillability	FI ≤ 5.5[3]	Fillability test

[1] Modified to include verification at only 24 hr. and 28 days.
[2] Moist cure specimens at 73°F ±3°F for 26 days. At 26 days, condition water, cut specimens to size, and dry and coat sides with epoxy gel. At 27 days, place prepared samples under vacuum as per method. Test at 28 days.
[3] Refer to Subsection on "Comparison of Fillability and Infiltration Length"
Note: Contact CST/M&P for more information regarding this test method.

Disqualification

Any change in cement or admixtures of a particular grout may result in removal from the MPL and disqualification for Department use. The material must be re-qualified for acceptance. The manufacturer may resubmit their product for requalification consideration, after following the procedures stated in 'Prequalification Requirements.

The current specifications require that the pre-packaged PT grouts will qualify for post-tensioning applications only if they do not contain either aluminum powder, gas generating components that produce hydrogen gas, carbon dioxide, oxygen, expansive admixtures, or admixtures containing chlorides. The grouts containing gas generating components are disqualified because these grouts can result in the formation of entrapped voids due to generation of gases. Grouts with expansive admixtures are disqualified because the grout expansion may result in the cracking of HDPE ducts, which can lead to durability issues. The addition of aluminum powder can also contribute to the expansion by liberating hydrogen gas which can form voids within the grout – this can also result in durability issues. Therefore, grouts with aluminum powder should continue to be disqualified.

The addition of two new tests, the wet density test and the fillability test, to the current DMS-4670 specifications, is technically justified based on this research. It is also important to justify the impact of these additional tests on the overall project costs, and whether the costs associated with these tests are significant. Consider that a quality control inspector can perform the wet density test in the field once for each grout mixture prepared. The fillability test, on the other hand, needs to be performed in the laboratory before selecting the grout for post-tensioning.

The total cost associated with these tests should conservatively be less than $5,000 for the repair of an existing PT bridge. Because this cost is small it can be ignored when comparing it with the overall project cost, which can be of the order of several million dollars. Therefore, allocating a minimal budget to ensure better fillability and durability of the grout is certainly justified.

Table 4-38 shows grout characteristics that met the modified TxDOT specification DMS-4670 for Class A, C-1, C-2, and C-3 grouts. Note that all grouts met the requirements of the current TxDOT specifications. However, according to the modified DMS-4670 specification, only Class C-1 and C-2 grouts qualify for the grouting of new PT structures and for repair of existing PT structures. Class C-3 grout did not exhibit good fillability. It also contained fine aggregates with maximum particle size larger than No. 100 Sieve (150 μm) which could clog the

flow of grout through small openings and result in more voids. This was confirmed with actual repairs of ducts.

Table 4-38. Grout Characteristics that Met the Modified DMS-4670 Specification.

Grout Characteristic	Class A	C-1	C-2	C-3
Wick-induced bleed	×	√	√	√
Fluidity (immediately after mixing)	×	√	√	√
Viscosity (immediately after mixing)	NR	NR	NR	NR
Wet density	√	√	√	√
Initial setting time	√	√	√	√
Gradation maximum size	√	√	√	×
Compressive strength	√	√	√	√
Volume change	√	√	√	√
Chloride diffusivity	NR	NR	NR	NR
pH	NR	NR	NR	NR
Fillability	√	√	√	×

√ indicates grout meet modified DMS-4670 specifications

× indicates grout did not meet modified DMS-4670 specifications

NR indicates grout characteristic not required in modified DMS-4670 specifications

5. MITIGATION AND REPAIR STRATEGIES: EXPERIMENTAL PROGRAM AND RESULTS

5.1. EXPERIMENTAL PROGRAM

The objective of the research presented in this section is to develop and propose an effective method for repairing voids in tendons on PT bridges. Three different repair grouting methods were evaluated for 1) filling capability in voided ducts, 2) repair performance, and 3) economic feasibility. In addition to evaluating grouting methods, various grout types were assessed as possible repair materials.

This section describes the experimental program including the test materials, the test methodologies, and the analysis. This section first introduces the descriptions of the test materials and test procedures. Next, the proposed methodologies for repairing tendons are presented. The analysis plan of the data obtained from the test program is then presented and effective repair methods for filling voids in ducts are proposed.

5.1.1. Experimental setup

In this research 16 prototype external tendon specimens were fabricated. These specimens contained inclined and horizontal tendons. This tendon set-up was designed, fabricated, and used to evaluate different repair grouting methods and different grouting materials (refer to Figure 3-1 in Subsection 3.3.1).

5.1.2. Grouting techniques

5.1.2.1. Grout types

In this research, the initial grout used to fill ducts is a Class A grout. The repair grouts used are high performance grouts, classified as Class C grouts, that are commercially available pre-packaged grouts. The three Class C grouts were assessed in this program and are identified

as Class C-1, C-2, and C-3 in the same manner as Subsection 4.2.1. Table 5-1 shows the grout names and experimental design. The research evaluated three different grouts and three different repair methods. Duplicate tests were planned for each combination, but the Class C-3 grout was found to be difficult to use in the repair methods assessed in this program. As a result of this, only one PET specimen each with the Class C-3 grout in the VG and PVG repair methods (discussed later). The w/p of each repair grout was based on the manufacturer's recommendation. In general, the color of initial and repair grouts are similar. Hence, to distinguish between the initial grout and repair grout, a small amount of colorant was added to the grouts.

Table 5-1. Repair Materials and the Test Matrix.

Grout Materials		No. of Specimens for Each Repair Grouting Methods		
Repair Grouts	**w/p**	**PG**	**VG**	**PVG**
Class C-1	0.30	2	2	2
Class C-2	0.26	2	2	2
Class C-3	0.27	2	1	1

5.1.2.2. Grout mixer and mixing procedures

Two types of mixers are used to prepare Class A grout. At first, the Class A grout was mixed (for 5 minutes) using an air-powered paddle mixer as shown in Figure 5-1. Then, mixing was stopped to add colorant, and then further mixing (for one additional minute) was performed using a 2500 rpm drill with a mixing paddle (Figure 5-2). Further mixing was then performed with the air-powered grout mixer for an additional 5 minutes. Thus, the total mixing time was 11 minutes for the Class A grout.

Figure 5-1. Grout Mixer for Initial Grouts and Grout Pump.

To mix the high performance Class C grouts used for the repairs, portable drills and mixing paddles were used to mimic field practices when small amounts of grout are required for tendon repairs (see Figure 5-2). The amount of grout required for each repair was 0.9 cubic feet (0.025 cubic meters); therefore, the grout was divided into two batches, mixed separately for the recommended mixing time, then combined in 15-gallon (56.8-liter) buckets. The grout was then mixed for an additional 2 minutes. Mixing times for each repair grout is provided in Table 5-2.

Figure 5-2. Drill and Mixing Paddle.

Table 5-2. Recommended Mixing Time and Drill for Repair Grouts

Repair grouts	Mixing time (minutes)	Mixing drill (rpm)
Class C-1	5	2500
Class C-2	6	2500
Class C-3	20	4000

5.1.2.3. Material tests for grouts

Because small changes in environmental conditions can have a significant influence on grout flow, the flow cone test was performed to measure the efflux time of the grouts. Procedures provided in Tex-437-A Method 2 (TxDOT 1999) were followed. In addition, the wick-induced bleed test was conducted following Tex-441-A (TxDOT 2003). The compressive strength test of cubic molds was carried out to verify the performance of hardened grouts. Three cubes were cast for each grout and were tested for compressive strength at 7 and 28 days following Tex-442-A (TxDOT 2006). The results of the compressive strength test are shown in Appendix C. All grout materials exceeded the required strength (4 ksi at 7 days and 4.6 ksi at 28 days).

Figure 5-3. Flow Cone (a) and Wick-induced Bleed Test (b).

5.1.3. Methodology of repair grouting

FDOT (2001a) reported that the VG method is more effective than the PG method. However, the FDOT did not employ the use of air outlets for the PG method and grout was injected by pressure into sealed specimens. This can significantly reduce the effectiveness of the PG method, making it more difficult to fill the voids in ducts. In this research, the PG method is applied with an air outlet on the voided duct.

A preliminary test using the PG method was performed to determine an appropriate location for grout injection. The first injection location for the repair grout is grout vent #1 (Figure 5-4). This location was selected because grout should be injected from a low point to reduce the amount of entrapped air inside the tendon. When injected at this point the grout filled the voids below the injection hole and did not fill the void above the injection point. As a result of this, the repair grout was injected into grout vent #2. The grout infiltrated the ducts below this point and did not fill thevoid above this point. Finally, the repair grout is injected into grout vent #3. The grout filled the lower voids up to grout vent #2. Although grout can be injected near the anchorage zone in this setup where the large voids were located, in actual structures the anchorage diaphragms will likely prevent access to these areas. In most cases, diaphragms range from 5 to 9 ft (1.52 to 2.74 m) long, so they will prevent the access of ducts where large voids are present near anchorage areas.

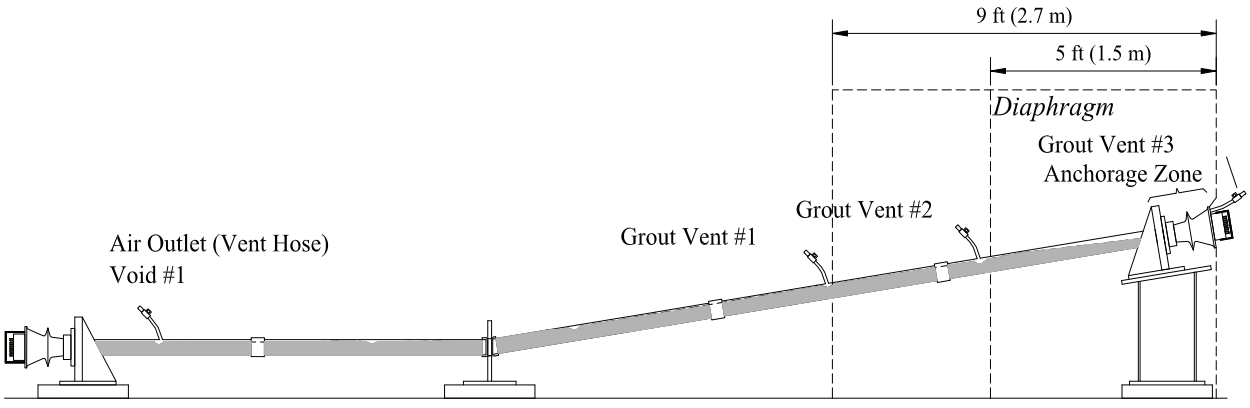

Figure 5-4. Preliminary Test for the PG Method.

Therefore, the injection location and the air outlet for the PG method were developed based on preliminary testing and industry practices. The test set-ups for the different methods are shown in Figure 5-5. All the injection grout inlets for each repair grouting method are at the ports located in the anchor plate of the upper anchorage (Figure 3-1).

5.1.3.1. Pressure-grouting method

The grout injection in the PG method can be applied by using an air-powered grout pump. However, a sealed portion of the ducts could burst when this pressure is applied. To prevent sealed ducts from bursting while under pressure, a hand grout pump was used which does not typically increase the pressure inside the duct to a high level (Figure 3-2).

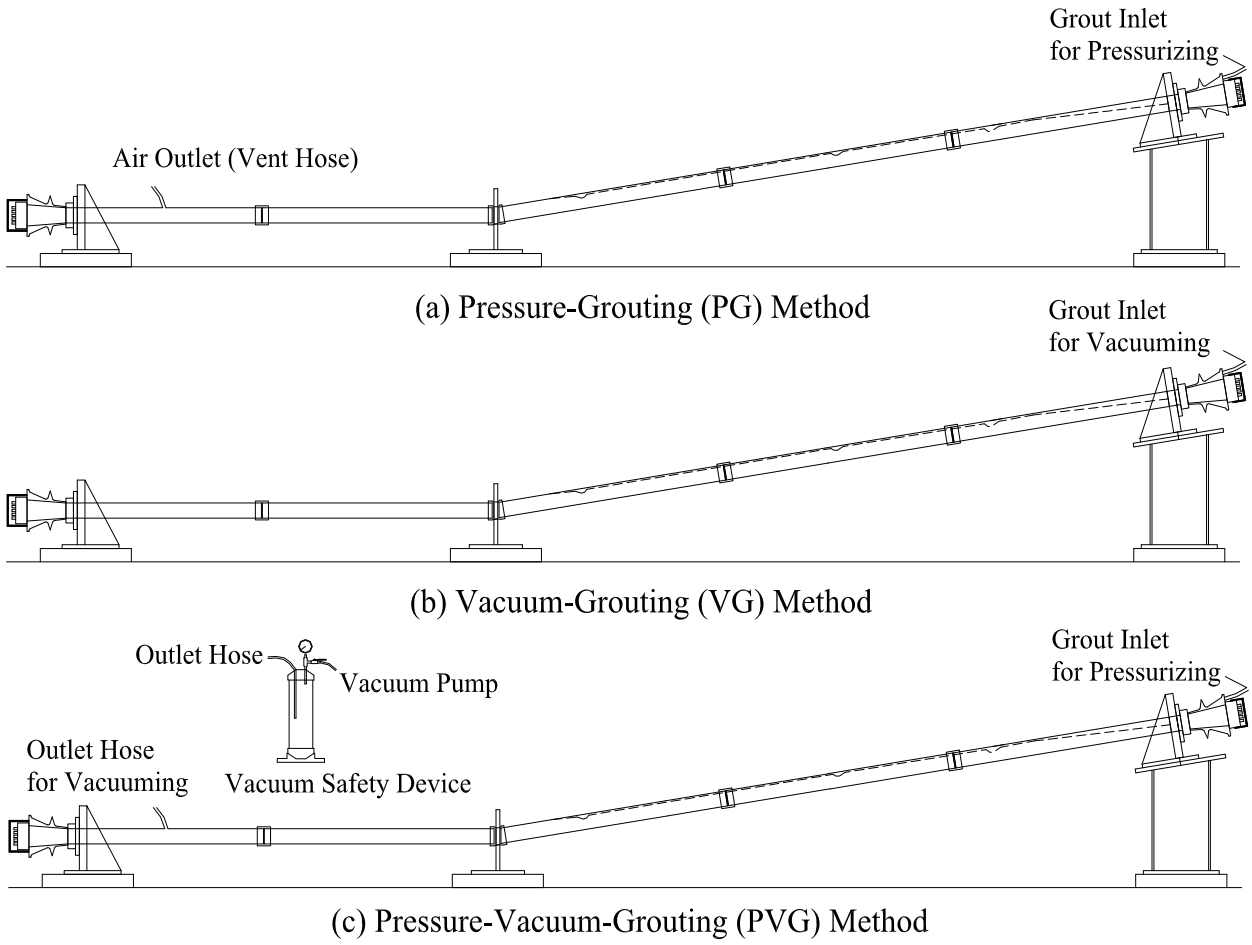

Figure 5-5. Schematic of PET Specimens Showing the Inlet and Outlet Holes.

5.1.3.2. Vacuum-grouting method

The VG method uses only one grout port and no outlet port. The vacuum pump is connected to one end of a T-connection valve, and the grout storage tank is connected to the other end (Figure 5-6). The vacuum grout inlet is connected to the third opening of the T-connection valve. When activating the vacuum pump the valve connecting the storage tank has to be closed. After a vacuum is created inside the tendon the valve for the vacuum pump is closed and the storage tank valve is opened. Repair grout will flow into the duct due to the reduced pressure in the duct. However, in order to create the reduced pressure required to fill the voids an air-tight condition is required. This has been a challenge of using the VG method in the field.

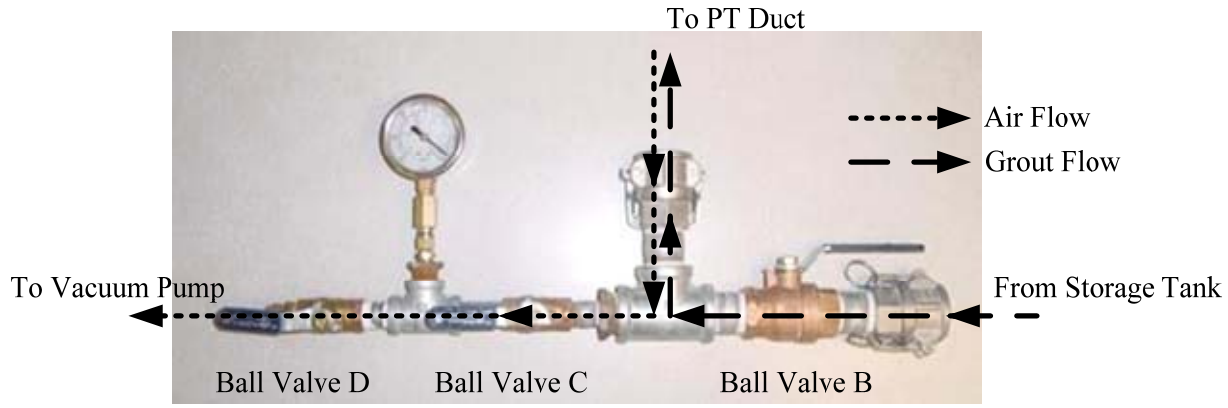

Figure 5-6. T-connection Valve for Vacuum Grouting Method.

5.1.3.3. Pressure-vacuum-grouting method

The PVG method requires the simultaneous use of a hand grout pump and a vacuum pump. The use of a vacuum pump is required to reduce the pressure in the duct, which I turn will help improve the flow of grout into the duct. The vacuum pump is to be connected to the air outlet near the lower anchorage of the PET specimen to improve the filling capability of the repair grouts. Because the PVG method does not require an air-tight duct, it may be more practical for field applications than the VG method. To protect the vacuum pump from being contaminated with repair grout, a safety device was designed and connected between the outlet

hose and the vacuum pump (see Figure 5-9). If grout does flow from the duct, the grout will be retained in the vacuum pump container.

5.1.4. Step-wise procedures for repair grouting methods

The detailed procedures for using PG, VG, and PVG repair methods are described in the following sub-sections.

5.1.4.1. Pressure-grouting method

This method requires an injection port and an air outlet. After these are connected, the following procedure was performed.

- Make connections and apply pressure grout with hand grout pump from top grout port (Figure 5-7).
- Inject repair grout until resistance on hand pump is significant.
- If the repair grout flows out from outlet, close valve at grout outlet and then pump until resistance on hand pump is significant.
- If the repair grout does not flow out until resistance on hand pump is significant, close valves at grout inlet and outlet.
- Remove connection to valves and clean equipment.

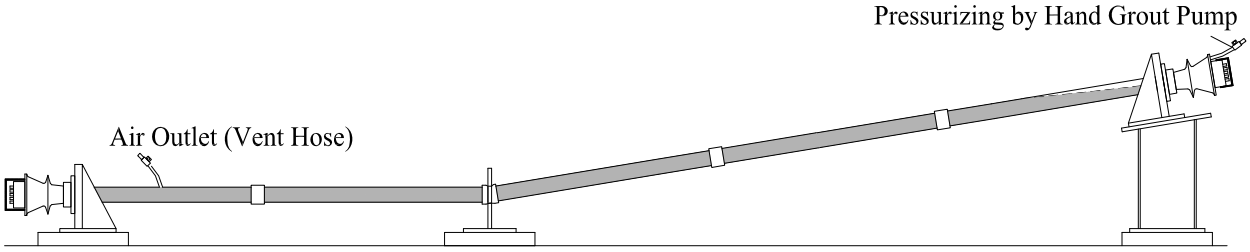

Figure 5-7. Set-up of the PG Method.

5.1.4.2. Vacuum-grouting method

This procedure assumes that all leaks in the system have been sealed. Methods include applying epoxy, chalking, and other materials to leaking areas. After sealing, the researchers used the following procedure:

- Close ball valve B, and open storage tank valve (Figure 5-8).
- Open ball valves A, C, and D (not B).
- Turn on the vacuum pump to reduce pressure by 90% of the atmospheric pressure (26.9 in Hg).
- Close ball valve D and check air-tight status of entire ducts (be reading vacuum gage).
- If vacuum is held, close ball valve C. If vaccum is not maintained, repair leak and start process again.
- Pour repair grout into storage tank.
- Open ball valve B (repair grout will flow into duct).
- Close ball valve A after grout stops flowing.
- Close ball valve B and storage tank valve.
- Remove connection and clean equipment.

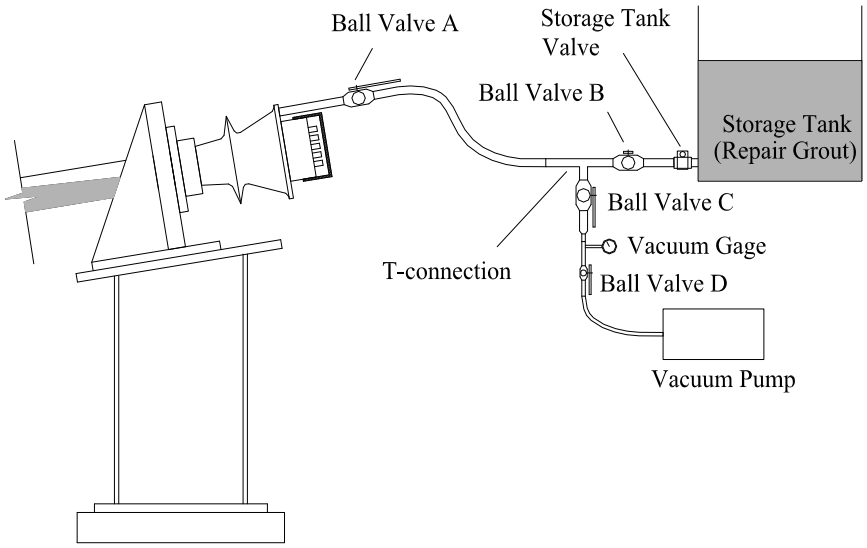

Figure 5-8. Set-up of the VG Method.

5.1.4.3. Pressure-vacuum-grouting method

This method uses both vacuum and pressure to inject repair grout into the voided ducts. The advantages of this method include not having to repair all vacuum leaks and relatively easy repair procedures. To perform the PVG grouting method, the following steps are performed.

- Connect vacuum safety device to air outlet and to vacuum pump (Figure 5-9).
- Connect hand grout pump to top grout port.
- Apply vacuum pump to reduce pressure by 80% (or as much as possible) of the atmospheric pressure (23.9 in Hg).
- Open grout inlet and inject repair grout with hand grout pump.
- If the repair grout flow out from the air outlet, close valve B at air outlet, close valve A at safety device, and then pump until resistance on hand pump is significant.
- If the repair grout does not flow out from the air outlet, close valve A at safety device, and then pump until resistance on hand pump is significant.
- Close valve of grout inlet at upper anchorage.
- Turn off vacuum pump.
- Disconnect tubing from valves and clean equipment.

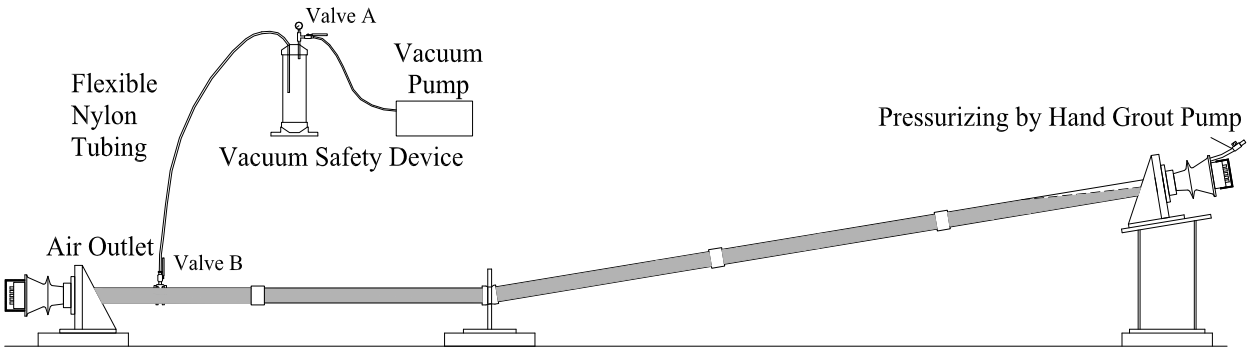

Figure 5-9. Set-up of the PVG Method.

5.1.5. Methodology to evaluate the repair methods and materials

To examine the effectiveness of each grouting method and each grout material, this study performs the following analysis to assess the filling capability (FC), performance, and economic feasibility. The term FC is defined as the ability of the repair method-material combination to fill the voids.

5.1.5.1. Filling capability of repair methods and materials

To compare the FC of each specimen, the length that the repair grout infiltrated the duct was investigated. The infiltration length is measured from the reference point at the upper anchorage and measured along the inclined ducts (Figure 5-10 and Figure 5-11).

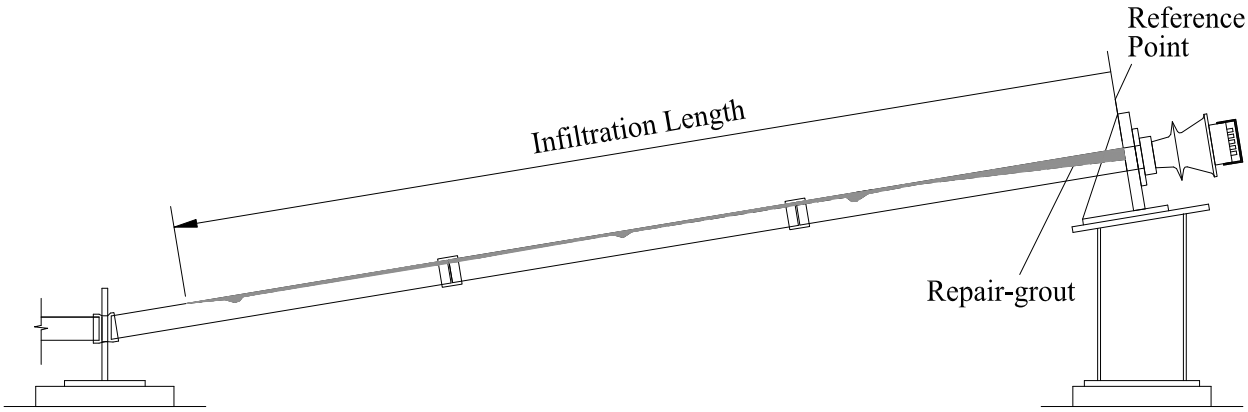

Figure 5-10. The Infiltration Length Measured from the Reference Point.

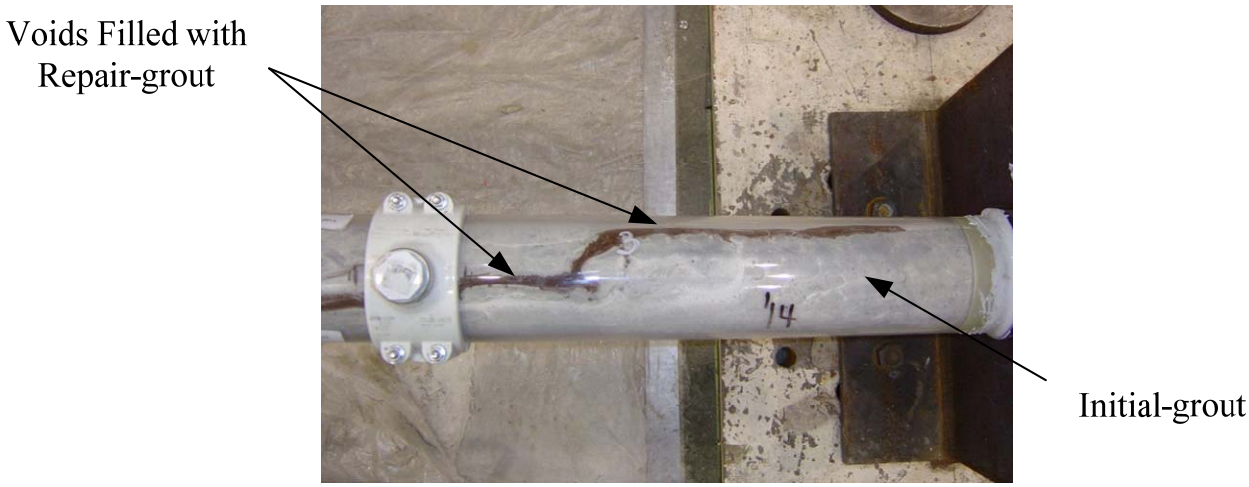

Figure 5-11. Top View of the PET Specimen Showing the Infiltration of Repair Grouts.

The path and width of the bleed line and the shape of the voids varied from one PET specimen to another. This research compares the amount of voids filled by a repair grout using an analysis of cut sections, as presented in Figure 5-12 (a) and discussed earlier. Sections were cut using a steel band saw at the locations shown in Figure 5-12 (a). The following subsection discusses how these were analyzied.

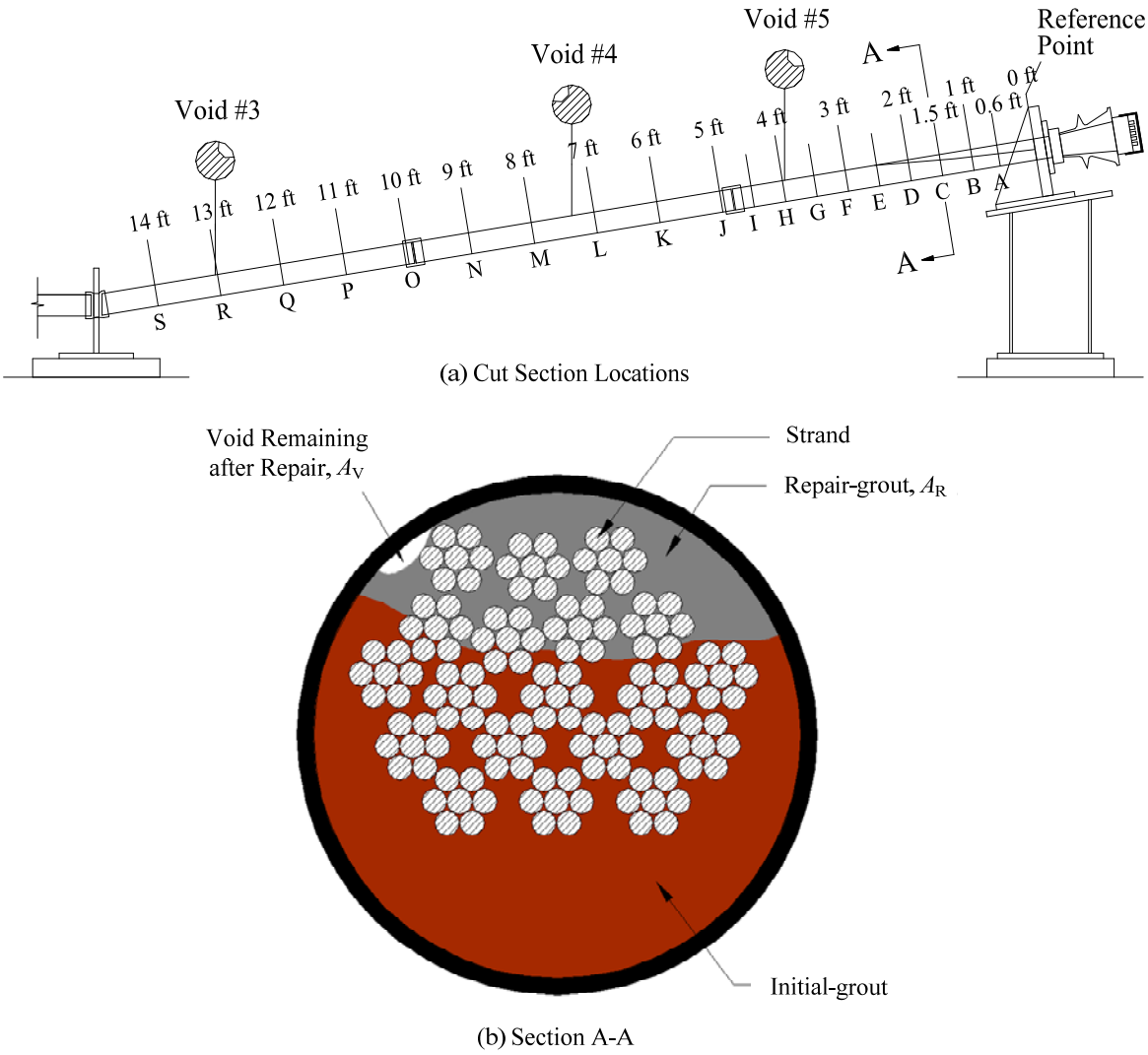

Figure 5-12. (a) Cut Section Locations of Repaired Ducts (b) and Cut Section of A-A.

5.1.5.2. Performance of repair grouts

As already noted the repair grouting was performed by three different methods and three different grout materials such that recommendation in an appropriate and economical repair grouting method for external PT systems can be developed. Figure 5-12 (b) shows an example of cut sections in a repaired duct. Note that small and sometimes isolated voids remain after

grouting and these remaining voids could still leave the tendon vulnerable to corrosion. Therefore, this study evaluated and compared the performance of repair grouts using remaining void ratios from cut sections. The void ratio, η, in the repair grout was defined as follows:

$$\eta = \frac{A_V}{A_R} 100\ \% \tag{5.1}$$

The remaining void ratio can be obtained using the following procedure. First, the cut-section area of a repair grout, A_R, is estimated using figures in AutoCAD®. This area does not include the area of the strands that are covered with repair grout. The area of the remaining voids after repair in the cut section, A_V, is then estimated by outlining the voids in AutoCAD®. After the pre- and post-repair section are generated, comparisons were made in the effectiveness of each repair-grout combination.

5.1.5.3. Economic feasibility

One objective of this research is to propose the most practical repair grouting method to use in the field. Therefore, the preparation time required for each repair method is a critical factor because of its close relationship with the overall repair costs. As mentioned in Section 5.1.3, each repair method requires different amount of sealing and preparation time. Each grout material also has dissimilar times for mixing. Thus, a time analysis of the sealing and mixing procedure will be performed to compare the economic feasibility of each repair method - grout combination.

5.2. MITIGATION OR REPAIR STRATEGIES: RESULTS

This section contains the experimental results and analyses of the repair methods and materials. The objective of this analysis is to provide details on an appropriate repair method and repair grout for field applications. Using test results from the infiltration length and cut sections from each specimen, the analysis was performed to evaluate the FC and performance for each repair

method and grout type. The economic feasibility for the study for the different combinations were also analyzed using estimates of preparation and grout mixing time.

Specimen identification and notation consists of three character groups with each group separated by a hyphen. The first character set denotes the name of the repair grouting method (VG, PG, or PVG) while the grout type is assigned to the second group (C1, C2, or C3). The third and final number represents the specimen number (1 or 2). For example, the classification VG-C1-2 denotes that it is the second specimen using vacuum grouting procedures with Class C-1 grout.

5.2.1. Filling capability of repair grouts

To assess the FC for the different systems the infiltration length and minimum repaired area in cut sections, which means how small voids were repaired in specimens, were analyzed. The following section provides a description of the analysis procedure.

5.2.1.1. Analysis of infiltration length of repair method - grout combination

The FC of the repair methods and repair grouts can be analyzed using the infiltration length measurements assuming that all of the specimens are subjected to the same initial conditions. For example, Specimen VG-C1-2 had 14.3 ft (4.36 m) of the infiltration length from the reference point (Figure 5-13).

The infiltration lengths for all other specimens are provided in Appendix B. From Table 5-3, it can be seen that the VG and PVG methods using Class C-1 and Class C-2 grouts have a better FC than the other combinations. The infiltration lengths also resulted in similar trends when comparing the average value of each repair method and grout. Figure 5-14 and Figure 5-15 show average infiltration lengths and their standard deviations. It can be seen that the VG and PVG methods have higher infiltration lengths than the PG method, on average. Also, Class C-1 and Class C-2 grouts, on average, have better infiltration lengths than does the Class C-3 grout.

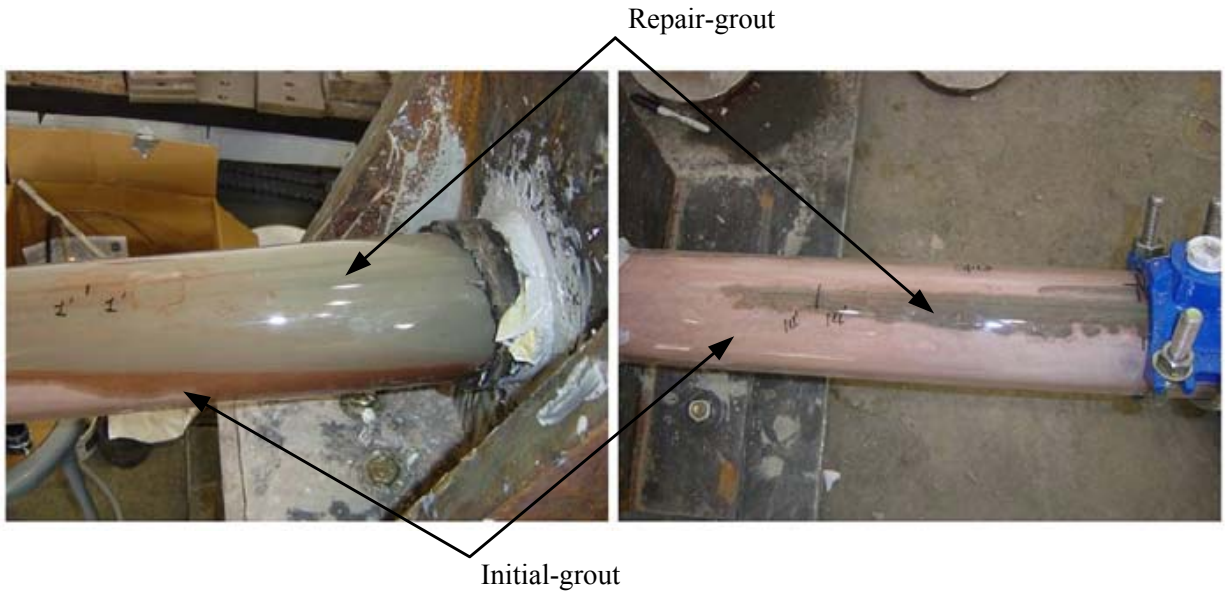

Figure 5-13. Specimen VG-C1-2 Showing Initial and Repair Grouts.

Table 5-3. Results of Repair (Infiltration Length from the Standard Point).

Repair grouts		Infiltration Length of Repair Grouts, ft (m)		
Type	**w/p**	**PG**	**VG**	**PVG**
Class C-1	0.30	11.5 (3.51) / 9.3 (2.83)	14.5 (4.42) / 14.3 (4.36)	15.0 (4.57) / 14.5 (4.42)
Class C-2	0.26	4.6 (1.40) / 14.4 (4.39)	13.4 (4.08) / 14.4 (4.39)	14.4 (4.39) / 14.3 (4.36)
Class C-3	0.27	7.3 (2.23) / 13.2 (4.02)	4.8 (1.46)	3.9 (1.19)

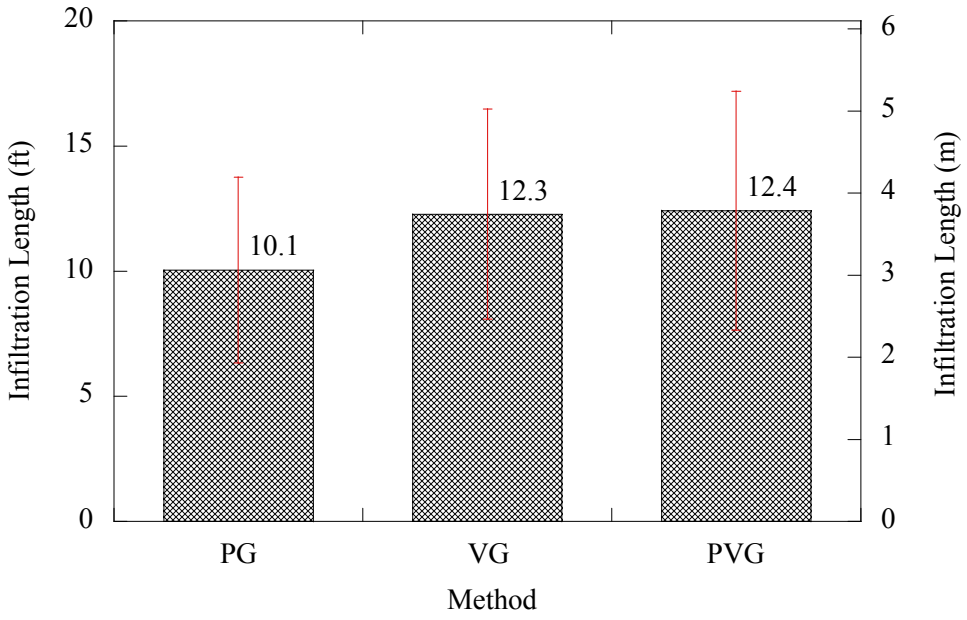

Figure 5-14. Comparison of Infiltration Lengths Obtained with Different Repair Methods.

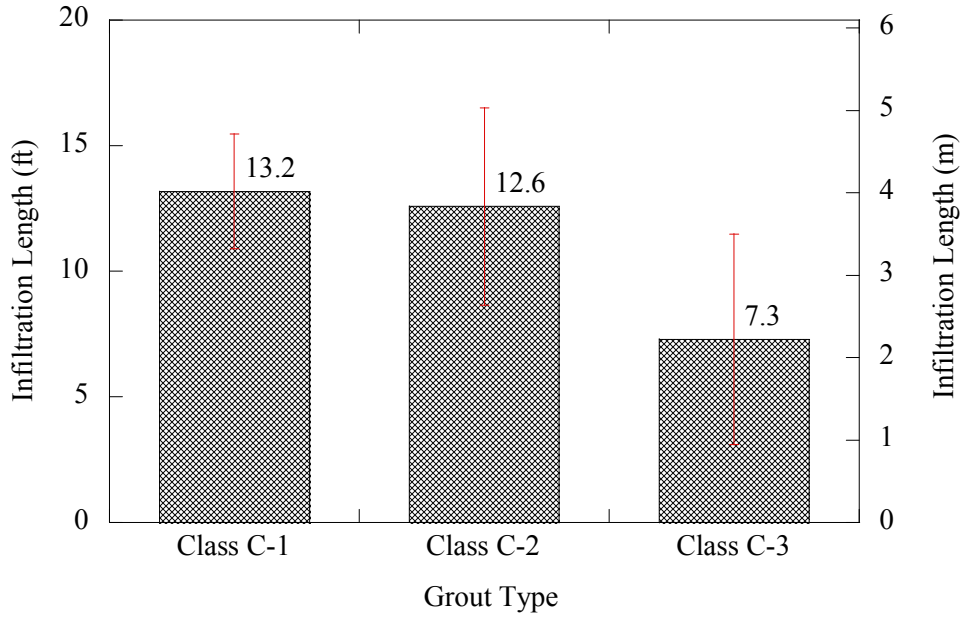

Figure 5-15. Comparison of Infiltration Lengths Obtained with Different Repair Grouts.

A two-factor factorial experiment design was used to analyze the differences between infiltration lengths of the various repair methods and repair grouts. In this experiment the two

factors are repair methods (PG, VG, and PVG) and repair grout materials (Class C-1, Class C-2, and Class C-3). The linear statistical model of the two-factor factorial is defined by

$$Y_{ijk} = \mu + \tau_i + \beta_j + (\tau\beta)_{ij} + \varepsilon_{ijk} \begin{cases} i = 1,2,3 \\ j = 1,2,3 \\ k = 1 \text{ or } 1,2 \end{cases}, \tag{5.2}$$

where μ is the overall mean effect, τ_i is the effect of the repair methods, β_j is the effect of the repair grout materials, $(\tau\beta)_{ij}$ is the effect of the interaction between repair methods and repair grouts, and ε_{ijk} is a random error component having a normal distribution with a mean zero and variance σ^2. The null and alternate hypotheses are defined as

$$\begin{aligned}
&1.\ H_0 = \tau_1 = \tau_2 = \tau_3 = 0 && \text{(no main effect of repair methods)} \\
&\quad H_1 = \tau_i \neq 0 \ \text{ at least one } i \\
&2.\ H_0 = \beta_1 = \beta_2 = \beta_3 = 0 && \text{(no main effect of repair grouts)} \\
&\quad H_1 = \beta_j \neq 0 \ \text{ at least one } j \\
&3.\ H_0 = (\tau\beta)_{11} = (\tau\beta)_{12} = \cdots = (\tau\beta)_{33} = 0 && \text{(no interaction)} \\
&\quad H_1 = \text{at least one } (\tau\beta)_{ij} \neq 0
\end{aligned} \tag{5.3}$$

The analysis of variance (ANOVA) is performed to test these hypotheses. Table 5-4 shows the ANOVA results for the infiltration length. At the 0.05 level of significance, the ANOVA results show that different grouts affect the FC of repair grouting (*p*-value of repair grouts is less than 0.05) while the repair methods do not reveal a significant difference for filling voids (*p*-value of repair grouts is not less than 0.05).

Table 5-4. ANOVA for the Infiltration Length.

Source	Type III Sum of Square	Degree of Freedom	Mean Square	F Statistic	*p*-value
Repair Methods	3.367	2	1.683	0.172	0.845
Repair grouts	120.492	2	60.246	6.157	0.029
Methods×Grouts	77.792	4	19.493	1.992	0.200
Error	68.495	7	9.785		
Total	250.398	15			

While the ANOVA test are capable of showing that different repair grouts have an influence on filling voids in ducts, it is not capable of identifying which grout is superior. Hence, Fisher's *least significant difference* (LSD) method using the 0.05 level of significance is applied to determine which repair grout is preferred (Montgomery and Runger 2007). The mean values for each repair grout are compared with the null hypothesis:

$$H_0:\ \mu_i = \mu_j \ \text{for all}\ i \neq j \tag{5.4}$$

According to Fisher's LSD, the pair of means for infiltration length would be concluded to be significantly different if

$$|\bar{y}_{i.} - \bar{y}_{j.}| > \text{LSD}$$

$$\text{where, LSD} = t_{\alpha/2,N-a}\sqrt{MS_E\left(\frac{1}{n_i}+\frac{1}{n_j}\right)} \tag{5.5}$$

where $t_{\alpha/2,a(n-1)}$ is a two sided *t*-statistic with α level of significance, a is the number of treatments applied (repair grouts), N is the total sample number, and MS_E is the mean square error when the sample sizes are different. The mean values for the repair grouts are compared in Table 5-5.

Table 5-5. The Comparisons of Void Ratios Corresponding to the Repair Grouts.

Comparison	Difference of Means	LSD	Results
(C-1)-(C-2)	0.6	3.901	No difference
(C-1)-(C-3)	5.883	4.361	C-3 is lower than C-1
(C-2)-(C-3)	5.823	4.361	C-3 is lower than C-2

However, Fisher's LSD test is susceptible to a high probability of Type I errors (also, known as α-error) because of its inability to consider multiple comparisons. Thus, Tukey's Honestly Significant Differences (HSD) test and Student-Newman-Keuls (SNK) test were performed using the program SPSS™, a statistical software package. Tukey's HSD test is a fairly conservative measure of differences among groups while the SNK test is a more sensible alternative to Duncan's test, which is designed for comparing samples with significantly different means. The results of both tests are provided in Table 5-6. The results show that the Class C-3 grout has a lower FC than the Class C-1 grout in Tukey's HSD test. The Class C-3 grout also shows a lower FC than both the Class C-1 and C-2 grouts in the SNK test.

Table 5-6. The Grouping Results of Tukey's HSD and SNK Tests.

Method	Source	N	Subset	Source	N	Subset	
			1			1	2
Tukey's HSD Test	PG VG PVG	6 5 5	10.050 12.280 12.420	C-1 C-2 C-3	6 6 4	13.183 12.583 -	- 12.583 7.300
Student-Newman-Keuls Test	PG VG PVG	6 5 5	10.050 12.280 12.420	C-1 C-2 C-3	6 6 4	13.183 12.583 -	- - 7.300

From the results shown in Table 5-6, it can be reasonably concluded that the Class C-3 grout has a lower FC than the other grouts. In addition, the Class C-3 grout has different infiltration lengths when used in conjunction with the VG and PVG methods, compared to the Class C-1 and C-2 grouts. Thus, the FC of each repair method will be further evaluated to

identify if one repair method has a better FC using the Class C-1 and Class C-2 grouts. Figure 5-16 shows the comparison of average infiltration lengths for the Class C-1 and Class C-2 grouts. The graph shows that the PG method seems to have a lower FC than the VG and PVG methods.

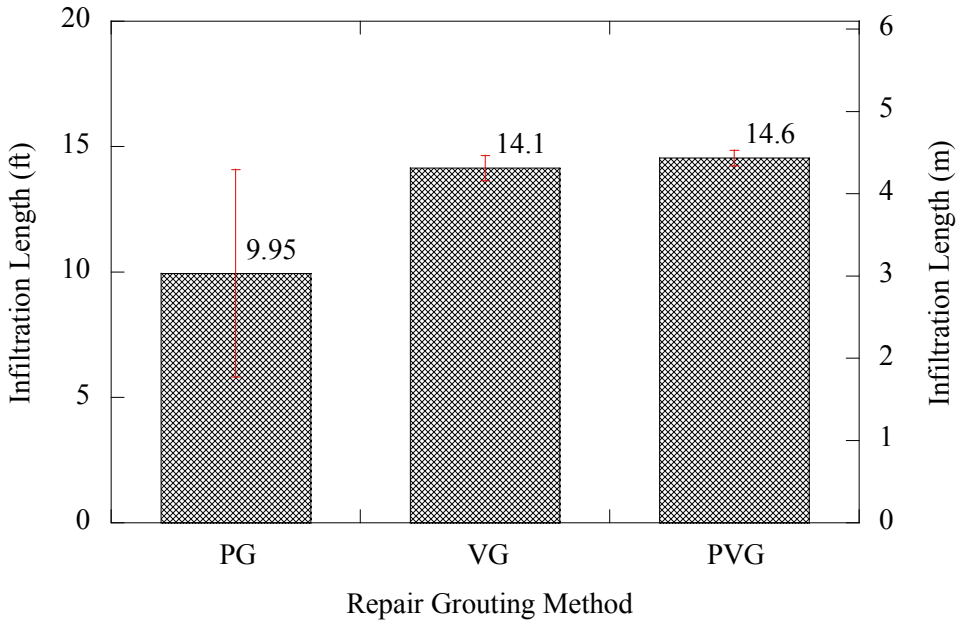

Figure 5-16. Comparison of Infiltration Length in Each Repair Method (Based on Results from Class C-1 and C-2 Grouts).

To compare the repair grouting methods in more detail, a two-factor factorial experiment was applied (the Class C-3 grout is not considered in this analysis). The two factors considered are the repair methods (PG, VG, and PVG) and the repair grouts (Class C-1 and Class C-2). The linear statistical model of the two-factor factorial is provided in Equation (5.2), where j is 1 and 2 because Class C-3 grout is not considered. The null and alternate hypotheses are defined as follows:

$$
\begin{aligned}
&1.\ H_0 = \tau_1 = \tau_2 = \tau_3 = 0 && \text{(no main effect of repair methods)}\\
&\quad H_1 = \tau_i \neq 0 \ \text{ at least one } i\\
&2.\ H_0 = \beta_1 = \beta_2 = 0 && \text{(no main effect of repair grouts)}\\
&\quad H_1 = \beta_j \neq 0 \ \text{ at least one } j\\
&3.\ H_0 = (\tau\beta)_{11} = (\tau\beta)_{12} = \cdots = (\tau\beta)_{32} = 0 && \text{(no interaction)}\\
&\quad H_1 = \text{at least one } (\tau\beta)_{ij} \neq 0
\end{aligned}
\qquad (5.6)
$$

The ANOVA tests are performed again to test these hypotheses. Table 5-7 shows the ANOVA results for the infiltration results. For the 0.05 level of significance, the ANOVA shows that the repair methods do not affect the FC of the repair grouts. It should be noted that these results do not consider the amount of preparation work required to perform each repair method. They simply indicate that once prepared correctly, each method has the same potential to fill the voids.

Table 5-7. ANOVA Table for the Infiltration Results (Only C-1 and C-2 are Considered).

Source	Type III Sum of Square	Degree of Freedom	Mean Square	F Statistic	*p*-value
Repair Methods	51.947	2	25.973	3.050	0.122
Repair grouts	1.080	1	1.080	0.127	0.734
Methods×Grouts	0.140	2	0.070	0.008	0.992
Error	51.090	6	8.515		
Total	104.257	11			

5.2.1.2. Analysis of minimum repaired area in cut sections.

Another way to evaluate the FC of the repair grouts is to analyze the minimum repaired area of each specimen from its cut sections. Improved FC should be represented by a reduced value in the minimum repaired area of the cut sections. In another way, a grout - method combination having low FC cannot fill small voids in ducts. Figure 5-17 shows the cross-section views of the cut sections obtained from Specimen VG-C1-2. From the cut sections, it is noted that the repair grout successfully filled the main voids and the #3, #4, and #5 large voids (see Figure 5-12).

However, small voids still exist inside the repaired ducts, especially in-between strands (see cut sections, C, D, E, and F in Figure 5-17). Those voids cannot be repaired because the voids are isolated from the "bleed line," which are routes for the repair grouts.

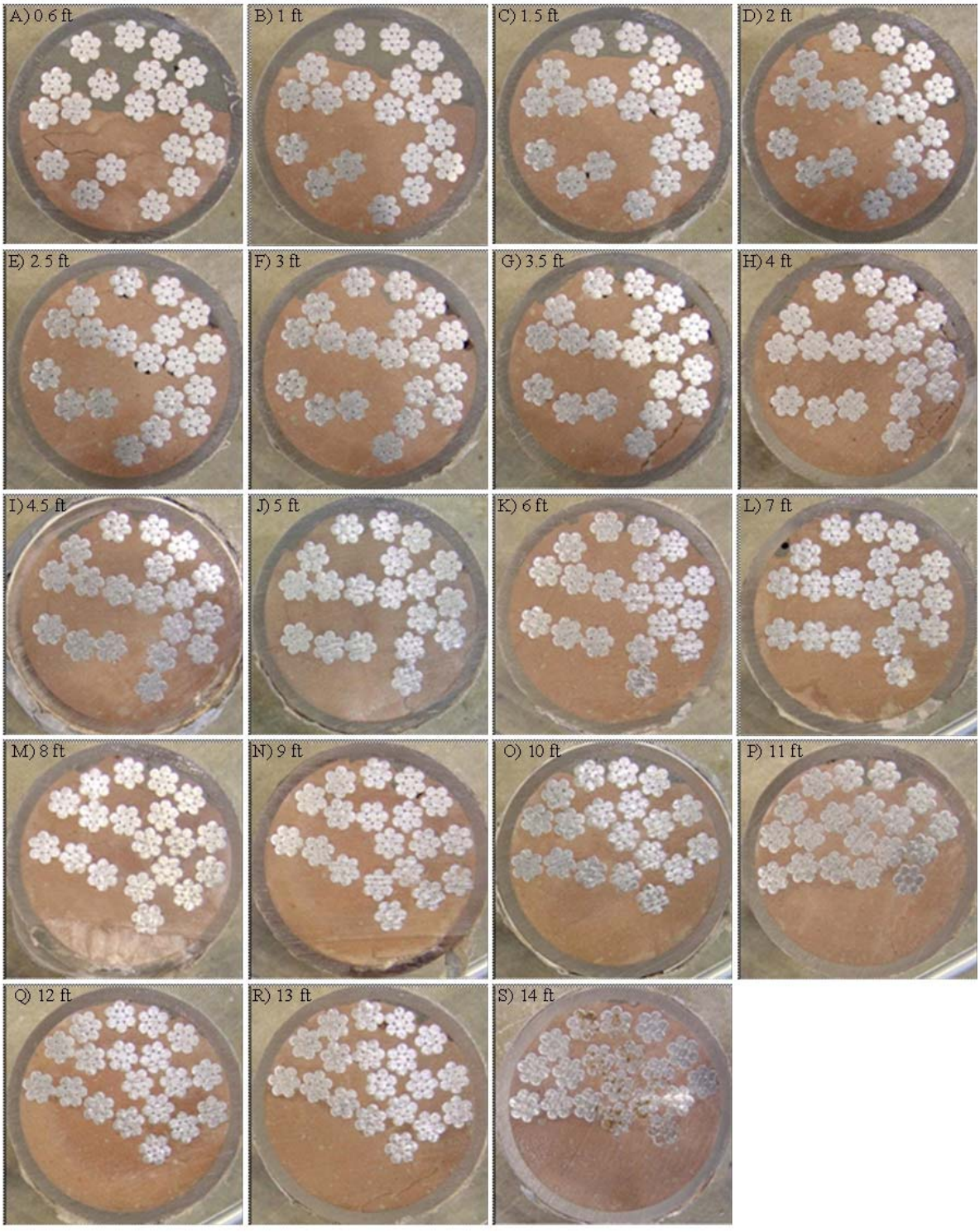

Figure 5-17. Cut Sections of Specimen VG-C1-2 for the FC of Repair Method –Grout Combination. (Note: See top left corner of each figure for the location of cross-section.)

To compare the minimum repaired area in cut sections, repaired areas in each cut section are provided in Table 5-8. The repaired area was calculated using AutoCAD® (See Subsection 5.1.5.2 for details).

Table 5-8. The Void Area Remaing after Repair of Specimen VG-C1-2.

Cut Sections, ft (m)		Repaired Area, A_R, inch^2(10^{-4} m^2)	Void Area, A_V, inch^2(10^{-4} m^2)	Void Ratio, η (%)
A	0.6 (0.18)	2.528 (16.31)	0.0095 (0.061)	0.38
B	1 (0.30)	1.525 (9.84)	0.0045 (0.029)	0.30
C	1.5 (0.46)	0.783 (5.05)	0.0044 (0.028)	0.56
D	2 (0.61)	0.515 (3.32)	0.0066 (0.043)	1.28
E	2.5 (0.76)	0.333 (2.15)	0.0111 (0.072)	3.33
F	3 (0.91)	0.288 (1.86)	0.0024 (0.015)	0.83
G	3.5 (1.07)	0.216 (1.39)	0.0012 (0.008)	0.56
H	4 (1.22)	0.198 (1.28)	0.0099 (0.064)	5.01
I	4.5 (1.37)	0.185 (1.19)	0.0020 (0.013)	1.08
J	5 (1.52)	0.339 (2.19)	0.0060 (0.039)	1.77
K	6 (1.83)	0.202 (1.30)	0.0009 (0.006)	0.45
L	7 (2.13)	0.254 (1.64)	0.0184 (0.119)	7.24
M	8 (2.44)	0.212 (1.37)	0.0042 (0.027)	1.98
N	9 (2.74)	0.223 (1.44)	0.0027 (0.017)	1.21
O	10 (3.05)	0.331 (2.13)	0.0056 (0.036)	1.69
P	11 (3.35)	0.261 (1.68)	0.0088 (0.057)	3.38
Q	12 (3.66)	0.096 (0.62)	0.0069 (0.045)	7.23
R	13 (3.96)	0.119 (0.77)	0.0082 (0.053)	6.87
S	14 (4.27)	0.060 (0.39)	0.0029 (0.019)	4.81
Sum		8.667 (55.92)	0.1162 (0.750)	1.34

The minimum repaired area of Specimen VG-C2-1 is provided in cut section S in Table 5-8 (0.060 inch^2, 0.39×10^{-4} m^2). Table 5-9 shows the minimum repaired area for every PET specimen. The values from the other specimens are given in Appendix B.

Table 5-9. Results of Repair grouts (Minimum Repaired Area in Cut Sections).

Grout Type	Minimum Repaired Area in Cut Sections, inch^2 (10^{-4} m^2)		
	PG	VG	PVG
Class C-1	0.033 (0.21) / 0.181 (1.17)	0.030 (0.19) / 0.060 (0.39)	0.051 (0.33) / 0.021 (0.13)
Class C-2	0.040 (0.26) / 0.120 (0.77)	0.019 (0.12)	0.053 (0.34) / 0.031 (0.20)
Class C-3	0.186 (1.20) / 0.141 (0.91)	0.094 (0.61)	0.074 (0.48)

Figure 5-18 and Figure 5-19 show the average and standard deviation of the minimum repaired area for each repair method and repair grout, respectively. Through the comparison of the minimum repaired area in each grout method it was determined that the VG and PVG methods have better FC than the PG method, on average. It can also be seen that, from the comparison of the repair grouts, the Class C-1 and Class C-2 grouts have better FC than the Class C-3 grout, on average.

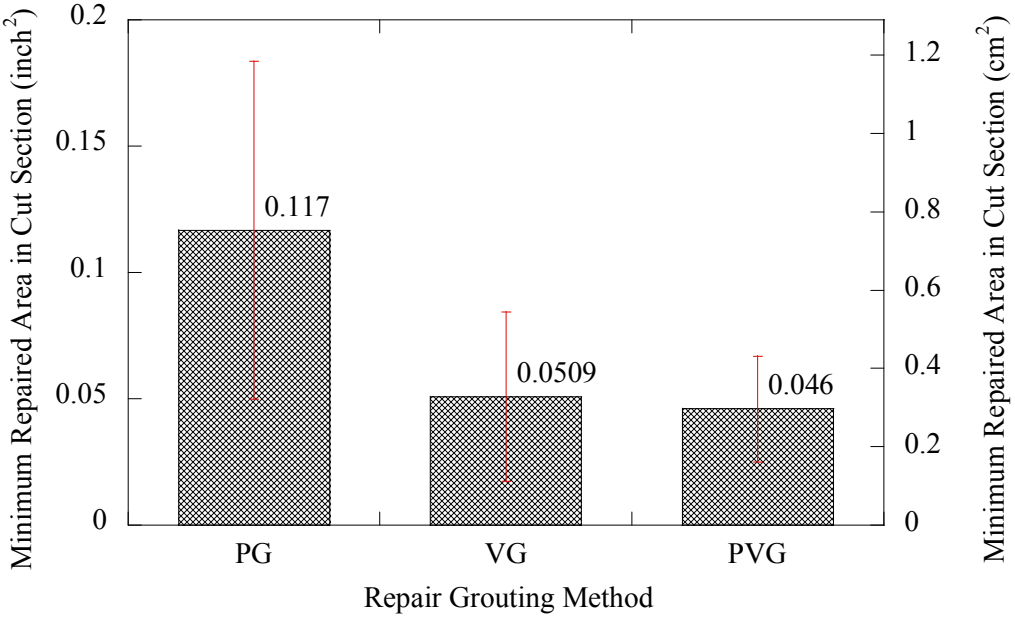

Figure 5-18. Comparison of Minimum Repaired Area for Different Repair Methods.

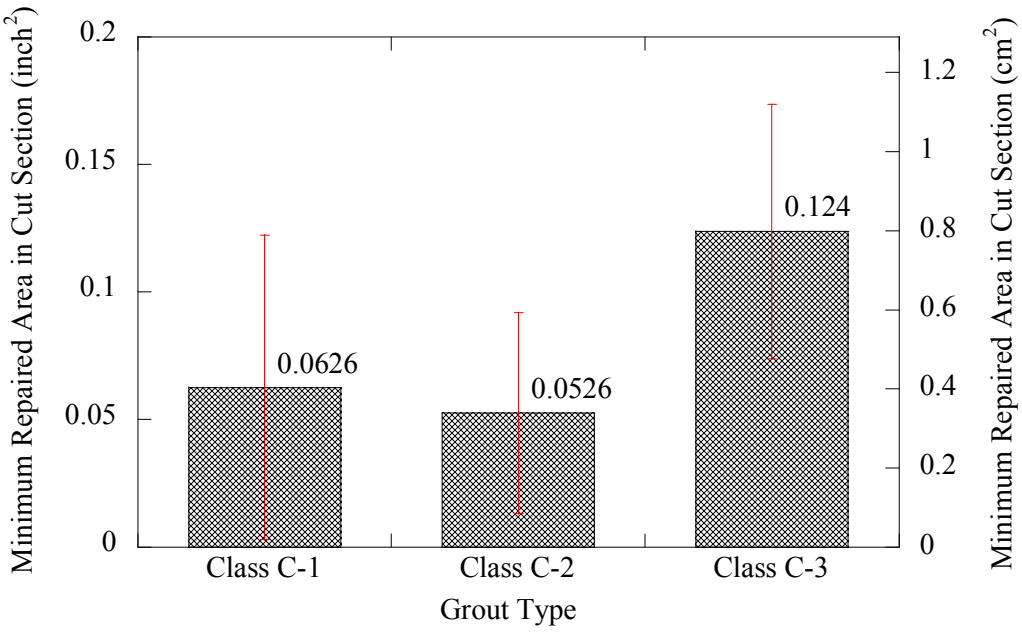

Figure 5-19. Comparison of Minimum Repaired Area Corresponding to Different Grouts.

The two-factor factorial experiment was again used to analyze the differences between the minimum repaired area of each specimen with respect to the repair method and repair grout. The two factors used are the repair methods (PG, VG, and PVG) and repair grout materials (Class C-1, C-2, and C-3 grouts). The linear statistical model of the two-factor factorial design is provided in Equation (5.2), and the null and alternative hypotheses were shown earlier in Equation (5.3).

The ANOVA tests were performed to test these hypotheses. Table 5-10 shows the results of the ANOVA table for the minimum repaired area in the sections. For the 95% confidence limit, the ANOVA shows that different repair methods and grouts do not significantly affect the FC (minimum repaired area in specimen) of the repair grouting. However, based on the comparisons of the graphs and results of the ANOVA, the PG method seems to have lower FC than the VG and PVG methods.

Table 5-10. ANOVA for the Minimum Repaired Area in Cut Sections.

Source	Type III Sum of Square	Degree of Freedom	Mean Square	F Statistic	*p*-value
Repair Methods	0.015	2	0.007	2.690	0.147
Repair grouts	0.009	2	0.004	1.589	0.279
Methods×Grouts	0.001	4	0.000	0.117	0.972
Error	0.016	6	0.003		
Total	0.044	14			

5.2.1.3. Analysis of influence factors in filling capability

Although significant efforts have been made to ensure consistency between the specimens, the grout levels from test setups do have slight differences from specimen to specimen. Also, void shapes in ducts could have formed differently due to differences in bleed water and entrapped air. Different void shapes and sizes in specimens have an influence on the resistance force, P, generated against the flow of repair grout. For the flow of a fluid element in a void a constant cross sectional area, A, a perimeter, U, and length, dx, (Figure 5-20), the the term P is evaluated. The unit resistance pressure, p, in a small void is estimated as follows:

$$\left(p+\frac{1}{2}\mathrm{d}p\right)A-\left(p-\frac{1}{2}\mathrm{d}p\right)A=\tau_0 U\,\mathrm{d}x$$
$$\mathrm{d}p=\frac{U}{A}\tau_0\,\mathrm{d}x \tag{5.7}$$

For an arbitrarily shaped void, the resistance stresses, τ_0, are generated opposite to the direction of grout flow around the perimeter U of the void (Figure 5-20). For the unit length, dx, the relation between the unit resistance pressure, p, and the resistance force, P, for a given length, l, are given by:

$$P=\int_0^l \mathrm{d}p=\int_0^l \frac{U}{A}\tau_0\,\mathrm{d}x \tag{5.8}$$

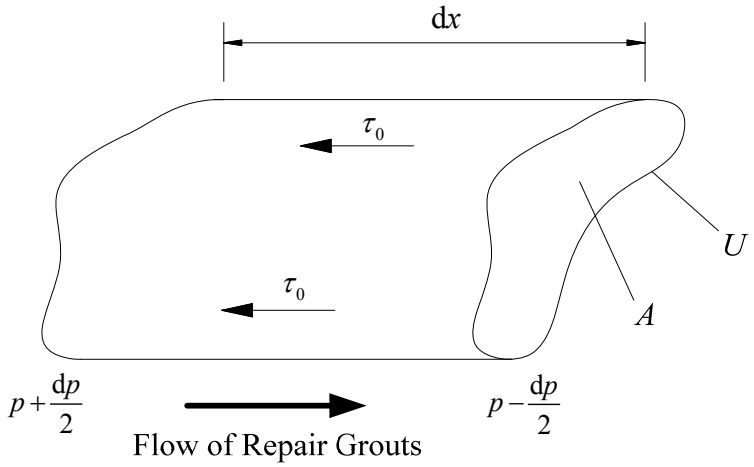

Figure 5-20. Schematic of Resistance Stresses for Grout Flow in Voids.

Because the resistance stresses in repair grouts are analogous to shear stress in a fluid flow, the principles of fluid mechanics are used to estimate this stress for a steady uniform flow (Cruise et al. 2007):

$$\tau_0 = \frac{f \rho V^2}{8} \tag{5.9}$$

where, V is the fluid velocity. The factor, f, is a dimensionless parameter representing the roughness between the fluid flow and the ducts, while the factor, ρ, represents the density of the fluid. Substituting Equation 5.9 into Equation 5.8 and then integrating results in:

$$P = \frac{U}{A} l \frac{f \rho V^2}{8} \tag{5.10}$$

where, the specific weight of the fluid, γ, is expressed as $\gamma = \rho g$. Thus, the term P is determined as follows:

$$P = \frac{l}{R_h} f \frac{\gamma V^2}{8g} \tag{5.11}$$

where, the hydraulic radius R_h is defined as A/U, and l is the infiltration length when the applied force is P. In Equation (5.11), the friction factors are considered constant in this case due to the slow rate of flow. However, R_h and V are critical parameters that directly affect the infiltration length, l, in the repair grouts. From the basic principle of fluid motion, the mass flow rate is as follows:

$$Q = AV = \text{const.} \tag{5.12}$$

A fluid with a constant mass flow rate will have a velocity that is inversely proportional to the cross-sectional area, A, of the void. Therefore, A directly impacts the resistance force, P, in ducts. Summarizing the infiltration length, l, can be determined as follows:

$$l = 8 \cdot \frac{P}{f} \frac{g}{\gamma} R_h \frac{A^2}{Q^2} \tag{5.13}$$

when the applied force is constant in the duct. The value of P/f is a constant that represents an applied force divided by the friction factor in the duct.

To analyze the factors affecting the filling of voids, correlations between infiltration length and varying geometric and material conditions across the specimens were evaluated. For the geometric conditions of specimens, the average square area, A^2, of the voids and hydraulic radius, R_h, are considered in the analysis. The efflux time of each repair grout is estimated by considering the different fluidity conditions of the grouts. Table 5-11 was generated using estimates from section cuts and the results of the flow cone test. Table 5-12 shows the correlation matrix for all of the specimens.

Table 5-11. Description of Experimental Data on Influence Factors.

Specimen	Infiltration Length, ft (m)	Average R_h of Voids, inch (10^{-2} m)	Average A^2 of Voids, inch^2 (10^{-4} m^2)	Efflux Time of Repair grout (s)
VG-C1-1	14.5 (4.4)	0.066 (0.17)	0.43 (2.8)	9.91
VG-C1-2	14.3 (4.4)	0.044 (0.11)	0.46 (2.9)	8.34
VG-C2-2	14.4 (4.4)	0.037 (0.09)	0.41 (2.6)	12.06
VG-C3-1	4.8 (1.5)	0.053 (0.14)	0.81 (5.2)	22.57
PG-C1-1	11.5 (3.5)	0.084 (0.21)	0.95 (6.1)	7.8
PG-C1-2	9.3 (2.8)	0.057 (0.14)	0.59 (3.8)	8.72
PG-C2-1	4.6 (1.4)	0.040 (0.10)	0.35 (2.3)	15.31
PG-C2-2	14.4 (4.4)	0.054 (0.14)	0.49 (3.2)	12.59
PG-C3-1	7.3 (2.2)	0.049 (0.13)	0.76 (4.9)	19.12
PG-C3-2	13.2 (4.0)	0.088 (0.22)	1.04 (6.7)	23.14
PVG-C1-1	15 (4.6)	0.061 (0.15)	0.57 (3.7)	9.97
PVG-C1-2	14.5 (4.4)	0.061 (0.16)	0.63 (4.1)	8.75
PVG-C2-1	14.4 (4.4)	0.053 (0.13)	0.82 (5.3)	14.16
PVG-C2-2	14.3 (4.4)	0.047 (0.12)	0.44 (2.8)	10.84
PVG-C3-1	3.9 (1.2)	0.056 (0.14)	0.68 (4.4)	25.63

Table 5-12. Correlation Matrix of Repaired Specimens.

	Infiltration Length	Average A^2 of Voids	Average R_h of Voids	Efflux Time of Repair grouts
Infiltration Length	1	-0.121	0.166	-0.646
Average A^2 of Voids	-0.121	1	0.755	0.441
Average R_h of Voids	0.166	0.755	1	0.073
Efflux Time of Repair grouts	-0.646	0.441	0.073	1

From Table 5-12, the geometric conditions of voids (R_h and A^2) do not affect the infiltration length of the repair grouts; however, the efflux time has a slight negative correlation

with the infiltration length of the repair grouts. The correlation coefficient factors show different trends in Table 5-12 when they are estimated by each repair grouting method.

The correlation coefficient factors obtained are shown in Table 5-13, Table 5-14, and Table 5-15. Table 5-13 shows that the correlation coefficient between the infiltration length and A^2. This correlation is highly negative when using the VG method. However, this correlation conflicts with the theory involving resistance force in ducts derived in Equation 5.13. The reason for this is that the flow rate Q in the VG method is not constant; thus, the velocity of the fluid in a small void is not inversely proportional to the flow rate. Therefore, the A^2 does not affect the infiltration length when using the VG method. From Table 5-14, the average R_h has a slight linear correlation with infiltration length obtained when using the PG method but not when using the VG and PVG methods. The efflux time of the repair grouts has a negative correlation with the infiltration length for the VG and PVG methods but not in the PG method. Therefore, the correlation matrix for the PG method is obtained separately as shown in Table 5-16. The VG and PVG methods are assessed together to estimate the correlation matrix (Table 5-17).

Table 5-13. Correlation Coefficient between Infiltration Length and Average A^2 of Voids.

Average A^2 of Voids	Infiltration Length		
	PG	VG	PVG
PG	0.458	-	-
VG	-	-0.998	-
PVG	-	-	-0.166

Note: "-" indicates no correlation between factors.

Table 5-14. Correlation Coefficient between Infiltration Length and Average R_h of Voids.

Average R_h of Voids	Infiltration Length		
	PG	VG	PVG
PG	0.654	-	-
VG	-	-0.169	-
PVG	-	-	0.012

Note: "-" indicates no correlation between factors.

Table 5-15. Correlation Coefficient between Infiltration Length and Efflux Time of Grouts.

Efflux Time of Repair grouts	Infiltration Length		
	PG	VG	PVG
PG	-0.032	-	-
VG	-	-0.970	-
PVG	-	-	-0.961

Note: "-" indicates no correlation between factors.

Table 5-16. Correlation Matrix of PG Methods.

	Infiltration Length	Average A^2 of Voids	Average R_h of Voids	Efflux Time of Repair grouts
Infiltration Length	1	0.458	0.654	-0.032
Average A^2 of Voids	0.458	1	0.920	0.336
Average R_h of Voids	0.654	0.920	1	0.083
Efflux Time of Repair grouts	-0.032	0.336	0.083	1

From Table 5-16 one can conclude that the average R_h has a slightly positive and linear relationship with infiltration length when using the PG method. However, the infiltration length for the PG method does not reveal any correlation with the efflux time of the repair grouts. Figure 5-21 shows the scatter plot between infiltration length and the average R_h value when using the PG method. Although the correlation coefficient between these variables is not highly positive, they can be rationalized based on the fact that the FC of the PG method is dominated by geometric conditions.

Table 5-17. Correlation Matrix of VG and PVG Methods.

	Infiltration Length	Average A^2 of Voids	Average R_h of Voids	Efflux Time of Repair grouts
Infiltration Length	1	-0.538	-0.073	-0.958
Average A^2 of Voids	-0.538	1	0.248	0.619
Average R_h of Voids	-0.073	0.248	1	0.023
Efflux Time of Repair grouts	-0.958	0.619	0.023	1

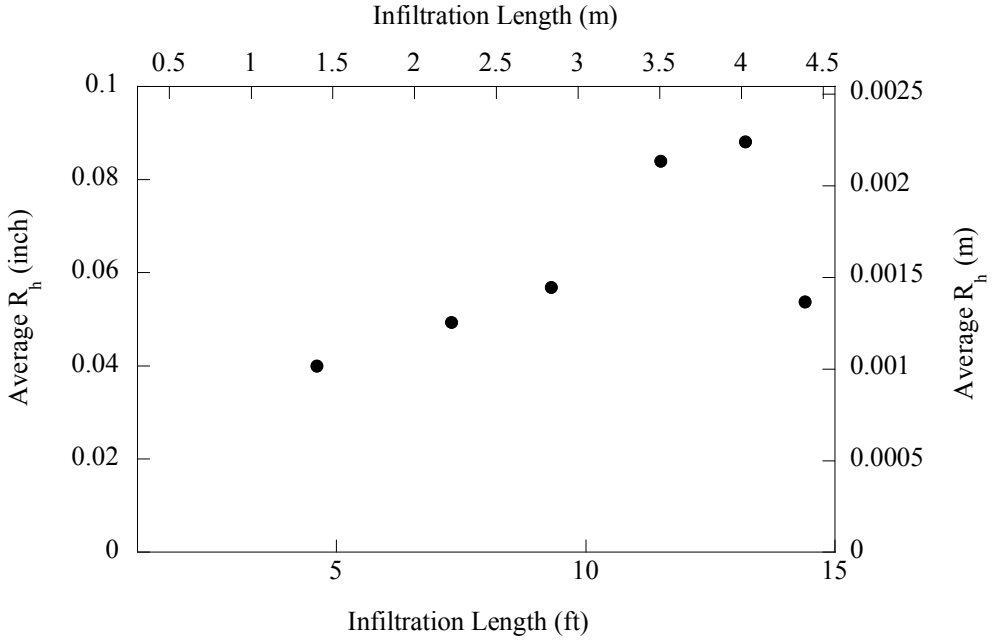

Figure 5-21. Scatter Plot between Infiltration Lengths and Average R_h.

When the VG and PVG methods were used (Table 5-17), the correlation between the infiltration length and the efflux time of the repair grouts was highly negative. Thus, it is shown that when the efflux time is lower the FC is higher. However, the FC of these methods does not

have any correlation with the geometric condition, R_h. Figure 5-22 shows the scatter plot between infiltration length and the initial efflux time of repair grouts when applying the VG and PVG methods. Although the correlation coefficient between the infiltration lengths and the initial efflux time is highly negative, the scatter plot shows that there are no data points between low infiltration lengths and high infiltration lengths. In addition, the two data points with low infiltration lengths are from the Class C-3 grout. When considering only the Class C-1 and C-2 grouts, the relationships between infiltration length and efflux time do not show negative correlations, and therefore it is difficult to conclude that the FC of the VG and PVG methods are dominated by the initial efflux time of the repair grouts.

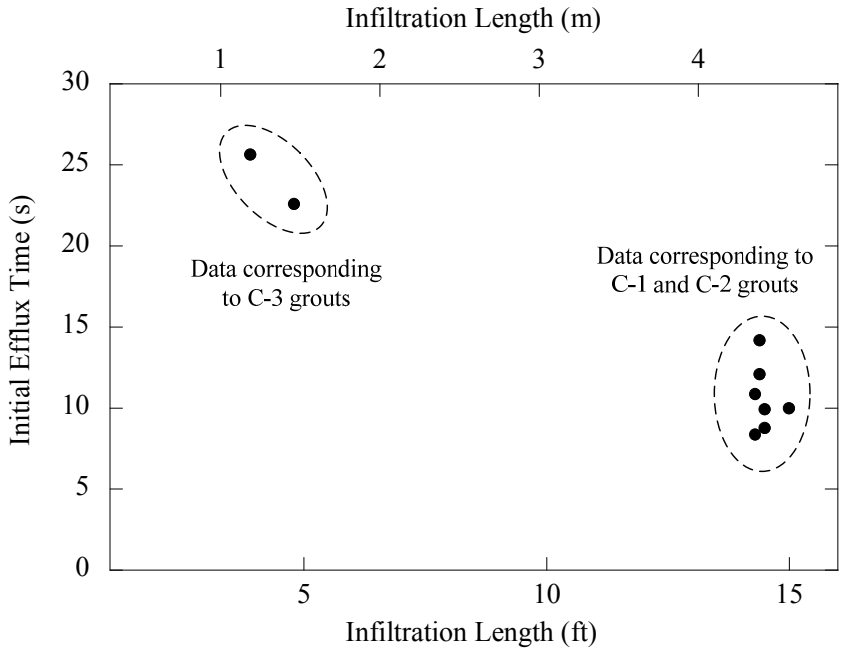

Figure 5-22. Scatter Plots between Infiltration Lengths and Initial Efflux Time.

In summary, the PG method seems to be significantly affected by the geometric condition, R_h, when filling voided ducts. Conversely, the VG and PVG methods' filling capabilities are shown to be relatively unaffected by a void's geometric conditions, leaving the engineer few options in optimizes the repair process.

5.2.2. Filling performance of repair grouts

Class C grouts tested in this research do not show any signs of having bleeding water when the wick-induced bleed test was performed. However, entrapped air may be introduced when repairing. Although isolated voids created by entrapped air are usually not typically associated with strand corrosion in ducts, these voids can be used as an index for evaluating the filling performance of repair grouts. To compare the performance of repair grouts, the void ratio, η, (defined as A_V / A_R) is estimated. The A_R and A_V are calculated using AutoCAD® tools (Section 5.1.5.2). Table 5-8 shows the values of A_R and A_V for each cut section. From Table 5-8, the value of η, obtained from the analysis, is 1.34% for Specimen VG-C1-2. The void ratios for all other specimens are provided in Appendix B, and all the results are summarized in Table 5-18.

The remaining voids in repaired specimens were estimated using the cut section analysis. However, the value of η can be magnified when the remaining voids exist only in small repaired area. Thus, the filling performance for each specimen is provided considering the summation over all of the cut sections for each specimen. The results of the filling performance of each specimen are shown in Table 5-18.

Table 5-18. Results of Void Performance in Each Specimen.

Grout Type	Void Ratio, η, in Each Specimen (%)		
	PG	VG	PVG
Class C-1	0.22 / 1.76	0.60 / 1.34	0.66 / 0.67
Class C-2	1.13 / 0.78	0.99	0.92 / 0.51
Class C-3	1.56 / 0.98	0.57	2.16

Figure 5-23 and Figure 5-24 show the average and the standard deviation of the η for each repair method and repair grout, respectively.

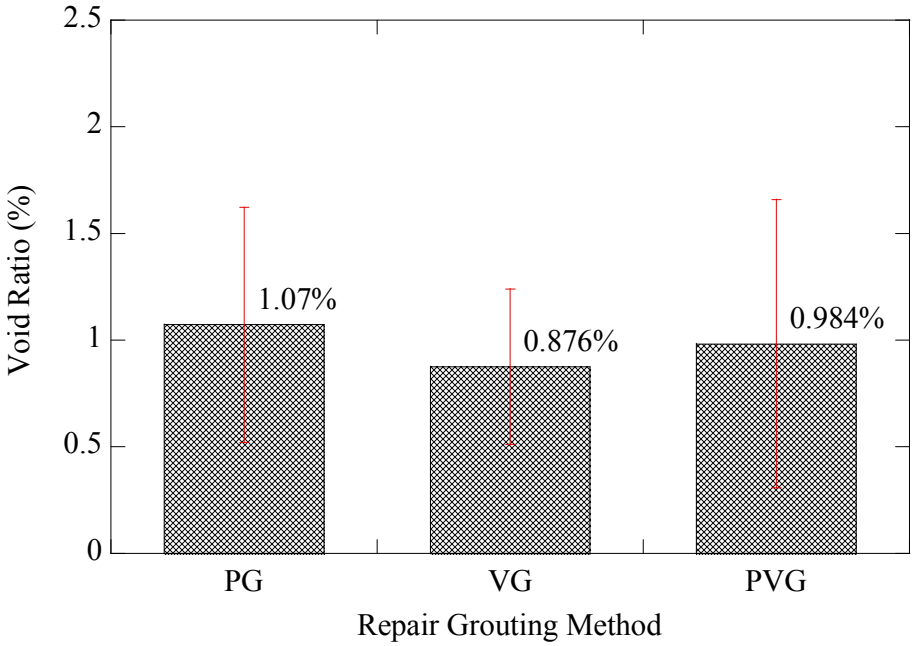

Figure 5-23. Comparison of Void Ratio, η, in Each Repair Method.

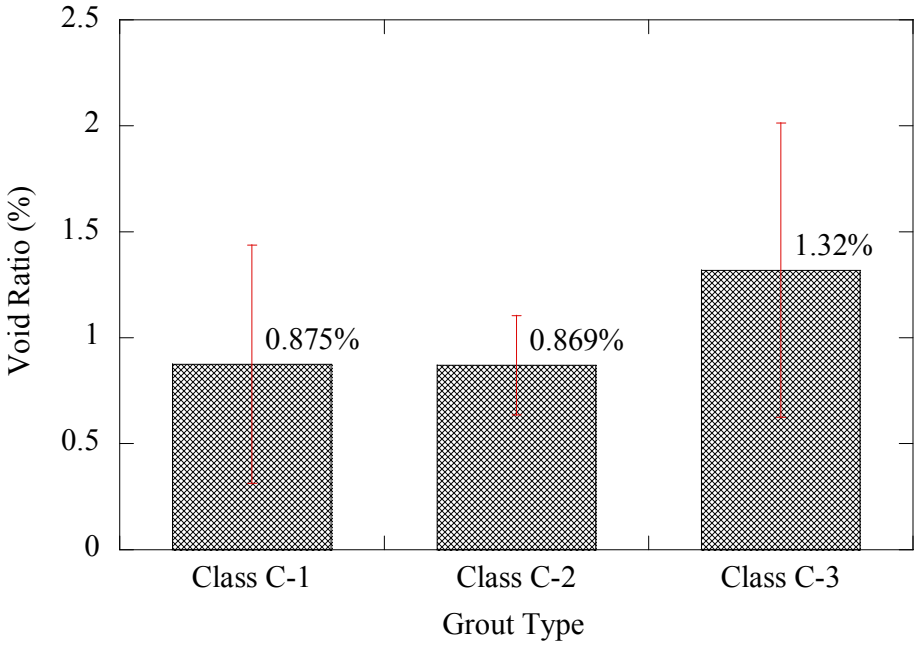

Figure 5-24. Comparison of Void Ratio, η, in Each Repair Grout.

The comparison of ηs obtained from each grouting method, all repair methods seem to have similar amounts of remaining voids (Figure 5-23). The comparison of the repair grouts indicate that the specimens repaired with the Class C-3 grout show slightly more voids than the Class C-1 and C-2 grouts, on average (Figure 5-24).

A two-factor factorial experiment was again considered to analyze the differences between void performance of repair methods and repair grouts. The two factors used are repair methods (PG, VG, and PVG) and repair grout materials (Class C-1, Class C-2, and Class C-3). The linear statistical model of the two-factor factorial was provided in Equation 5.2, and the null and alternative hypotheses were shown in Equation 5.3.

An ANOVA test was performed to test these hypotheses. Table 5-19 shows the ANOVA table for the η of the test specimens. For the 0.05 level of significance, the ANOVA table concludes that different repair methods and grouts do not significantly affect filling performance.

Table 5-19. ANOVA Table for the Void Ratio, η, of Test Specimens.

Source	Type III Sum of Square	Degree of Freedom	Mean Square	*F* Statistic	*p*-value
Repair Methods	0.231	2	0.116	0.396	0.690
Repair grouts	0.554	2	0.277	0.948	0.439
Methods×Grouts	1.425	4	0.356	1.219	0.394
Error	1.754	6	0.292		
Total	3.833	14			

5.2.3. Economic feasibility based on repair methods and grouts

The economic feasibility of each repair method and grout can be represented by the time required to effectively apply each method and grout. Longer repair time increases the demands on labor which can lead to higher costs. Also, leaving a structure under repair for longer periods of time increases the chance of failures as other sections of the structure may become overstressed in order to accommodate the area under repair. Therefore, the optimal repair method

and grout should be selected based on its required time to implement and the performance of the repaired system.

5.2.3.1. Feasibility of repair grouts

From the data collected on mixing time for the repair grouts, the Class C-3 grout was found to have the least feasibility for field applications. The Class C-3 grout required 20 minutes of mixing time and as a consequence led to overheating and breakdown of mixers (Table 5-2). Furthermore, in some cases the efflux time did not satisfy the requirements of Tex-437-A Method 2. The Class C-1 and C-2 grouts required relatively shorter mixing times, and both grouts met the requirements of Tex-437-A Method 2. Considering the grout mixing times, efflux requirements, and required equipment, the Class C-1 and C-2 grouts are considered to be feasible for filling voids.

5.2.3.2. Feasibility of repair grouting methods

For the assessment of repair grouting methods, the preparation time for each specimen was documented. Table 5-20 shows the time schedule for sealing ducts for Specimen VG-C1-2. It also shows the steps required to achieve an air-tight condition. The total sealing time for Specimen VG-C1-2 was three days and 5 hours.

Table 5-20. Sealing Time Schedule of Specimen VG-C1-2.

Sealing Procedure	Working Day	Working Time (min.)
Connect hose and silicone	Day 1	11
Installing pipe saddle tap with grease	Day 1	35
Setting end rubber cover and silicone	Day 1	11
Mixing epoxy and sealing	Day 1	35
Wait	1 day	
Connect T-connection and check air-tight	Day 2	65
RTV silicone sealing	Day 2	12
Check air-tight condition	Day 2	11
RTV silicone sealing	Day 2	10
Mixing epoxy and sealing	Day 2	30
Wait	1 day	
Check air-tight and seal with RTV silicone	Day 3	80
Sum	**3 days**	**300 (5 hours)**

The preparation time for all other specimens are provided in Appendix B. The time estimates for the required sealing time for each specimen is shown in Table 5-21. The preparation times for Specimens VG-C1-1 and VG-C2-1 were not considered in this analysis because both these specimens required a considerable amount of trial and error before it was possible to create an air-tight condition in the test specimens. On Specimen PVG-C1-2 even after working for 12.5 hours an air-tight condition could not be created. Table 5-21 and Table 5-22 show the required preparation time and schedule for applying each method. The term "sealing schedule" in the following discussions is defined as the laboratory work-days required to prepare each PET specimen. Although the sealing schedule was delayed occasionally due to lab conditions and scheduling, the delayed time is compensated in Table 5-21 and Table 5-22.

Table 5-21. Sealing Time Required for Each PET Specimen.

Repair Methods	Sealing Time for Repair (hours)						Average
	PET Speicmen No.						
	1	2	3	4	5	6	
PG	1.03	0.88	0.85	0.65	0.97	0.88	0.88
VG	10.92	5	12.53	3.63			8.02
PVG	2.83	2.33	2.25	1.57	1.50		2.10

Table 5-22. Sealing Schedule Required for Each PET Specimen.

Repair Methods	Sealing Schedule for Repair (days)						Average
	PET Speicmen No.						
	1	2	3	4	5	6	
PG	3	2	2	2	2	2	0.88
VG	7	3	9	3			8.02
PVG	4	1	2	2	2		2.10

Figure 5-25 is provided to compare the mean time requirements needed to repair using each method. The results show that the VG method requires significantly more sealing time than the other methods. Also, the PG method requires much less preparation time than with the PVG method. Figure 5-26 shows the preparation schedule required before applying each repair method. This figure also shows that the VG method seems to involve more preparation than the PG and PVG methods.

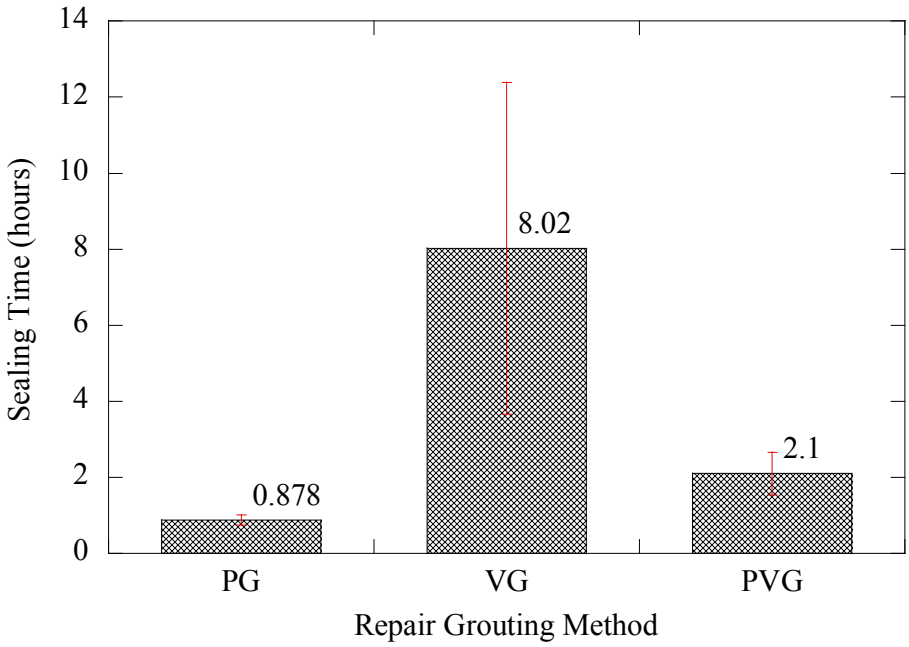

Figure 5-25. Sealing Time Required for Applying Repair Methods.

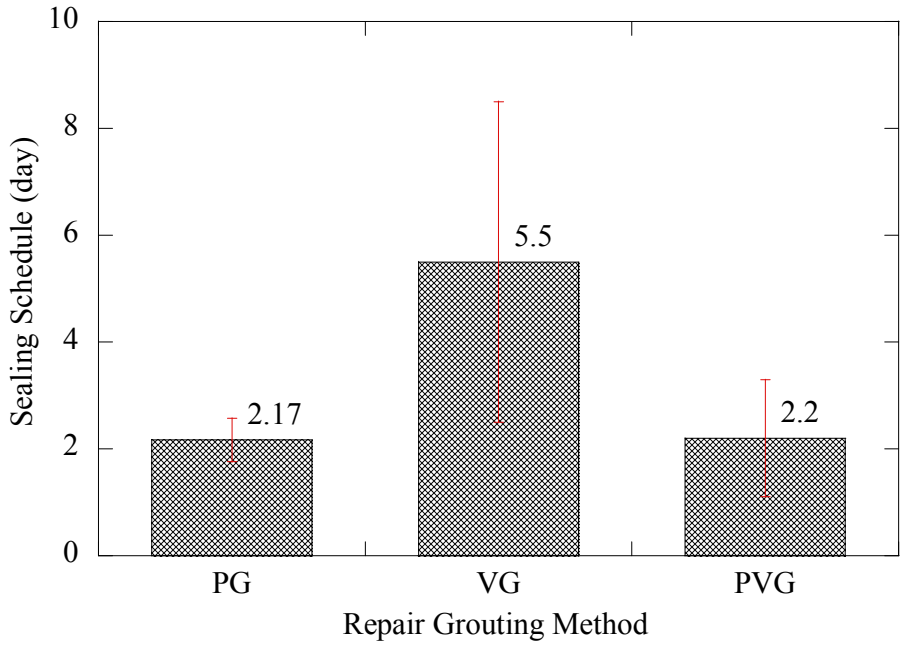

Figure 5-26. Sealing Schedule Required for Applying Repair Methods.

To further analyze the time required for each repair method, a single-factor factorial experiment was performed to compare the differences of preparation time and scheduling among

repair methods. The single factor is the repair methods (PG, VG, and PVG), where the response for each repair method is considered as a random variable. The linear statistical model of a single-factor experiment is defined by:

$$Y_{ij} = \mu + \tau_i + \varepsilon_{ij} \begin{cases} i = 1,2,3 \\ j = 1,2,\cdots,n_i \end{cases}, \tag{5.14}$$

where μ is the overall mean effect, τ_i is the effect of the repair methods, and ε_{ij} is a random error component having a normal distribution with mean of zero and a variance σ^2. The null and alternate hypotheses are defined as:

$$\begin{aligned} &H_0 = \tau_1 = \tau_2 = \tau_3 = 0 \qquad \text{(no main effect of repair methods)} \\ &H_1 = \tau_i \neq 0 \text{ at least one } i \end{aligned} \tag{5.15}$$

An ANOVA test was performed to test these hypotheses. Table 5-23 and Table 5-24 show the ANOVA table for sealing time and scheduling for the application of the repair methods, respectively. For the 0.05 level of significance, the analysis shows that different repair methods require different preparation times and schedules.

Table 5-23. The ANOVA Table for the Sealing Time for Preparing Repair.

Source	Type III Sum of Square	Degree of Freedom	Mean Square	*F* Statistic	*p*-value
Repair Methods	131.409	2	65.704	13.483	0.001
Error	58.476	12	4.873		
Total	189.885	14			

Table 5-24. ANOVA Table for the Sealing Schedule for Preparing Repair.

Source	Type III Sum of Square	Degree of Freedom	Mean Square	*F* Statistic	*p*-value
Repair Methods	32.300	2	16.150	5.939	0.016
Error	32.633	12	2.719		
Total	64.933	14			

Tukey's HSD test and Student-Newman-Keuls (SNK) test were performed using SPSS. The results of both tests are shown in Table 5-25 and Table 5-26. Table 5-25 and Table 5-26 shows that the VG method requires a longer sealing time for conducting repairs than the other methods. However, the tables also reveal that there is no significant difference in preparation time between the PG and PVG methods. Thus, the PG and PVG methods are more economical and feasible for repairing voids in the field than the VG method.

Table 5-25. Grouping Results of Tukey's HSD and SNK Tests for Preparation Time.

Method	Source	N	Subset	
			1	2
Tukey's HSD Test	PG PVG VG	6 5 4	52.67 125.80 -	- - 481.25
Student-Newman-Keuls Test	PG PVG VG	6 5 4	52.67 125.80 -	- - 481.25

Table 5-26. Grouping Results of Tukey's HSD and SNK Tests for Preparation Schedule.

Method	Source	N	Subset	
			1	2
Tukey's HSD Test	PG PVG VG	6 5 4	2.167 2.200 -	- - 5.500
Student-Newman-Keuls Test	PG PVG VG	6 5 4	2.167 2.200 -	- - 5.500

5.3. COMPARISON OF FILLABILITY AND INFILTRATION LENGTH

The fillability index of different repair grouts was determined in Section 4. This FI is now compared with infiltration lengths for the PVG method. Only PVG method is compared as it is the grouting procedure recommended by this research project. Table 5-27 shows the infiltration length for the three Class C grouts along with their fillability indices.

Table 5-27. Fillability Index along with Infiltration Lengths.

Grouting Method	Grouts	Fillability Index			Infiltration Length, ft (m)	
		1	2	3	1	2
PVG	Class C-1	4.1	4.3	4.2	15.0 (4.57)	14.5 (4.42)
	Class C-2	5.3	5.2	5.2	14.4 (4.39)	14.3 (4.36)
	Class C-3	7.5	6.4	6.3	3.9 (1.19)	-

Because the fillability indices and infiltration length datasets were not of the same size (in terms of the number of observations), a many-to-many relationship between the fillability index and infiltration length was formulated and is shown in the Figure 5-27.

Based on the relationship obtained between the fillability index and infiltration length, it is observed that Class C-1 and C-2 grouts have fillability indeces below 5.3 and the infiltration length above 14.3 ft. Based on these results, it is recommended that the grouts with a fillability index of 5.5 or less will be appropriate for repairing PT ducts. On the other hand, grouts with a fillability index above 5.5 are not recommended for repair grouting.

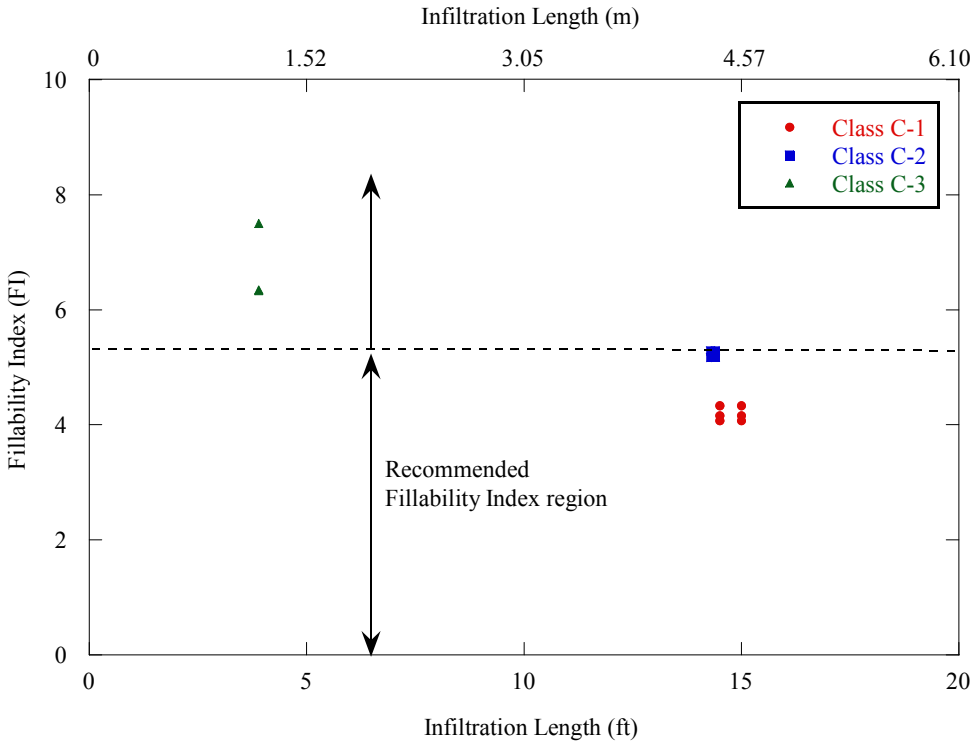

Figure 5-27. Relationship between Fillability Index and Infiltration Length.

5.4. RECOMMENDATION

Repairing voids before severe corrosion is significant to reduce maintenance cost as well as potential factors of corrosion failure. Based on the results of this research, the pressure-vacuum combination repair method is recommended for filling voids in the field. This method exhibits good filling capability and better economic feasibility. Application of the PVG method for repairing voids can reduce the time and cost will providing good fillability of the voids. In addition, no parameter was identified to assist engineers in selecting the most appropriate repair method and material combination. However, repair grouts with fillability indices less than 5.5 should provide good fillability of voided ducts. The reader is encouraged to review the Inspection and Repair Manual if specific questions regarding processes need to be answered.

6. ECONOMIC RISK ASSESSMENT: ANALYTICAL PROGRAM AND RESULTS

6.1. INTRODUCTION

The reliability or performance of a network of bridges should always be maintained as highly as possible in bridge system management; however, transportation agencies usually have only limited annual maintenance budgets. Over time, the performance of every bridge in the network must be kept above a specified limit for public safety reasons. Because the health condition of each bridge is different, and the limited budget is usually not sufficient for all bridges in a network at the same time, it is important to know when to maintain a bridge and what maintenance actions to take to achieve the optimum management goal given a required periodic inspection. Not only should the minimum reliability of every bridge be satisfied but also the total reliability of a network of bridges should be maximized subject to budget limitations. Maintenance and repair strategies for multiple PT bridges are first investigated by formulating the optimal maintenance/repair problem as a 0/1 knapsack problem (Martello and Toth 1990). Each bridge in a transportation network is coded with either 0 when no maintenance action is required and 1 when action is necessary in each year of its time horizon. The obtained solution vector includes only 0 and 1 to indicate whether action is needed in each year for each bridge in the system so that the maintenance or cost does not exceed a specified maintenance annual budget while maximizing the total reliability of the entire system of PT bridges. Optimum maintenance policies obtained using the random search approach is presented next. These two methodologies are followed by numerical examples for illustration. Formulating the maintenance/repair problem as a 0/1 knapsack problem can reduce the complexity of an optimization problem and produces results quickly. However, the random search method is more flexible in terms of applying constraints to the optimization problem, though the computing time is usually longer than the former method.

6.2. FORMULATION OF THE OPTIMAL MAINTENANCE/REPAIR PROBLEM AS A 0/1 KNAPSACK PROBLEM

Given N_i types of maintenance action and a population of N_j bridges in a bridge network, an optimum maintenance/repair policy can be determined for the network so that the total expenditure in year *k*, $E(k)$, does not exceed the maximum expenditure budget for that year, $Budget(k)$, for any year in a time horizon of N_k years as follows:

Let *i* be the type of maintenance or repair treatment: $1 \le i \le N_i$,

Let *j* be the bridge number in the network: $1 \le j \le N_j$, and

Let *k* be the time index or year: $1 \le k \le N_k$.

If $c_{i,j,k}$ and $\beta_{i,j,k}$ are respectively the cost incurred and the reliability or performance benefit obtained due to application of treatment *i* to bridge *j* in year *k*, a binary variable, $x_{i,j,k}$, is to be determined such that

$$E(k) = \sum_{i=1}^{N_i} \sum_{j=1}^{N_j} c_{i,j,k} \cdot x_{i,j,k}; \;\; E(k) \le Budget(k), \forall k \tag{6.1}$$

$$Bt = \sum_{i=1}^{N_i} \sum_{j=1}^{N_j} \sum_{k=1}^{N_k} \beta_{i,j,k} \cdot x_{i,j,k}; \;\; Bt = Maximum \tag{6.2}$$

where, Bt is the total benefit in terms of reliability of the bridge network and should be maximized for the time horizon being considered. It is noted that an importance factor can be included in term $\beta_{i,j,k}$ to account for the fact that some bridges are more important than others.

In order to solve the integer linear programming (LP) problem, the solution variable, $x_{i,j,k}$, is expressed in the form of a solution vector, $\{x_{ijk}\}$, such that a maintenance/repair

strategy consists of $N_i \cdot N_j \cdot N_k$ elements (Mathworks 2008). Each element of the solution vector is solved for a value of 0 or 1 and is obtained from computing $x_{i,j,k}$. A benefit vector, $\{\beta_{ijk}\}$, that includes $N_i \cdot N_j \cdot N_k$ elements and contains the coefficients of the linear objective function [Equation (6.2)] can be determined corresponding to the solution vector.

$$\{\beta_{ijk}\}^T = \left[\underbrace{\underbrace{\beta_{1,1,1} \cdots \beta_{1,1,N_k}}_{bridge-1} \cdots \underbrace{\beta_{1,N_j,1} \cdots \beta_{1,N_j,N_k}}_{bridge-N_j}}_{treatment-1} \cdots \underbrace{\underbrace{\beta_{1,1,1} \cdots \beta_{1,1,N_k}}_{bridge-1} \cdots \underbrace{\beta_{1,N_j,1} \cdots \beta_{1,N_j,N_k}}_{bridge-N_j}}_{treatment-N_i} \right] \tag{6.3}$$

The objective function can therefore be expressed as follows:

$$Bt = \{\beta_{ijk}\}^T \times \{x_{ijk}\} \tag{6.4}$$

Accordingly, the constrained budget is to be expressed as a vector $\{C_k\}$ containing N_k elements, and each element has C_k as a budget value limit for year *k*. If $[cM_j]$ is a cost matrix [Equation (6.5)] for bridge *j*, the cost matrix for the system of bridges, $[Ct]$, is formulated as follows:

$$[cM_j] = \begin{bmatrix} c_{1,j,1} & & & 0 \\ & \ddots & & \\ & & c_{1,j,k} & \\ & & & \ddots \\ 0 & & & c_{1,j,N_k} \end{bmatrix} \tag{6.5}$$

$$[Ct] = \left[[cM_1] \quad \cdots \quad [cM_j] \quad \cdots \quad [cM_{N_j}] \right] \tag{6.6}$$

The constraint condition [Equation (6.1)] can be given as:

$$[Ct]\times\{x_{ijk}\}\le\{C_k\} \tag{6.7}$$

Figure 6-1 illustrates how a LP solver finds an optimal solution for a 4-binary-variable problem. Each element of vector $\{x_{ijk}\}$ is equivalent to one variable in such a solution tree, and the order of the variables is not necessarily that of the vector subscripts. Without an efficient search algorithm the computer program would need to enumerate and compare all possible options ($N_i \cdot N_j \cdot N_k$) to get the solution with the greatest benefit. However, the branch-and-bound algorithm speeds up the solution process. The algorithm considers the constraints at each node of the algorithm tree and compares with results that have been obtained from the previous node to set a search bound. The algorithm helps one decide whether to continue branching at a node or to investigate the next node based on the constraints and the newly found bound.

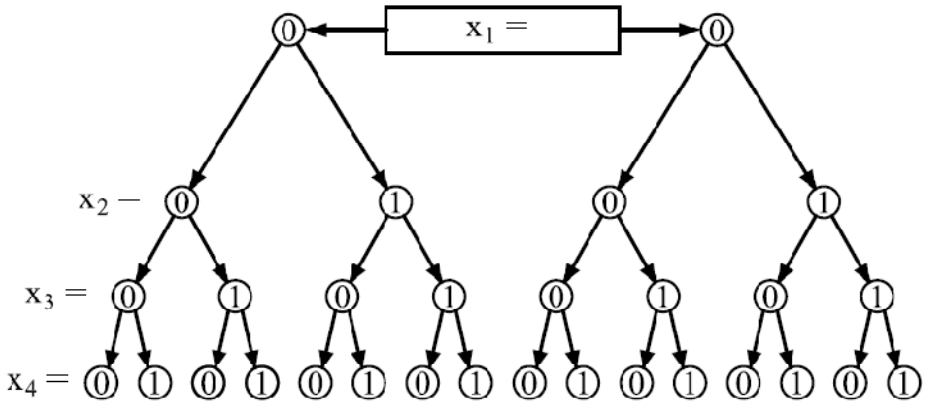

Figure 6-1. Solution of a Linear Programming Problem.

6.3. DEVELOPMENT OF A RANDOM SEARCH METHOD FOR THE OPTIMIZATION PROBLEM

A population of bridges is to be maintained so that the reliability of none of the bridges decays below a minimum reliability over a planned time horizon. The allocated annual maintenance budget cannot allow all the bridges to be repaired at the same time. Thus, it is important to know when to repair a bridge in the population before its performance deteriorates below a minimum limit over some time horizon. It is assumed that enough resources are provided to keep all the bridges safe over the time horizon, otherwise, a solution would become infeasible, and some bridges would have to be shut down during the planned horizon. It is also noted that none of the bridges is structurally deficient. In the event that more resources are provided than are needed, transportation agencies may want to keep the reliability of each bridge not just above the minimum limit but also well above this limit in order to reduce the total vulnerability of the bridges. The random search method can easily be applied to attain these goals.

A flowchart describing the process of finding optimal solutions of maintenance and repair using the random search approach is given in Figure 6-2. The initial total expenditure over a given time horizon, *minTE*, is first set to a very large number (infinity is applicable in MATLAB). In this way, every next random generation of a strategy of maintenance and repair (*it*+1) that has a lower total expenditure than the previously generated strategy (*it*) can be captured and considered a newly found solution. The number of iterations needed to generate a strategy of maintenance and repair can be very large depending on the extent of a problem. For small problems, the program can generate a converged solution quickly after a small number of simulations. Thus, there is no need to wait for a program to try all possible simulations when a solution is found. Based on this rule, an algorithm is developed to stop the program after a significantly large number of iterations without obtaining a new solution. If the later iterations produce a larger total expenditure than the earlier ones, the number of consecutive steps without obtaining a new optimal solution is specified by $Nstep$ to stop the iteration and export the best solution at the END circle in the flowchart. As shown in the chart, the index *Signal_4* is used to count those steps every time the iteration does not produce a new optimal solution.

In each iteration, the expenditure in year k is expressed as $E(k)$ and $E(0)$ is zero, as shown in Figure 6-2. It is then updated every time if a feasible treatment of maintenance is

applied to a bridge in that year. The oval shapes in the flowchart indicate random selections of bridges, maintenance actions, and years of treatment. It is noted that random selection of each individual of a type has an equal probability. The first oval is a random selection of bridge *j* in a population of N_j bridges in that each bridge is selected only once per iteration. The reliability index of bridge *j* in every year, $\beta_{j,k}$, over the time horizon of N_k years is determined and compared with the specified limit of reliability, $\beta_{\min}$. The bridges that are estimated to have their reliability index higher than this limit are not considered for repairs; thus, repair actions in any year during the time horizon is set to zero as shown in Figure 6-2, *Action*(*j*, *k*) = 0. For each of the rest of the bridge population, a repair treatment *i* is selected randomly from N_i available treatments and is applied randomly to a year (year *j* in the figure) that its reliability index is higher than the minimum limit ($\beta_{j,k} > \beta_{\min}$). By doing this, it is assured that necessary repair actions are taken before a bridge becomes structurally deficient during the time horizon.

In some cases, the budget for the selected year, *k*, has already been exhausted for other bridges, or the treatment cost is greater than the remaining budget. Thus, it is not always possible to repair any more bridges in that year, and the cost of treatment *i*, *Cost* (*i*,*k*) , is calculated to deterimine if the budget permits the treatment. As shown in Figure 6-2, the expenditure in the year *k*, *E*(*k*), is updated by adding the newly calculated cost. If the budget is not enough for the selected year, the selected treatment is applied randomly to a different year seeking resource feasibility, $E(k) \leq Budget(k)$. If no other years satisfy this constraint (Signal_3 > N_k), other treatments hopefully less expensive are randomly selected to try all possible interested years. No feasible solution is found when none of these constraints is met (Signal_3 > N_i), or when no available resources are provided to repair the selected bridge. In this case, the reliability index of the bridge is estimated to decrease below the required limit and may have to be shut down. However, if it is feasible to apply the selected treatment in year *k* for bridge *j*, the repair treatment is taken, *Action* (*j*, *k*) = *i*, in that year as shown in Figure 6-2. The total expenditure is determined by adding the expenditure in every year of the time horizon, and it is compared to the total expenditure known from the earlier iterations to define the lowest maintenance and repair expenditure, *minTE*.

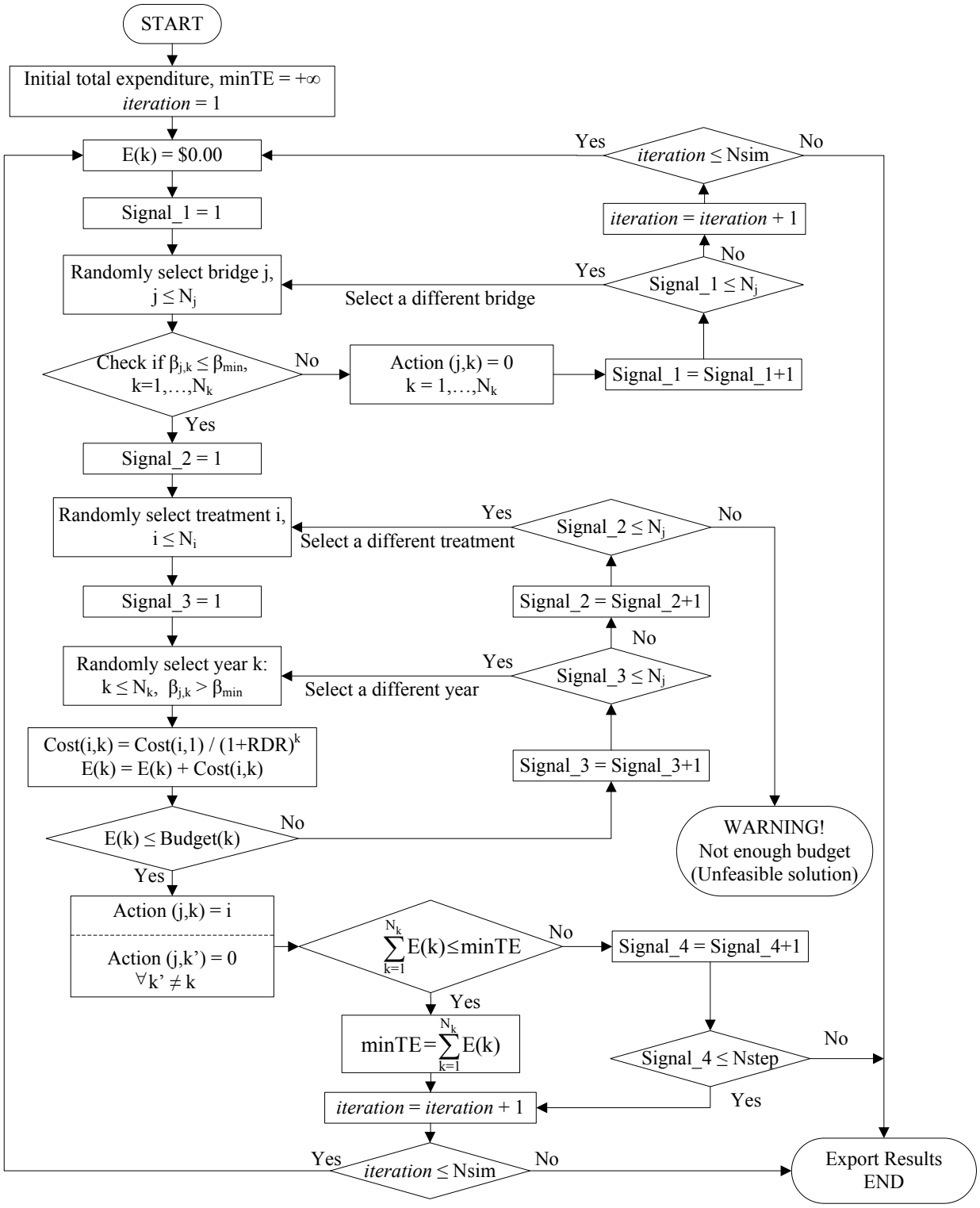

Figure 6-2. The Random Search Method for Optimization Solution.

6.4. NUMERICAL EXAMPLES

Five box-girder PT bridges with spans of 30.5 m (100 ft) exposed to the same environmental conditions are taken as examples. Each of these bridges is 17.7 m (58 ft) wide and has 3 traffic lanes. Without any maintenance intervention, the deterioration functions of these similar bridges are assumed to be identical, and their ages are 3, 8, 13, 18, and 23 years old (Figure 6-3). The bridges are, therefore, in different states due to aging. A maintenance policy is to be established for this group of bridges over a planning time horizon of 20 years. The reliability analysis of these structures is presented in Chapter 8 of Volume 1 of this report.

If a maintenance action of grouting voids in the ducts is applied to a bridge, it is considered that the steel strands are covered with protective grout isolating the strands from further attack of corrosive agents, especially chlorides, and water. Therefore, it is assumed that after grouting the reliability of the bridge stops degrading and stays the same as shown in Figure 6-4, when grouting occurs at the tenth year. Note that this is an assumption and this may not be the case in the field. Instead of grouting all the tendons that have voids and corroded strands, a decision to replace deteriorated tendons with new tendons and subsequent grouting results in a bridge that has no voids in its ducts and tendons with the original cross-sectional area. The capacity of the bridge after this repair is assumed to recover to its initial state with no further deterioration, as illustrated in Figure 6-5. These assumptions are the most optimistic assumptions that can be made. Results obtained from the field indicate that tendons of strands in PT bridges are not subject to considerable corrosion if they are fully covered with grout. The assumptions about no further decrease in performance need to be validated by experimental tests.

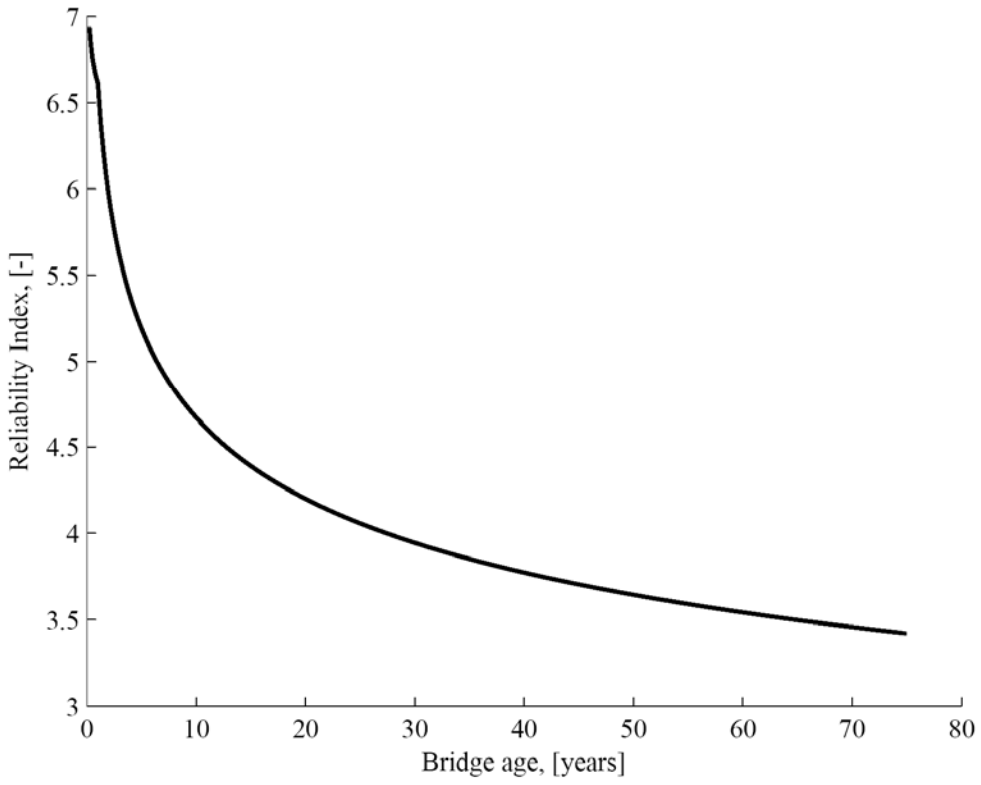

Figure 6-3. Performance Degradation Due to Corrosion of Post-Tensioned Strands.

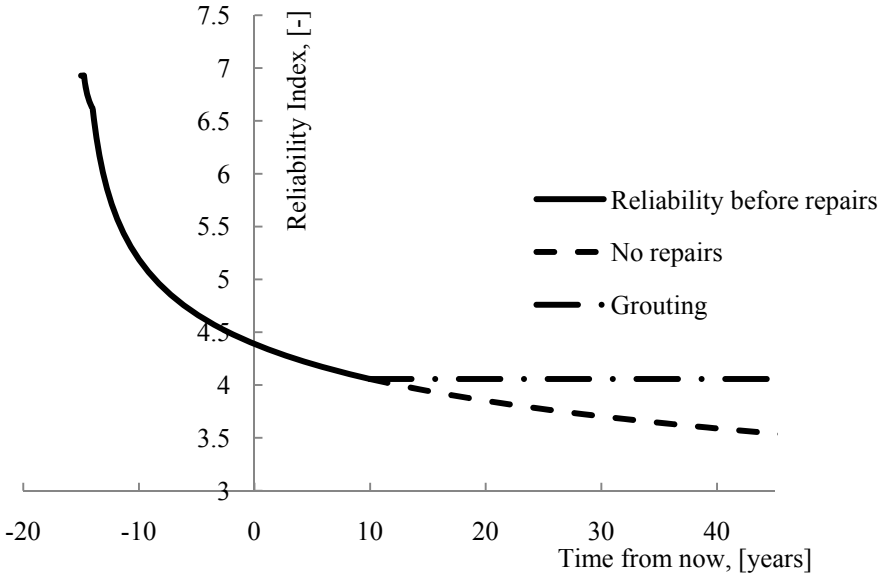

Figure 6-4. Reliability Benefit from Grouting Tendons with Corroded PT Strands.

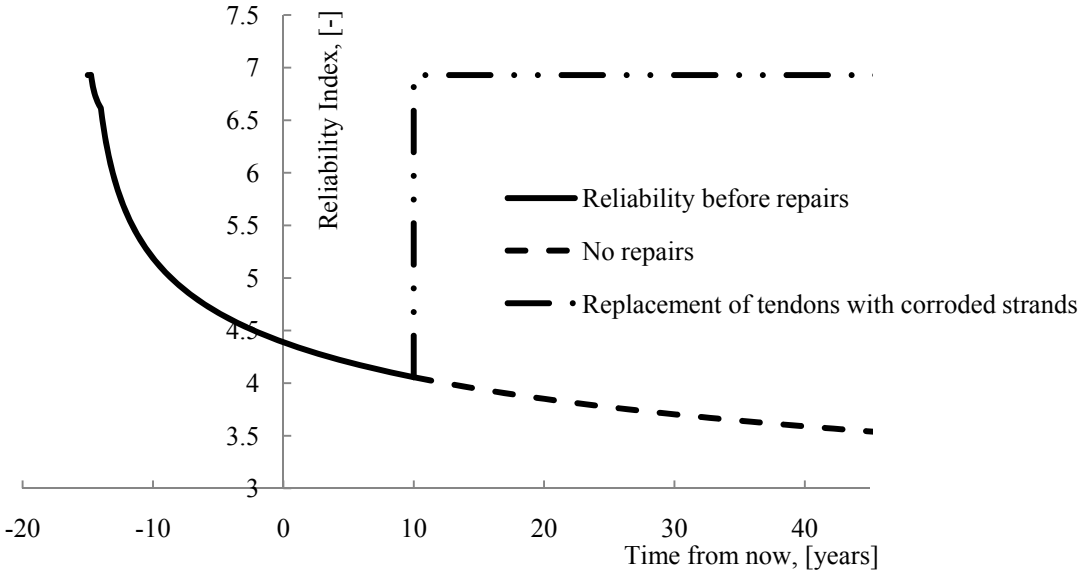

Figure 6-5. Reliability Benefit from the Replacement of Corroded Tendons.

The costs of different maintenance actions for this type of bridge are estimated for the current time and presented in Table 6-1. For reference, the State of New York does inspection for all bridges once every two years, and the average inspection cost is approximately $2,300 per year for one bridge (NYDOT 2002). The replacement cost can be estimated based on the total mass of prestressing steel, $7.50/kg (KDOT 1999). The total mass of prestressing steel of the bridge in this example is approximately 11,000 kg. For this example, the cost of grouting will be estimated to be one fifth of the replacement cost. To investigate how the proposed optimization suggests an optimal strategy for maintenance, a constrained annual budget of $50,000 will be allotted for this group of bridges.

Table 6-1. Estimate of Expected Cost of Maintenance

Type of maintenance	Cost ($)
Periodic inspection (once every 2 years)	3,500
Protective grouting 20% of tendons	4,000
Replacement 20% of tendons	20,000

It is noted that the real discount rate, RDR, is used to forecast maintenance expenditure in the future. In this study, the discount rate of 2.8% is taken from the instructions about discount rates for cost effectiveness analysis of federal programs (OMB 2008). By using RDR, the financial markets are considered free of risk and are protected from inflation (NCHRP 483). In this case, if $c_{i,j,0}$ is the maintenance cost for applying treatment i to bridge j, and the maintenance is delayed to year k, the cost becomes:

$$c_{i,j,k} = c_{i,j,0} \cdot \frac{1}{(1+RDR)^k} \tag{6.8}$$

6.5. RESULTS AND DISCUSSIONS

The solution for an optimal maintenance policy for the group of bridges based on the given constraints is presented in Table 6-2. The bridges are listed in order of decreasing importance in the way that if the repair of two bridges in a year produces the same reliability benefit the bridge listed first is prioritized. Letters G and R in the table are suggested maintenance actions of grouting and repair or replacement of corroded tendons respectively. Zero indicates that only regular inspections take place in each year. Maximizing the total performance of the group of PT bridges is obtained and how performance of each bridge in the group changes is shown in Figure 6-6. The optimization solution suggests that repair of older bridges results in the higher total reliability of the population of bridges. These results indicate means that old bridges should be prioritized for repairs (but realize that in this analysis all bridges degrade at the same rate, which is likely an oversimplification). Table 6-2 suggests that the two most important bridges need to be repaired now, two others in the next year, and the youngest one be repaired last, after the last repair of the other bridges. As long as expenditure in a year does not exceed the limiting maintenance budget, the results indicate that the earlier the replacement of the corroded tendons for deteriorating PT bridges occurs, the more benefit is gained.

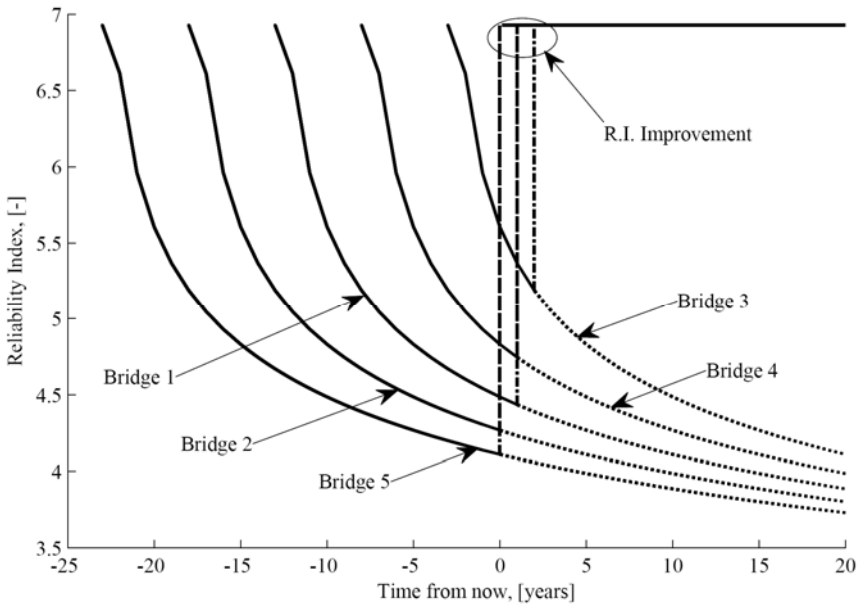

Figure 6-6. Optimal Solution for Improvement of Performance of Every Bridge Under Considerarion.

The optimum maintenance policy applies only for the current year; the analysis recommends that Bridge 2 (18 years old) and Bridge 5 (23 years old) should have tendon replacement in the current year. In the following year, the optimization program should be re-run with updated cost information; changes in costs or other assumptions may lead to different solutions. The problem is solved by using a random search method. The objective is to find the minimum cost to keep all the bridges safe. The safety level is selected at $\beta = 4.1$,which is equivalent to a failure probability of approximately 2.1×10^{-5}. The optimum solution obtained recommends an optimum strategy of maintenance and repair in terms of expenditure as presented in Table 6-3.

Table 6-2. Optimum Maintenance Policy for the Group of PT Bridges.

Year in the future	Bridge Number				
	1	2	3	4	5
	Agen of bridge (years)				
	13	18	3	8	23
0	0	R	0	0	R
1	R	0	0	R	0
2	0	0	R	0	0
3	0	0	0	0	0
4	0	0	0	0	0
5	0	0	0	0	0
6	0	0	0	0	0
7	0	0	0	0	0
8	0	0	0	0	0
9	0	0	0	0	0
10	0	0	0	0	0
11	0	0	0	0	0
12	0	0	0	0	0
13	0	0	0	0	0
14	0	0	0	0	0
15	0	0	0	0	0
16	0	0	0	0	0
17	0	0	0	0	0
18	0	0	0	0	0
19	0	0	0	0	0
20	0	0	0	0	0
21	0	0	0	0	0

Note: 0-do nothing; G-grout ducts; R-replace tendons.

Table 6-3. Optimum Maintenance Policy Using the Random Search.

Year in future	Bridge Number				
	1	2	3	4	5
	Age of bridge (years)				
	13	18	3	8	23
0	0	0	0	0	G
1	0	0	0	0	0
2	0	0	0	0	0
3	0	0	0	0	0
4	0	0	0	0	0
5	0	0	0	0	0
6	0	G	0	0	0
7	0	0	0	0	0
8	0	0	0	0	0
9	0	0	0	0	0
10	G	0	0	0	0
11	0	0	0	0	0
12	0	0	0	0	0
13	0	0	0	0	0
14	0	0	0	0	0
15	0	0	0	0	0
16	0	0	0	G	0
17	0	0	0	0	0
18	0	0	0	0	0
19	0	0	0	0	0
20	0	0	0	0	0
21	0	0	0	0	0

Note: 0-do nothing; G-grout ducts; R-replace tendons.

Unlike the repair policy to maximize the reliability of all PT bridges in which replacement of tendons is suggested in the early years of the time horizon (Figure 6-6), only grouting is recommended in this case, as shown in Table 6-3. The reason is that the management objective is to find the most cost-effective policy that is able to keep the entire bridges considered in the evaluation safe over a time horizon; grouting is only one fifth as expensive as the tendon replacement (Table 6-1). Figure 6-7 shows how grouting actions help maintain all the bridges. Because of the application of the discount factor, grouting is delayed as late as possible to reduce the total cost of maintenance. Furthermore, not any repair action is scheduled for

Bridge 3 because, as estimated, the reliability index of this bridge never drops below the minimum limit in any year of the time horizon.

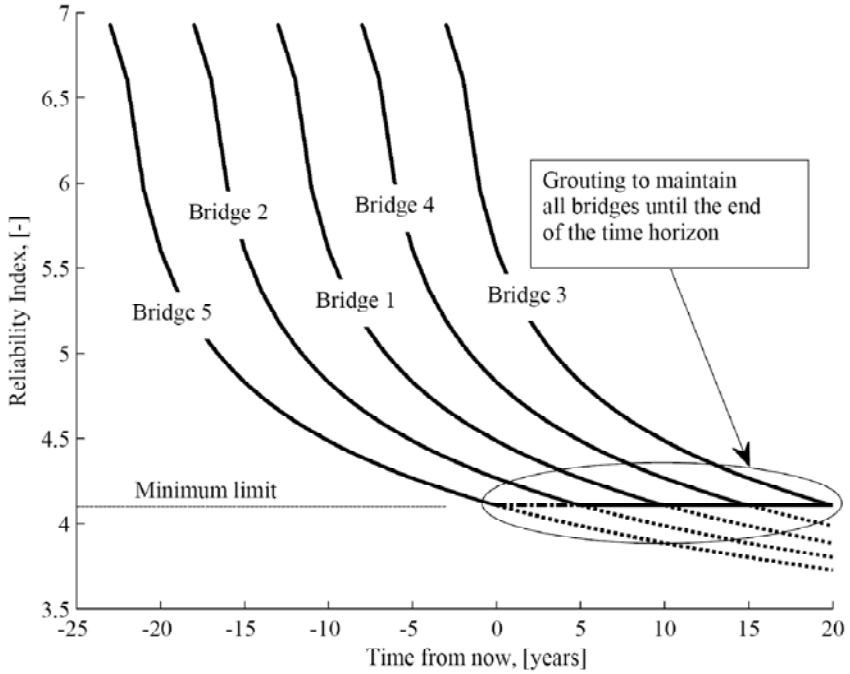

Figure 6-7: Optimal Solution for Improvement of Performance Using the Random Search.

7. CONCLUSIONS AND RECOMMENDATIONS

7.1. REPAIR GROUT MATERIALS

The current TxDOT specifications for grouts provide test methods and threshold values for cement grouts. These standards fail to provide specifications to test pre-packaged proprietary cementitious-based grouts for the ability of a particular grout to fill voids. Also, some TxDOT recommendations (desirable limits of efflux time) may not be appropriate.

Significant voids have been found in ducts in a number of PT bridges in Texas constructed before year 2000. These bridges may require repair of the voided PT ducts by filling with a suitable grout. The three prepackaged Class C grouts evaluated in this research conformed to the current TxDOT grout specifications. These grout exhibited zero bleed, limited shrinkage, and good fluidity. However, grout C-3 exhibited poor fillability.

The Class C grouts exhibited a slow increase in the viscosity over time. This is due to the hydration of these grouts. Characterization of pre-packaged grouts is very important as it provides ample time for material engineers to assess applicability of these pre-packaged grouts.

The effects of mixer type, mixture volume, and w/p on the grout characteristics were evaluated to determine the sensitivity of each grout due to the change in these factors. It was found that the fluidity and viscosity were, to some extent, affected by the change in mixer type. Two mixers with different rotating speeds were used and the mixer with the higher rpm (M2 mixer) resulted in better fluidity of the grouts. However, this mixer was not designed to be used at the loads required to mix grout, and the M1 mixer will likely be more durable.

Three different mixture volumes were evaluated in this research to study the effect of the mixture volume on a grout's fresh characteristics. The fluidity and viscosity were the two main characteristics affected by the change in mixture volume. As the mixture volume increased the fluidity decreased; lower volumes resulted in grouts with lower viscosity values. However, no significant change in the grout's fluidity was observed with the change in mixture volume for any of the grouts studied at a 5% level of significance.

The sensitivity of the w/p was also evaluated in this research. As expected, the fluidity of all grouts increased as the w/p increased. This increase in fluidity was due the increase of water content of the mixture. Viscosity and density also decreased with an increase in w/p.

The newly developed fillability test procedure was found to be a useful procedure in differentiating the pre-packaged PT grouts in terms of their void filling ability. The fillability test results indicate that Class C-1 and C-2 grouts performed well in terms of their void filling ability with a fillability index less than 5.5. The Class C-3 grout resulted in a higher fillability index (> 5.5) indicating that it will not fill smaller voids efficiently. The fillability test procedure can assist constructors and engineers in determining a suitable pre-packaged PT grout for use in PT tendons, either for new or repair scenarios.

Testing from this research indicates that the following changes to the current DMS-4670 specifications may be warranted:

- The maximum size fine aggregates allowed in a PT grout should be reduced from No. 50 Sieve (300 μm) to No. 100 sieve (150 μm).
- The minimum efflux time should be lowered from 9 seconds to 5 seconds when grouting is performed with a positive head (i.e., when grouting is done from the lowest duct elevation).
- The minimum initial setting time should be increased from 3 hours to 4 hours. Although an increase in the initial setting time does not increase the workability time, it may provide a grout mixture with better fillability.
- The wet density test using a Baroid mud balance should be required for all grouting of PT ducts. The wet density value determined in the field should be within the limit shown in the Equation 5.12.
- The fillability test developed in this research should be used to assess the fillability of grouts. The fillability index should be less than or equal to 5.5.

This research provides recommendations to modify the current TxDOT specifications for PT grouts (DMS-4670 Grouts for Post-tensioning) such that these grouts can be objectively assessed and grouts that can fill voids more efficiently will be used for grouting PT ducts. The recommendations made in this research is expected to improve the durability of PT structures,

however before grouting it is imperative that the possible issue at the formation of galvanic cells be addressed.

7.2. INSPECTION AND MITIGATION ASSESSMENT

Recent investigations of PT bridges have uncovered problems related to tendon failure due to excessive corrosion. Furthermore, the failure of an individual tendon due to corrosion can lead to structural failure. PT structures are designed with the intention of having the post tensioning force in place throughout its design life. The loss of tendons could overstress other portions of PT structure and cause failure. Even if the consequences of a PT tendon are not catastrophic they still involve costly repairs and could affect the bridge's performance. Thus, it is critical to protect tendons from deterioration caused by corrosion using an appropriate inspection and repair method. Currently, the recommended repair method is the vacuum grouting method. This method requires air-tight conditions throughout the entire duct which can be extremely difficult to do in the field. In addition, constrained working conditions in box girders further complicate the use of vacuum grouting. In this research, test on an external PT tendon system were conducted to assess methods for filling voids in ducts.

Based on these tests, the proposed repair grouting methods, pressure grouting (PG), pressure-vacuum grouting (PVG), and vacuum grouting (VG) were evaluated with respect to their filling capabilities, filling performance, and economic feasibility. To estimate the filling capability of these repair methods, the infiltration length and minimum repaired area in cut sections were estimated. Although the different grouting repair methods did not show significant differences in their filling capability at a 95 percent confidence limit, the PG method seems to have a lower filling capability than the VG and PVG methods. To evaluate the filling performance, the void ratio of repaired grouts was estimated using cut sections; however, no significant differences were identified between the different grouting methods.

Preparation time and scheduling for each repair grouting method have been estimated to evaluate the economic feasibility of each method. The analysis contained in this report concludes that the VG method requires more sealing time than the PG and PVG method. Thus, the PG and PVG methods are more economical methods for repairing voids than the VG method. Because

the PG method exhibited lower filling capability and the VG method requires extensive preparation time, the PVG method is recommended for filling voids in the field. Note that this method should only be used if it is determined that galvanic cells do not form at existing-new grout interfaces.

The mock-up test for filling voids in ducts was performed using commercially available pre-packaged grouts. Three grouts, identified as Class C-1, C-2, and C-3, were assessed.

Sounding inspections are commonly used to inspect voided ducts in the field. This inspection is proper for employing in the field because it can be applied without a power supply and is simple. While most non-destructive inspection methods are sensitive to ambient vibrations resulting from wind and traffic, the sounding inspection is not affected by these field conditions. This research evaluated the effectiveness of the sounding inspection using transparent ducts. Voided areas were identified using soundings and were compared with actual void conditions. Although the voids identified with the sounding inspection were not identical to the voids found with a visual inspection, statistical analysis shows that both inspections are highly correlated. The analysis results show that the sounding inspection underestimates the size of the voids; however, the inspected locations have a close correlation with actual voids in ducts. Thus, the sounding inspection can be applied as an effective inspection tool in the field to assess void volume.

In summary, this research proposes that the PVG method is the most effective method for repair grouting in the field. For appropriate repairs, grouts meeting the proposed revised specification should be used. The sounding inspection can assess void locations in ducts and provide the required volume of repair grout material. It should be noted that grouting of voided tendons was not performed in this research because of potential issures with accelerated corrosion at the existing-repair grout interface. Until this issue can be resolved, repairing with grouts should not be performed.

7.3. ECONOMIC RISK MODELING

A review of the literature shows that it is important to develop a proper approach for optimization of the maintenance policy of PT bridges in the State of Texas. Two approaches

have been developed and applied to a test group of PT bridges. The optimization solutions obtained using these two models offer important recommendations for maintenance optimization of this particular type of bridge.

The random search method was used to solve the optimization challenges; it can be applied not only to PT bridges but also to any type of structures where information on their reliability can be predicted or obtained as a function of time. This method is simple to use, and constraints can be flexibly applied to the objective function. However, the random search is inefficient, and consideration should be given to replace this with the Genetic Algorithm or some other evolutionary algorithm if the optimization models are extended to encompass larger problems.

Uncertainties always exist in design, analysis, construction of structures, associated expenditures, and environmental conditions. Thus, it is important to have sound robust models to predict the behavior of both structural components and structural systems from which the reliability of the entire structural system in a network can be reasonably predicted. This system should be based on collected inspection data and developed models for structural deterioration.

REFERENCES

ACI. (1989). "Building code requirements for reinforced concrete." *ACI Standard 318-89*, Detroit, Michigan.

Adey, B. (2002). "A Supply and Demand System Approach to the Development of Bridge Management Strategies," Thesis 2519, Swiss Federal Institute of Technology, Lausanne.

Adey, B., Bruhwiler, E., and Hajdin, R. "Supply and Demand System Approach to Developing Bridge Management Strategies - Comparison with Two Existing Approaches." *9th International Bridge Management Conference*, Orlando, Florida, 3-14.

Alonso, C., Recio, F. J., Sanchez, M., and Andrade, C. (2008). "Chloride Threshold Determination in Prestressing Steel Beams." *Proc. in 11DBMC International Conference on Durability of Building Materials and Components*, Istanbul, Turkey.

e DVAmadei, B. (2000). "A Mathematical Model for Flow of Bingham Material in Fractures." *Proc. 4th NARMS Conf.: Pacific Rocks 2000, "Rock around the rim,"* J. Girard, M. Liebman, C. Breeds, and T. Doe, eds., Seattle, WA.

ASBI. (2000a). "American segmental bridge institute grouting committee: Interim statement on grouting practices." American Segmental Bridge Institute (ASBI), Phoenix, AZ, USA.

ASBI. (2000b). "Interim Statement on Grouting Practices." American Segmental Bridge Institute, Grouting Committee, Phoenix, AZ.

ASTM Standard C 1556. (2003). "Standard Test Method for Determining the Apparent Chloride Diffusion Coefficient of Cementitious Mixtures by Bulk Diffusion." ASTM C1556-03, ASTM, West Conshohocken, PA.

ASTM Stantard C 942. (1986). "Standard Test Method for Compressive Strength of Grouts for Preplaced-Aggregate Concrete in the Laboratory." ASTM C942-86, ASTM, West Conshohocken, PA.

Barneyback, R. S., and Diamond, S. (1981). "Expression and analysis of pore fluids from hardened cement pastes and mortars." *Cement and Concrete Research*, 11(2), 279-285.

Beyer, W. H. (1978). *CRC Handbook of Mathematical Sciences*, CRC Press, Boca Raton, FL.

Blitz, J., and Simpson, G. (1996). *Ultrasonic Methods of Non-destructive Testing*, Chapman and Hall, London.

Blum, F. (2003). "A Focused, Two Dimensional, Air-coupled Ultrasonic Array for Non-Contact Generation," University of Stuttgart.

Carino, N. J., and Sansalone, M. "Impact-echo: a New Method for Inspecting Construction Materials." *Proceedings, Conference on NDT&E for Manufacturing and Construction*, Urbana, IL, 209-223.

Carino, N. J., and Sansalone, M. (1992). "Detection of Voids in Grouted Ducts Using the Impact-Echo Method." *ACI Material Journal*, 89(3), 296-303.

Chaqui, M. (2006). "How many components in a grout mix?" *Geotechnical News*, 24(1), 52-57.

Choe, D.E., Gardoni, P., Rosowsky, D., and Haukaas, T. (2008a). "Seismic fragility estimates for reinforced concrete bridges subject to corrosion." *Structural Safety*, In Press, Corrected Proof.

Choe, D. E., Gardoni, P., Rosowsky, D., and Haukaas, T. (2008b). "Probabilistic capacity models and seismic fragility estimates for RC columns subject to corrosion." *Reliability Engineering & System Safety*, 93(3), 383-393.

Clark, G., and Ganz, H.-R. (2002). "Grouting of Tendons in Prestressed Concrete." *fib Bulletin 20*, Federal Institute of Technology Lausanne (EPFL), Laussane, Switzerland.

Cruise, J. F., Sherif, M. M., and Singh, V. P. (2007). *Elementary Hydraulics*, Nelson Education, Toronto, Ontario.

Della Vedova, M., and Elsener, B. "Enhanced Durability, Quality Control and Monitoring of Electrically Isolated Tendons." *Proceedings of the 2nd FIB International Congress*, Italy, 1-12.

Earley, W. (2004). "Lasting line of defense." *Roads & Bridges*, 38-49.

Elsener, B. "Experience with Electrically Isolated Tendons in Switzerland." *Proceedings of the first workshop of COST 534 on NDT Assessment and New Systems in Prestressed Concrete Structures*, Switzerland, 89-97.

Eriksson, M., and Stille, H. (2003). "A Method for Measuring and Evaluating the Penetrability of Grouts." *Proc. 3rd International Specialty Conference on Grouting and Ground Treatment, Grouting 2003*, L. F. Johnson, D. A. Bruce, and M. J. Byle, eds., ASCE, New Orleans, Louisiana, USA, 79-79.

Eriksson, M., Stille, H., and Andersson, J. (2000). "Numerical calculations for prediction of grout spread with account for filtration and varying aperture." *Tunnelling and Underground Space Technology*, 15(4), 353-364.

Estes, A. C., and Frangopol, D. M. "Updating Time-Dependent Reliability of Highway Bridges with Pontis Bridge Management System Inspection Results." *9th International Bridge Management*, Orlando, Florida, 229-238.

FDOT. (1999). "Corrosion Evaluation of Post-Tensioned Tendons on the Niles Channel Bridge." Florida Department of Transportation, Tallahassee, FL, USA.

FDOT. (2001a). "Mid-Bay Bridge Post-Tensioning Evaluation – Final Report." Florida Department of Transportation, Corven Engineering, Inc, Tallahassee, FL.

FDOT. (2001b). "Sunshine skyway bridge post-tensioned tendons investigation." Florida Department of Transportation, Parsons Brinckerhoff Quade and Douglas, Inc., Tallahassee, FL.

Ferraris, C. F. (1999). "Measurement of the rheological properties of high performance concrete: State of the art report." *Journal of Research of the National Institute of Standards and Technology*, 104(5), 461-478.

FHWA. (2004). "Post-Tensioning Tendon Installation and Grouting Manual." Federal Highway Administration, Washington, D.C.

Gallagher, K. A. (1989). "Concrete bridge deterioration - Research into the problem by TRRL." *Construction & Building Materials*, 3(4), 184-190.

Ganz, H. R. (2001). "Evolution of Prestressing Systems." Belgium.

Goodwin, F. (2002). "Corrosion in bonded post-tensioned structures." *Materials Performance*, 41(10), 38-43.

Hakansson, U., Hassler, L., and Stille, H. (1992). "Rheological properties of microfine cement grouts." *Tunneling and Underground Space Technology*, 7(4), 453-458.

Hansen, B. (2007). "Tendon failure raises questions about grout in posttensioned bridges." Forensic Engineering: Civil Engineering News, 17-18.

Hawk, H., and Small, E. P. (1998). "The BRIDGIT Bridge Management System." *Structural Engineering International, Journal of IABSE*, 8(1998), 309-314.

Hemmings, R. T., and Cornelius, B. J. (1991). "Optimization of a Cement Grout Formulation for Ducts Containing Post-Tensioned Cables." *MAT-91-08*, The Research and Development Branch, Ontario Ministry of Transportation, Canada, Ontario.

Herman, G. T. (1980). *Image Reconstruction from Projections: the Fundamentals of Computerized Tomography*, Academic Press, New York.

Hope, B. B., and Ip, A. K. C. (1988). "Grout for post-tensioning ducts." *ACI Materials Journal*, 234-240.

Hu, Q., and Yue, W. (2008). *Markov decision processes with their applications*, Springer, New York.

Huang, Q., Gardoni, P., and Hurlebaus, S. (2008). "Probabilistic Capacity Models and Fragility Estimates for Reinforced Concrete Columns using Nondestructive Testing." *Submitted to ASCE Journal of Engineering Mechanics*.

Hurlebaus, S., Jacobs, L. J., and Jarzynski, J. (1998). "Laser Techniques to Characterize the Effect of Geometry on Acoustic Emission Signals." *Journal of Nondestructive Testing and Evaluation*, 14, 21-37.

Iyer, S., Schokker, A. J., and Sinha, S. K. (2003). "Ultrasonic C-Scan Imaging: Preliminary Evaluation for Corrosion and Void Detection in Posttensioned Tendons " *Transportation Research Record: Journal of the Transportation Research Board*, 1827, 44-52.

Iyer, S. R., Sinha, S. K., and Schokker, A. J. (2005). "Ultrasonic C-Scan Imaging of Post-Tensioned Concrete Bridge Structures for Detection of Corrosion and Voids." *Computer-Aided Civil and Infrastructure Engineering*, 20(2), 79-94.

Karaoğuz, M., Bilgütay, N., Akgül, T., and Popovics, S. (1998). "Defect Detection in Concrete Using Split Spectrum Processing." *IEEE Ultrasonics symposium*, 1, 843-846.

Kil, H. G., Jarzynski, J., and Berthelot, Y. H. (1998). "Wave decomposition of the vibrations of a cylindrical shell with an automated scanning laser vibrometer." *Journal of the Acoustic Society of America*, 104(6), 3161-3168.

Kong, J. S., and Frangopol, D. M. "System Reliability Modelling in Bridge Management." *9th International Bridge Management*, Orlando, Florida, 348-360.

Kosmatka, S., Kerkhoff, B., and Panarese, W. (2002). *Design and Control of Concrete Mixtures*, EB001, 14th edition, Portland Cement Association, Skokie, IL.

Krause, H. J., Wolf, W., Glaas, W., Zimmermann, E., Faley, M. I., Sawade, G., Neudert, G., Gampe, U., and Krieger, J. (2001). "SQUID System for Magnetic Inspection of Prestressed Tendons on Concrete Bridges." *Insight Nondestructive Testing and Condition Monitoring*, 43(7), 458-461.

Krause, M., Maierhofer, C., and Wiggenhauser, H. "Thickness Measurement of Concrete Elements Using Radar and Ultrasonic Impulse Echo Techniques." *Proceeding International Conference on Structural Faults and Repair-95*, London, UK, 17-24.

Kumar, R., Gardoni, P., and Sanchez-Silva, M. (2008). "Effect of cumulative seismic damage and corrosion on the life-cycle cost of reinforced concrete bridges." *Earthquake Engineering & Structural Dynamics*, 9999(9999).

Kundu, T. (2000). "Chapter 12: Nondestructive Testing Techniques for Material Characterization." Modeling in Geomechanics, M. Zaman, G. Gioda, and J. Booker, eds., John Wiley & Sons, 267-298.

Kuznetsov, V. M., Tseitlin, G., Hitrov, V. A., Zaitchik, J. U., Brodski, G., Brodskaia, E., Enutin, Y. A., and Shesterikov, V. I. "Bridge Management System for City of Moscow." *9th International Bridge Management*, Orlando, Florida.

Locke, C. E. (1986). "Corrosion of Steel in Portland Cement Concrete: Fundamental Studies." Corrosion Effects of Stray Currents and the Techniques for Evaluating Corrosion of Rebars in Concrete, ASTM STP 906, V. Chaker, ed., American Society for Testing and Materials, Philadelphia, 5-14.

Martello, S., and Toth, P. (1990). *Knapsack Problems-Algorithm and Computer Implementations*, Wiley, New York.

Martin, J., Broughton, K. J., Giannopolous, A., Hardy, M. S. A., and Forde, M. C. (2001). "Ultrasonic Tomography of Grouted Duct Post-Tensioned Reinforced Concrete Bridge Beams." *NDT&E International*, 34, 107-113.

Martínez, O., Akhnak, M., Ullate, L. G., and Espinosa, F. M. (2003). "A Small 2D Ultrasonic Array for NDT Application." *NDT&E International*, 36(1), 57-63.

Martz, H. E., Roberson, G. P., Skeate, M. F., Schneberk, D. J., and Azevedo, S. G. (1991). "Computerized Tomography Studies of Concrete Samples." *Nuclear Instruments and Methods in Physics Research Section B*, 58(2), 216-226.

Martz, H. E., Scheberk, D. J., Roberson, G. P., and Monteiro, P. J. M. (1993). "Computerized Tomography Analysis of Reinforced Concrete." *ACI Materials Journal*, 90(3), 259-264.

Mathworks. (2008). "*Binary Integer Programming, Version 7.7.0.471*."

Mendelsohn, Y., and Wiener-Avnear, E. (2002). "Simulations of circular 2D phase-array ultrasonic imaging transducers." *Ultrasonics*, 39(9), 657-666.

Mindess, S., Young, J. F., and Darwin, D. (2003). *Concrete*, Pearson Education Inc., Upper Saddle River, NJ 07458.

Montgomery, D. C., and Runger, G. C. (2007). *Applied Statistics and Probability for Engineers*, 4th Edition, John Wiley & Sons, Inc, New York, NY.

Moon, H. K., and Song, M. K. (1997). "Numerical Studies of Groundwater Flow, Grouting and Solute Transport in Jointed Rock Mass." *International Journal of Rock Mechanics and Mining Sciences and Geomechanics Abstracts*, 34, 490-490.

Mori, Y., and Ellingwood, B. R. (1994a). "Maintaining Reliability of Concrete Structures. I: Role of Inspection/Repair." *Structural Engineering*, 120(3), 824-845.

Mori, Y., and Ellingwood, B. R. (1994b). "Maintaining Reliability of Concrete Structures. II: Optimum Inspection/Repair." *Structural Engineering*, 120(3), 846-862.

NCHRP. (1998a). "Durability of Precast Segmental Bridges." *Project 20-7/Task 92*, National Cooperative Highway Research Program (NCHRP): Transportation Research Board: National Research Council, Washington, D.C.

NCHRP. (1998b). "Durability of Precast Segmental Bridges." National Cooperative Highway Research Program (NCHRP): Transportation Research Board: National Research Council, Washington, D.C.

PCI. (1997). "Chapter 3: Fabrication and Construction." PCI Bridge Design Manual, Prestressed Concrete Institute, Chicago, IL.

Pearson-Kirk, D. "The Performance of Post-tensioned Bridge." *Role of Concrete Bridges in Sustainable Development – Proceedings of the International Symposium*, 129-140.

Pessiki, S. P., and Carino, N. J. (1988). "SettingTime and Strength of Concrete Using the Impact-Echo Method." *ACI Materials Journal*, 85(5), 389-399.

Pielstick, B. (2002). "Grouting of Segmental Posttensioned Bridges in America." *Transportation Research Record*, 1813(-1), 235-241.

Pillai, R. G., Gardoni, P., Hueste, M. D., Reinschmidt, K., and Trejo, D. "Flexural Reliability of Corroding Segmental Post-tensioned Bridges." *The 10th International Conference on Structural Safety and Reliability*, Osaka, Japan.

Poulsen, E., and Mejlbro, L. (2006). *Diffusion of Chloride in Concrete: Theory and Application*, Taylor & Francis, London.

Powers, T. C. "The Bleeding of Portland Cement Paste, Mortar, and Concrete - Treated as a Special Case of Sedimentation." *Proceedings of the American Concrete Institute*, Detroit , MI, 465-479.

PTI. (2001). *Guide Specification for Grouting of Post-Tensioned Structures*, Post-Tensioning Institute, Phoenix, AZ.

PTI. (2003a). *Specification for Grouting Post-Tensioned Structures*, Post-Tensioning Institute, Phoenix, AZ.

PTI. (2003b). *Specification for Grouting Post-Tensioned Structures*, Post-Tensioning Institute, Phoenix, AZ.

Qian, T., Wei, S., Jiaping, L., and Changwen, M. (2004). "Performance of Grouts for Post-tensioned Prestressed Structures." *Journal of Southeast University*, 20(4), 492-497.

Raiss, M. (1995). "Post-tensioned Concrete Bridges: the UK Debate." *Concrete International*, 29(2), 23-26.

Ritchie, A. G. B. (1965). "The rheology of cement grout." *Cement and Lime Manufacture*, 9-17.

Robert, W. E., Marshall, A. R., Shepard, R. W., and Aldayuz, J. "Pontis Bridge Management System: State of the Practice in Implementation and Development." *The 9th International Bridge Management*, Orlando, Florida, 49-60.

Sansalone, M., and Carino, N. J. (1989). "Laboratory and Field Studies of the Impact-Echo Method for Flaw Detection in Concrete." *ACI Special Publication*, 112, 1-20.

Schickert, M. "Towards SAFT-Imaging in Ultrasonic Inspection of Concrete " *Proceeding International Symposium of Non-destructive Testing in Civil Engineering (NDT-CE)*, 411-418.

Schokker, A. J., Breen, J. E., and Kreger, M. E. (2001a). "Grouts for Bonded Post-Tensioning in Corrosive Environments." *ACI Materials Journal*, 98(4), 296-305.

Schokker, A. J., Breen, J. E., and Kreger, M. E. (2001b). "High Performance Grouts for Durable Post-Tensioning." *First International Structural Engineering and Construction Conference,* 'Creative Systems in Structural and Construction Engineering', A. Singh, ed., Taylor & Francis, Balkema, Rotterdam, 429-433.

Schokker, A. J., Breen, J. E., and Kreger, M. E. (2002). "Simulated field testing of high performance grouts for post-tensioning." *Journal of Bridge Engineering*, 7(2), 127-133.

Schupack, M. (2004). "PT Grout: Bleed Water Voids." *Concrete International*, 26(8), 69-77.

Scruby, C. B., and Drain, L. E. (1990). *Laser Ultrasonics: Techniques and Applications*, Adam Hilger.

Shoji, N., Noritaka, S., Yasushi, K., and Koichiro, S. (2003). "Development of Repair Method for Poorly Grouting of PC Structures." *Concrete Journal*, 41(11), 31-43.

Sivakumar, B., Minervino, C. M., and Edberg, W. "New Bridge Performance Measures for Prioritizing Bridges." *The 9th International Bridge Management*, Orlando, Florida, 348-360.

Smith, L. J., and Wood, R. (2001). "Grouting of External Tendons: A Practical Perspective." *Proceeding of the Institution of Civil Engineers: Structures & Buildings*, 146(1), 93-100.

Sprinkel, M., and Napier, C. S. "VDOT Experience with Grouted Tendons in Varina-Enon Precast Segmental Post-tensioned Bridge." *Virginia Concrete Conference*.

Thompson, P. D., Sobanjo, J. O., and Kerr, R. "Florida Project-Level Models for Pontis." *The 9th International Bridge Management*, Orlando, Florida, 70-84.

Tilly, G. P. (2002). "Performance and management of post-tensioned structures." *Proceedings of the Institution of Civil Engineers*, 152(1), 3-16.

Tinkey, Y., Olson, L. D., and Wiggenhauser, H. (2005). "Impact Echo Scanning for Discontinuity Detection and Imaging in Posttensioned Concrete Bridges and Other Sturctures." *Materials Evaluation*, 63(1), 64-69

TxDOT. (1999). "Tex-437-A: Test for Flow of Grout Mixtures (Flow Cone Method)." Texas Department of Transportation, Austin, TX.

TxDOT. (2003). "Tex-441-A, Wick-induced Bleed Test of Freshly Mixed Grouts." T. D. O. Transportation, ed., Texas Department of Transportation, Austin, TX.

TxDOT. (2004). "DMS-4670: Grouts for Post-tensioning." Texas Department of Transportation, Austin, TX.

TxDOT. (2006). "Tex-442-A, Determining Compressive Strength of Grouts." Texas Department of Transportation, Austin, TX.

VSL. (2002). "Grouting of Post-Tensioning Tendons." *Report Series 5*, VSL International Ltd., Lyssach/ Switzerland.

Warner, J. (2004). *Practical Handbook of Grouting*, John Wiley & Sons, Inc, Hoboken, NJ.

Woodward, R. J. (1980). "Conditions within Concrete Ducts in Post Tensioned Prestressed Concrete Bridges." *TRRL Report LR 980*, Transport and Road Research Laboratory, Department of Transport, Crowthorne, UK.

Woodward, R. J., and Miller, E. (1990). "Grouting Post-tensioned Concrete Bridges: the Prevention of Voids." *Highways and Transportation*, 37(6), 9-17.

Yahia, A., and Khayat, K. (2003). "Applicability of rheological models to high-performance grouts containing supplementary cementitious materials and viscosity enhancing admixture." *Materials and Structures*, 36(6), 402-412.

Yanev, B., Testa, R. B., and Garvin, M. "Maintenance Strategy to Minimize Bridge Life-Cycle Costs." *The 9th International Bridge Management*, Orlando, Florida, 189-200.

APPENDICES

APPENDIX A. MATERIAL CHARACTERIZATION TEST PROCEDURES

A.1 VISCOSITY MEASUREMENTS USING THE DV-III+ PROGRAMMABLE RHEOMETER FROM BROOKFIELD ENGINEERING

1. Read all directions before performing the viscosity measurements.
2. Personnel, material, and equipment requirements
    a. One person
    b. DV-III+ Programmable Rheometer from Brookfield Engineering
    c. Model D Helipath™ Stand from Brookfield Engineering
    d. Computer Program - Rheocalc V2.4 or newer version
    e. Appropriate computer to run the computer program and connect to the rheometer

    f. Cement
    g. Water
    h. Scoop
    i. Balance – accurate to at least ± 0.000353 ounces (0.01 g)
    j. Black cylinder molds – 4 × 8 inch (101.6 × 203.2 mm) for testing
    k. Tape – Scotch Magic™ Tape will work
    l. Small beaker – 16.9 ounces or 33.8 ounces (500 ml or 1000 ml) to help clean the spindle and temperature probe after each test
    m. Paper towels

3. Assembling the Helipath™ Stand

    a. Remove the screw and washer from the upright rod.

    b. Place the rod and clamp assembly into the hole in the top of the base.

    c. Rotate the rod/clamp assembly slightly until the slot on the bottom of the rod intersects the pin located in the base.

    d. While holding the rod and base together, insert the slotted screw and washer and tighten securely.

4. Mounting the DV-III+ to the Helipath™ Stand

    a. Insert the viscometer mounting rod on the back of the DV-III+ into the hole (with the cut away slot) in the clamp assembly.

    b. Check the lateral position of the viscometer relative to the base.

    c. Make adjustments and retighten the screw as required to center the viscometer between the base legs.

    d. Referring to the stand bubble level, adjust the base leveling screws until the stand is level.

    e. Adjust the instrument level until the bubble is centered from right to left and tighten the clamp knob (clockwise).

    f. Use the leveling screws to "fine" adjust the viscometer level. (Caution: Position power cords so they do not interfere with the travel of the drive unit.)

5. Turn the DV-III+ power switch on. The switch is located on the right backside of the base unit.

6. Once the DV-III+ is turned on, you can open the Rheocalc program on the computer. Rheocalc V2.4 was used for this study.

7. The screen on the DV-III+ will read as follows:

Brookfield
DV-III+ Rheometer
1 = EXTERNAL CONTROL
2 = STANDALONE MODE

Press the control key, 1, on the face of the DV-III+ Rheometer for external control through the computer.

8. The Rheocalc program will start on the Dashboard page. On this page you must select which spindle to use. There is a pull down menu under the heading Spindle that allows you to select which spindle is being used. Spindle T-A (#91) will be used for the tests.

9. Zeroing the Rheometer

    a. Before readings may be taken, the rheometer must be autozeroed. It is important to let the rheometer warm up for about 10 minutes before zeroing the machine.

    b. The Zero button is in the lower left hand corner of the Dashboard page.

    c. The rheometer must be zeroed while the unit is balanced and before the spindle is attached. The unit can be balanced by using the leveling screws on the bottom of the base stand. Once the Zero button is pressed, a Warning message will appear on the computer screen:

    d. Rheometer will now be zeroed. Please ensure the rheometer is level and the spindle is removed.

    e. Click on the zero button and allow approximately 15 seconds for the rheometer to zero.

10. Attaching the Spindle

    a. Select a T-bar spindle.

    b. Attach the weight to the closer piece of the chuck assembly.

    c. Slide the spindle through the weight and closer into the chuck and tighten before attaching the chuck to the viscometer.

d. Connect the chuck/closer/weight assembly, with spindle, to the viscometer.

11. Grout Sample

a. After completion of mixing, collect grout sample in a 4 × 8-inch (101.6 × 203.2 mm) cylinder mold.

b. This is an appropriate size container for the spindle to spin freely in the grout mixture while not touching the sides of the container.

c. The sample can now be taken to the Brookfield Rheometer.

12. Test Setup

a. Once the grout is in the testing cylinder, the temperature probe can be taped to the inside of the container right above the grout level.

b. Then place the container under the rheometer.

c. If the rheometer is high on the stand and the spindle is not in the grout, lower the spindle into the grout by depressing the disengaging lever on the Helipath™ drive unit.

d. The recommended initial spindle immersion is when the cross-bar of the T spindle is ¼ inch (6.35 mm) below the surface of the grout.

e. At this time the reversing rod on the drive unit should be pushed down. Make sure that the drive unit is OFF (the light on top of the drive unit will not be illuminated).

f. Set the adjustable stops to accommodate the travel of the Helipath™ that will provide the desired penetration of the spindle [recommended 1.5 inch (38.1 mm)]. The top stop should be lowered to the top of the drive unit so that the drive unit will not move any higher and thus raise the cross-bar of the T-spindle to where it has less than ¼ inch (6.35 mm) of material above it.

g. The testing can then be started at five minutes after the completion of mixing or at any other appropriate time while the grout is still in its fluid state. When the program

is started the Helipath™ drive unit should be turned on also (the light on the drive unit will now be illuminated).

13. Test Program

    a. Click on the Programs tab in the Rheocalc program.

    b. The written program that was used for this test was as follows:

        SSN 010.

        DCI 00:15

        WTI 15:00

    c. This means that the rheometer will be set to a rotational speed of 10 rpm and that it will record data every 15 seconds for 15 minutes.

    d. The progress of the program can be viewed on the Programs tab or the measurements can be seen continuously on the Dashboard tab.

14. Data Collection

    a. Once the program has run completely, the collected data will be shown on the View/Edit tab. On this tab, you can save, print, and export to a MicrosoftExcel™ file the collected data.

    b. The data can also be plotted. Click on the Plot tab and print out a plot using any of the recorded variables.

15. Test Cleanup

    a. When the test is completed, turn the Helipath™ drive unit off.

    b. Depress the disengaging lever on the Helipath™ drive unit to raise the spindle out of the grout.

        a. The drive unit will come into contact with the upper adjustable stopper before the spindle is removed from the grout. The adjustable stopper can be raised so that the spindle is out of the grout, but if several comparable tests are being

run, the adjustable stoppers should probably not be moved so that each test will be confidently the same. If this is the case, the spindle can be lifted at an angle to a height in which the container holding the grout can be removed from under the Helipath™ stand.

b. The temperature probe can be removed from the container and then the container can be discarded appropriately.

c. It is important to thoroughly clean the temperature probe and the spindle with water and paper towels right after each test. If the spindle is not cleaned completely after each test, grout deposits remaining on the spindle would result in larger torque % readings and thus a larger and erroneous viscosity measurement.

16. Report

a. Date and identification number of the test specimen

b. Identification of the test equipment and instruments used

c. Written program used and the start time of the test from the addition of water to the grout

d. Any deviation from the test method together with other information of importance

e. A plot showing the measured viscosity versus time and temperature versus time

A.2 PROCEDURE FOR pH TEST OF THE PORE SOLUTION OF GROUT

1. Read all directions before performing the viscosity measurements.
2. Personnel, material, and equipment requirements:
    a. One person
    b. Pore Fluid Expression Device – consisting of support cylinder, platen, die body, and piston assembly

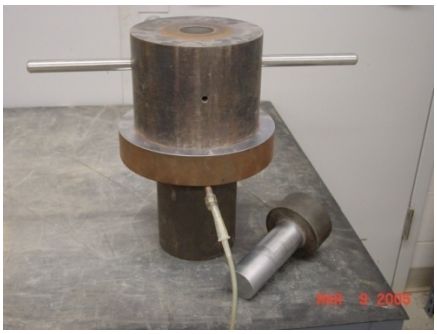

    c. Small rubber hose
    d. Disposable plastic syringe
    e. 6-mm thick Teflon seal – inserted between the top of the specimen and the bottom surface of the piston
    f. 2 × 4-inch (50.8 × 101.6 mm) black plastic cylindrical molds with top
    g. Tinius Olsen Compression Machine
    h. Plastic pipettes
    i. Denver Instrument Company – Model 250 pH/Ion/Conductivity Meter (any of the other models, Model 215, 220, 225, would also be sufficient)
    j. Plastic bags
3. Sample Preparation
    a. Once the grout has been mixed, fill 4 of the 2 × 4-inch (50.8 × 101.6 mm) plastic molds with the grout.
    b. Close the containers with the provided tops so that moisture is not allowed to escape.
    c. Label the different specimens.

d. Store these specimens together in a constant temperature environment.

e. After initial set, remove the specimens from their molds and leave them in curing environment.

4. Test Setup

a. Place the support cylinder on the lower bearing surface of the compression machine.

b. At this time, check the platen for any debris in the fluid drain or area where the test specimen will be placed.

c. Once the platen has been cleaned appropriately, place the platen on top of the support cylinder so that the support cylinder fits into the provided grooves on the bottom of the platen and so that the fluid drain is accessible.

d. Two designs can be used at the fluid drain. A small rubber hose can be pushed up into the drain hole to receive the fluid or a small threaded pipe can be screwed into the drain with some Teflon tape wrapped around the threads. With this setup, the rubber hose can be fitted to the end of the small pipe.

e. A small plastic disposable syringe without the needle can be fitted into the end of the rubber hose to later retrieve the water.

f. Spray a thin coating of film-bonding grade fluorocarbon over the mating surfaces of the die body and platen, over the bore of the die body, and the shaft of the piston.

g. The die body can then be centered in the grooves on the upper surface of the platen.

5. Pore Solution Collection Procedure

a. Make sure your test apparatus is completely set up in the compression machine.

b. Take one of your samples and remove it from its plastic mold. The container may have to be cut if the specimen will not slide out.

c. The specimen should be placed directly into the bore of the die body. If the specimen is already removed from its mold, it should be retrieved from the curing environment and promptly placed in the mold. This will reduce its exposure to ambient air.

d. Place the 6 mm-thick Teflon seal on top of the specimen.

e. Then place the piston assembly in the bore on top of the Teflon seal and test specimen.

f. The piston should then be loaded at a rate equivalent to a compressive stress increase of about 400 psi/s (about 2.8 MPa/s).

g. The rate should increase until the maximum pressure of 78.3 ksi (540 MPa) is reached or a sustained pressure that allows for the collection of a sufficient quantity of pore fluid [0.1 to 0.14 ounces (3 to 4 ml)] in a plastic syringe through the fluid drain.

h. The plunger on the plastic syringe should be pulled out a short distance to put a slight negative pressure on the pore fluid drainage system.

i. It is also helpful to temporarily withdraw the syringe from the rubber hose to allow some of the accumulated gases to escape from it several times during each test.

j. If sufficient pore fluid is not collected on this first cycle, the pressure should be reduced to about 50.8 ksi (350 MPa) to allow some elastic rebound to occur. On increasing the pressure back to the maximum level additional pore fluid can be withdrawn into the syringe. This can be repeated for several steps, but it is seldom possible to recover more fluid after 3 or 4 times.

k. It is important to avoid undue exposure of the pore solution to air. It should be sealed in a plastic container until the time of analysis.

6. pH Analysis

a. Once 0.07 to 0.1 ounces (2 to 3 ml) of pore solution is collected in the syringe, the solution can be transferred into a small container that will receive a pH glass electrode. (We will use a plastic pipette that has the shaft end cut off.)

b. Hold the plastic pipette half under the pH glass electrode.

c. The initial reading on the pH meter is the desired reading. The pH reading will drop after this initial reading due to the exposure to air.

d. This test can be performed at 1, 7, 14, and 28 days.

7. Cleaning the test apparatus

a. It is necessary to disassemble the apparatus, recover the remolded specimen, and clean all surfaces immediately after recovery of the expressed fluid.

b. The die body is removed from the platen and the platen surface and its drain system are flushed with absolute ethanol and wiped clean with soft facial tissue at least twice, and until no residue remains.

c. After the platen is cleaned and the fluid drain is flushed, it can be removed from the top of the support cylinder.

d. If the remolded specimen is too tightly packed into the die body, the die body should be placed onto the support cylinder, the piston cap removed from the piston, and pressure is applied to the top of the piston to eject the remolded specimen from the bore into the central opening of the support cylinder.

e. The apparatus can be disassembled and the specimen recovered and sealed in a plastic bag for storage or further analysis.

f. The piston and die are cleaned using absolute ethanol and facial tissue until all residual material is removed.

g. All surfaces are then recoated with a fresh coating of fluorocarbon.

A.3 PROCEDURE FOR FILLABILITY TEST OF GROUT

(Developed in laboratory based on the penetrability meter developed by Eriksson and Stille)

1. Read all directions before performing the fillability test.
2. Personnel, material, and equipment requirements:
    a. One person
    b. Fillability meter developed in laboratory by PVC schedule 40 and schedule 80 fittings, including different size stainless steel screen filters
    c. Pressurized nitrogen gas cylinder assembly
    d. One 4.23 pint (2 l) scoop and four 2.11 pint (1000 ml) graduated cylinders
    e. One stop watch
3. Sample preparation
    a. Prepare the grout by mixing a known amount of grout with a known amount of water based on the mixture proportions

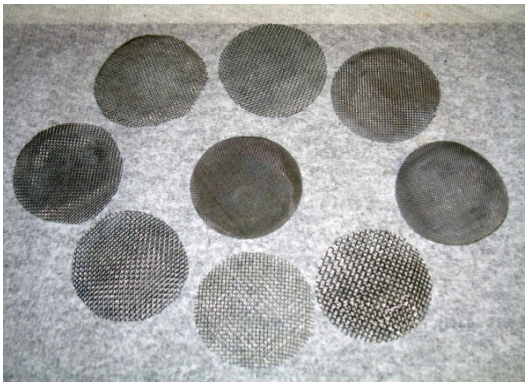

    b. Mix the grout for 5 minutes unless otherwise mentioned in the mixing procedure
    c. Immediately after the mixing, measure 4.23 pint (2000 ml) of grout in the scoop and pour it in the fillability meter with check valve closed
    d. Close the fillability meter from the top by using the threaded cover and connect the hose with the barbed hose adapter.

e. Put a protective wire mesh cover on the fillability meter

4. Test setup

    a. Place a 2-liter graduated beaker below the fillability meter bottom outlet to collect the grout.

    b. Once the fillability meter is covered with protective wire cage, open the pressure cylinder valve and maintain a constant pressure of 20 psi (0.138 MPa). The grout will now start flowing out of the bottom outlet under the pressure. Let the grout flow under this pressure.

    c. Measure the volume of grout collected in the beaker once the grout stops flowing.

    d. Stop pressure supply when no further grout flows through the bottom outlet or no grout left in the meter. Release air pressure, remove the air supply and clean the fillability meter and filter immediately.

5. Repeat steps 4 and 5 for different filter sizes for all three grouts in study and measure the volume of grout passing each filter.

6. Plot a graph between the filter size and volume of grout passed for the three thixotropic grouts under study. Compare the passing ability of each grout.

APPENDIX B. EXPERIMENTAL RESULTS OF REPAIR GROUTING

The experimental results of repair grouting for analysis are summarized in this appendix. First, void profiles mapped by a sounding and visual inspection are provided to evaluate the effectiveness of sounding technique for detecting voids in ducts. Also, the infiltration length of repair grout and results obtained from the cut sections are represented to compare FC and performance of different repair methods and grouts. Finally, the sealing time and schedule are recorded to assess economic feasibility of different repair methods.

B.1 SPECIMEN VG-C1-1

Figure B-1 depicts the initial void profiles of the sounding inspection and of the visual inspection before grouting.

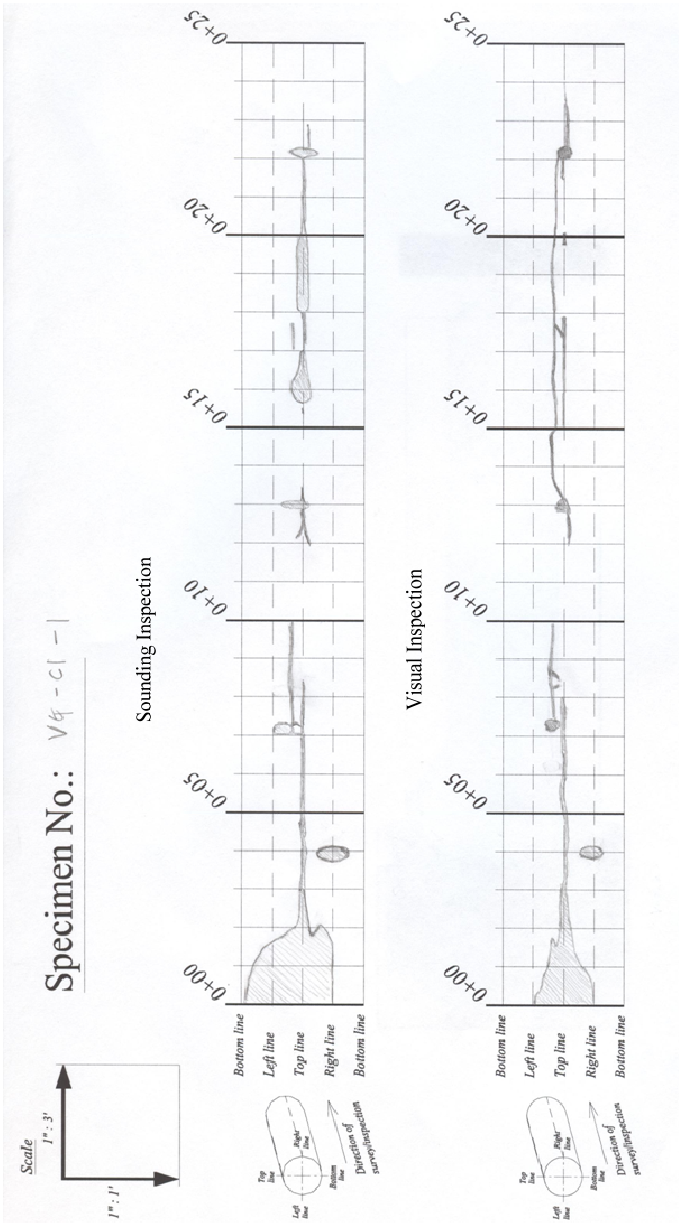

Figure B-1. Void Map of Specimen VG-C1-1.

The areas of both void profiles are estimated using AutoCAD® and provided in Table B-1.

Table B-1. Estimation of Void Profile in Specimen VG-C1-1.

Section, ft (m)	Sounding Inspection (SI), inch^2 (10^{-4} m^2)	Visual Inspection (VI), inch^2 (10^{-4} m^2)	SI - VI, inch^2 (10^{-4} m^2)
0~1 (0~0.3)	104.82 (676.2)	62.18 (401.2)	42.64 (275.1)
1~2 (0.3~0.6)	75.85 (489.3)	28.21 (182.0)	47.63 (307.3)
2~3 (0.6~0.9)	10.57 (68.2)	10.23 (66.0)	0.34 (2.2)
3~4 (0.9~1.2)	14.95 (96.5)	8.78 (56.7)	6.17 (39.8)
4~5 (1.2~1.5)	8.57 (55.3)	7.39 (47.7)	1.18 (7.6)
5~6 (1.5~1.8)	4.84 (31.2)	4.79 (30.9)	0.05 (0.3)
6~7 (1.8~2.1)	4.90 (31.6)	5.18 (33.4)	-0.28 (-1.8)
7~8 (2.1~2.4)	13.69 (88.3)	12.41 (80.1)	1.28 (8.3)
8~9 (2.4~2.7)	5.74 (37.0)	6.92 (44.6)	-1.18 (-7.6)
9~10 (2.7~3.0)	3.57 (23.1)	3.68 (23.8)	-0.11 (-0.7)
10~11 (3.0~3.4)	0.00 (0.0)	0.00 (0.0)	0.00 (0.0)
11~12 (3.4~3.7)	0.16 (1.0)	0.08 (0.5)	0.08 (0.5)
12~13 (3.7~4.0)	8.43 (54.4)	6.83 (44.0)	1.60 (10.3)
13~14 (4.0~4.3)	4.20 (27.1)	5.22 (33.7)	-1.03 (-6.6)
14~15 (4.3~4.6)	0.00 (0.0)	4.11 (26.5)	-4.11 (-26.5)
15~16 (4.6~4.9)	7.75 (50.0)	5.75 (37.1)	2.00 (12.9)
16~17 (4.9~5.2)	14.65 (94.5)	7.74 (50.0)	6.90 (44.5)
17~18 (5.2~5.5)	5.66 (36.5)	8.58 (55.4)	-2.92 (-18.8)
18~19 (5.5~5.8)	14.55 (93.9)	3.87 (25.0)	10.68 (68.9)
19~20 (5.8~6.1)	13.99 (90.3)	4.01 (25.9)	9.99 (64.4)
20~21 (6.1~6.4)	5.98 (38.6)	2.65 (17.1)	3.33 (21.5)
21~22 (6.4~6.7)	4.78 (30.9)	4.45 (28.7)	0.33 (2.1)
22~23 (6.7~7.0)	8.38 (54.1)	8.87 (57.2)	-0.48 (-3.1)
23~24 (7.0~7.3)	0.00 (0.0)	2.48 (16.0)	-2.48 (-16.0)

Repair grout is infiltrated from the top grout port and the main voids are filled successfully. The repair grout is infiltrated to 14.5 ft (4.42 m) from the reference point (Figure B-2).

Figure B-2. Repair Grouted Ducts of Specimen VG-C1-1.

Figure B-3 shows the cross-sectional views of the cut sections obtained from Specimen VG-C1-1. For the Specimen VG-C1-1, a colorant is added in the repair grout. Through the preliminary test on Class C-1 grout, it is confirmed that the added colorant does not affect the fluidity of this grout. However, the colorant is added onward to the initial grout in order to minimize the effect in repair grouts.

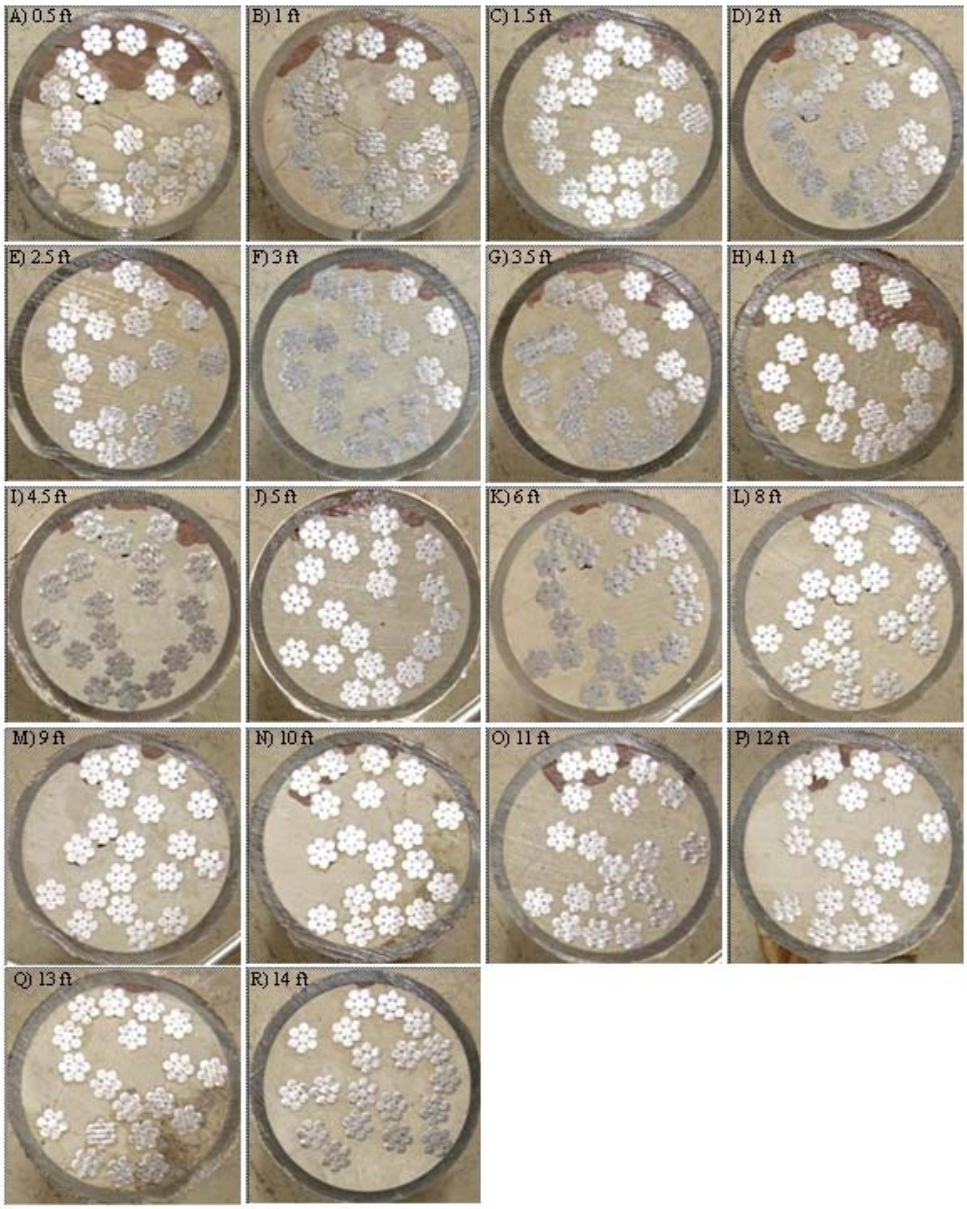

Figure B-3. Cut Sections of Specimen VG-C1-1 for the Filling Analysis of Repair Grout.

To compare the performance of repair grouts, the ratio of the remaining void area after repair to the repaired area is estimated. The repaired area and area of voids after repair are calculated using AutoCAD® (Table B-2).

Table B-2. Void Area of Specimen VG-C1-1.

Cut Sections, ft (m)		Repaired Area, A_R, inch^2(10^{-4} m^2)	Void Area, A_V, inch^2(10^{-4} m^2)	Void Ratio, η (%)
A	0.5 (0.15)	1.810 (12.20)	0.0031 (0.020)	0.17
B	1 (0.30)	0.797 (5.14)	0.0000 (0.000)	0.00
C	1.5 (0.46)	0.413 (2.67)	0.0000 (0.000)	0.00
D	2 (0.61)	0.339 (2.18)	0.0000 (0.000)	0.00
E	2.5 (0.76)	0.336 (2.17)	0.0010 (0.006)	0.30
F	3 (0.91)	0.402 (2.60)	0.0000 (0.000)	0.00
G	3.5 (1.07)	0.539 (3.48)	0.0012 (0.008)	0.22
H	4.1 (1.26)	1.200 (7.74)	0.0095 (0.061)	0.79
I	4.5 (1.37)	0.343 (2.21)	0.0052 (0.034)	1.52
J	5 (1.52)	0.350 (2.26)	0.0043 (0.028)	1.23
K	6 (1.83)	0.105 (0.68)	0.0022 (0.014)	2.10
L	8 (2.44)	0.113 (0.73)	0.0009 (0.006)	0.80
M	9 (2.74)	0.130 (0.84)	0.0020 (0.013)	1.54
N	10 (3.05)	0.187 (1.20)	0.0022 (0.014)	1.18
O	11 (3.35)	0.409 (2.64)	0.0060 (0.039)	1.47
P	12 (3.66)	0.212 (1.37)	0.0092 (0.059)	4.33
Q	13 (3.96)	0.091 (0.59)	0.0002 (0.001)	0.22
R	14 (4.27)	0.030 (0.19)	0.0000 (0.000)	0.00
Sum		**7.805 (50.36)**	**0.0470 (0.303)**	**0.60**

From the analysis, remaining voids in the repair grout are estimated in each cut section, but the void ratio in a section can be magnified when the remaining voids exist in a small repaired area. Thus, the filling performance for Specimen VG-C1-1 is evaluated using the summation of the estimated sections of Specimen VG-C1-1. The remaining void ratio after repair obtained from the analysis comes out to be 0.60% for Specimen VG-C1-1. The initial void area, the repaired area, as shown in Table B-2 ranges over 0.1 inch^2 (0.65×10^{-4} m^2) or more in Section P; however, these voids include small voids from Section Q.

The time analysis for repair preparation is not considered in Specimen VG-C1-1 and VG-C2-1 because both specimens required a significant amount of trial and error to find an appropriate way to seal the test specimens.

B.2 SPECIMEN VG-C2-1

Since Specimen VG-C2-1 is the first setup of its kind, a sufficient amount of grouts for initial grouting are mixed. The initial grouts are mixed separately in 2 batches using the air-powered grout mixer, and two high shear mixers are then used in the grout storage tank (Figure B-4) to ensure consistency between grouts mixed in two batches. The flow cone test (Method 1) is performed on both batches and the final batch according to the ASTM 939-02 (ASTM 2002) standard. The flow cone test for repair grouts is performed by Tex-437-A Method 2 (TxDOT 1999).

Figure B-4. Grout Storage Tank and High Shear Mixer.

The preparation for repair grouting in Specimen VG-C2-1 took a considerable of time (4 months) to construct since an air-tight PT system is required. While performing sealing procedures a trial and error method is used in order to find a better sealing method.

Repair grout is infiltrated from the top grout port and the main voids are filled successfully. The repair grout is infiltrated to 13.4 ft (4.08 m) from the reference point (Figure B-5).

Figure B-5. Repair Grouted Ducts of Specimen VG-C2-1.

For the Specimen VG-C2-1, however, the colorant is not added in the initial grouting. Thus, the performance of repaired grout is not considered because the difference between initial grouts and repair grouts is difficult to identify.

B.3 SPECIMEN VG-C2-2

Figure B-6 depicts the initial void profiles of the sounding inspection and of the visual inspection before grouting for Specimen VG-C2-2.

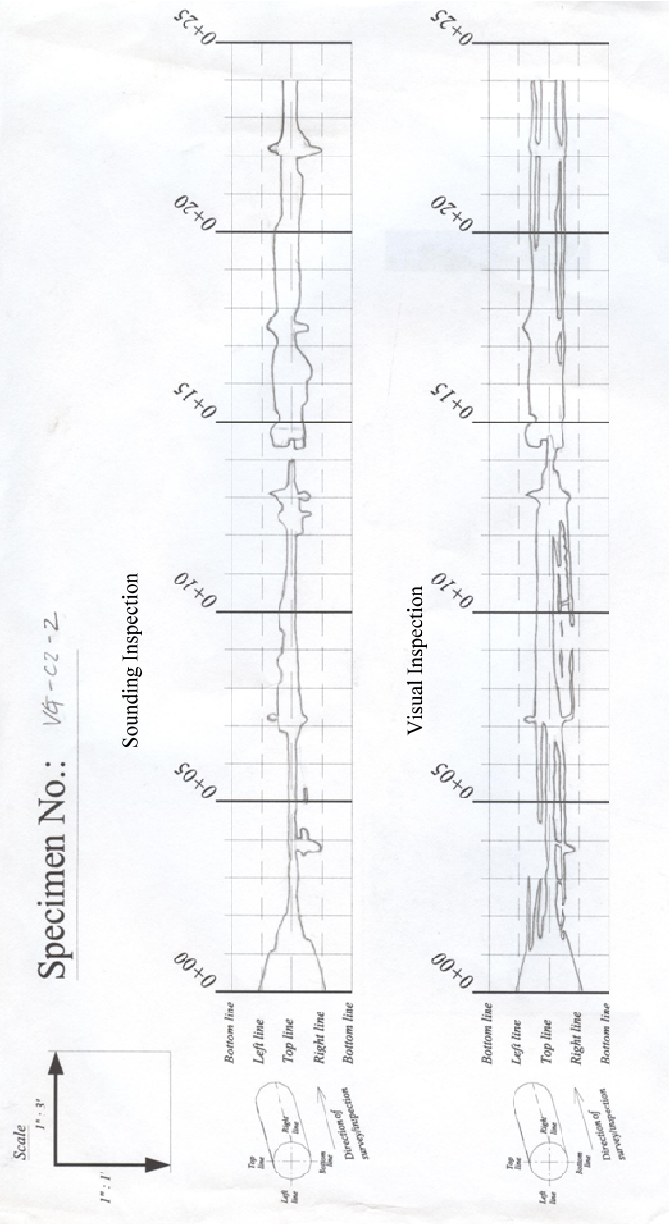

Figure B-6. Void Map of Specimen VG-C2-2.

The areas of both void profiles are estimated using AutoCAD® and provided in Table B-3.

Table B-3. Estimation of Void Profile in Specimen VG-C2-2.

Section, ft (m)	Sounding Inspection (SI), inch^2 (10^{-4} m^2)	Visual Inspection (VI), inch^2 (10^{-4} m^2)	SI - VI, inch^2 (10^{-4} m^2)
0~1 (0~0.3)	71.62 (462.1)	70.70 (456.2)	0.92 (5.9)
1~2 (0.3~0.6)	36.38 (234.7)	41.36 (266.8)	-4.98 (-32.1)
2~3 (0.6~0.9)	11.42 (73.7)	23.31 (150.4)	-11.89 (-76.7)
3~4 (0.9~1.2)	18.78 (121.2)	19.57 (126.3)	-0.79 (-5.1)
4~5 (1.2~1.5)	11.57 (74.6)	19.32 (124.7)	-7.76 (-50.0)
5~6 (1.5~1.8)	10.18 (65.7)	23.65 (152.6)	-13.46 (-86.9)
6~7 (1.8~2.1)	12.82 (82.7)	25.15 (162.3)	-12.34 (-79.6)
7~8 (2.1~2.4)	32.29 (208.3)	35.75 (230.7)	-3.46 (-22.4)
8~9 (2.4~2.7)	22.93 (147.9)	27.95 (180.3)	-5.02 (-32.4)
9~10 (2.7~3.0)	18.37 (118.5)	23.42 (151.1)	-5.05 (-32.6)
10~11 (3.0~3.4)	15.50 (100.0)	27.47 (177.2)	-11.97 (-77.2)
11~12 (3.4~3.7)	10.91 (70.4)	29.18 (188.2)	-18.27 (-117.9)
12~13 (3.7~4.0)	26.19 (168.9)	36.43 (235.0)	-10.24 (-66.1)
13~14 (4.0~4.3)	14.99 (96.7)	23.19 (149.6)	-8.19 (-52.9)
14~15 (4.3~4.6)	25.95 (167.4)	31.44 (202.8)	-5.49 (-35.4)
15~16 (4.6~4.9)	36.98 (238.6)	41.41 (267.1)	-4.43 (-28.6)
16~17 (4.9~5.2)	42.95 (277.1)	41.01 (264.6)	1.94 (12.5)
17~18 (5.2~5.5)	31.90 (205.8)	42.94 (277.1)	-11.04 (-71.2)
18~19 (5.5~5.8)	30.81 (198.8)	34.25 (221.0)	-3.45 (-22.2)
19~20 (5.8~6.1)	31.27 (201.8)	33.64 (217.1)	-2.37 (-15.3)
20~21 (6.1~6.4)	24.78 (159.9)	34.04 (219.6)	-9.26 (-59.7)
21~22 (6.4~6.7)	23.84 (153.8)	37.16 (239.8)	-13.32 (-86.0)
22~23 (6.7~7.0)	34.29 (221.2)	36.01 (232.4)	-1.72 (-11.1)
23~24 (7.0~7.3)	16.55 (106.8)	25.56 (164.9)	-9.01 (-58.1)

The repair grout is filled from the top grout port and infiltrated to 14.4 ft (4.39 m) from the reference point (Figure B-7).

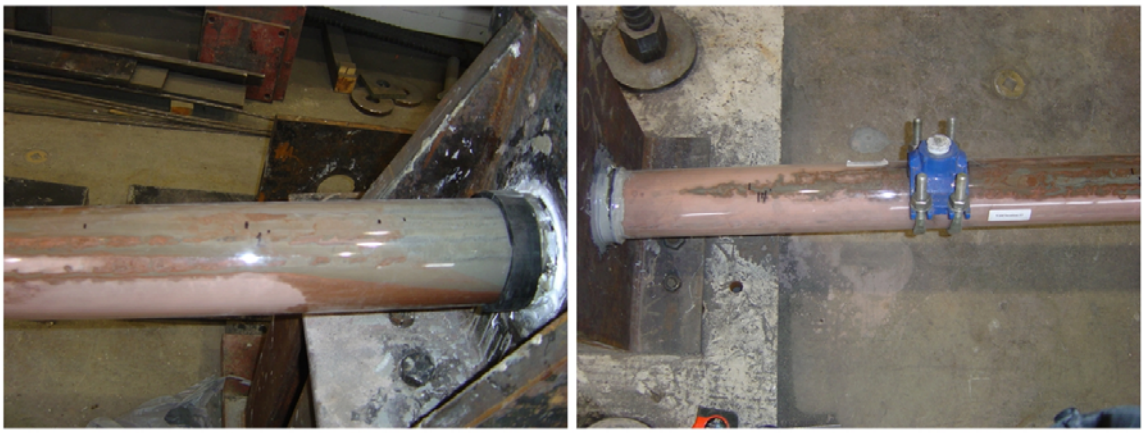

Figure B-7. Repair Grouted Ducts of Specimen VG-C2-2.

Figure B-8 shows the cross-sectional views of the cut sections obtained from Specimen VG-C2-2. From the cut sections, it is noted that the repair grouts successfully replaces the main voids and repairs local large voids #3, #4, and #5. The small voids still exist inside the initially grouted ducts, especially in-between strands.

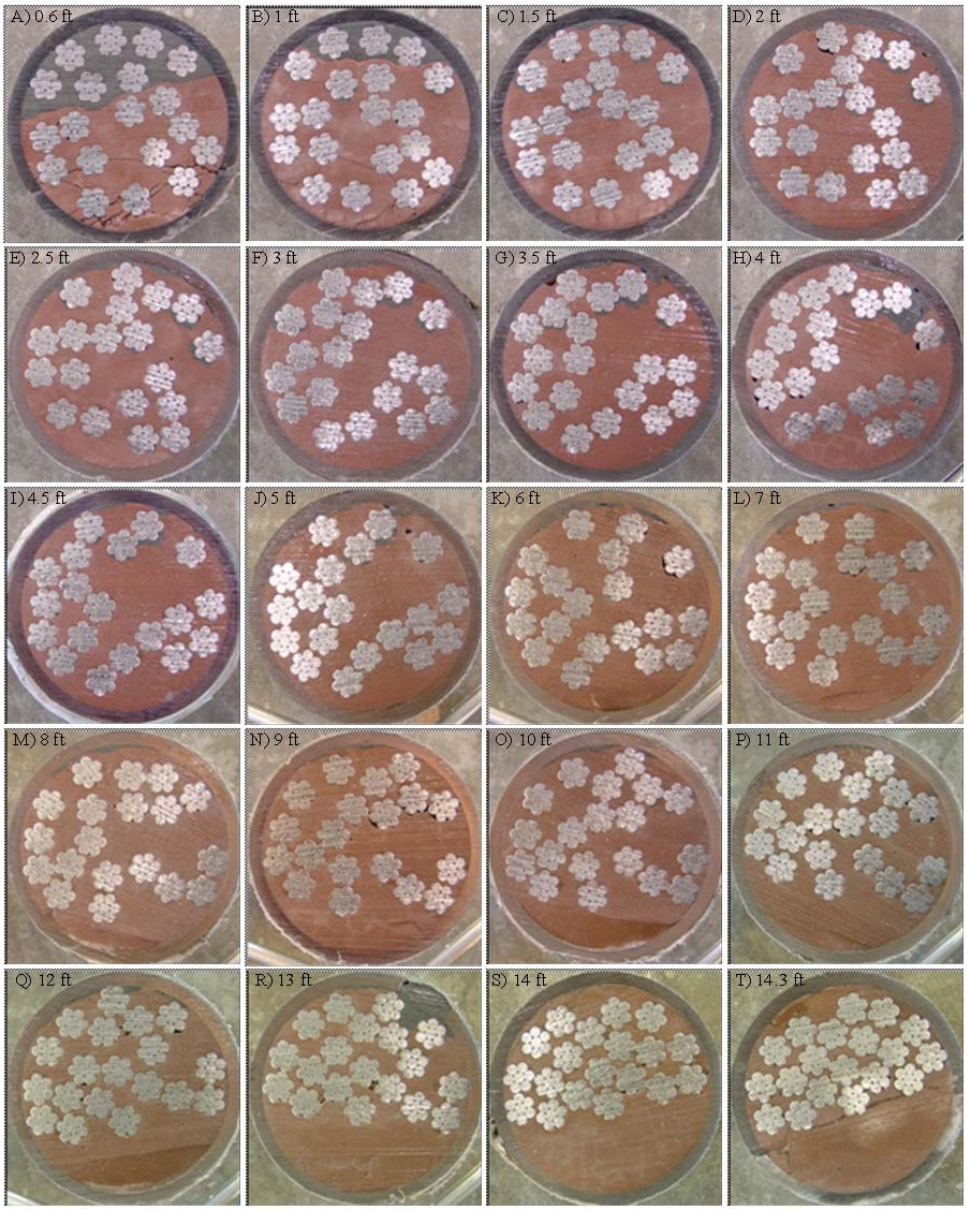

Figure B-8. Cut Sections of VG-C2-2 for the Filling Analysis of Repair Grout.

To compare the performance of repair grouts, the ratio of the remaining void area after repair to the repaired area is estimated. The repaired area and area of voids after repair are calculated using AutoCAD® (Table B-4).

Table B-4. Void Area of Specimen VG-C2-2.

Cut Sections, ft (m)		Repaired Area, A_R, inch^2(10^{-4} m^2)	Void Area, A_V, inch^2(10^{-4} m^2)	Void Ratio, η (%)
A	0.6 (0.18)	2.365 (15.26)	0.0134 (0.086)	0.57
B	1 (0.30)	0.952 (6.14)	0.0044 (0.028)	0.46
C	1.5 (0.46)	0.337 (2.17)	0.0000 (0.000)	0.00
D	2 (0.61)	0.325 (2.09)	0.0000 (0.000)	0.00
E	2.5 (0.76)	0.380 (2.45)	0.0089 (0.057)	2.34
F	3 (0.91)	0.278 (1.79)	0.0013 (0.008)	0.47
G	3.5 (1.07)	0.325 (2.10)	0.0055 (0.035)	1.69
H	4 (1.22)	0.542 (3.49)	0.0111 (0.072)	2.05
I	4.5 (1.37)	0.229 (1.48)	0.0006 (0.004)	0.26
J	5 (1.52)	0.279 (1.80)	0.0062 (0.040)	2.22
K	6 (1.83)	0.179 (1.16)	0.0126 (0.081)	7.03
L	7 (2.13)	0.223 (1.44)	0.0076 (0.049)	3.40
M	8 (2.44)	0.176 (1.14)	0.0000 (0.000)	0.00
N	9 (2.74)	0.117 (0.75)	0.0000 (0.000)	0.00
O	10 (3.05)	0.196 (1.26)	0.0000 (0.000)	0.00
P	11 (3.35)	0.119 (0.77)	0.0019 (0.012)	1.59
Q	12 (3.66)	0.198 (1.28)	0.0036 (0.023)	1.82
R	13 (3.96)	0.497 (3.20)	0.0000 (0.000)	0.00
S	14 (4.27)	0.033 (0.22)	0.0000 (0.000)	0.00
T	14.3 (4.37)	0.019 (0.12)	0.0000 (0.000)	0.00
Sum		**7.768 (50.12)**	**0.0771 (0.497)**	**0.99**

From the analysis of the cut sections, Specimen VG-C2-2 has the remaining void ratio, after repair, of 0.99% on average. The initial void area ranges over 0.1 inch^2 (0.65×10^{-4} m^2) or more from the reference point to Section R, however, these voids include a small contribution from Section S.

Table B-5 shows the time schedule for sealing ducts for Specimen VG-C2-2. Total sealing time for Specimen VG-C2-2 is 3 days and 3.63 hours before applying the repair grout.

Table B-5. Sealing Time Schedule of Specimen VG-C2-2.

Sealing Procedure	Working Day	Working Time (min.)
Installing pipe saddle tap with grease	Day 1	32
Setting rubber end caps and sealing hose	Day 1	5
Assembling T-connection, sealing with silicone, and checking air tight condition	Day 1	35
Sealing end rubber caps with silicone	Day 1	32
Sealing with epoxy	Day 1	27
Wait	1 day	
Checking air-tight condition and sealing	Day 2	13
Checking air-tight condition	Day 2	3
Sealing with epoxy	Day 2	45
Wait	1 day	
Checking air-tight condition	Day 3	5
Reassembling T-connection and checking air-tight condition	Day 3	16
Sealing with silicone	Day 3	5
Sum	**3 days**	**218 (3.6 hours)**

B.4 SPECIMEN VG-C3-1

Figure B-9 depicts the initial void profiles of the sounding inspection and of the visual inspection before grouting for Specimen VG-C3-1.

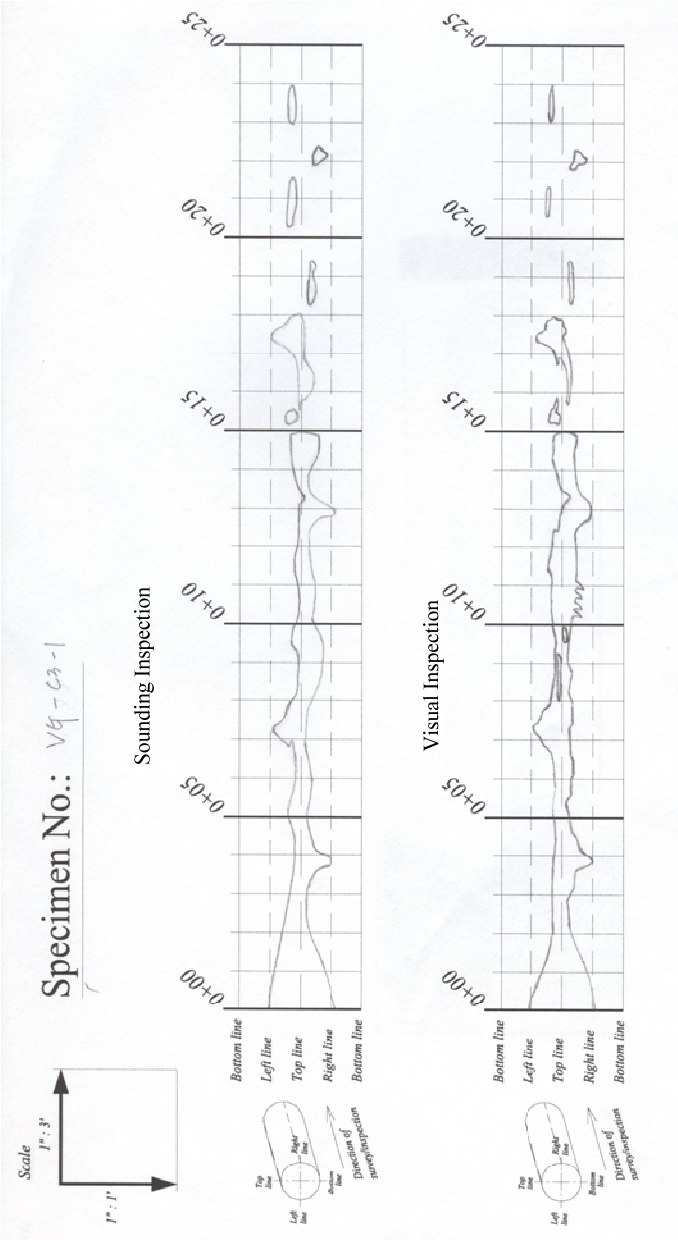

Figure B-9. Void Map of Specimen VG-C3-1.

The areas of both void profiles are estimated using AutoCAD® and provided in Table B-6.

Table B-6. Estimation of Void Profile in Specimen VG-C3-1.

Section, ft (m)	Sounding Inspection (SI), inch^2 (10^{-4} m^2)	Visual Inspection (VI), inch^2 (10^{-4} m^2)	SI - VI, inch^2 (10^{-4} m^2)
0~1 (0~0.3)	73.90 (476.8)	70.20 (425.9)	3.70 (23.9)
1~2 (0.3~0.6)	48.58 (313.4)	38.47 (248.2)	10.11 (65.2)
2~3 (0.6~0.9)	26.03 (167.9)	20.29 (130.9)	5.74 (37.0)
3~4 (0.9~1.2)	30.12 (194.3)	32.75 (211.3)	-2.63 (-17.0)
4~5 (1.2~1.5)	22.69 (146.4)	25.44 (164.1)	-2.75 (-17.8)
5~6 (1.5~1.8)	22.84 (147.3)	18.72 (120.7)	4.12 (26.6)
6~7 (1.8~2.1)	18.11 (116.8)	25.83 (166.7)	-7.72 (-49.8)
7~8 (2.1~2.4)	31.58 (203.7)	37.83 (244.1)	-6.25 (-40.3)
8~9 (2.4~2.7)	26.56 (171.4)	18.13 (117.0)	8.43 (54.4)
9~10 (2.7~3.0)	33.12 (213.7)	14.58 (94.1)	18.54 (119.6)
10~11 (3.0~3.4)	19.71 (127.2)	31.33 (202.1)	-11.62 (-75.0)
11~12 (3.4~3.7)	19.83 (128.0)	32.57 (210.1)	-12.74 (-82.2)
12~13 (3.7~4.0)	22.54 (145.4)	30.42 (196.3)	-7.88 (-50.8)
13~14 (4.0~4.3)	18.66 (120.4)	23.79 (153.5)	-5.13 (-33.1)
14~15 (4.3~4.6)	29.56 (190.7)	25.70 (165.8)	3.86 (24.9)
15~16 (4.6~4.9)	7.34 (47.4)	6.02 (38.8)	1.32 (8.5)
16~17 (4.9~5.2)	16.35 (105.5)	8.03 (51.8)	8.32 (53.7)
17~18 (5.2~5.5)	28.07 (181.1)	23.77 (153.3)	4.31 (27.8)
18~19 (5.5~5.8)	6.96 (44.9)	3.82 (24.6)	3.15 (20.3)
19~20 (5.8~6.1)	2.49 (16.1)	2.22 (14.3)	0.27 (1.8)
20~21 (6.1~6.4)	6.79 (43.8)	2.11 (13.6)	4.69 (30.2)
21~22 (6.4~6.7)	5.83 (37.6)	4.09 (26.4)	1.74 (11.2)
22~23 (6.7~7.0)	5.31 (34.2)	3.53 (22.8)	1.77 (11.4)
23~24 (7.0~7.3)	8.16 (52.7)	4.75 (30.6)	3.41 (22.0)

The repair grout is filled from the top grout port and infiltrated to 4.8 ft (1.46 m) from the reference point (Figure B-10).

Figure B-10. Repair Grouted Ducts of Specimen VG-C3-1.

Figure B-11 shows the cross-sectional views of the cut sections obtained from Specimen VG-C3-1. From the cut sections, it is noted that the repair grout successfully replaces the main voids up to 3 ft (0.91 m) from the reference point, but after that voids are only partially repaired. Also, this repair grout does not fill the #5 void, located in Section H. The small voids still exist inside the initially grouted ducts, especially in-between strands.

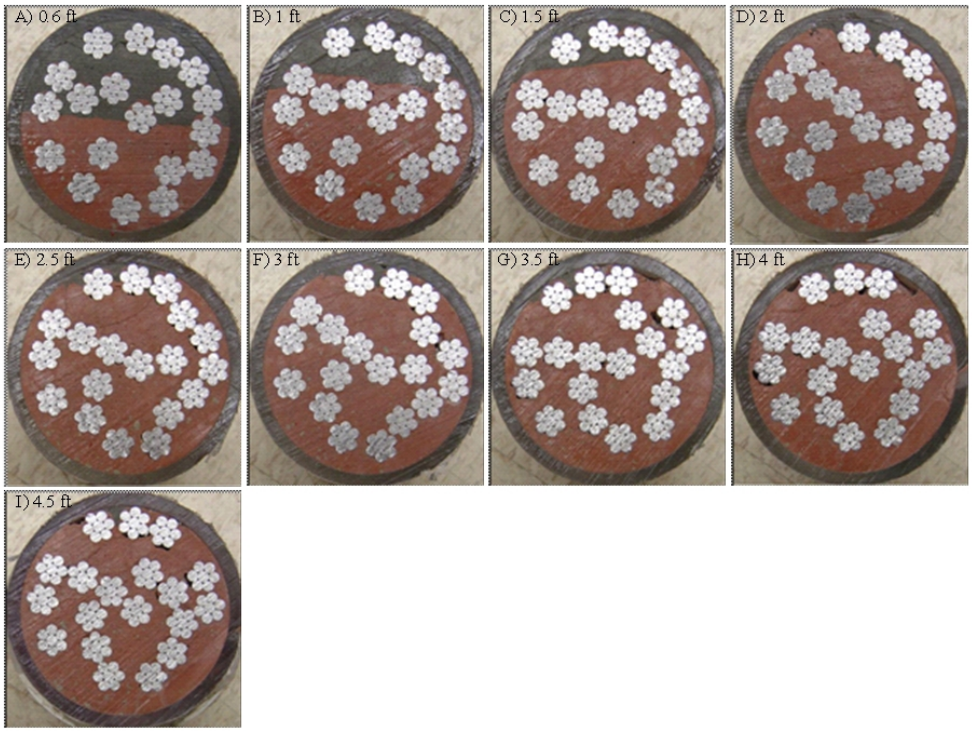

Figure B-11. Cut Sections of Specimen VG-C3-1 for the Filling Analysis of Repair Grout.

To compare the performance of repair grouts, the ratio of the remaining void area after repair to the repaired area is estimated. The repaired area and area of voids after repair are calculated using AutoCAD® (Table B-7).

Table B-7. Void Area of Specimen VG-C3-1.

Cut Sections, ft (m)		Repaired Area, A_R, inch^2(10^{-4} m^2)	Void Area, A_V, inch^2(10^{-4} m^2)	Void Ratio, η (%)
A	0.6 (0.18)	3.150 (20.32)	0.0117 (0.075)	0.37
B	1 (0.30)	2.019 (13.02)	0.0078 (0.050)	0.39
C	1.5 (0.46)	0.954 (6.16)	0.0004 (0.003)	0.04
D	2 (0.61)	0.336 (2.17)	0.0038 (0.025)	1.13
E	2.5 (0.76)	0.261 (1.69)	0.0020 (0.013)	0.77
F	3 (0.91)	0.216 (1.39)	0.0037 (0.024)	1.71
G	3.5 (1.07)	0.164 (1.06)	0.0120 (0.077)	7.32
H	4 (1.22)	0.104 (0.67)	0.0000 (0.000)	0.00
I	4.5 (1.37)	0.094 (0.61)	0.0002 (0.000)	0.21
Sum		**7.299 (47.09)**	**0.0416 (0.268)**	**0.57**

From the analysis of cut sections, Specimen VG-C3-1 has a remaining void ratio, after repair grouting, of 0.57% on average. The initial void area ranges over 0.1 inch^2 (0.65×10^{-4} m^2) or more from the reference point to Section H, however, the voids include small amount from Section I.

Table B-8 shows the time schedule of sealing ducts and preparation of repair grouting for Specimen VG-C3-1. Total sealing time of Specimen VG-C3-1 is 7 days and 10.92 hours before applying repair grout.

Table B-8. Sealing Time Schedule of Specimen VG-C3-1.

Sealing Procedure	Working Day	Working Time (min.)
Setting rubber end caps and sealing with epoxy	Day 1	55
Wait	1 day	
Installing pipe saddle tap with grease	Day 2	50
Assembling T-connection and checking air-tight condition	Day 2	110
Sealing with RTV silicone	Day 2	20
Checking air-tight condition	Day 3	50
Reassembling T-connection and checking air-tight condition	Day 4	150
Checking air-tight condition and sealing with epoxy	Day 5	60
Wait	1 day	
Checking air-tight condition and sealing	Day 6	30
Checking air-tight condition and sealing	Day 7	130
Sum	**7 days**	**655 (10.92 hours)**

B.5 SPECIMEN PG-C1-1

Figure B-12 depicts the initial void profiles of the sounding inspection and of the visual inspection before grouting for Specimen PG-C1-1.

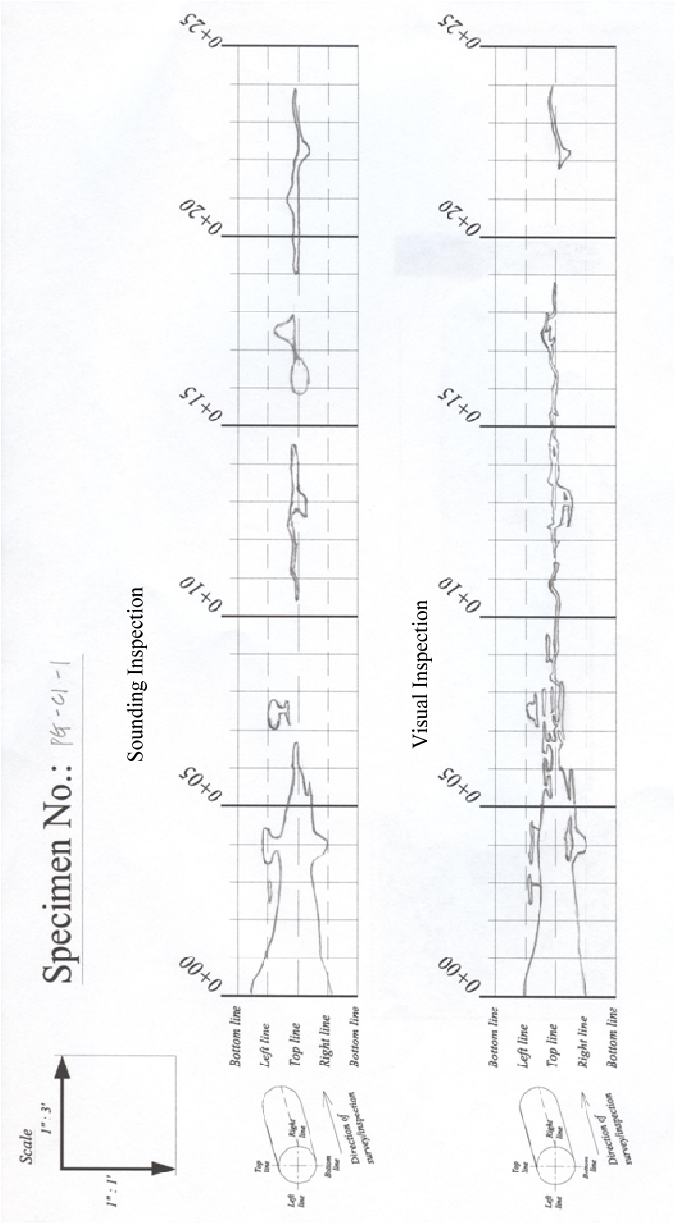

Figure B-12. Void Map of Specimen PG-C1-1.

The areas of both void profiles are estimated using AutoCAD® and provided in Table B-9.

Table B-9. Estimation of Void Profile in Specimen PG-C1-1.

Section, ft (m)	Sounding Inspection (SI), inch^2 (10^{-4} m^2)	Visual Inspection (VI), inch^2 (10^{-4} m^2)	SI - VI, inch^2 (10^{-4} m^2)
0~1 (0~0.3)	89.02 (574.3)	70.86 (457.1)	18.17 (117.2)
1~2 (0.3~0.6)	61.25 (395.2)	54.40 (351.0)	6.86 (44.2)
2~3 (0.6~0.9)	49.61 (320.0)	47.71 (307.8)	1.90 (12.2)
3~4 (0.9~1.2)	55.39 (357.4)	47.52 (306.6)	7.87 (50.7)
4~5 (1.2~1.5)	47.82 (308.5)	47.43 (306.0)	0.39 (2.5)
5~6 (1.5~1.8)	19.71 (127.1)	31.10 (200.6)	-11.39 (-73.5)
6~7 (1.8~2.1)	3.89 (25.1)	15.67 (101.1)	-11.78 (-76.0)
7~8 (2.1~2.4)	11.97 (77.2)	18.50 (119.4)	-6.53 (-42.2)
8~9 (2.4~2.7)	0.00 (0.0)	6.53 (42.1)	-6.53 (-42.1)
9~10 (2.7~3.0)	0.00 (0.0)	6.85 (44.2)	-6.85 (-44.2)
10~11 (3.0~3.4)	2.67 (17.2)	4.23 (27.3)	-1.56 (-10.1)
11~12 (3.4~3.7)	5.21 (33.6)	3.78 (24.4)	1.42 (9.2)
12~13 (3.7~4.0)	9.48 (61.2)	11.70 (75.5)	-2.21 (-14.3)
13~14 (4.0~4.3)	10.10 (65.1)	13.84 (89.3)	-3.74 (-24.2)
14~15 (4.3~4.6)	3.57 (23.0)	6.77 (43.7)	-3.21 (-20.7)
15~16 (4.6~4.9)	2.26 (14.6)	4.13 (26.6)	-1.87 (-12.1)
16~17 (4.9~5.2)	15.43 (99.5)	4.00 (25.8)	11.42 (73.7)
17~18 (5.2~5.5)	12.08 (77.9)	7.53 (48.6)	4.55 (29.3)
18~19 (5.5~5.8)	0.00 (0.0)	2.50 (16.1)	-2.50 (-16.1)
19~20 (5.8~6.1)	5.94 (38.3)	0.00 (0.0)	5.94 (38.3)
20~21 (6.1~6.4)	8.95 (57.8)	0.00 (0.0)	8.95 (57.8)
21~22 (6.4~6.7)	9.05 (58.4)	0.88 (5.7)	8.17 (52.7)
22~23 (6.7~7.0)	8.58 (55.4)	6.54 (42.2)	2.04 (13.1)
23~24 (7.0~7.3)	3.50 (22.6)	3.08 (19.9)	0.42 (2.7)

The repair grout is filled from the top grout port and infiltrated to 11.5 ft (3.51 m) from the reference point (Figure B-13).

Figure B-13. Repair Grouted Ducts of Specimen PG-C1-1.

Figure B-14 shows the cross-sectional views of the cut sections obtained from Specimen PG-C1-1. From the cut sections, it is noted that the repair grout successfully replaces the main voids and repairs local large voids #3, #4, and #5. The small voids still exist inside the initially grouted ducts, especially in-between strands. However, those voids cannot be repaired because the voids are isolated from the "bug holes" which is a route for repair grouts.

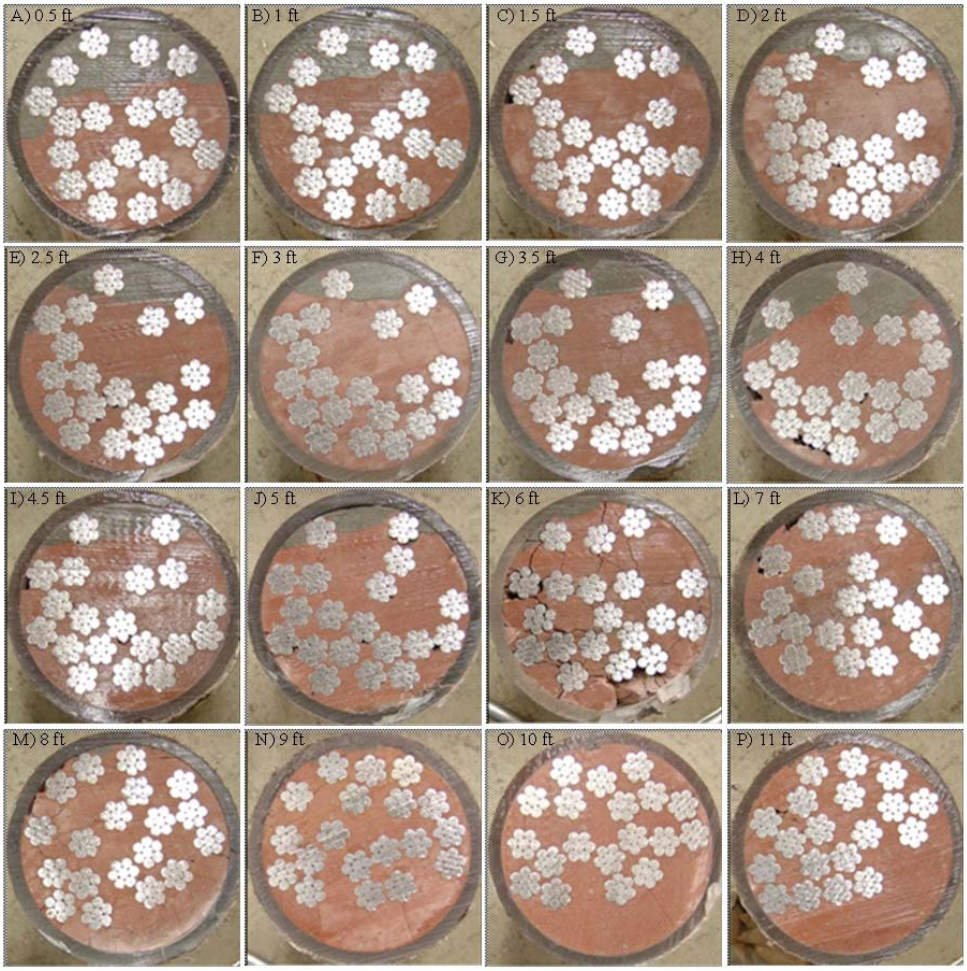

Figure B-14. Cut Sections of Specimen PG-C1-1 for the Filling Analysis of Repair Grout.

To compare the performance of repair grouts, the ratio of the remaining void area after repair to the repaired area is estimated. The repaired area and area of voids after repair are calculated using AutoCAD® (Table B-10).

Table B-10. Void Area of Specimen PG-C1-1.

Cut Sections, ft (m)		Repaired Area, A_R, inch^2(10^{-4} m^2)	Void Area, A_V, inch^2(10^{-4} m^2)	Void Ratio, η (%)
A	0.5 (0.15)	2.874 (18.54)	0.0118 (0.076)	0.41
B	1 (0.30)	1.825 (11.78)	0.0026 (0.017)	0.14
C	1.5 (0.46)	1.483 (9.57)	0.0078 (0.050)	0.53
D	2 (0.61)	1.272 (8.21)	0.0009 (0.006)	0.07
E	2.5 (0.76)	1.269 (8.19)	0.0008 (0.005)	0.06
F	3 (0.91)	1.050 (6.78)	0.0000 (0.000)	0.00
G	3.5 (1.07)	0.948 (6.11)	0.0000 (0.000)	0.00
H	4 (1.22)	2.158 (13.92)	0.0012 (0.008)	0.06
I	4.5 (1.37)	0.944 (6.09)	0.0000 (0.000)	0.00
J	5 (1.52)	0.753 (4.86)	0.0023 (0.015)	0.31
K	6 (1.83)	0.267 (1.73)	0.0000 (0.000)	0.00
L	7 (2.13)	0.099 (0.64)	0.0058 (0.037)	5.89
M	8 (2.44)	0.083 (0.53)	0.0000 (0.000)	0.00
N	9 (2.74)	0.113 (0.73)	0.0000 (0.000)	0.00
O	10 (3.05)	0.033 (0.21)	0.0008 (0.005)	2.43
P	11 (3.35)	0.064 (0.41)	0.0002 (0.001)	0.31
Sum		**15.234 (98.28)**	**0.0342 (0.221)**	**0.22**

The remaining void ratio after repair, obtained from the analysis, comes out to be 0.22% for Specimen PG-C1-1. The initial void area ranges over 0.1 inch^2 (0.65×10^{-4} m^2) or more from the reference point to Section K, however, the voids include a small contribution from Section L excluding Section N.

Table B-11 shows the time schedule for sealing ducts and preparation of repair grouting for Specimen PG-C1-1. Total sealing time for Specimen PG-C1-1 is 2 days and 0.88 hours before applying repair grout.

Table B-11. Sealing Time Schedule of Specimen PG-C1-1.

Sealing Procedure	Working Day	Working Time (min.)
Setting rubber end caps (one side)	Day 1	1
Installing pipe saddle tap	Day 1	20
Mixing epoxy and sealing (one side)	Day 1	20
Wait	1 day	
Connect pressure grout pump and reseal	Day 2	12
Sum	**2 days**	**53 (0.88 hours)**

B.6 SPECIMEN PG-C1-2

Figure B-15 shows depicts the initial void profiles of the sounding inspection and of the visual inspection before grouting for Specimen PG-C1-2.

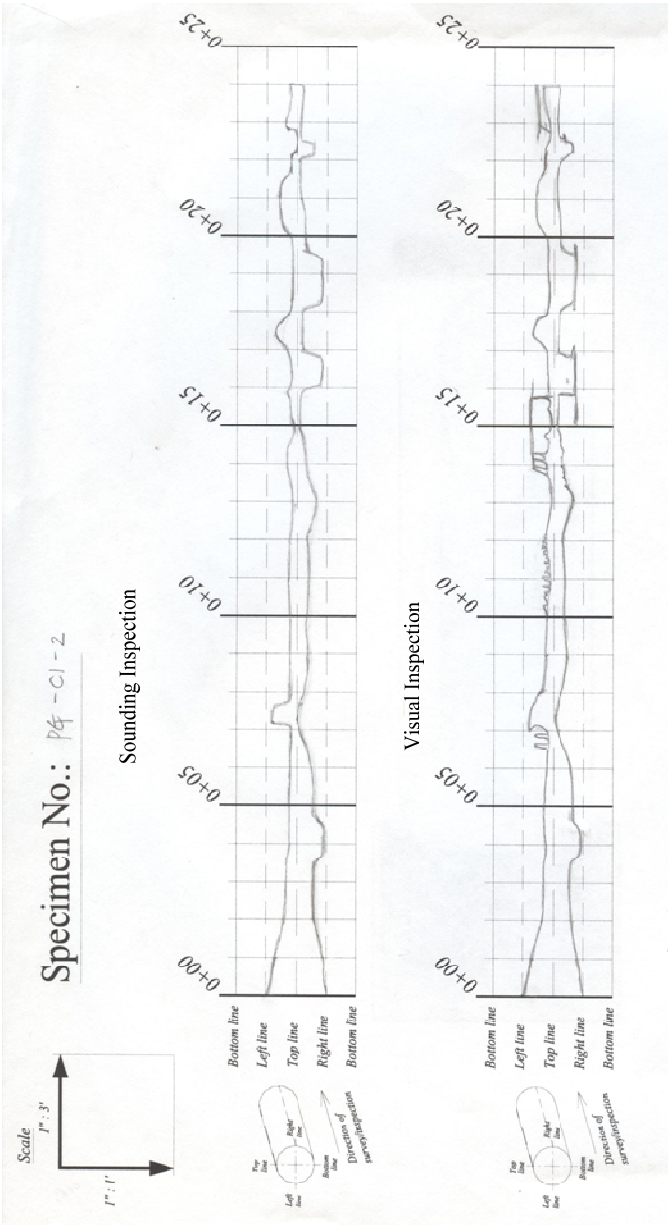

Figure B-15. Void Map of Specimen PG-C1-2.

The areas of both void profiles are estimated using AutoCAD® and provided in Table B-12.

Table B-12. Estimation of Void Profile in Specimen PG-C1-2.

Section, ft (m)	Sounding Inspection (SI), inch^2 (10^{-4} m^2)	Visual Inspection (VI), inch^2 (10^{-4} m^2)	SI - VI, inch^2 (10^{-4} m^2)
0~1 (0~0.3)	67.05 (432.6)	66.04 (426.1)	1.01 (6.5)
1~2 (0.3~0.6)	49.73 (320.9)	47.15 (304.2)	2.58 (16.7)
2~3 (0.6~0.9)	36.20 (233.6)	34.42 (222.0)	1.78 (11.5)
3~4 (0.9~1.2)	38.21 (246.5)	37.12 (239.5)	1.10 (7.1)
4~5 (1.2~1.5)	38.47 (248.2)	40.93 (264.1)	-2.47 (-15.9)
5~6 (1.5~1.8)	30.24 (195.1)	34.53 (222.8)	-4.30 (-27.7)
6~7 (1.8~2.1)	20.37 (131.4)	25.12 (162.1)	-4.76 (-30.7)
7~8 (2.1~2.4)	23.65 (152.6)	29.88 (192.8)	-6.23 (-40.2)
8~9 (2.4~2.7)	22.05 (142.2)	26.28 (169.6)	-4.24 (-27.3)
9~10 (2.7~3.0)	22.03 (142.1)	25.19 (162.5)	-3.17 (-20.4)
10~11 (3.0~3.4)	24.78 (159.9)	23.37 (150.7)	1.42 (9.2)
11~12 (3.4~3.7)	25.63 (165.4)	24.21 (156.2)	1.42 (9.2)
12~13 (3.7~4.0)	26.34 (169.9)	24.18 (156.0)	2.15 (13.9)
13~14 (4.0~4.3)	26.95 (173.9)	25.95 (167.4)	1.00 (6.5)
14~15 (4.3~4.6)	18.99 (122.5)	23.58 (152.1)	-4.59 (-29.6)
15~16 (4.6~4.9)	14.09 (90.9)	21.32 (137.5)	-7.22 (-46.6)
16~17 (4.9~5.2)	36.99 (238.6)	33.82 (218.2)	3.17 (20.5)
17~18 (5.2~5.5)	27.88 (179.9)	26.78 (172.8)	1.10 (7.1)
18~19 (5.5~5.8)	34.88 (225.0)	30.34 (195.8)	4.53 (29.2)
19~20 (5.8~6.1)	28.91 (186.5)	30.49 (196.7)	-1.58 (-10.2)
20~21 (6.1~6.4)	29.02 (187.2)	27.29 (176.1)	1.73 (11.1)
21~22 (6.4~6.7)	20.64 (133.2)	22.24 (143.5)	-1.60 (-10.3)
22~23 (6.7~7.0)	16.20 (104.5)	25.23 (162.8)	-9.02 (-58.2)
23~24 (7.0~7.3)	17.46 (112.6)	21.33 (137.6)	-3.88 (-25.0)

The repair grout is filled from the top grout port and infiltrated to 9.3 ft (2.86 m) from the reference point (Figure B-16).

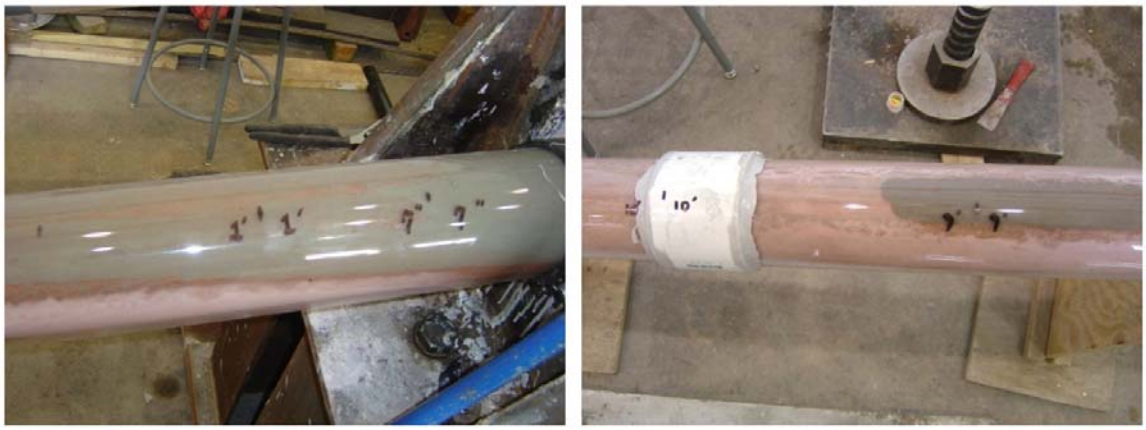

Figure B-16. Repair Grouted Ducts of Specimen PG-C1-2.

Figure B-17 shows the cross-sectional views of the cut sections obtained from Specimen PG-C1-2. From the cut sections, it is noted that the repair grouts successfully replaces the main voids up to 6 ft (1.83 m) from the reference point, but after that voids are only partially repaired. The local large void #5 is filled completely by repair grout; however, small voids still exist inside the initially grouted ducts, especially in-between strands.

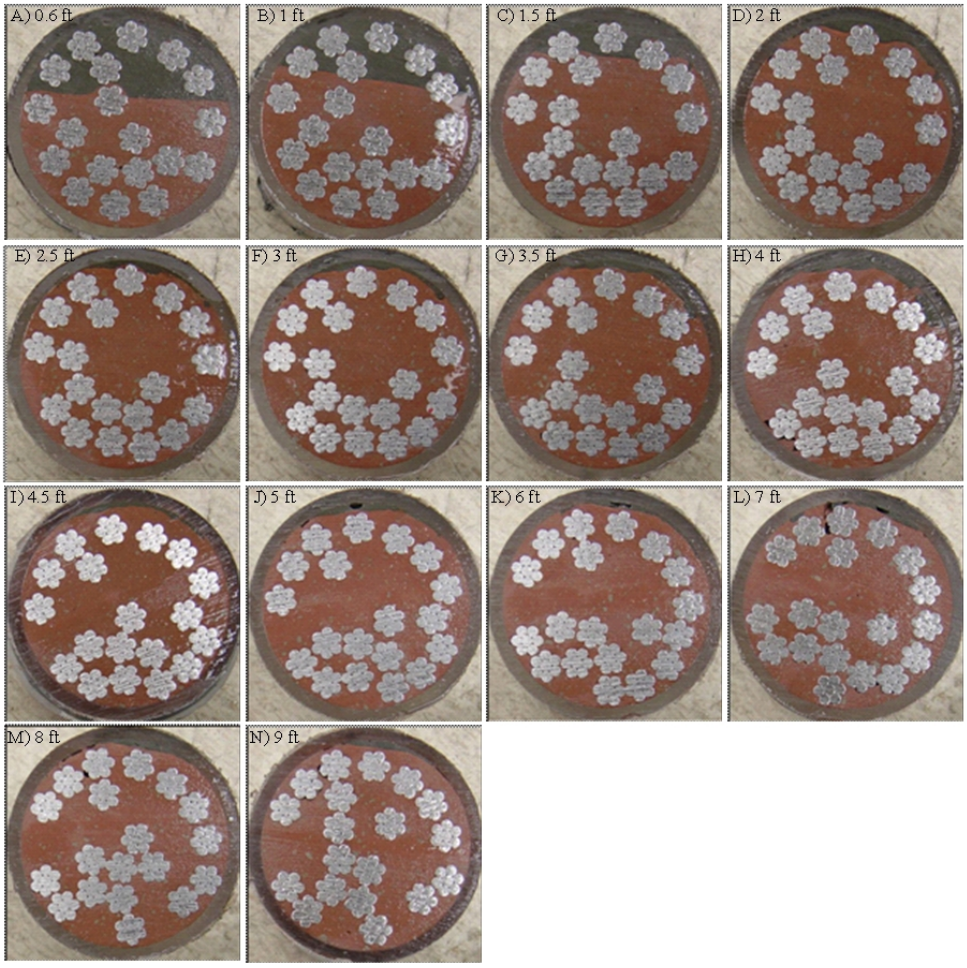

Figure B-17. Cut Sections of Specimen PG-C1-2 for the Filling Analysis of Repair Grout.

To compare the performance of repair grouts, the ratio of the remaining void area after repair to the repaired area is estimated. The repaired area and area of voids after repair are calculated using AutoCAD® (Table B-13).

Table B-13. Void Area of Specimen PG-C1-2.

Cut Sections, ft (m)		Repaired Area, A_R, inch^2(10^{-4} m^2)	Void Area, A_V, inch^2(10^{-4} m^2)	Void Ratio, η (%)
A	0.6 (0.18)	2.592 (16.72)	0.0063 (0.041)	0.24
B	1 (0.30)	1.614 (10.41)	0.0000 (0.000)	0.00
C	1.5 (0.46)	0.872 (5.62)	0.0039 (0.025)	0.45
D	2 (0.61)	0.384 (2.48)	0.0000 (0.000)	0.00
E	2.5 (0.76)	0.267 (1.72)	0.0008 (0.005)	0.30
F	3 (0.91)	0.301 (1.94)	0.0000 (0.000)	0.00
G	3.5 (1.07)	0.369 (2.38)	0.0000 (0.000)	0.00
H	4 (1.22)	0.467 (3.02)	0.0041 (0.026)	0.88
I	4.5 (1.37)	0.227 (1.46)	0.0021 (0.014)	0.93
J	5 (1.52)	0.264 (1.70)	0.0278 (0.179)	10.55
K	6 (1.83)	0.237 (1.53)	0.0300 (0.194)	12.68
L	7 (2.13)	0.225 (1.45)	0.0531 (0.343)	23.58
M	8 (2.44)	0.213 (1.37)	0.0135 (0.087)	6.35
N	9 (2.74)	0.181 (1.17)	0.0025 (0.016)	1.38
Sum		**8.211 (52.97)**	**0.1441 (0.930)**	**1.76**

From the analysis of the cut sections, Specimen PG-C1-2 has a remaining void ratio, after repair, of 1.76% on average. The initial void area ranges over 0.1 inch^2 (0.65×10^{-4} m^2) or more about all the repaired sections. Therefore, the PG method with Class C-1 grout in Specimen PG-C1-2 has a lower FC than other previously evaluated. Table B-14 shows the time schedule for sealing ducts for Specimen PG-C1-2. Total sealing time for Specimen PG-C1-2 is 2 days and 0.65 hours before applying repair grout.

Table B-14. Sealing Time Schedule of Specimen PG-C1-2.

Sealing Procedure	Working Day	Working Time (min.)
Installing pipe saddle tap	Day 1	22
RTV silicone sealing	Day 1	5
Wait	1 day	
Connect pressure grout pump and reseal	Day 2	12
Sum	**2 days**	**39 (0.65 hours)**

B.7 SPECIMEN PG-C2-1

The initial void profiles before repair grouting are represented and shown in Figure B-18.

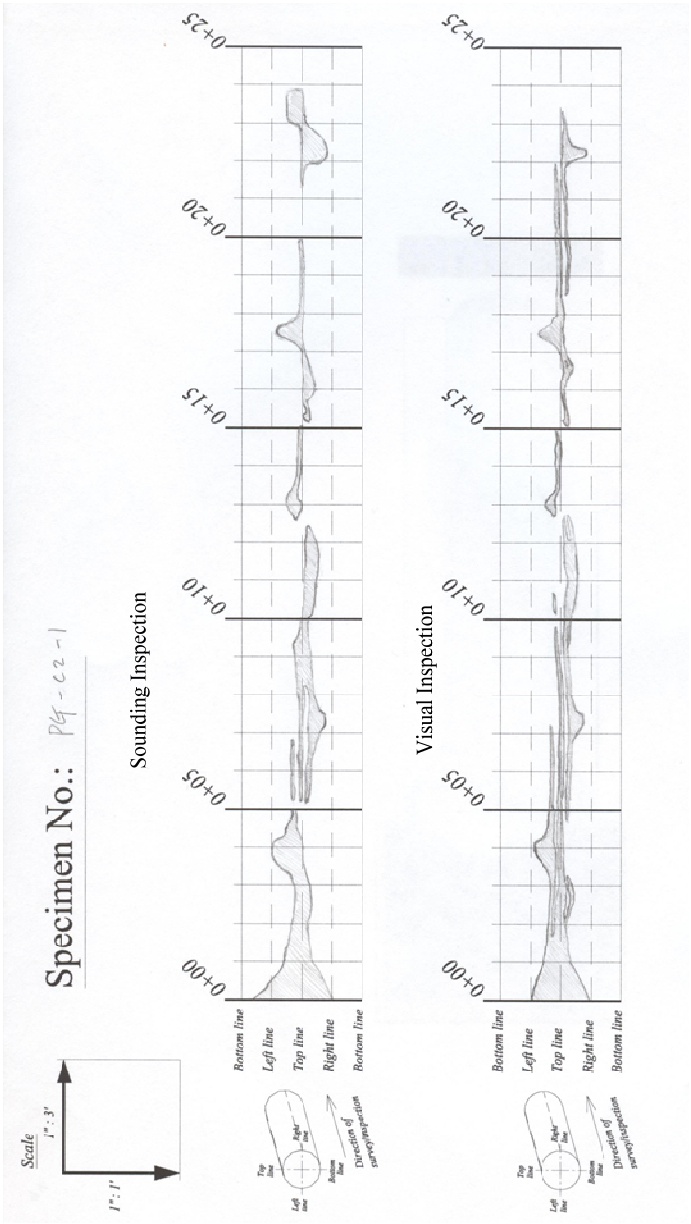

Figure B-18. Void Map of Specimen PG-C2-1.

The areas of both void profiles are estimated using AutoCAD® and provided in Table B-12.

Table B-15. Estimation of Void Profile in Specimen PG-C2-1.

Section, ft (m)	Sounding Inspection (SI), inch^2 (10^{-4} m^2)	Visual Inspection (VI), inch^2 (10^{-4} m^2)	SI - VI, inch^2 (10^{-4} m^2)
0~1 (0~0.3)	66.40 (428.4)	54.89 (354.1)	11.51 (74.3)
1~2 (0.3~0.6)	28.33 (182.7)	26.29 (169.6)	2.04 (13.1)
2~3 (0.6~0.9)	21.88 (141.2)	21.29 (137.3)	0.59 (3.8)
3~4 (0.9~1.2)	30.08 (194.0)	23.50 (151.6)	6.58 (42.4)
4~5 (1.2~1.5)	16.38 (105.7)	19.62 (126.6)	-3.24 (-20.9)
5~6 (1.5~1.8)	13.48 (87.0)	14.21 (91.7)	-0.73 (-4.7)
6~7 (1.8~2.1)	19.95 (128.7)	15.32 (98.8)	4.63 (29.9)
7~8 (2.1~2.4)	21.56 (139.1)	18.28 (117.9)	3.29 (21.2)
8~9 (2.4~2.7)	20.29 (130.9)	10.69 (69.0)	9.60 (62.0)
9~10 (2.7~3.0)	16.23 (104.7)	10.53 (68.0)	5.70 (36.8)
10~11 (3.0~3.4)	13.36 (86.2)	13.17 (85.0)	0.19 (1.2)
11~12 (3.4~3.7)	16.10 (103.9)	14.43 (93.1)	1.67 (10.8)
12~13 (3.7~4.0)	8.60 (55.5)	8.79 (56.7)	-0.20 (-1.3)
13~14 (4.0~4.3)	8.58 (55.3)	5.82 (37.5)	2.76 (17.8)
14~15 (4.3~4.6)	5.56 (35.9)	5.17 (33.4)	0.39 (2.5)
15~16 (4.6~4.9)	7.39 (47.7)	4.12 (26.6)	3.27 (21.1)
16~17 (4.9~5.2)	10.96 (70.7)	8.18 (52.8)	2.78 (17.9)
17~18 (5.2~5.5)	18.54 (119.6)	18.25 (117.8)	0.28 (1.8)
18~19 (5.5~5.8)	6.35 (40.9)	8.36 (54.0)	-2.02 (-13.0)
19~20 (5.8~6.1)	5.64 (36.4)	9.55 (61.6)	-3.91 (-25.3)
20~21 (6.1~6.4)	0.00 (0.0)	8.39 (54.1)	-8.39 (-54.1)
21~22 (6.4~6.7)	4.61 (29.8)	8.29 (53.5)	-3.68 (-23.7)
22~23 (6.7~7.0)	26.46 (170.7)	13.59 (87.7)	12.87 (83.0)
23~24 (7.0~7.3)	18.79 (121.2)	1.01 (6.5)	17.79 (114.7)

The repair grout is filled from the top grout port and infiltrated to 4.6 ft (1.40 m) from the reference point (Figure B-19).

Figure B-19. Repair Grouted Ducts of Specimen PG-C2-1.

Figure B-20 shows the cross-sectional views of the cut sections obtained from Specimen PG-C2-1. The repair grout successfully fills the voids up to 3.5 ft (1.07m) from the reference point, but it does not fill void #5 located at 4 ft (1.22 m) from the reference point since the void is isolated from the "bug hole." Because the five local large voids are fabricated intentionally by vacuuming, in some cases, the voids are not connected with a void route located on the top surface. The small voids still exist inside the initially grouted ducts, especially in-between strands.

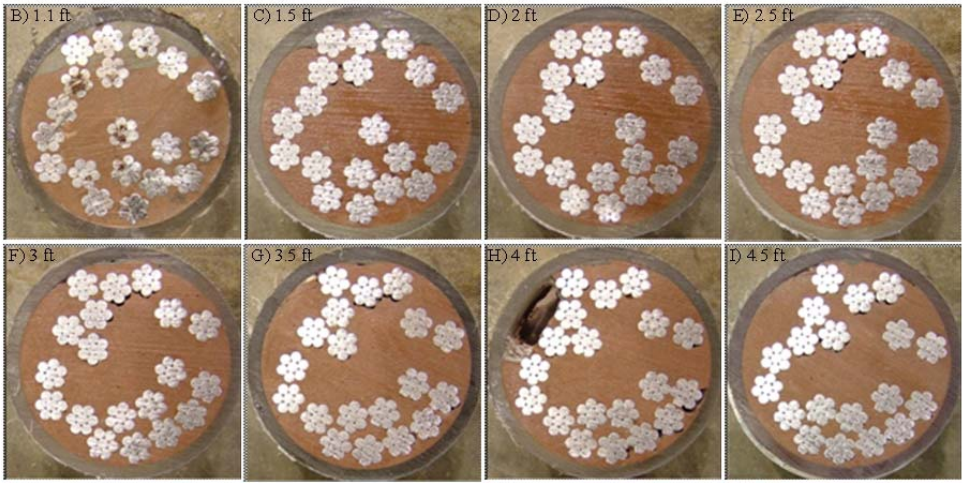

Figure B-20. Cut Sections of Specimen PG-C2-1 for the Filling Analysis of Repair Grout.

To compare the performance of repair grouts, the ratio of the remaining void area after repair to the repaired area is estimated. The repaired area and area of voids after repair are calculated using AutoCAD® (Table B-16).

Table B-16. Void Area of Specimen PG-C2-1.

Cut Sections, ft (m)		Repaired Area, A_R, inch^2(10^{-4} m^2)	Void Area, A_V, inch^2(10^{-4} m^2)	Void Ratio, η (%)
B	1.1 (0.34)	1.164 (7.51)	0.0079 (0.051)	0.68
C	1.5 (0.46)	0.436 (2.81)	0.0036 (0.023)	0.86
D	2 (0.61)	0.430 (2.77)	0.0021 (0.014)	0.49
E	2.5 (0.76)	0.182 (1.17)	0.0027 (0.017)	1.48
F	3 (0.91)	0.125 (0.81)	0.0057 (0.037)	4.56
G	3.5 (1.07)	0.081 (0.52)	0.0038 (0.025)	4.71
H	4 (1.22)	0.066 (0.43)	0.0026 (0.017)	3.92
I	4.5 (1.37)	0.040 (0.26)	0.0000 (0.000)	0.00
Sum		**2.524 (16.28)**	**0.0284 (0.183)**	**1.13**

From the analysis of the cut sections, Specimen PG-C2-1 has the remaining void ratio, after repair, of 1.13%. Since the initial void area is significantly less [under 0.1 inch^2 (0.65×10^{-4}

m^2)] from Section G, the repair grouts cannot be depended on to adequately fill Specimen PG-C2-1 when compared to other specimens.

Table B-17 shows the time schedule for sealing ducts and preparation of repair grouting for Specimen PG-C2-1. Total sealing time for Specimen PG-C2-1 is 3 days and 1.03 hours before applying repair grout.

Table B-17. Sealing Time Schedule of Specimen PG-C2-1.

Sealing Procedure	Working Day	Working Time (min.)
Mixing epoxy and sealing	Day 1	25
Wait	1 day	
Setting rubber end cap (one side)	Day 2	2
Installing pipe saddle tap	Day 2	25
Connect pressure grout pump and reseal	Day 3	10
Sum	**3 days**	**62 (1.03 hours)**

B.8 SPECIMEN PG-C2-2

Figure B-21 depicts the initial void profiles of the sounding inspection and of the visual inspection before grouting for Specimen PG-C2-2.

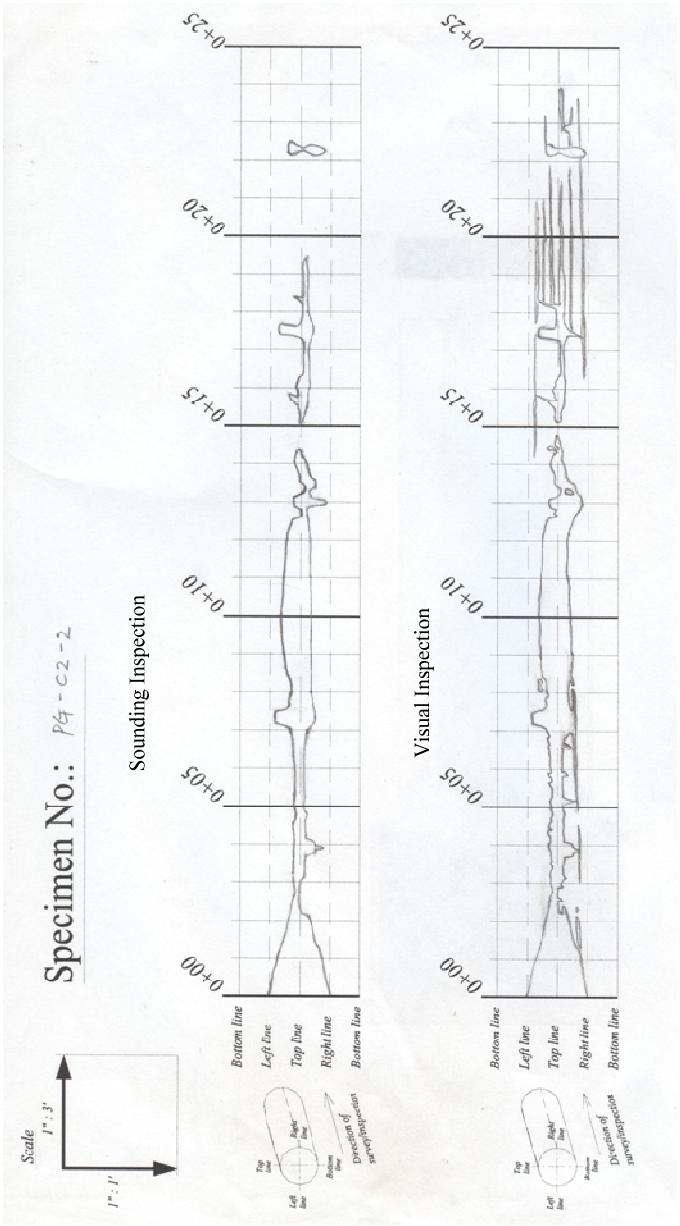

Figure B-21. Void Map of Specimen PG-C2-2.

The areas of both void profiles are estimated using AutoCAD® and provided in Table B-18.

Table B-18. Estimation of Void Profile in Specimen PG-C2-2.

Section, ft (m)	Sounding Inspection (SI), inch^2 (10^{-4} m^2)	Visual Inspection (VI), inch^2 (10^{-4} m^2)	SI - VI, inch^2 (10^{-4} m^2)
0~1 (0~0.3)	66.52 (429.1)	66.19 (427.0)	0.32 (2.1)
1~2 (0.3~0.6)	40.54 (261.5)	43.93 (283.4)	-3.39 (-21.9)
2~3 (0.6~0.9)	11.28 (72.8)	15.96 (103.0)	-4.68 (-30.2)
3~4 (0.9~1.2)	17.91 (115.5)	21.72 (140.1)	-3.81 (-24.6)
4~5 (1.2~1.5)	15.31 (98.8)	18.51 (119.4)	-3.20 (-20.6)
5~6 (1.5~1.8)	11.74 (75.7)	19.38 (125.0)	-7.64 (-49.3)
6~7 (1.8~2.1)	15.08 (97.3)	23.15 (149.3)	-8.07 (-52.1)
7~8 (2.1~2.4)	36.90 (238.0)	40.95 (264.2)	-4.05 (-26.1)
8~9 (2.4~2.7)	29.27 (188.8)	37.26 (240.4)	-7.99 (-51.6)
9~10 (2.7~3.0)	35.95 (231.9)	39.66 (255.9)	-3.71 (-24.0)
10~11 (3.0~3.4)	35.10 (226.5)	37.74 (243.5)	-2.64 (-17.1)
11~12 (3.4~3.7)	30.72 (198.2)	31.56 (203.6)	-0.84 (-5.4)
12~13 (3.7~4.0)	20.69 (133.5)	31.14 (200.9)	-10.45 (-67.4)
13~14 (4.0~4.3)	17.03 (109.9)	20.56 (132.7)	-3.53 (-22.8)
14~15 (4.3~4.6)	3.89 (25.1)	9.34 (60.3)	-5.45 (-35.2)
15~16 (4.6~4.9)	10.73 (69.2)	14.03 (90.5)	-3.30 (-21.3)
16~17 (4.9~5.2)	9.61 (62.0)	10.48 (67.6)	-0.87 (-5.6)
17~18 (5.2~5.5)	19.37 (125.0)	23.46 (151.3)	-4.09 (-26.4)
18~19 (5.5~5.8)	7.00 (45.2)	24.09 (155.4)	-17.09 (-110.3)
19~20 (5.8~6.1)	2.26 (14.6)	19.76 (127.5)	-17.50 (-112.9)
20~21 (6.1~6.4)	0.00 (0.0)	15.65 (101.0)	-15.65 (-101.0)
21~22 (6.4~6.7)	0.00 (0.0)	6.74 (43.5)	-6.74 (-43.5)
22~23 (6.7~7.0)	9.80 (63.2)	15.57 (100.4)	-5.76 (-37.2)
23~24 (7.0~7.3)	0.00 (0.0)	6.21 (40.1)	-6.21 (-40.1)

The repair grout is filled from the top grout port and infiltrated to 14.4 ft (4.39 m) from the reference point (Figure B-22).

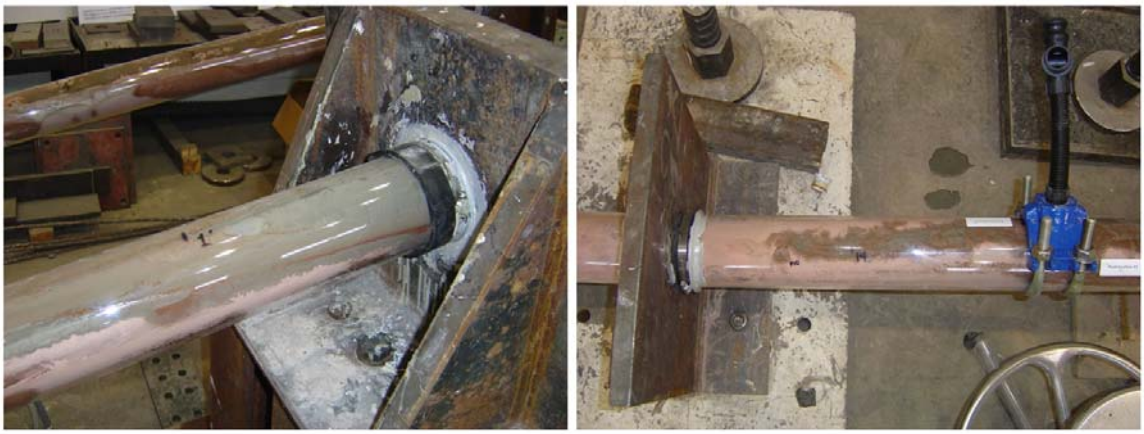

Figure B-22. Repair Grouted Ducts of Specimen PG-C2-2.

Figure B-23 shows the cross-sectional views of the cut sections obtained from Specimen PG-C2-2. From the cut sections, it is noted that the repair grouts successfully replaces the main voids and repairs local large voids #3, #4, and #5.

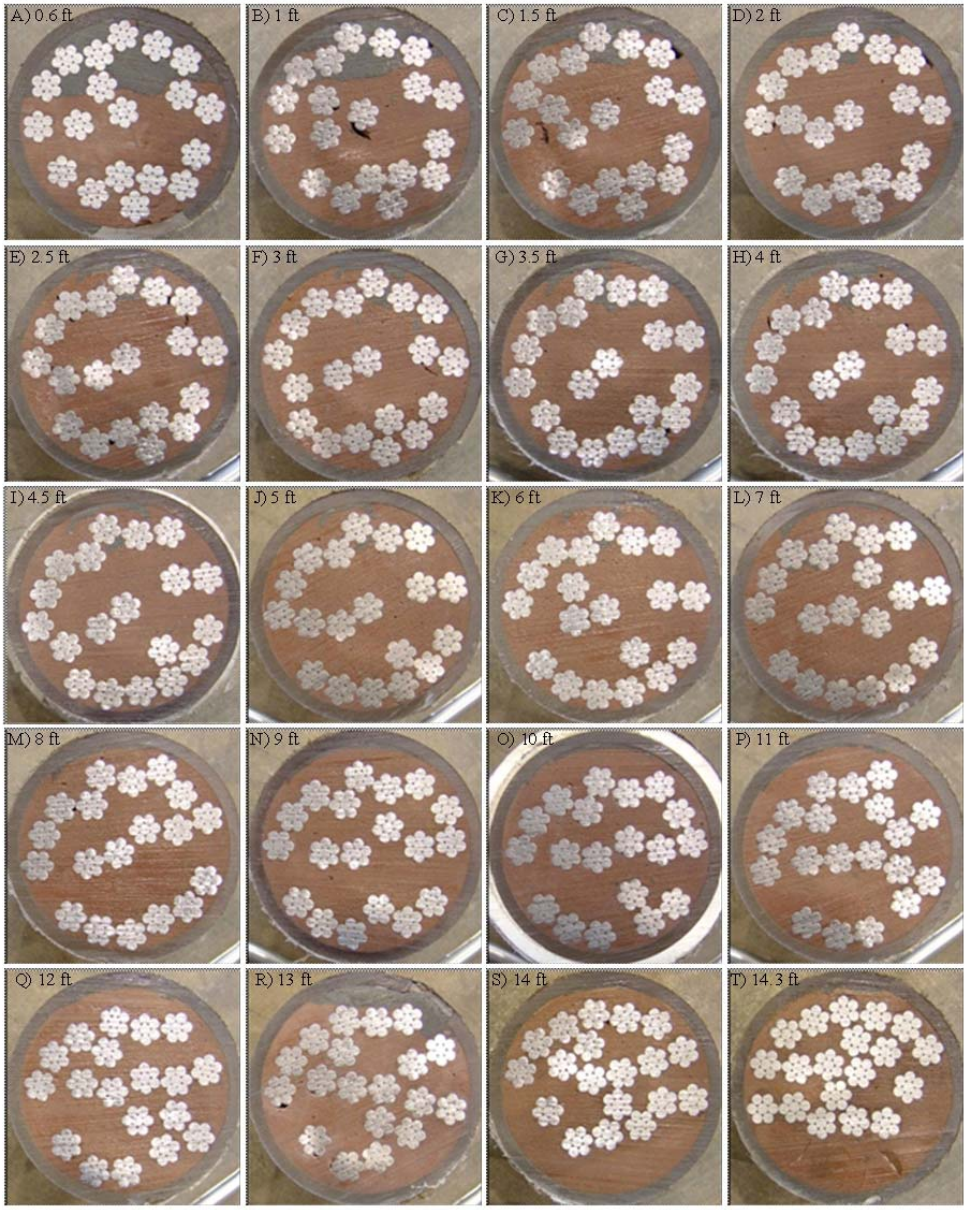

Figure B-23. Cut Sections of Specimen PG-C2-2 for the Filling Analysis of Repair Grout.

To compare the performance of repair grouts, the ratio of remaining void area after repair to the repaired area is estimated. The repaired area and area of voids after repair are calculated using AutoCAD® (Table B-19).

Table B-19. Void Area of Specimen PG-C2-2.

Cut Sections, ft (m)		Repaired Area, A_R, inch^2(10^{-4} m^2)	Void Area, A_V, inch^2(10^{-4} m^2)	Void Ratio, η (%)
A	0.6 (0.18)	2.033 (13.12)	0.0025 (0.016)	0.12
B	1 (0.30)	1.349 (8.71)	0.0174 (0.112)	1.29
C	1.5 (0.46)	0.673 (4.34)	0.0289 (0.186)	4.29
D	2 (0.61)	0.469 (3.03)	0.0023 (0.015)	0.49
E	2.5 (0.76)	0.281 (1.81)	0.0040 (0.026)	1.43
F	3 (0.91)	0.327 (2.11)	0.0021 (0.014)	0.64
G	3.5 (1.07)	0.371 (2.39)	0.0009 (0.006)	0.24
H	4 (1.22)	0.462 (2.98)	0.0025 (0.016)	0.54
I	4.5 (1.37)	0.302 (1.95)	0.0018 (0.012)	0.60
J	5 (1.52)	0.245 (1.58)	0.0010 (0.006)	0.41
K	6 (1.83)	0.272 (1.76)	0.0015 (0.010)	0.55
L	7 (2.13)	0.367 (2.37)	0.0026 (0.017)	0.71
M	8 (2.44)	0.284 (1.83)	0.0000 (0.000)	0.00
N	9 (2.74)	0.250 (1.61)	0.0014 (0.009)	0.56
O	10 (3.05)	0.235 (1.52)	0.0000 (0.000)	0.00
	11 (3.35)	0.221 (1.43)	0.0004 (0.003)	0.18
Q	12 (3.66)	0.215 (1.39)	0.0018 (0.012)	0.84
R	13 (3.96)	0.909 (5.87)	0.0042 (0.027)	0.46
S	14 (4.27)	0.120 (0.77)	0.0000 (0.000)	0.00
T	14.3 (4.37)	0.205 (1.32)	0.0000 (0.000)	0.00
Sum		**9.590 (61.87)**	**0.0753 (0.486)**	**0.79**

From the analysis of cut sections, the Specimen PG-C2-2 has the remaining void ratio, after repair, of 0.79% on average. The initial void area ranges over 0.1 inch^2 (0.65×10^{-4} m^2) or more about all the repaired sections. Therefore, the initial void condition for Specimen PG-C2-2 provides an easier condition for filling grouts when compared to others.

Table B-20 shows the time schedule for sealing ducts for Specimen PG-C2-2. Total sealing time for Specimen PG-C2-2 is 2 days and 0.88 hours before applying repair grout.

Table B-20. Sealing Time Schedule of Specimen PG-C2-2.

Sealing Procedure	Working Day	Working Time (min.)
Installing pipe saddle tap	Day 1	18
Connect grout hose and silicone sealing	Day 1	5
Mixing epoxy and sealing	Day 1	25
Wait	1 day	
Connect grout pump and reseal	Day 2	5
Sum	**2 days**	**53 (0.88 hours)**

B.9 SPECIMEN PG-C3-1

Figure B-24 depicts the initial void profiles of the sounding inspection and of the visual inspection before grouting for Specimen PG-C3-1.

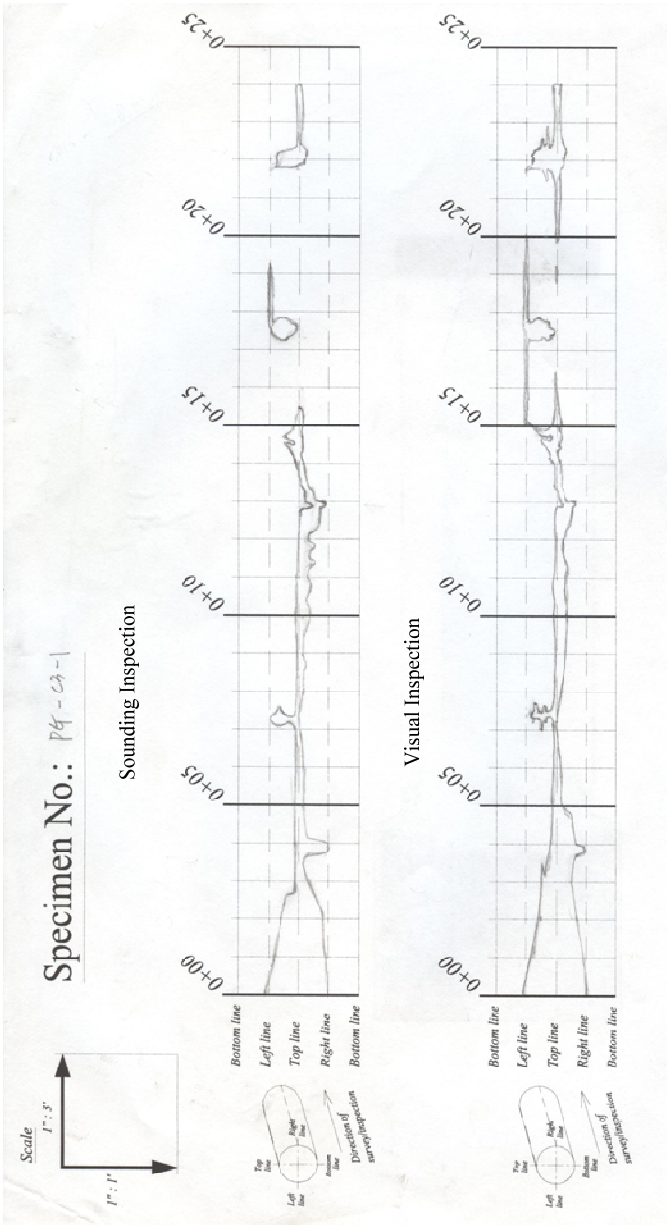

Figure B-24. Void Map of Specimen PG-C3-1.

The areas of both void profiles are estimated using AutoCAD® and provided in Table B-21.

Table B-21. Estimation of Void Profile in Specimen PG-C3-1.

Section, ft (m)	Sounding Inspection (SI), inch^2 (10^{-4} m^2)	Visual Inspection (VI), inch^2 (10^{-4} m^2)	SI - VI, inch^2 (10^{-4} m^2)
0~1 (0~0.3)	72.67 (468.9)	73.92(476.9)	-1.24 (-8.0)
1~2 (0.3~0.6)	56.95 (367.4)	57.77 (372.7)	-0.82 (-5.3)
2~3 (0.6~0.9)	35.90 (231.6)	43.46 (280.4)	-7.55 (-48.7)
3~4 (0.9~1.2)	20.97 (135.3)	38.20 (246.4)	-17.23 (-111.2)
4~5 (1.2~1.5)	15.01 (96.8)	26.25 (169.4)	-11.24 (-72.5)
5~6 (1.5~1.8)	10.47 (67.5)	10.96 (70.7)	-0.49 (-3.2)
6~7 (1.8~2.1)	7.48 (48.2)	6.41 (41.4)	1.07 (6.9)
7~8 (2.1~2.4)	14.92 (96.3)	14.63 (94.4)	0.29 (1.9)
8~9 (2.4~2.7)	8.55 (55.2)	11.47 (74.0)	-2.92 (-18.8)
9~10 (2.7~3.0)	11.45 (73.9)	15.98 (103.1)	-4.53 (-29.2)
10~11 (3.0~3.4)	15.68 (101.2)	16.74 (108.0)	-1.05 (-6.8)
11~12 (3.4~3.7)	15.79 (101.8)	13.33 (86.0)	2.46 (15.8)
12~13 (3.7~4.0)	20.46 (132.0)	18.57 (119.8)	1.90 (12.2)
13~14 (4.0~4.3)	9.44 (60.9)	9.05 (58.4)	0.39 (2.5)
14~15 (4.3~4.6)	14.42 (93.0)	17.59 (113.5)	-3.17 (-20.5)
15~16 (4.6~4.9)	3.62 (23.4)	12.38 (79.9)	-8.76 (-56.5)
16~17 (4.9~5.2)	0.00 (0.0)	6.15 (39.7)	-6.15 (-39.7)
17~18 (5.2~5.5)	16.81 (108.5)	20.46 (132.0)	-3.65 (-23.5)
18~19 (5.5~5.8)	6.40 (41.3)	6.49 (41.9)	-0.09 (-0.6)
19~20 (5.8~6.1)	1.01 (6.5)	4.14 (26.7)	-3.14 (-20.2)
20~21 (6.1~6.4)	0.00 (0.0)	6.17 (39.8)	-6.17 (-39.8)
21~22 (6.4~6.7)	6.52 (42.1)	17.16 (110.7)	-10.64 (-68.7)
22~23 (6.7~7.0)	14.11 (91.0)	23.99 (154.7)	-9.88 (-63.7)
23~24 (7.0~7.3)	7.27 (46.9)	7.83 (50.5)	-0.56 (-3.6)

The repair grout is filled from the top grout port and infiltrated to 7.3 ft (2.23 m) from the reference point (Figure B-25).

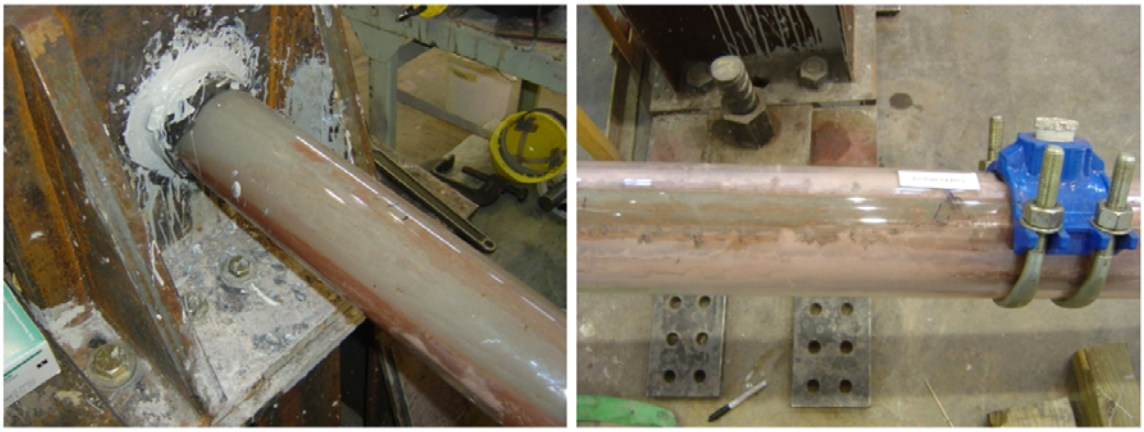

Figure B-25. Repair Grouted Ducts of Specimen PG-C3-1.

Figure B-26 shows the cross-sectional views of the cut sections obtained from Specimen PG-C3-1. From the cut sections, it is noted that the repair grout successfully replaces the main voids up to 6 ft (1.83 m) from the reference point, but after that voids were only partially repaired. The local large void #5 is filled completely by repair grout. The small voids still exist inside the initially grouted ducts, especially in-between strands. However, those voids cannot be repaired because the voids are isolated from the "bug holes" which is a route for repair grouts.

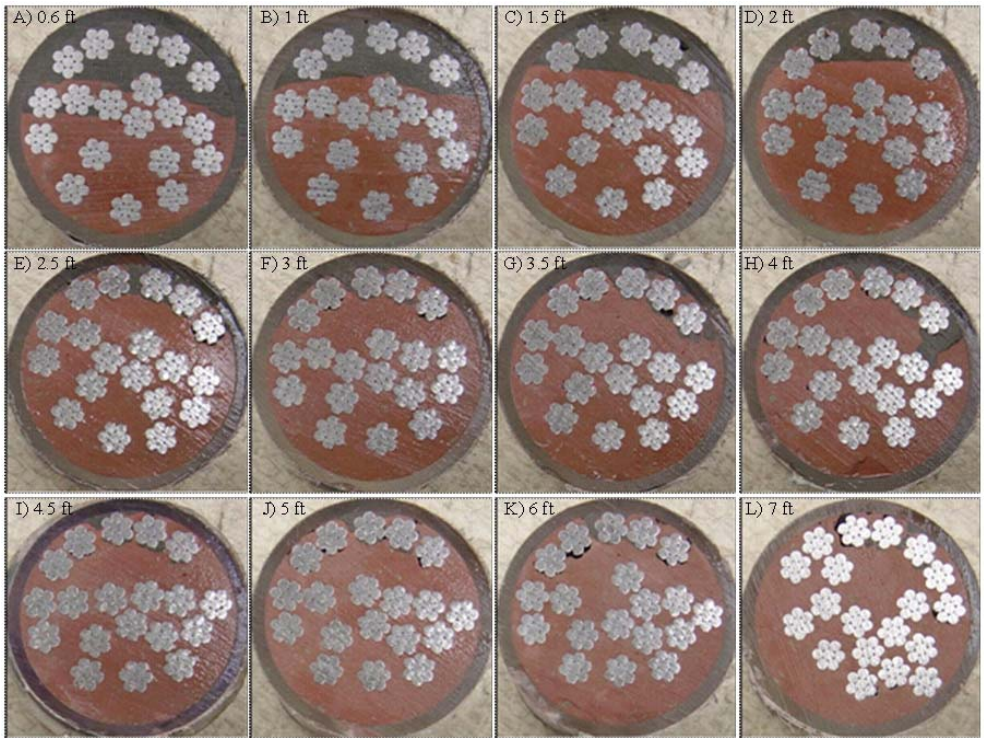

Figure B-26. Cut Sections of Specimen PG-C3-1 for the Filling Analysis of Repair Grout.

To compare the performance of repair grouts, the ratio of remaining void area after repair to the repaired area is estimated. The repaired area and area of voids after repair are calculated using AutoCAD® (Table B-22).

Table B-22. Void Area of Specimen PG-C3-1.

Cut Sections, ft (m)		Repaired Area, A_R, inch^2(10^{-4} m^2)	Void Area, A_V, inch^2(10^{-4} m^2)	Void Ratio, η (%)
A	0.6 (0.18)	2.395 (15.45)	0.0126 (0.081)	0.53
B	1 (0.30)	1.882 (12.14)	0.0089 (0.057)	0.47
C	1.5 (0.46)	1.407 (9.08)	0.0322 (0.208)	2.28
D	2 (0.61)	0.796 (5.13)	0.0032 (0.021)	0.40
E	2.5 (0.76)	0.487 (3.15)	0.0159 (0.103)	3.26
F	3 (0.91)	0.285 (1.84)	0.0080 (0.052)	2.81
G	3.5 (1.07)	0.440 (2.84)	0.0349 (0.225)	7.93
H	4 (1.22)	0.638 (4.12)	0.0120 (0.077)	1.88
I	4.5 (1.37)	0.239 (1.54)	0.0039 (0.025)	1.63
J	5 (1.52)	0.220 (1.42)	0.0094 (0.061)	4.27
K	6 (1.83)	0.188 (1.21)	0.0020 (0.013)	1.07
L	7 (2.13)	0.186 (1.20)	0.0000 (0.000)	0.00
Sum		**9.164 (59.12)**	**0.1430 (0.923)**	**1.56**

From the analysis of cut sections, the Specimen PG-C3-1 has the remaining void ratio, after repair, of 1.56% on average. The initial void area ranges over 0.1 inch^2 (0.65×10^{-4} m^2) or more about all the repaired sections. Therefore, the PG method with Class C-3 grout in Specimen PG-C3-1 has a lower FC than others.

Table B-23 shows the time schedule for sealing ducts for Specimen PG-C3-1. Total sealing time for Specimen PG-C3-1 is 3 days and 0.85 hours before applying repair grout.

Table B-23. Sealing Time Schedule of Specimen PG-C3-1.

Sealing Procedure	Working Day	Working Time (min.)
Mixing epoxy and sealing (one side)	Day 1	25
Wait	1 day	
Installing pipe saddle tap	Day 2	18
Connect pressure grout pump and reseal	Day 2	8
Sum	**2 days**	**51 0.85 hours**

B.10 SPECIMEN PG-C3-2

Figure B-27 depicts the initial void profiles of the sounding inspection and of the visual inspection before grouting for Specimen PG-C3-2.

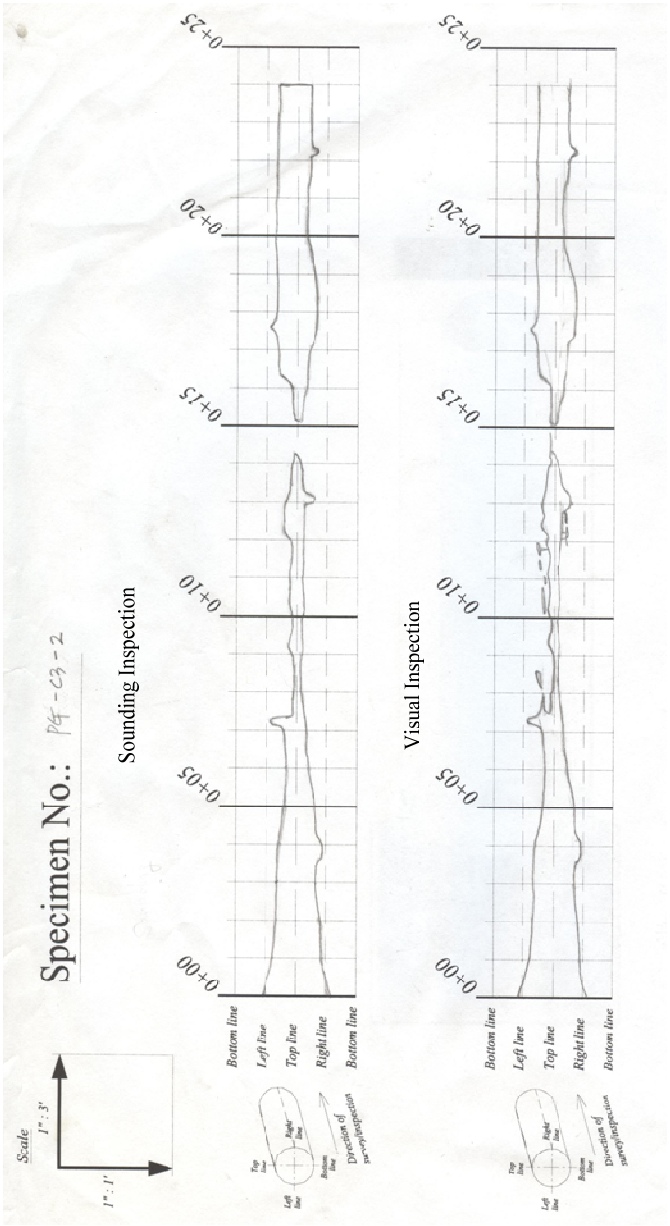

Figure B-27. Void Map of Specimen PG-C3-2.

The areas of both void profiles are estimated using AutoCAD® and provided in Table B-24.

Table B-24. Estimation of Void Profile in Specimen PG-C3-2.

Section, ft (m)	Sounding Inspection (SI), inch^2 (10^{-4} m^2)	Visual Inspection (VI), inch^2 (10^{-4} m^2)	SI - VI, inch^2 (10^{-4} m^2)
0~1 (0~0.3)	72.74 (469.3)	72.92 (470.5)	-0.18 (-1.2)
1~2 (0.3~0.6)	58.93 (380.2)	60.08 (387.6)	-1.15 (-7.4)
2~3 (0.6~0.9)	51.81 (334.2)	53.21 (343.3)	-1.40 (-9.0)
3~4 (0.9~1.2)	52.01 (335.6)	54.57 (352.0)	-2.56 (-16.5)
4~5 (1.2~1.5)	44.87 (289.5)	46.82 (302.1)	-1.96 (-12.6)
5~6 (1.5~1.8)	32.84 (211.9)	34.83 (224.7)	-1.98 (-12.8)
6~7 (1.8~2.1)	26.48 (170.9)	27.48 (117.3)	-0.99 (-6.4)
7~8 (2.1~2.4)	21.06 (135.9)	26.38 (170.2)	-5.32 (-34.3)
8~9 (2.4~2.7)	8.80 (56.8)	8.45 (54.5)	0.34 (2.2)
9~10 (2.7~3.0)	13.70 (88.4)	10.05 (64.9)	3.64 (23.5)
10~11 (3.0~3.4)	16.16 (104.3)	14.96 (96.5)	1.20 (7.8)
11~12 (3.4~3.7)	14.97 (96.6)	16.74 (108.0)	-1.77 (-11.4)
12~13 (3.7~4.0)	23.60 (152.3)	27.08 (174.7)	-3.48 (-22.4)
13~14 (4.0~4.3)	18.98 (122.5)	23.85 (153.9)	-4.86 (-31.4)
14~15 (4.3~4.6)	1.91 (12.3)	3.55 (22.9)	-1.64 (-10.6)
15~16 (4.6~4.9)	11.12 (71.8)	11.15 (71.9)	-0.02 (-0.1)
16~17 (4.9~5.2)	32.11 (207.1)	30.95 (199.6)	1.16 (7.5)
17~18 (5.2~5.5)	49.13 (316.9)	46.88 (302.5)	2.24 (14.5)
18~19 (5.5~5.8)	49.28 (317.9)	47.43 (306.0)	1.85 (11.9)
19~20 (5.8~6.1)	43.31 (279.4)	39.22 (253.0)	4.09 (26.4)
20~21 (6.1~6.4)	37.85 (244.2)	32.66 (210.7)	5.19 (33.5)
21~22 (6.4~6.7)	39.41 (254.3)	37.22 (240.1)	2.19 (14.1)
22~23 (6.7~7.0)	42.80 (276.1)	41.86 (270.1)	0.93 (6.0)
23~24 (7.0~7.3)	39.10 (252.3)	38.77 (250.1)	0.33 (2.1)

The repair grout is filled from the top grout port and infiltrated to 13.2 ft (4.02 m) from the reference point (Figure B-28).

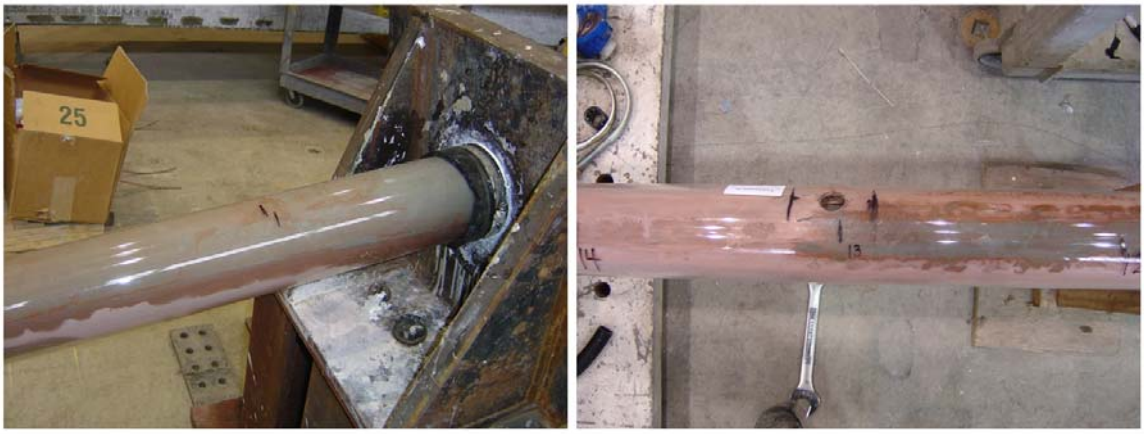

Figure B-28. Repair Grouted Ducts of Specimen PG-C3-2.

Figure B-29 shows the cross-sectional views of the cut sections obtained from Specimen PG-C3-2. From the cut sections, it is noted that the repair grouts successfully replaces the main voids up to 12 ft (3.66 m) from the reference point, but after that voids are only partially repaired. The local large void #4 and #5 are filled completely by repair grout.

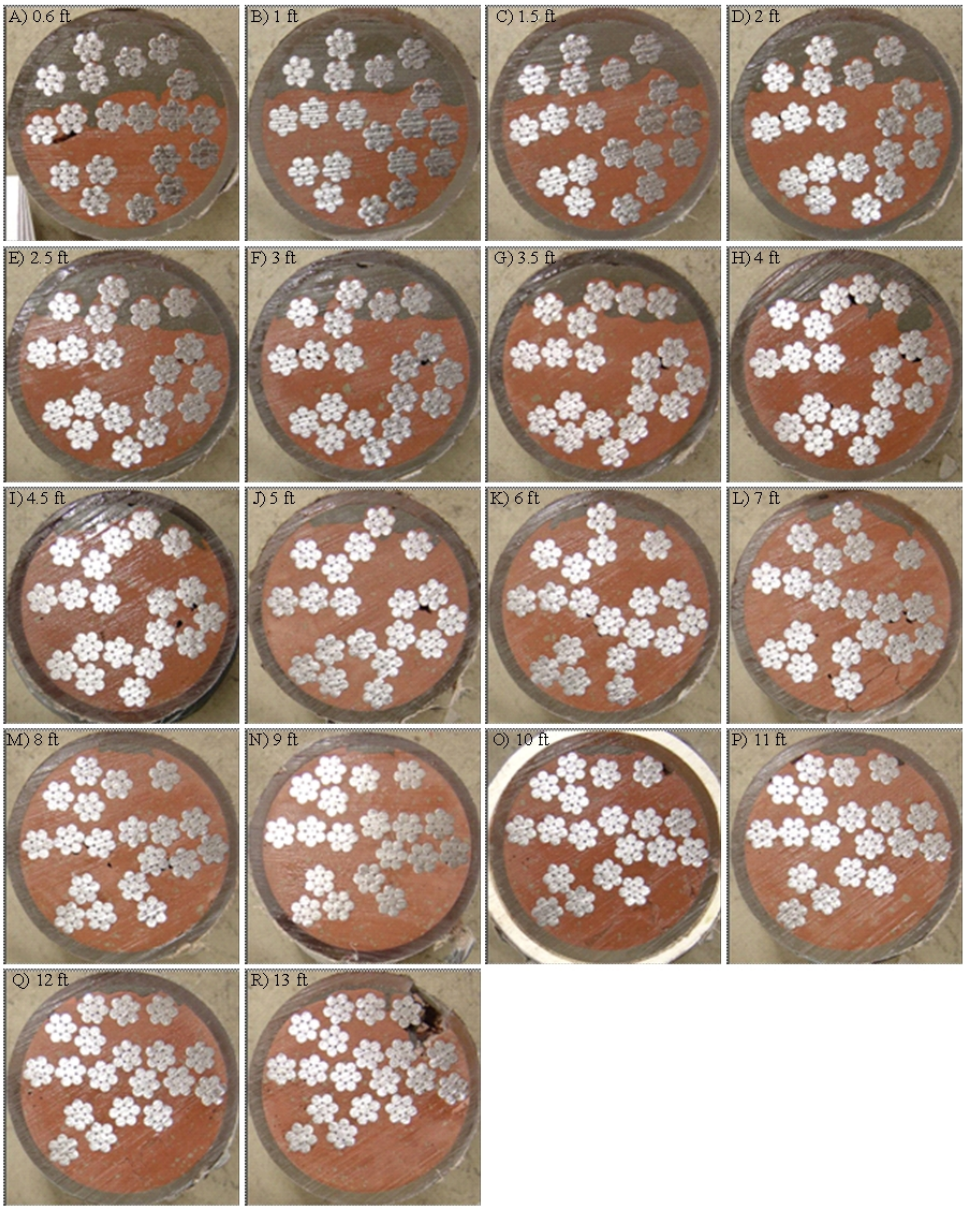

Figure B-29. Cut Sections of Specimen PG-C3-2 for the Filling Analysis of Repair Grout.

To compare the performance of repair grouts, the ratio of remaining void area after repair to the repaired area is estimated. The repaired area and area of voids after repair are calculated using AutoCAD® (Table B-25).

Table B-25. Void Area of Specimen PG-C3-2.

Cut Sections, ft (m)		Repaired Area, A_R, inch^2(10^{-4} m^2)	Void Area, A_V, inch^2(10^{-4} m^2)	Void Ratio, η (%)
A	0.6 (0.18)	2.927 (18.89)	0.0088 (0.057)	0.30
B	1 (0.30)	2.518 (16.24)	0.0400 (0.258)	1.59
C	1.5 (0.46)	2.164 (13.96)	0.0119 (0.077)	0.55
D	2 (0.61)	1.927 (12.43)	0.0027 (0.017)	0.14
E	2.5 (0.76)	1.771 (11.43)	0.0083 (0.054)	0.47
F	3 (0.91)	1.509 (9.74)	0.0324 (0.209)	2.15
G	3.5 (1.07)	1.319 (8.51)	0.0261 (0.168)	1.98
H	4 (1.22)	1.336 (8.62)	0.0046 (0.030)	0.34
I	4.5 (1.37)	0.764 (4.93)	0.0128 (0.083)	1.68
J	5 (1.52)	0.630 (4.06)	0.0106 (0.068)	1.68
K	6 (1.83)	0.374 (2.42)	0.0084 (0.054)	2.24
L	7 (2.13)	0.349 (2.25)	0.0031 (0.020)	0.89
M	8 (2.44)	0.188 (1.22^2)	0.0022 (0.014)	1.17
N	9 (2.74)	0.141 (0.91)	0.0000 (0.000)	0.00
O	10 (3.05)	0.180 (1.16)	0.0005 (0.003)	0.28
P	11 (3.35)	0.160 (1.04)	0.0016 (0.010)	1.00
Q	12 (3.66)	0.227 (1.46)	0.0061 (0.039)	2.69
R	13 (3.96)	0.297 (1.92)	0.0043 (0.028)	1.45
Sum		**18.781 (121.17)**	**0.1844 (1.190)**	**0.98**

From the analysis of cut sections, the Specimen PG-C3-2 has the remaining void ratio, after repair, of 0.98% on average. The initial void area ranges over 0.1 inch^2 (0.65×10^{-4} m^2) or more about all the repaired sections. Therefore, the PG method with Class C-3 grout in Specimen PG-C3-2 has a lower FC than others.

Table B-26 shows the time schedule of sealing ducts for Specimen PG-C3-2. Total sealing time for Specimen PG-C3-2 is 2 days and 0.97 hours before applying repair grout.

Table B-26. Sealing Time Schedule of Specimen PG-C3-2.

Sealing Procedure	Working Day	Working Time (min.)
Installing pipe saddle tap	Day 1	25
Connect hose and silicone sealing	Day 1	6
Mixing epoxy and sealing	Day 1	20
Wait	1 day	
Connect pressure grout pump and reseal	Day 2	7
Sum	**2 days**	**58 (0.97 hours)**

B.11 SPECIMEN PVG-C1-1

The initial void profiles produced by using both sounding inspection and visual inspection before repair grouting is shown in Figure B-30.

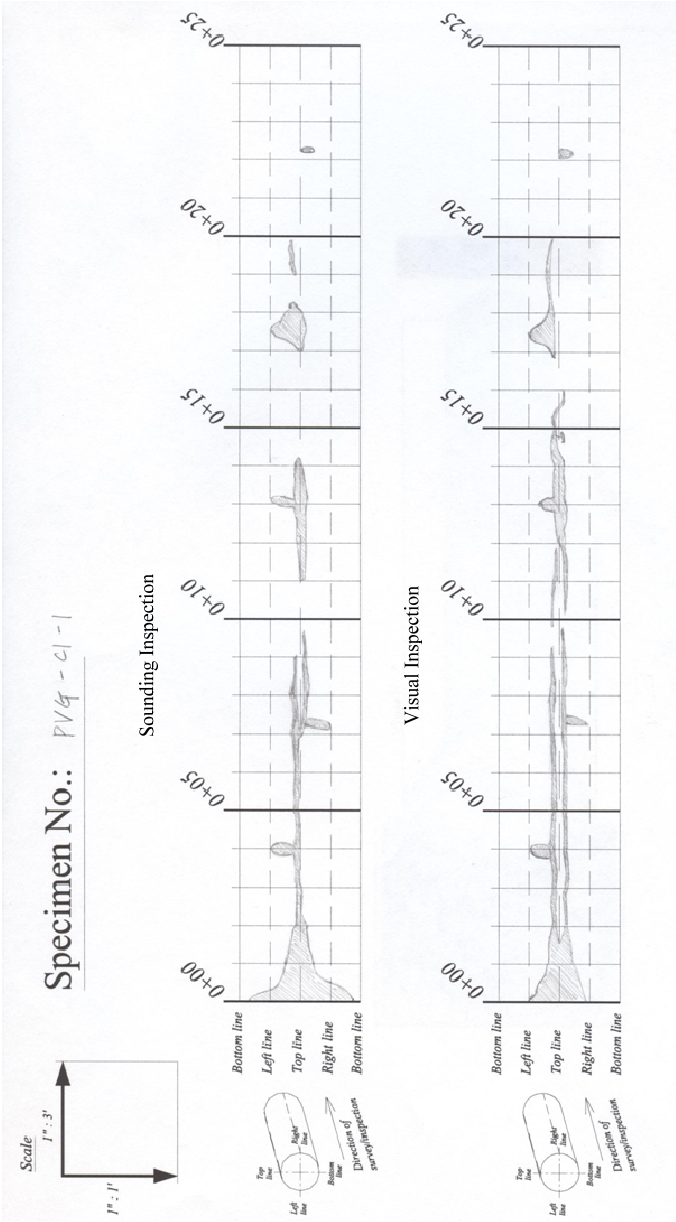

Figure B-30. Void Map of Specimen PVG-C1-1.

The areas of both void profiles are estimated using AutoCAD® and provided in Table B-27.

Table B-27. Estimation of Void Profile in Specimen PVG-C1-1.

Section, ft (m)	Sounding Inspection (SI), inch^2 (10^{-4} m^2)	Visual Inspection (VI), inch^2 (10^{-4} m^2)	SI - VI, inch^2 (10^{-4} m^2)
0~1 (0~0.3)	73.52 (474.3)	50.94 (328.7)	22.58 (145.6)
1~2 (0.3~0.6)	23.95 (154.5)	24.55 (158.4)	-0.61 (-3.9)
2~3 (0.6~0.9)	7.42 (47.8)	10.66 (68.8)	-3.24 (-20.9)
3~4 (0.9~1.2)	10.22 (65.9)	16.48 (106.3)	-6.26 (-40.4)
4~5 (1.2~1.5)	9.01 (58.1)	14.04 (90.6)	-5.03 (-32.4)
5~6 (1.5~1.8)	6.75 (43.5)	12.58 (81.1)	-5.83 (-37.6)
6~7 (1.8~2.1)	7.66 (49.4)	11.68 (75.3)	-4.02 (-25.9)
7~8 (2.1~2.4)	19.56 (126.2)	17.61 (113.6)	1.95 (12.6)
8~9 (2.4~2.7)	12.48 (80.5)	12.02 (77.5)	0.46 (3.0)
9~10 (2.7~3.0)	2.83 (18.2)	4.60 (29.7)	-1.77 (-11.4)
10~11 (3.0~3.4)	0.00 (0.0)	7.09 (45.7)	-7.08 (-45.7)
11~12 (3.4~3.7)	8.51 (54.9)	10.51 (67.8)	-1.99 (-12.9)
12~13 (3.7~4.0)	14.37 (92.7)	16.14 (104.1)	-1.77 (-11.4)
13~14 (4.0~4.3)	19.21 (124.0)	17.42 (112.4)	1.80 (11.6)
14~15 (4.3~4.6)	1.56 (10.1)	11.39 (73.5)	-9.84 (-63.5)
15~16 (4.6~4.9)	0.00 (0.0)	4.57 (29.5)	-4.57 (-29.5)
16~17 (4.9~5.2)	0.00 (0.0)	0.52 (3.4)	-0.52 (-3.4)
17~18 (5.2~5.5)	28.38 (183.1)	19.75 (127.4)	8.63 (55.7)
18~19 (5.5~5.8)	3.32 (21.4)	5.25 (33.8)	-1.93 (-12.4)
19~20 (5.8~6.1)	4.48 (28.9)	4.47 (28.8)	0.01 (0.1)
20~21 (6.1~6.4)	0.00 (0.0)	0.00 (0.0)	0.00 (0.0)
21~22 (6.4~6.7)	0.00 (0.0)	0.00 (0.0)	0.00 (0.0)
22~23 (6.7~7.0)	2.55 (16.4)	4.23 (27.3)	-1.68 (-10.8)
23~24 (7.0~7.3)	0.00 (0.0)	0.00 (0.0)	0.00 (0.0)

The repair grout is filled from the top grout port and infiltrated to 15.0 ft (4.57 m) from the reference point (Figure B-31).

Figure B-31. Repair Grouted Ducts of Specimen PVG-C1-1.

Figure B-32 shows the cross-sectional views of the cut sections obtained from Specimen PVG-C1-1. From the cut sections, it is noted that the repair grout successfully replaces the main voids and repairs local large voids #3, #4, and #5. The small voids still exist inside the initially grouted ducts, especially in-between strands. However, those voids could not be repaired because the voids are isolated from the "bug holes," which is a route for repair grouts.

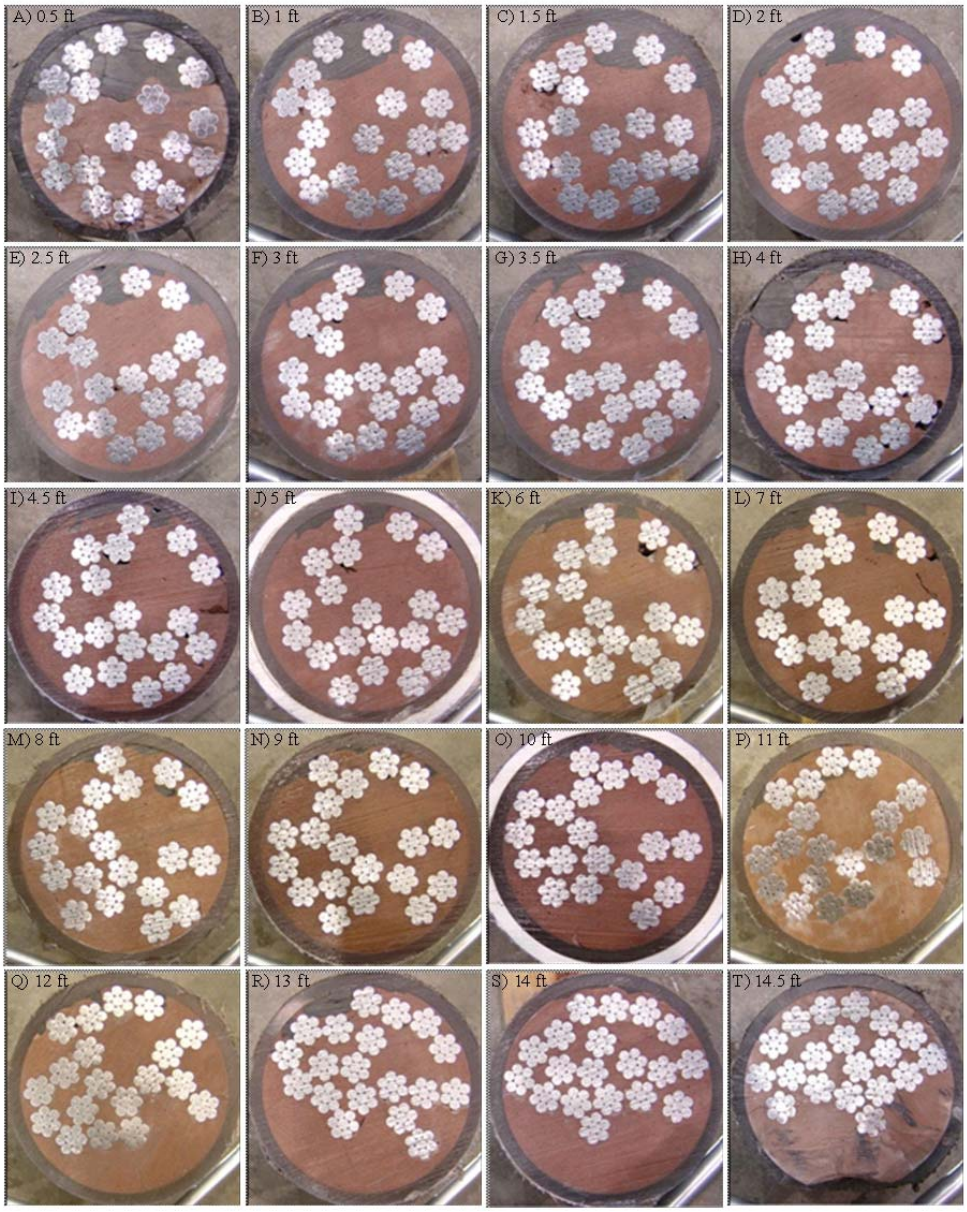

Figure B-32. Cut Sections of Specimen PVG-C1-1 for the Filling Analysis of Repair Grout.

To compare the performance of repair grouts, the ratio of remaining void area after repair to the repaired area is estimated. The repaired area and area of voids after repair are calculated using AutoCAD® (Table B-28).

Table B-28. Void Area of Specimen PVG-C1-1.

Cut Sections, ft (m)		Repaired Area, A_R, inch^2(10^{-4} m^2)	Void Area, A_V, inch^2(10^{-4} m^2)	Void Ratio, η (%)
A	0.5 (0.15)	2.280 (14.71)	0.0000 (0.000)	0.00
B	1 (0.30)	1.247 (8.05)	0.0000 (0.000)	0.00
C	1.5 (0.46)	0.871 (5.62)	0.0003 (0.002)	0.03
D	2 (0.61)	0.786 (5.07)	0.0264 (0.170)	3.36
E	2.5 (0.76)	0.714 (4.61)	0.0111 (0.072)	1.55
F	3 (0.91)	0.599 (3.87)	0.0000 (0.000)	0.00
G	3.5 (1.07)	0.491 (3.17)	0.0034 (0.022)	0.69
H	4 (1.22)	1.047 (6.75)	0.0039 (0.025)	0.37
I	4.5 (1.37)	0.408 (2.64)	0.0075 (0.048)	1.84
J	5 (1.52)	0.427 (2.75)	0.0044 (0.028)	1.03
K	6 (1.83)	0.284 (1.84)	0.0023 (0.015)	0.81
L	7 (2.13)	0.421 (2.72)	0.0012 (0.008)	0.29
M	8 (2.44)	0.327 (2.09)	0.0032 (0.021)	0.99
N	9 (2.74)	0.257 (1.66)	0.0047 (0.030)	1.83
O	10 (3.05)	0.156 (1.01)	0.0007 (0.005)	0.45
P	11 (3.35)	0.145 (0.94)	0.0000 (0.000)	0.00
Q	12 (3.66)	0.225 (1.45)	0.0000 (0.000)	0.00
R	13 (3.96)	0.552 (3.56)	0.0057 (0.037)	1.03
S	14 (4.27)	0.126 (0.81)	0.0004 (0.003)	0.32
T	14.5 (4.42)	0.051 (0.33)	0.0000 (0.000)	0.00
Sum		**11.413 (73.63)**	**0.0752 (0.485)**	**0.66**

From the analysis, remaining voids in the repair grout are estimated in each cut section; however, the void ratio in a section can be magnified when the remaining voids exist in a small repaired area. Thus, the filling performance for Specimen PVG-C1-1 is evaluated using the summation of estimated sections for Specimen PVG-C1-1. The remaining void ratio, after repair, obtained from the analysis comes out to be 0.66% for Specimen PVG-C1-1. The initial void area which is the repaired area as shown in Table B-28 ranges over 0.1 inch^2 (0.65×10^{-4} m^2) or more by Section S, however, the voids include small voids from Section T.

Table B-29 shows the time schedule of sealing ducts and preparation of repair grouting for Specimen PVG-C1-1. Total sealing time for Specimen PVG-C1-1 is 5 days and 2.83 hours before applying repair grout.

Table B-29. Sealing Time Schedule of Specimen PVG-C1-1.

Sealing Procedure	Working Day	Working Time (min.)
Setting rubber end caps and sealing with silicone	Day 1	20
Installing pipe saddle tap with grease	Day 1	40
Mixing epoxy and sealing	Day 2	35
Wait	1 day	
Checking air-tight condition	Day 3	15
Searching leaking part and sealing	Day 3	20
Connect grout hose and checking air-tight condition	Day 4	20
Sealing with RTV silicone	Day 4	15
Checking air-tight condition and sealing	Day 4	5
Sum	**4 days**	**170 (2.83 hours)**

B.12 SPECIMEN PVG-C1-2

Figure B-33 shows depicts the initial void profiles of the sounding inspection and of the visual inspection before grouting for Specimen PVG-C1-2.

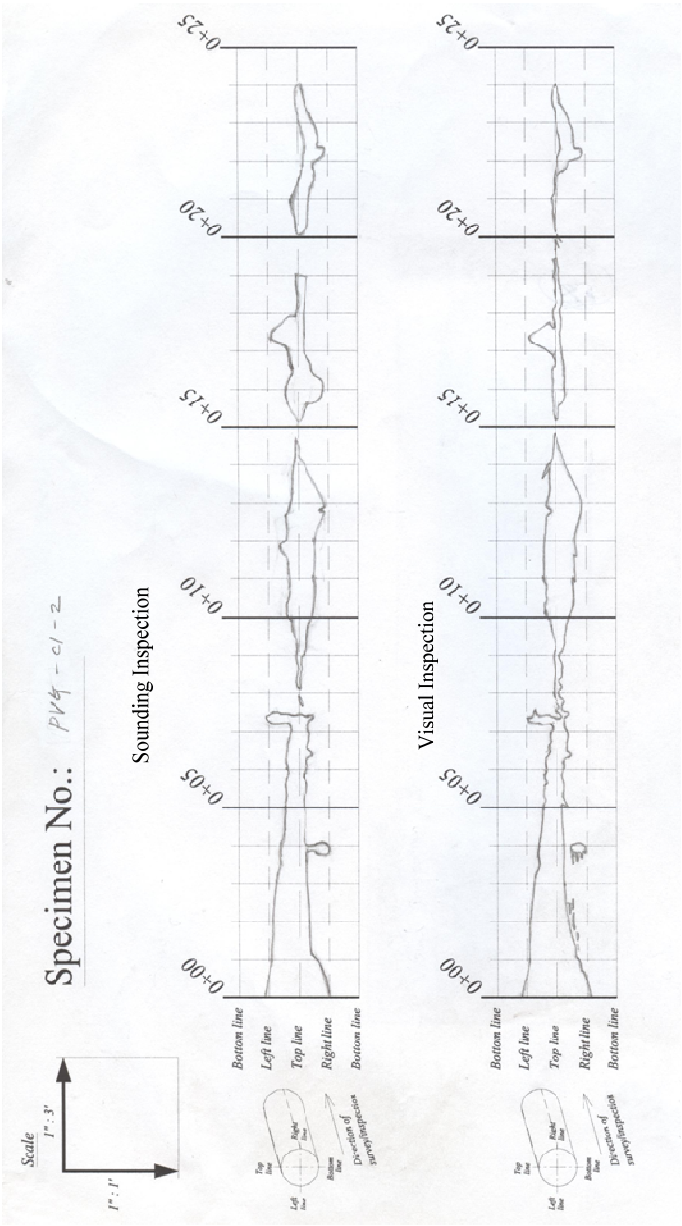

Figure B-33. Void Map of Specimen PVG-C1-2.

The areas of both void profiles are estimated using AutoCAD® and provided in Table B-27.

Table B-30. Estimation of Void Profile in Specimen PVG-C1-2.

Section, ft (m)	Sounding Inspection (SI), inch^2 (10^{-4} m^2)	Visual Inspection (VI), inch^2 (10^{-4} m^2)	SI - VI, inch^2 (10^{-4} m^2)
0~1 (0~0.3)	70.27 (453.4)	74.65 (481.6)	-4.38 (-28.3)
1~2 (0.3~0.6)	48.21 (311.0)	56.19 (362.5)	-7.97 (-51.4)
2~3 (0.6~0.9)	43.16 (278.5)	45.58 (294.1)	-2.42 (-15.6)
3~4 (0.9~1.2)	40.05 (258.4)	39.65 (255.8)	0.41 (2.6)
4~5 (1.2~1.5)	27.25 (175.8)	27.88 (179.9)	-0.63 (-4.1)
5~6 (1.5~1.8)	23.55 (152.0)	24.86 (160.4)	-1.31 (-8.5)
6~7 (1.8~2.1)	26.48 (170.9)	24.44 (157.7)	2.04 (13.2)
7~8 (2.1~2.4)	18.07 (116.5)	18.63 (120.2)	-0.56 (-3.6)
8~9 (2.4~2.7)	3.91 (25.2)	8.93 (57.6)	-5.02 (-32.4)
9~10 (2.7~3.0)	17.10 (110.3)	16.00 (103.2)	1.09 (7.1)
10~11 (3.0~3.4)	32.90 (212.3)	35.23 (227.3)	-2.33 (-15.0)
11~12 (3.4~3.7)	36.88 (237.9)	40.07 (258.5)	-3.19 (-20.6)
12~13 (3.7~4.0)	41.71 (269.1)	40.93 (264.1)	0.78 (5.0)
13~14 (4.0~4.3)	28.29 (182.5)	33.71 (217.5)	-5.42 (-35.0)
14~15 (4.3~4.6)	3.84 (24.8)	8.29 (53.5)	-4.45 (-28.7)
15~16 (4.6~4.9)	23.36 (150.7)	8.80 (56.7)	14.57 (94.0)
16~17 (4.9~5.2)	31.02 (200.1)	14.80 (95.5)	16.22 (104.6)
17~18 (5.2~5.5)	29.35 (189.4)	24.81 (160.1)	4.54 (29.3)
18~19 (5.5~5.8)	11.09 (71.5)	8.30 (53.6)	2.78 (18.0)
19~20 (5.8~6.1)	0.17 (1.1)	4.79 (30.9)	-4.62 (-29.8)
20~21 (6.1~6.4)	16.61 (107.2)	3.62 (23.3)	12.99 (83.8)
21~22 (6.4~6.7)	18.73 (120.8)	7.60 (49.0)	11.13 (71.8)
22~23 (6.7~7.0)	20.83 (134.4)	21.24 (137.0)	-0.41 (-2.7)
23~24 (7.0~7.3)	12.67 (81.8)	11.80 (76.1)	0.88 (5.7)

The repair grout is filled from the top grout port and infiltrated to 14.5 ft (4.42 m) from the reference point (Figure B-34).

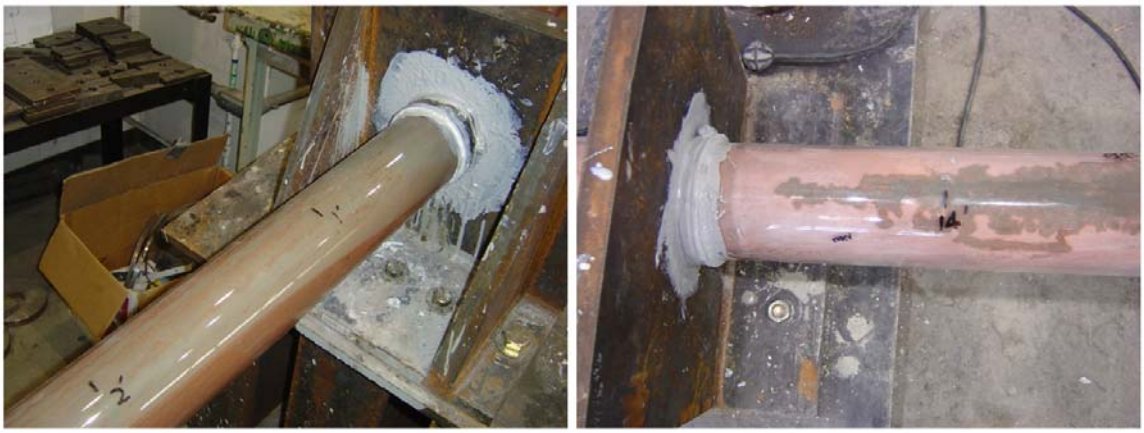

Figure B-34. Repair Grouted Ducts of Specimen PVG-C1-2.

Figure B-35 shows the cross-sectional views of the cut sections obtained from Specimen PVG-C1-2. From the cut sections, it is noted that the repair grouts successfully replaces the main voids and repairs local large voids #3, #4, and #5. The small voids still exist inside the initially grouted ducts, especially in-between strands.

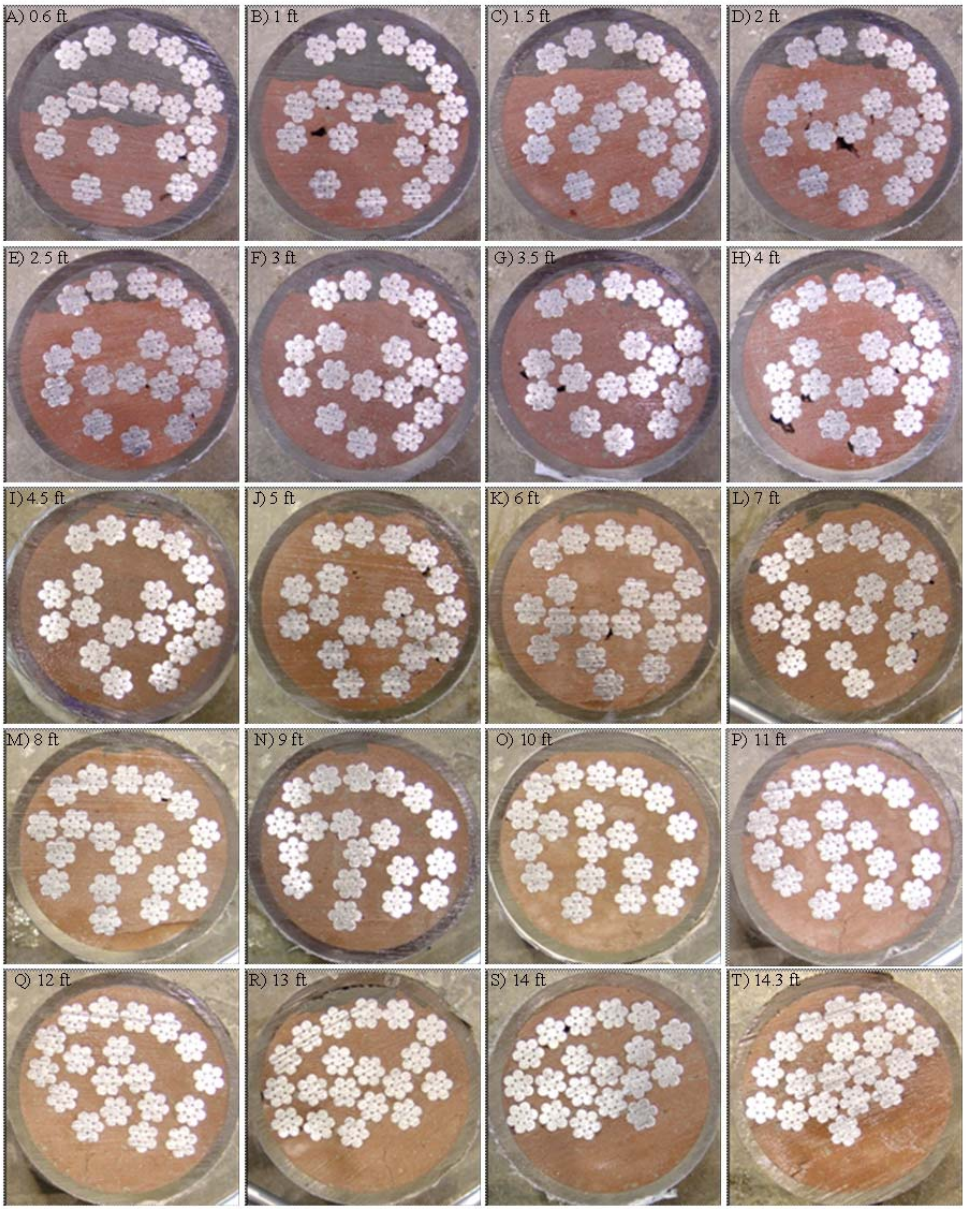

Figure B-35. Cut Sections of Specimen PVG-C1-2 for the Filling Analysis of Repair Grout.

To compare the performance of repair grouts, the ratio of remaining void area after repair to the repaired area is estimated. The repaired area and area of voids after repair are calculated using AutoCAD® (Table B-31).

Table B-31. Void Area of Specimen PVG-C1-2.

Cut Sections, ft (m)		Repaired Area, A_R, inch^2(10^{-4} m^2)	Void Area, A_V, inch^2(10^{-4} m^2)	Void Ratio, η (%)
A	0.6 (0.18)	2.981 (19.23)	0.0015 (0.010)	0.05
B	1 (0.30)	2.060 (13.29)	0.0010 (0.006)	0.05
C	1.5 (0.46)	1.110 (7.16)	0.0022 (0.014)	0.20
D	2 (0.61)	0.844 (5.44)	0.0008 (0.005)	0.09
E	2.5 (0.76)	0.716 (4.62)	0.0000 (0.000)	0.00
F	3 (0.91)	0.559 (3.61)	0.0000 (0.000)	0.00
G	3.5 (1.07)	0.419 (2.70)	0.0011 (0.007)	0.26
H	4 (1.22)	0.587 (3.79)	0.0028 (0.018)	0.48
I	4.5 (1.37)	0.299 (1.93)	0.0000 (0.000)	0.00
J	5 (1.52)	0.350 (2.26)	0.0028 (0.018)	0.80
K	6 (1.83)	0.253 (1.63)	0.0042 (0.027)	1.66
L	7 (2.13)	0.276 (1.78)	0.0058 (0.037)	2.10
M	8 (2.44)	0.125 (0.81)	0.0003 (0.002)	0.24
N	9 (2.74)	0.113 (0.73)	0.0000 (0.000)	0.00
O	10 (3.05)	0.273 (1.76)	0.0000 (0.000)	0.00
P	11 (3.35)	0.191 (1.23)	0.0003 (0.002)	0.16
Q	12 (3.66)	0.166 (1.07)	0.0000 (0.000)	0.00
R	13 (3.96)	0.615 (3.97)	0.0560 (0.361)	9.10
S	14 (4.27)	0.057 (0.37)	0.0016 (0.010)	2.81
T	14.3 (4.37)	0.021 (0.13)	0.0000 (0.000)	0.00
Sum		**12.013 (77.50)**	**0.0804 (0.519)**	**0.67**

The remaining void ratio, after repair, obtained from the analysis comes out to be 0.67% for Specimen PVG-C1-2. The initial void area ranges over 0.1 inch^2 (0.65×10^{-4} m^2) or more from the reference point to Section R, however, the voids include small contributions from Section S.

At first, the Specimen PVG-C1-2 was prepared for the VG method; however, it was replaced with the PVG method because it was not possible to create an air-tight condition. The Specimen took 9 days and 12.53 hours for preparation, but it was still leaking (see Table B-32). Although the preparation of VG method was failed, the sealing time schedule is considered at the analysis for economic feasibility because it shows the worst case for application of the VG method.

Table B-32. Fail to Prepare VG Methods in Specimen PVG-C1-2.

Sealing Procedure	Working Day	Working Time (min.)
Installing pipe saddle tap with grease	Day 1	35
Silicone and epoxy sealing	Day 1	40
Wait	1 day	
Setting rubber end caps and sealing with silicone	Day 2	15
Assemble T-connection and check air-tight condition	Day 3	40
Reassemble T-connection and change ball valve	Day 3	90
RTV silicone sealing and check air-tight condition	Day 3	40
Wait	1 day	
Check air-tight and silicone sealing	Day 4	45
Check air-tight and silicone sealing	Day 4	45
Epoxy mixing and sealing	Day 4	25
Wait	1 day	
Check air-tight and RTV silicone sealing	Day 5	36
Check air-tight, scrape epoxy, and seal with epoxy	Day 6	63
Retighten caps in pipe saddle tap using taflon tape	Day 6	19
Check air-tight and seal with epoxy and RTV silicone	Day 7	55
Check air-tight condition and seal with RTV silicone	Day 7	19
Epoxy mixing and sealing	Day 7	30
Check air-tight condition and reset end rubber caps	Day 8	30
Check air-tight and reinstall T-connection	Day 8	65
Checking air-tight condition and sealing	Day 8	18
Epoxy mixing and sealing	Day 8	32
Check air-tight condition	Day 9	10
FAIL to prepare VG method	**9 days**	**752 (12.53 hours)**

Table B-34 shows the time schedule of sealing ducts for Specimen PVG-C1-2. In the time schedule, the sealing procedures at day 2 are for replacing works with PVG method. The procedurs of epoxy sealing and setting end caps in Table B-32 are included in the sealing time schedule of Specimen PVG-C1-2. Total sealing time of PVG method for Specimen PVG-C1-2 is 2 days and 1.57 hours before applying repair grouts.

Table B-33. Sealing Time Schedule of Specimen PVG-C1-2.

Sealing Procedure	Working Day	Working Time (min.)
Setting rubber end caps and sealing with silicone	Day 1	15
Silicone and epoxy sealing	Day 1	40
Wait	1 day	
Connect hose and seal by silicone	Day 2	9
Connect vacuum safety device	Day 2	5
Reconnect pipe saddle tap with grease	Day 2	20
Check air-tight condition	Day 2	5
Sum	**2 days**	**94 (1.57 hours)**

B.13 SPECIMEN PVG-C2-1

Figure B-36 depicts the initial void profiles of the sounding inspection and of the visual inspection before grouting for Specimen PVG-C2-1.

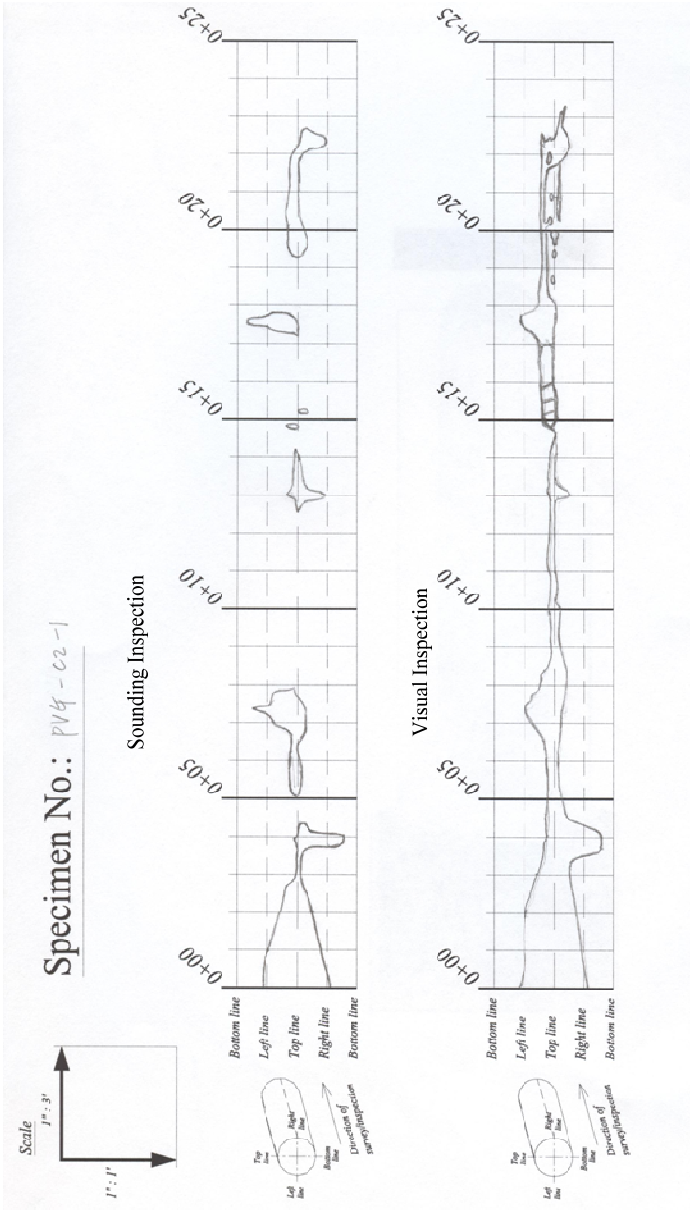

Figure B-36. Void Map of Specimen PVG-C2-1.

The areas of both void profiles are estimated using AutoCAD® and provided in Table B-34.

Table B-34. Estimation of Void Profile in Specimen PVG-C2-1.

Section, ft (m)	Sounding Inspection (SI), inch^2 (10^{-4} m^2)	Visual Inspection (VI), inch^2 (10^{-4} m^2)	SI - VI, inch^2 (10^{-4} m^2)
0~1 (0~0.3)	77.31 (498.8)	77.20 (498.1)	0.11 (0.7)
1~2 (0.3~0.6)	53.37 (344.3)	68.84 (444.1)	-15.48 (-99.8)
2~3 (0.6~0.9)	24.90 (160.6)	53.52 (345.3)	-28.62 (-184.7)
3~4 (0.9~1.2)	22.27 (143.7)	54.66 (352.7)	-32.39 (-209.0)
4~5 (1.2~1.5)	7.85 (50.7)	37.27 (240.5)	-29.42 (-189.8)
5~6 (1.5~1.8)	12.25 (79.0)	14.67 (94.6)	-2.42 (-15.6)
6~7 (1.8~2.1)	16.12 (104.0)	21.26 (137.2)	-5.14 (-33.2)
7~8 (2.1~2.4)	35.06 (226.2)	40.29 (259.9)	-5.23 (-33.8)
8~9 (2.4~2.7)	0.00 (0.0)	22.31 (144.0)	-22.31 (-144.0)
9~10 (2.7~3.0)	0.00 (0.0)	11.42 (73.7)	-11.42 (-73.7)
10~11 (3.0~3.4)	0.00 (0.0)	8.68 (56.0)	-8.68 (-56.0)
11~12 (3.4~3.7)	0.00 (0.0)	7.91 (51.1)	-7.91 (-51.1)
12~13 (3.7~4.0)	7.47 (48.2)	7.08 (45.7)	0.40 (2.6)
13~14 (4.0~4.3)	15.39 (99.3)	12.33 (79.6)	3.06 (19.8)
14~15 (4.3~4.6)	2.35 (15.2)	6.66 (43.0)	-4.31 (-27.8)
15~16 (4.6~4.9)	1.23 (8.0)	10.85 (70.0)	-9.62 (-62.0)
16~17 (4.9~5.2)	0.00 (0.0)	7.97 (51.4)	-7.97 (-51.4)
17~18 (5.2~5.5)	22.18 (143.1)	32.23 (207.9)	-10.05 (-64.8)
18~19 (5.5~5.8)	0.00 (0.0)	12.54 (80.9)	-12.54 (-80.9)
19~20 (5.8~6.1)	15.14 (97.7)	9.54 (61.5)	5.60 (36.1)
20~21 (6.1~6.4)	15.88 (102.5)	12.16 (78.5)	3.72 (24.0)
21~22 (6.4~6.7)	11.53 (74.4)	13.96 (90.1)	-2.43 (-15.7)
22~23 (6.7~7.0)	16.57 (106.9)	19.87 (128.2)	-3.30 (-21.3)
23~24 (7.0~7.3)	0.00 (0.0)	0.86 (5.5)	-0.86 (-5.5)

The repair grout is filled from the top grout port and infiltrated to 14.4 ft (4.39 m) from the reference point (Figure B-37).

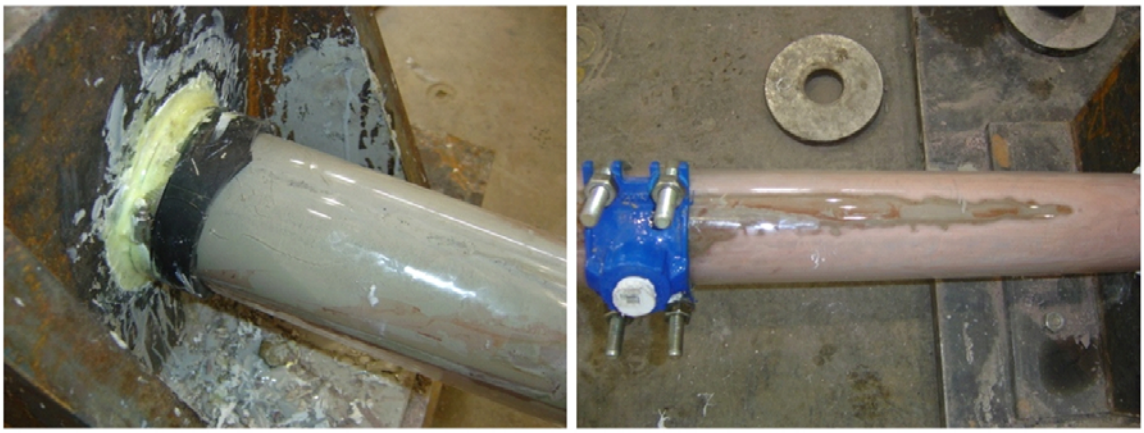

Figure B-37. Repair Grouted Ducts of Specimen PVG-C2-1.

Figure B-38 shows the cross-sectional views of the cut sections obtained from Specimen PVG-C2-1. From the cut sections, it is noted that the repair grout successfully replaces the main voids and repairs local large voids #3, #4, and #5.

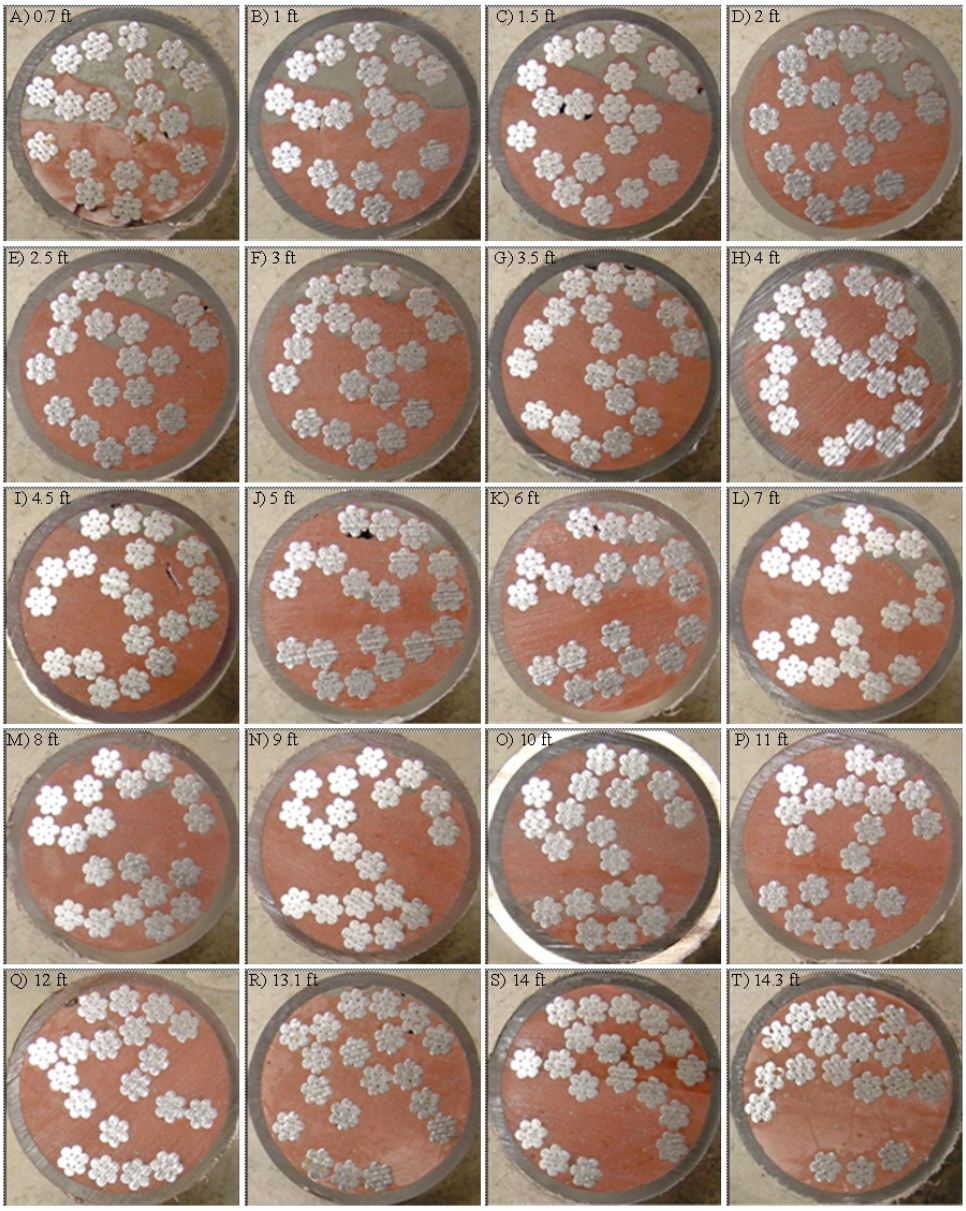

Figure B-38. Cut Sections of Specimen PVG-C2-1 for the Filling Analysis of Repair Grout.

To compare the performance of repair grouts, the ratio of remaining void area after repair to the repaired area is estimated. The repaired area and area of voids after repair are calculated using AutoCAD® (Table B-35).

Table B-35. Void Area of Specimen PVG-C2-1.

Cut Sections, ft (m)		Repaired Area, A_R, inch^2(10^{-4} m^2)	Void Area, A_V, inch^2(10^{-4} m^2)	Void Ratio, η (%)
A	0.7 (0.20)	2.980 (19.23)	0.0064 (0.041)	0.21
B	1 (0.30)	2.503 (16.15)	0.0073 (0.047)	0.29
C	1.5 (0.46)	1.613 (10.41)	0.0101 (0.065)	0.63
D	2 (0.61)	1.233 (7.95)	0.0028 (0.018)	0.23
E	2.5 (0.76)	0.943 (6.08)	0.0071 (0.046)	0.75
F	3 (0.91)	0.631 (4.07)	0.0015 (0.010)	0.24
G	3.5 (1.07)	0.557 (3.59)	0.0361 (0.233)	6.49
H	4 (1.22)	1.443 (9.31)	0.0062 (0.040)	0.43
I	4.5 (1.37)	0.521 (3.36)	0.0161 (0.104)	3.09
J	5 (1.52)	0.390 (2.52)	0.0013 (0.008)	0.33
K	6 (1.83)	0.593 (3.82)	0.0025 (0.016)	0.42
L	7 (2.13)	0.774 (4.99)	0.0000 (0.000)	0.00
M	8 (2.44)	0.314 (2.03)	0.0000 (0.000)	0.00
N	9 (2.74)	0.204 (1.31)	0.0000 (0.000)	0.00
O	10 (3.05)	0.162 (1.05)	0.0000 (0.000)	0.00
P	11 (3.35)	0.236 (1.52)	0.0023 (0.015)	0.98
Q	12 (3.66)	0.166 (1.07)	0.0281 (0.181)	16.98
R	13.1 (3.99)	0.253 (1.63)	0.0160 (0.103)	6.33
S	14 (4.27)	0.151 (0.98)	0.0005 (0.003)	0.33
T	14.3 (4.37)	0.053 (0.34)	0.0000 (0.000)	0.00
Sum		**15.717 (101.40)**	**0.1443 (0.931)**	**0.92**

From the analysis of cut sections, the Specimen PVG-C2-1 has the remaining void ratio, after repair, of 0.92% on average. The initial void area ranges over 0.1 inch^2 (0.65×10^{-4} m^2) or more from the reference point to Section S, however, the voids include small contributions from Section T.

Table B-36 shows the time schedule for sealing ducts and preparation of repair grouting for Specimen PVG-C2-1. Total sealing time for Specimen PVG-C2-1 is 1 day and 2.33 hours before applying repair grout.

Table B-36. Sealing Time Schedule of Specimen PVG-C2-1.

Sealing Procedure	Working Day	Working Time (min.)
Setting rubber end caps and sealing with silicone	Day 1	20
Installing pipe saddle tap with grease	Day 1	30
Checking air-tight condition	Day 1	20
Searching leaking part and sealing	Day 1	50
Connect grout hose and checking air-tight condition	Day 1	20
Sum	**1 day**	**140 (2.33 hours)**

B.14 SPECIMEN PVG-C2-2

Figure B-39 depicts the initial void profiles of the sounding inspection and of the visual inspection before grouting for Specimen PVG-C2-2.

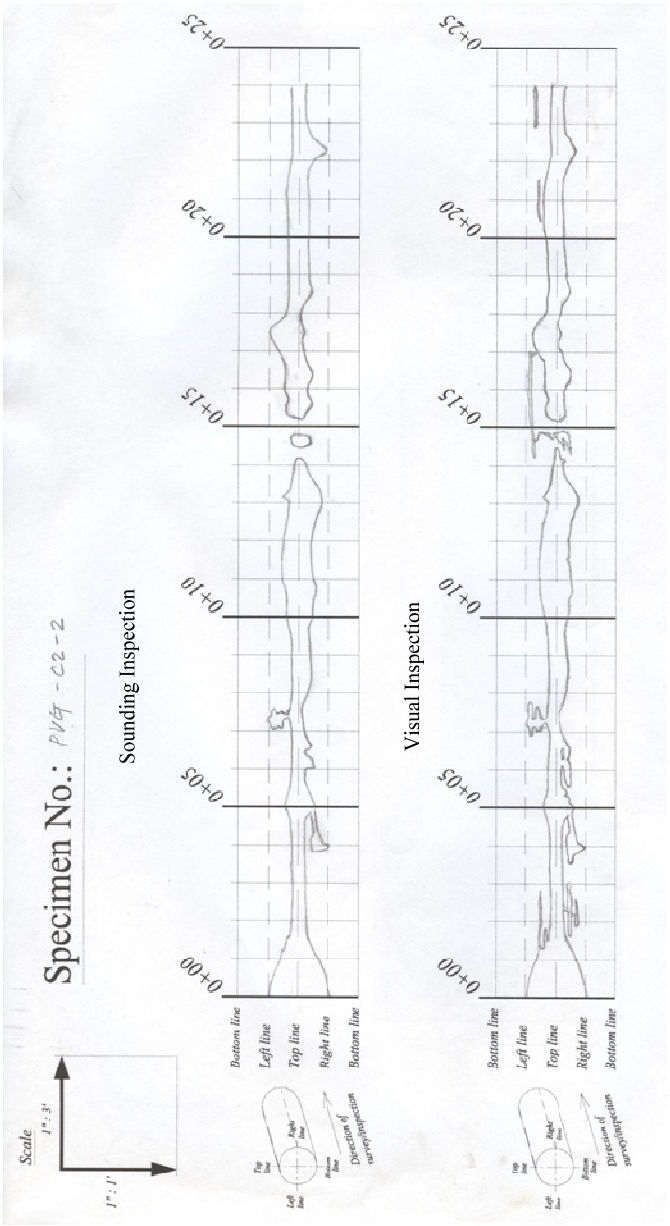

Figure B-39. Void Map of Specimen PVG-C2-2.

The areas of both void profiles are estimated using AutoCAD® and provided in Table B-37.

Table B-37. Estimation of Void Profile in Specimen PVG-C2-2.

Section, ft (m)	Sounding Inspection (SI), inch^2 (10^{-4} m^2)	Visual Inspection (VI), inch^2 (10^{-4} m^2)	SI - VI, inch^2 (10^{-4} m^2)
0~1 (0~0.3)	65.23 (420.9)	65.59 (423.155)	-0.35 (-2.3)
1~2 (0.3~0.6)	29.00 (187.1)	34.37 (221.743)	-5.37 (-34.6)
2~3 (0.6~0.9)	16.39 (105.8)	24.65 (159.061)	-8.26 (-53.3)
3~4 (0.9~1.2)	19.22 (124.0)	22.19 (143.140)	-2.97 (-19.2)
4~5 (1.2~1.5)	27.51 (177.5)	29.79 (192.186)	-2.28 (-14.7)
5~6 (1.5~1.8)	24.14 (155.7)	27.17 (175.314)	-3.04 (-19.6)
6~7 (1.8~2.1)	21.24 (137.0)	23.65 (152.604)	-2.41 (-15.6)
7~8 (2.1~2.4)	24.32 (156.9)	27.83 (179.536)	-3.51 (-22.7)
8~9 (2.4~2.7)	22.78 (147.0)	24.45 (157.771)	-1.68 (-10.8)
9~10 (2.7~3.0)	23.84 (153.8)	24.25 (156.462)	-0.41 (-2.7)
10~11 (3.0~3.4)	34.56 (223.0)	36.87 (237.852)	-2.31 (-14.9)
11~12 (3.4~3.7)	35.73 (230.5)	37.92 (244.676)	-2.19 (-14.1)
12~13 (3.7~4.0)	35.72 (230.5)	36.00 (232.241)	-0.28 (-1.8)
13~14 (4.0~4.3)	30.43 (196.3)	28.04 (180.889)	2.39 (15.4)
14~15 (4.3~4.6)	8.29 (53.5)	12.77 (82.364)	-4.48 (-28.9)
15~16 (4.6~4.9)	19.58 (126.3)	21.19 (136.723)	-1.61 (-10.4)
16~17 (4.9~5.2)	30.48 (196.7)	33.73 (217.607)	-3.25 (-21.0)
17~18 (5.2~5.5)	34.04 (219.6)	30.07 (194.024)	3.97 (25.6)
18~19 (5.5~5.8)	23.81 (153.6)	23.87 (154.002)	-0.06 (-0.4)
19~20 (5.8~6.1)	24.72 (159.5)	23.35 (150.651)	1.37 (8.8)
20~21 (6.1~6.4)	25.53 (164.7)	26.77 (172.694)	-1.23 (-8.0)
21~22 (6.4~6.7)	25.01 (161.3)	25.82 (166.611)	-0.82 (-5.3)
22~23 (6.7~7.0)	29.75 (191.9)	25.81 (166.534)	3.93 (25.4)
23~24 (7.0~7.3)	17.13 (110.5)	20.58 (132.756)	-3.45 (-22.2)

The repair grout is filled from the top grout port and infiltrated to 14.3 ft (4.36 m) from the reference point (Figure B-40).

Figure B-40. Repair Grouted Ducts of Specimen PVG-C2-2.

Figure B-41 shows the cross-sectional views of the cut sections obtained from Specimen PVG-C2-2. From the cut sections, it is noted that the repair grouts successfully replaces the main voids and repairs local large voids #3, #4, and #5. The small voids still exist inside the initially grouted ducts, especially in-between strands. However, those voids cannot be repaired because the voids are isolated from the "bug holes" which is a route for repair grouts.

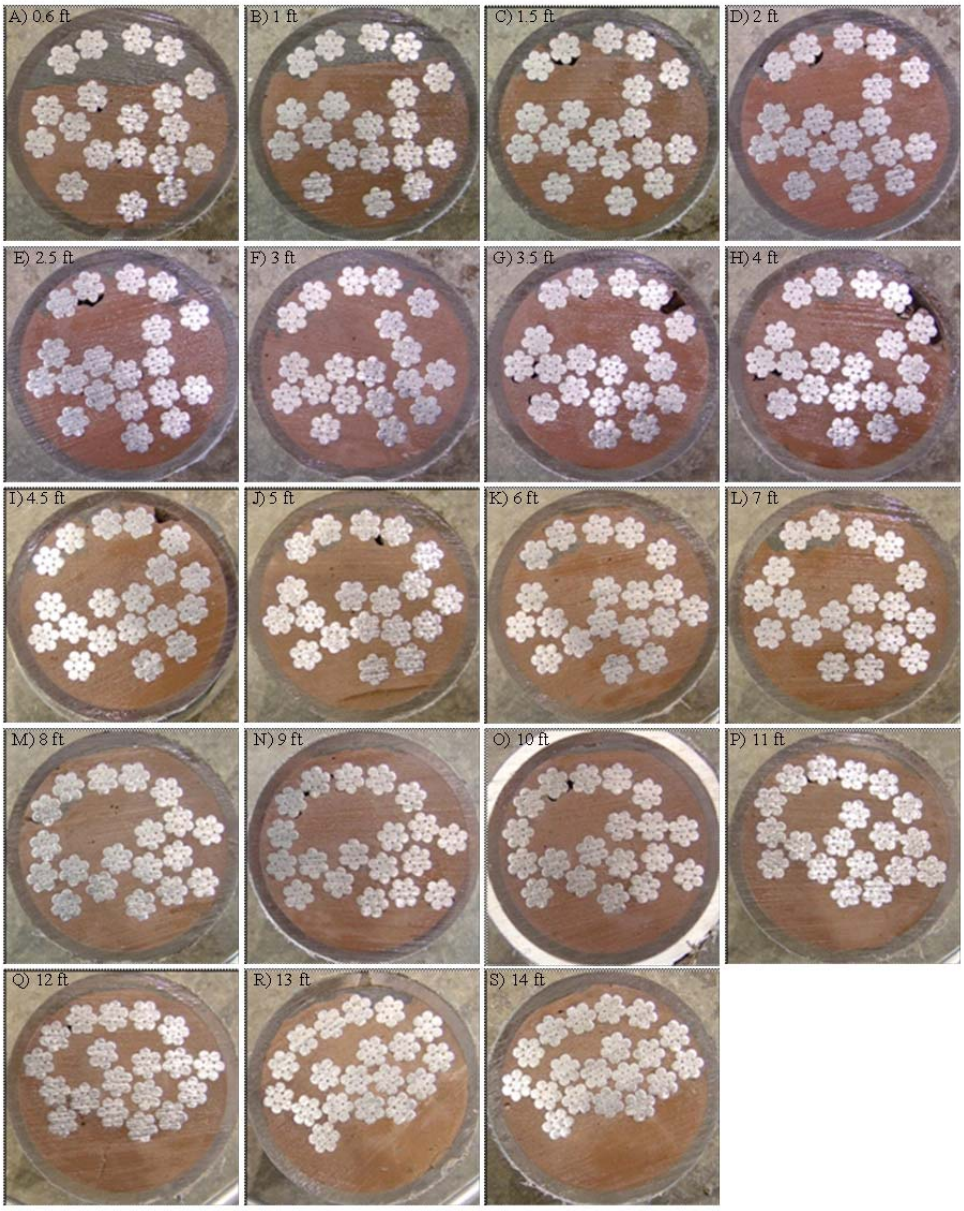

Figure B-41. Cut Sections of Specimen PVG-C2-2 for the Filling Analysis of Repair Grout.

To compare the performance of repair grouts, the ratio of remaining void area after repair to the repaired area is estimated. The repaired area and area of voids after repair are calculated using AutoCAD® (Table B-38).

Table B-38. Void Area of Specimen PVG-C2-2.

Cut Sections, ft (m)		Repaired Area, A_R, inch^2(10^{-4} m^2)	Void Area, A_V, inch^2(10^{-4} m^2)	Void Ratio, η (%)
A	0.6 (0.18)	2.274 (14.67)	0.0035 (0.023)	0.15
B	1 (0.30)	1.165 (7.52)	0.0022 (0.014)	0.19
C	1.5 (0.46)	0.490 (3.16)	0.0041 (0.026)	0.84
D	2 (0.61)	0.340 (2.19)	0.0095 (0.061)	2.80
E	2.5 (0.76)	0.351 (2.26)	0.0022 (0.014)	0.63
F	3 (0.91)	0.332 (2.14)	0.0017 (0.011)	0.51
G	3.5 (1.07)	0.257 (1.66)	0.0007 (0.005)	0.27
H	4 (1.22)	0.238 (1.53)	0.0006 (0.004)	0.25
I	4.5 (1.37)	0.291 (1.88)	0.0000 (0.000)	0.00
J	5 (1.52)	0.376 (2.42)	0.0000 (0.000)	0.00
K	6 (1.83)	0.352 (2.27)	0.0025 (0.016)	0.71
L	7 (2.13)	0.396 (2.56)	0.0021 (0.014)	0.53
M	8 (2.44)	0.214 (1.38)	0.0007 (0.005)	0.33
N	9 (2.74)	0.151 (0.97)	0.0005 (0.003)	0.33
O	10 (3.05)	0.194 (1.25)	0.0101 (0.065)	5.22
P	11 (3.35)	0.185 (1.19)	0.0017 (0.011)	0.92
Q	12 (3.66)	0.229 (1.48)	0.0000 (0.000)	0.00
R	13 (3.96)	0.405 (2.61)	0.0000 (0.000)	0.00
S	14 (4.27)	0.031 (0.20)	0.0000 (0.000)	0.00
Sum		**8.268 (53.34)**	**0.0421 (0.272)**	**0.51**

The remaining void ratio, after repair, obtained from the analysis comes out to be 0.51% for Specimen PVG-C2-2. The initial void area ranges over 0.1 inch^2 (0.65×10^{-4} m^2) or more from the reference point to Section R, but the voids include small contributions from Section S.

Table B-39 shows the time schedule of sealing ducts for Specimen PVG-C2-2. Total sealing time of Specimen PVG-C2-2 is 3 days and 1.53 hours before applying repair grout.

Table B-39. Sealing Time Schedule of Specimen PVG-C2-2.

Sealing Procedure	Working Day	Working Time (min.)
Installing pipe saddle tap with grease	Day 1	29
Setting end rubber cover and sealing	Day 1	4
Mixing epoxy and sealing	Day 1	27
Wait	1 day	
Checking air-tight condition	Day 2	17
Connecting grout hose and sealing	Day 2	8
Checking air-tight condition	Day 2	17
Connecting vacuum safety device and checking air-tight	Day 2	7
Sum	**2 days**	**90 (1.53 hours)**

B.15 SPECIMEN PVG-C3-1

Figure B-42 depicts the initial void profiles of the sounding inspection and of the visual inspection before grouting for Specimen PVG-C3-1.

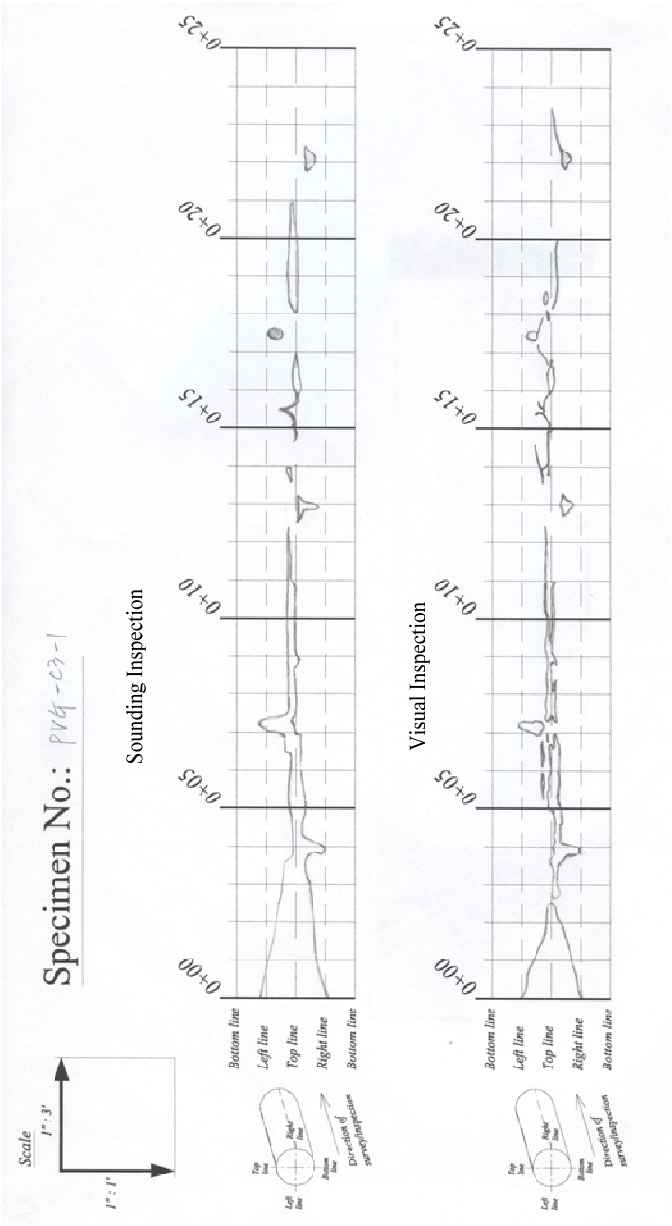

Figure B-42. Void Map of Specimen PVG-C3-1.

The areas of both void profiles are estimated using AutoCAD® and provided in Table B-37.

Table B-40. Estimation of Void Profile in Specimen PVG-C3-1.

Section, ft (m)	Sounding Inspection (SI), inch^2 (10^{-4} m^2)	Visual Inspection (VI), inch^2 (10^{-4} m^2)	SI - VI, inch^2 (10^{-4} m^2)
0~1 (0~0.3)	73.81 (476.2)	63.35 (408.7)	10.45 (67.4)
1~2 (0.3~0.6)	54.55 (351.9)	32.32 (208.5)	22.23 (143.4)
2~3 (0.6~0.9)	40.72 (262.7)	8.99 (58.0)	31.73 (204.7)
3~4 (0.9~1.2)	28.82 (185.9)	13.83 (89.3)	14.98 (96.7)
4~5 (1.2~1.5)	17.26 (111.3)	9.59 (61.9)	7.66 (49.4)
5~6 (1.5~1.8)	17.77 (114.6)	14.94 (96.4)	2.83 (18.2)
6~7 (1.8~2.1)	16.64 (107.3)	12.59 (81.2)	4.05 (26.1)
7~8 (2.1~2.4)	21.37 (137.9)	15.75 (101.6)	5.62 (36.3)
8~9 (2.4~2.7)	9.58 (61.8)	7.86 (50.7)	1.72 (11.1)
9~10 (2.7~3.0)	9.46 (61.1)	7.90 (51.0)	1.56 (10.1)
10~11 (3.0~3.4)	9.16 (59.1)	7.49 (48.3)	1.68 (10.8)
11~12 (3.4~3.7)	3.55 (22.9)	2.59 (16.7)	0.97 (6.2)
12~13 (3.7~4.0)	5.95 (38.4)	3.67 (23.7)	2.28 (14.7)
13~14 (4.0~4.3)	3.48 (22.4)	4.67 (30.1)	-1.19 (-7.7)
14~15 (4.3~4.6)	1.38 (8.9)	5.17 (33.4)	-3.79 (-24.5)
15~16 (4.6~4.9)	6.14 (39.6)	4.30 (27.7)	1.84 (11.9)
16~17 (4.9~5.2)	7.79 (50.3)	6.21 (40.0)	1.58 (10.2)
17~18 (5.2~5.5)	4.81 (31.0)	4.62 (29.8)	0.19 (1.2)
18~19 (5.5~5.8)	10.28 (66.3)	4.88 (31.5)	5.40 (34.8)
19~20 (5.8~6.1)	11.76 (75.9)	2.65 (17.1)	9.11 (58.8)
20~21 (6.1~6.4)	5.54 (35.8)	0.00 (0.0)	5.54 (35.8)
21~22 (6.4~6.7)	2.10 (13.5)	0.88 (5.7)	1.22 (7.9)
22~23 (6.7~7.0)	4.30 (27.7)	5.30 (34.2)	-1.00 (-6.5)
23~24 (7.0~7.3)	0.00 (0.0)	1.06 (6.8)	-1.06 (-6.8)

The repair grout is filled from the top grout port and infiltrated to 3.9 ft (1.19 m) from the reference point (Figure B-43).

Figure B-43. Repair Grouted Ducts of Specimen PVG-C3-1.

Figure B-44 shows the cross-sectional views of the cut sections obtained from Specimen PVG-C3-1. From the cut sections, it is noted that the repair grout successfully replaces the main voids up to 2.5 ft (0.76 m) from the reference point, but after that voids are only partially repaired. Also, it does not fill void #5 located in Section H. The small voids still exist inside the initially grouted ducts, especially in-between strands.

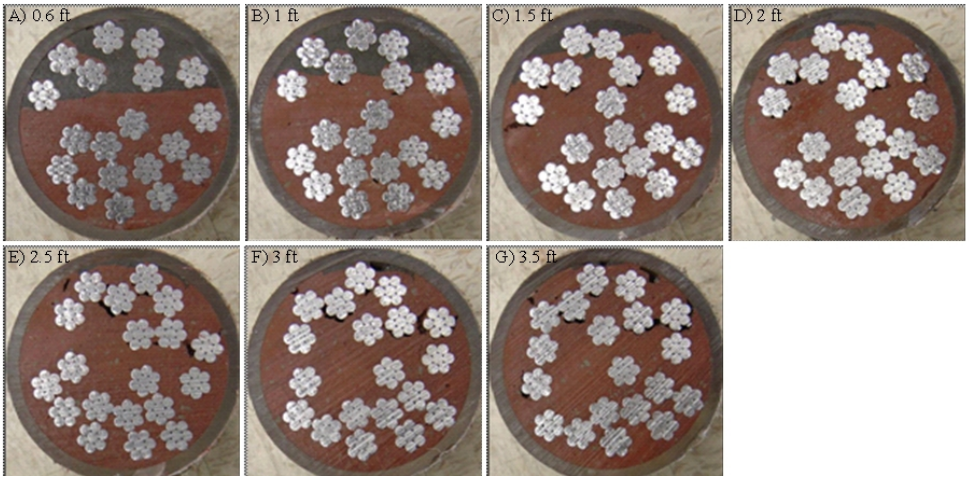

Figure B-44. Cut Sections of Specimen PVG-C3-1 for the Filling Analysis of Repair Grout.

To compare the performance of repair grouts, the ratio of remaining void area after repair to the repaired area is estimated. The repaired area and area of voids after repair are calculated using AutoCAD® (Table B-41).

Table B-41. Void Area of Specimen PVG-C3-1.

Cut Sections, ft (m)		Repaired Area, A_R, inch^2(10^{-4} m^2)	Void Area, A_V, inch^2(10^{-4} m^2)	Void Ratio, η (%)
A	0.6 (0.18)	2.182 (14.08)	0.0180 (0.116)	0.83
B	1 (0.30)	1.422 (9.17)	0.0054 (0.035)	0.38
C	1.5 (0.46)	0.551 (3.56)	0.0074 (0.048)	1.34
D	2 (0.61)	0.188 (1.21)	0.0018 (0.012)	0.96
E	2.5 (0.76)	0.163 (1.05)	0.0000 (0.000)	0.00
F	3 (0.91)	0.176 (1.14)	0.0526 (0.339)	29.84
G	3.5 (1.07)	0.074 (0.48)	0.0177 (0.114)	23.79
Sum		**4.756 (30.69)**	**0.1029 (0.664)**	**2.16**

From the analysis, remaining voids in repair grouts are estimated in each grout cut sections, however, a void ratio in a section can be magnified when the remaining voids exist only in a small repaired area. Thus, the filling performance for Specimen PVG-C3-1 is considered as using the summation of the estimated section. The remaining void ratio, after repair, obtained

from the analysis comes out to be 2.16% for Specimen PVG-C3-1. The initial void area ranges over 0.1 inch^2 (0.65×10^{-4} m^2) or more from the reference point to Section F, however, the voids include contribution from Section G.

Table B-42 shows the time schedule of sealing ducts for Specimen PVG-C3-1. Total sealing time of Specimen PVG-C3-1 is 2 days and 2.25 hours before applying repair grout.

Table B-42. Sealing Time Schedule of Specimen PVG-C3-1.

Sealing Procedure	Working Day	Working Time (min.)
Setting rubber end caps and sealing with epoxy	Day 1	50
Wait	1 day	
Installing pipe saddle tap with grease	Day 2	45
Connect grout hose	Day 2	10
Checking air-tight condition	Day 2	30
Sum	2 days	135 (2.25 hours)

APPENDIX C. STRENGTH TEST RESULTS OF GROUT

The compressive strength test of cubic molds is carried out to ensure the performance of hardened grouts, and it is executed by following Tex-442-A (TxDOT 2006). The test strength of initial grout and repair grout is provided in Table C-1.

Table C-1. Cube Strength of Grouts.

Specimen	Average Compressive Strength, ksi (10^4 kPa)			
	Initial Grout		Repair Grout	
	7 days	28 days	7 days	28 days
VG-C1-1	5.871 (4.048)	6.641 (4.579)	7.916 (5.458)	9.517 (6.562)
VG-C1-2	6.079 (4.191)	7.157 (4.935)	8.304 (5.726)	11.576 (7.982)
VG-C2-1	4.497 (3.101)	5.823 (4.015)	8.508 (5.866)	11.636 (8.023)
VG-C2-2	6.731 (4.641)	7.907 (5.452)	10.439 (7.198)	13.610 (9.384)
VG-C3-1	5.577 (3.845)	6.253 (4.311)	5.936 (4.093)	6.992 (4.821)
PG-C1-1	5.574 (3.843)	6.616 (4.562)	8.495 (5.857)	10.834 (7.470)
PG-C1-2	5.870 (4.047)	7.814 (5.388)	8.604 (5.932)	11.991 (8.268)
PG-C2-1	4.823 (3.325)	6.889 (4.750)	9.173 (6.325)	10.669 (7.356)
PG-C2-2	7.597 (5.238)	8.867 (6.114)	10.881 (7.502)	12.528 (8.638)
PG-C3-1	5.296 (3.652)	8.080 (5.571)	6.302 (4.345)	11.292 (7.786)
PG-C3-2	5.876 (4.052)	6.880 (4.744)	7.295 (5.030)	8.425 (5.809)
PVG-C1-1	5.840 (4.027)	7.525 (5.188)	7.518 (5.184)	9.640 (6.647)
PVG-C1-2	5.003 (3.450)	6.290 (4.337)	8.768 (6.046)	10.964 (7.560)
PVG-C2-1	5.523 (3.808)	6.698 (4.618)	7.695 (5.306)	11.352 (7.827)
PVG-C2-2	8.080 (5.571)	9.362 (6.455)	10.724 (7.394)	11.686 (8.057)
PVG-C3-1	5.405 (3.727)	5.916 (4.079)	5.720 (3.944)	8.056 (5.555)